A HIGH RESOLUTION MODEL FOR MULTIPLE SOURCE DISPERSION OF AIR POLLUTANTS UNDER COMPLEX ATMOSPHERIC STRUCTURE

BY

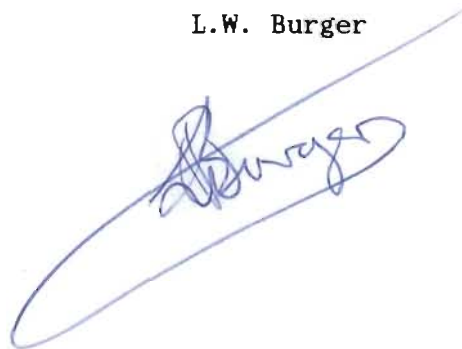Lucian Willem Burger B.Sc.Eng (Natal) M.Sc.Eng (Natal)

A thesis submitted in partial fulfilment of the requirements
for the degree of Doctor of Philosophy, in the Department of
Chemical Engineering, University of Natal,
Republic of South Africa.

Durban

December, 1986

DECLARATION:

The work described in this thesis was carried out in the Department of Chemical Engineering of the University of Natal. The work is original, except where other sources are specifically acknowledged in the text. No part of this thesis has been submitted for a degree at any other university.

L.W. Burger

Special thanks must go to Niels Kristensen whose programming ideas are greatly appreciated. I would like to also thank Paul den Hoed for proof reading the manuscript and Tracy Lavender who took on the great task of typing the thesis.

Finally I must thank my family for their support and encouragement for the duration of the project.

SUMMARY

A computer program is developed which predicts the distribution of air pollutants from multiple sources in a complex atmospheric structure. The dispersion of the pollutant is simulated by sequentially released puffs in an Eulerian reference frame. These puffs are divided into horizontal layers and the distribution within each layer is described by a bivariate normal distribution using the zero'th, first and second order moments (C_{00}, C_{10}, C_{20}, C_{01}, C_{02}, C_{11}). The moments are obtained by numerical solution of the advection-diffusion equation employing the method of fractional steps. Vertical diffusion is treated with an explicit finite difference numerical scheme. First-order chemical reaction, washout in rain, and dry deposition of the contaminants are accommodated. The rise of buoyant plumes and sedimentation are also included.

A mass-consistent three-dimensional wind field, including distortions due to topography and temperature anomalies, is constructed using a diagnostic model. This wind field produces key parameters describing the wind and diffusivity profiles used in the solution of the advection-diffusion equation. A pre-meteorological module computes the initial parameters of the wind field from available sparse measurements. A variety of meteorological measurement options are allowed as input to the package.

A high resolution puff-based (as opposed to grid-based) isopleth drawing routine supplies the concentration distribution at any height for any time interval. The wind field is represented in output plots by vectors drawn at a specified height and grid interval, together with curves for the wind and diffusivity profiles at a single chosen position in the study area.

The model is tested using measurements for two complex source configurations. The Durban Bluff area (13 x 4km) contains two relatively low hills and is situated on the coast. Excellent

Agreement between the predicted and observed concentrations is obtained. The second case study (Eastern Transvaal Highveld), covering a much larger area (120 x 84km), and containing nine elevated and twenty-four ground-level sources, gave acceptable results. These applications illustrate the enhanced horizontal spreads resulting from the interaction of wind-shear and vertical diffusion, particularly under unsteady conditions. The considerable value of high-resolution contour plots in distinguishing multiple sources is also apparent.

The program is easily adaptable to run on any medium-sized computer. The source code involves 15000 lines of FORTRAN 77 code (Burger 1986), and in a typical application requires 93K RAM for execution. It has been run on Sperry Univac 1100 (~1hr CPU/hr simulation), CDC Cyber 750 (~¼hr CPU/hr simulation) and IBM 4341 computers. The software is designed to be relatively independent of the output device, with HP2623 and Tektronix 4105 presently supported, and other graphics terminals easily added. An option for real-time operation has been provided.

TABLE OF CONTENTS

LIST OF FIGURES

LIST OF TABLES

CHAPTER 1

INTRODUCTION AND BRIEF OUTLINE

Air pollution is an inevitable offshoot of industrial progress. The question is: to what extent can we control the effect of these harmful and sometimes dangerous effluents? Strict control provides a solution, but seldom gives any economic advantage. Off-line simulation of the dispersion process under typical atmospheric and plant operation conditions allows decisions on plant sitings and stack dimensions. The objective is to maximise dilution of effluent gases before it effects urban areas. Real-time model prediction allows prompt responses to accidents involving the escape of dangerous gases (*e.g.* nuclear power plants). Dispersion modelling is obviously important in estimating the environmental impact of air pollution.

Many off-the-shelf dispersion packages assume greatly simplified atmospheric conditions *e.g.* Gaussian Puff and Plume models are derived under uniform wind and diffusivity profiles. Nonetheless, these models have found wide application and have shown reasonable accuracy under near neutral atmospheric conditions, and when applied in relatively flat terrain. The main advantages of these models are that they are fast and require little computer memory. Some models, on the other hand, are complex and often specifically designed for a particular application (dispersion down a valley, dispersion at a land/sea interface, dispersion under convective conditions, etc.).

Numerical techniques, applied to the dispersion equations, are normally capable of handling complex atmospheric structures. The majority of these, however, require large computer storage and are slow to run. In addition, spatial and temporal resolution is often lost as a result of discretisations. It is evident that a model, capable of simulating complex atmospheric conditions without large speed and memory requirements, and applicable to the majority of real situations, is desirable. This model should also exhibit sufficiently high spatial and temporal resolution.

Advection forms a major part of the dispersion process. An accurate discription of the wind field is therefore essential. Relevant background necessary to construct a wind field (under different atmospheric stabilities) in complex terrain, is presented in Chapter 2. The basic structure of the lowest part of the atmosphere, and the equations describing the heat and momentum transfer, are given. A review of three-dimensional wind field construction techniques is included.

Diffusion occurs through the action of turbulent eddies. As a result, a great deal of research has gone into establishing representative models to describe the nature of the turbulent eddies and how they affect the dispersion of gases. The basic equations describing these ideas are reviewed in Chapter 3. Additional factors affecting the dispersion of gases are ground retention, washout in rain, and chemical reactions. A brief review is included in the Chapter 3.

Chapter 4 contains the development of the dispersion package. This includes the submeteorological package, the three-dimensional wind and diffusivity fields, the diffusion process and the output package.

Numerical validation essential to indicate the accuracy of the model. This is done in Chapter 5. The ultimate test is to observe how the model predicts in real situations. Three case studies are included in the second part of Chapter 5.

CHAPTER 2

2. TRANSPORT OF AIRBORNE MATERIAL IN THE ATMOSPHERIC BOUNDARY LAYER

The ultimate objective of this study is to be able to predict the rate of dispersion of contaminants once they are introduced into the atmosphere. To achieve this objective it is essential to describe the nature of the transporting medium as accurately as possible.

The *atmospheric boundary layer* (ABL) or *planetary boundary layer* (PBL) is the lowest layer of the atmosphere under direct influence of the underlying surface (Figure 2.1). The turbulence within this layer is responsible for the transport of heat, water vapour, and pollutants. A great deal of work has already been done in describing the motion of air in this layer, with attention focusing on the more accessible lowest few metres. The lowest layer usually exhibits little change, with height, in the horizontal shearing stress and vertical turbulent fluxes of heat and vapour. It is this layer which is often referred to as the *surface layer* (SL), the *constant-stress layer* or the *surface-stress layer*, and is about ten per cent of the atmospheric boundary layer. It is the more complicated *outer layer* (OL) (or *Ekman layer*) above the surface layer that still remains to be described more accurately and most methods rely on parametric relations based on surface layer measurements. These two layers are described in more detail in Sections 2.1 and 2.2 .

Various forms exist for the definition of the *boundary layer height*

3

FREE ATMOSPHERE

Geostrophic wind. Motion of air approximates

that of an inviscid fluid

300-2000 m

OUTER LAYER

Region of transition. Variable shear stress

and heat flux. Wind structure influenced by

surface friction, density gradient and

rotation of earth. (Also known as the Ekman

or mixing layer)

ATMOSPHERIC

BOUNDARY

LAYER

50-300 m

SURFACE LAYER

Shear stress and heat flux (approximately) constant.

Wind structure primarily determined by nature of

surface and vertical gradient of temperature.

Earth's surface

Figure 2.1.   Definition of the lower atmosphere according

to air movements.

(BLH), but generally two approaches are taken (Section 2.2):

(i) diagnostic models, which give a direct relationship between the BLH and parameters characteristic of the surface layer.

(ii) prognostic models, which describe the BLH as a function of time by means of a rate equation.

The prediction of this height is particularly important since it is within this layer that all pollutants are trapped. The sources and sinks of turbulent energy which characterise this layer of variable depth all result directly or indirectly from the interactions between the atmosphere and the surface. The boundary layer can be either unstable if the sources of energy outweigh the sinks, or stable if the converse is true. During unstable conditions the PBL extends between 300 and 2000m, whereas during stable conditions this height extends from tens of metres to about 300m.

The wind and diffusion profiles also differ for different stability conditions. Methods for determining the stability condition of the atmosphere are numerous and are summarised in Section 2.3.

The prediction of the wind flow over smooth surfaces is easily estimated; however, in complex terrain, predicting the wind pattern remains a difficult task. For an accurate description of a wind field, closely spaced velocity and temperature measurements are necessary, but as this is not always possible, estimates from sparse measurements must often be used to model the flow. Diagnostic and prognostic models to construct three-dimensional wind fields are discussed in Section 2.4.1.

To construct a three-dimensional wind field from sparse measurements necessitates the use of numerical methods. Interpolation methods are required to interpolate measured data to grid locations which provide an initial estimate. The interpolated wind field is normally not mass consistent and errors (anomalous divergence) need to be reduced. Various objective analyses to minimise the anomolous divergence have been proposed. A selection of these are discussed in Section 2.4.2.

2.1 THE SURFACE LAYER AND THE MONIN-OBUKHOV SIMILARITY THEORY

Mean wind ($\bar{u}$) and temperature ($\bar{\theta}$) profiles in the fully developed region of the surface layer, well above the aerodynamic roughness elements, are considered to be well established from micrometeorological observations at homogeneous sites. The condition of the atmosphere can be neutral, stable or unstable depending on the vertical temperature gradient. This phenomonum is well treated in other texts (*e.g.* Seinfeld 1975, Sutton 1953).

Dimensional analysis, along the lines which have been used by Seinfeld (1975), leads to the flux-gradient relation for the neutral case

$$\frac{\partial \bar{u}}{\partial z} = \frac{u_*}{kz} \tag{2.1}$$

where

$\bar{u}$ = mean wind speed

u_* = τ/ρ = friction velocity

k = von Karmen constant

and

τ = shear stress

ρ = density of air

Integration of (2.1) leads to the well-known logarithmic wind profile for the neutral, constant flux, surface layer

$$\bar{u} = \frac{u_*}{k} \ln \frac{z}{z_0} \tag{2.2}$$

where the boundary integration constant, z_0, called the roughness length, is the level at which the mean wind speed is presumed to vanish. The von Karmen constant has been evaluated variously between 0,35 and 0,41.

When the surface layer is non-neutral, the similarity theory of Monin and Obukhov (1954) suggests that the vertical shear in the surface

layer may be represented by a modification of (2.1), namely,

$$\frac{\partial \bar{u}}{\partial z} = \frac{u_*}{kz} \phi_m(\frac{z}{L})$$ (2.3)

where $\phi_m(\frac{z}{L})$ is an empirical universal function and L is the Monin-Obukhov length, which depends on the turbulent fluxes as follows:

$$L = \frac{\bar{T} u_*^2}{gk^2\theta_*}$$ (2.4)

where
$\bar{T}$ = average temperature
g = gravitational acceleration constant
θ_* = $-H/(\rho c_p k u_*)$ = scaling temperature
H = sensible heat flux to the atmosphere
c_p = specific heat of air at constant pressure
ρ = density of air

$|L|$ may be interpreted as the height at which the magnitudes of mechanical and thermal production of turbulence are equal. It also provides a measure of the stability of the surface layer, $i.e.$,

$L > 0$ stable

$L = \infty$ neutral

$L < 0$ unstable.

A similar form is obtained for the potential temperature profile;

$$\frac{\partial \theta}{\partial z} = \frac{\theta_*}{kz} \phi_h(\frac{z}{L})$$ (2.5)

where ϕ_h is an empirical universal function and θ is the potential temperature, defined as the temperature exhibited by a parcel of air if it were brought adiabatically to a standard pressure at ground level. For a horizontal homogeneous atmosphere it follows that

$$\frac{\partial \theta}{\partial z} \cong \frac{\partial T}{\partial z} + \Gamma$$ (2.6)

where Γ is the adiabatic lapse rate and T the temperature. The dry

adiabatic lapse rate is 0.00986 K m^{-1}.

Integration of (2.3) and (2.5) leads to the expressions for wind and potential temperature profiles:

$$\bar{u} = \frac{u_*}{k} \, \Psi_m\left(\frac{z}{L}\right) \qquad (2.7)$$

$$\theta = \frac{\theta_*}{k} \, \Psi_h\left(\frac{z}{L}\right) + \theta_0 \qquad (2.8)$$

where

$$\Psi_m\left(\frac{z}{L}\right) = \int_{z_0/L}^{z/L} \frac{\phi_m(\xi)}{\xi} \, d\xi \qquad (2.9)$$

and

$$\Psi_h\left(\frac{z}{L}\right) = \int_{z_0/L}^{z/L} \frac{\phi_h(\xi)}{\xi} \, d\xi \qquad (2.10)$$

assuming that $\bar{u}(z_0) = 0$.

The surface layer is considered to be about 10% of the PBL; however Zeman (1979) suggested a relationship for stable conditions

$$h_s = \frac{0,3h_p}{1 + \frac{L}{h_p}} \qquad (2.11)$$

where h_p is the height of the boundary layer and h_s the surface layer height. For unstable and neutral layers Tennekes and Lumley (1972) maintained that

$$h_s \cong 0,1h_p \qquad (2.12)$$

Kaimal *et al.* (1976) limited the depth of the surface layer to a height range less than $|L|$ during convective conditions (very unstable conditions).

TABLE 2.1. A summary of universal functions for stable conditions

CONTRIBUTOR	YEAR	LIMITS ($\xi=\frac{z}{L}$)	MOMENTUM, ϕ_m	HEAT, ϕ_h	
Ito	1970	$0 \leq \xi < 1$	7ξ		
Webb	1970	$1 \leq \xi \leq 6,2$	$6,2$	$6,2$	
Carl *et al.*	1973	$\xi < 0,08$		$0,74+0,9\xi+29,6\xi^2$	
Pruitt *et al.*	1973	$0 \leq Ri \leq 0,3$	$0,8(1+18Ri)^{\frac{1}{3}}$	$(1+18Ri)^{\frac{1}{3}}$	
Kondo in Yamamato	1975	$0,3 < \xi < 10$	$(1+22,8\xi)^{\frac{1}{2}}$	$(1+22,8\xi)^{\frac{1}{2}}$	
Carson & Richards	1978	$0,5 < \xi < 10$	$8-\frac{4,25}{\xi}+\frac{1}{\xi^2}$		
Lettau	1979	$1 \leq \xi \leq 2,5$	$(1+5\xi)^{\frac{1}{4}}$	$(1+5\xi)^{\frac{1}{2}}$	
Monin–Obukhov	1954		$1 + \beta\xi$	$\alpha + \beta_2\xi$	
			β	α	β_2
Taylor	1960	$0 \leq \xi$	$2 \leq \beta \leq 10$		
Takeuchi	1961	$0 \leq \xi$	$2 \leq \beta \leq 10$		
McVehil	1964	$0 \leq \xi$	7		
Gurvich	1965	$0 \leq \xi$	10	1	10
Zilitinkevich & Chalikov	1969	$0 \leq \xi < 0,4$	10	1	10
Arya & Plate	1969	$0 \leq \xi$	10	1	17
Ito	1970	$0 \leq \xi \leq 1$	6		
Webb	1970	$0 \leq \xi \leq 1$	$5,2$	1	$5,2$
Businger *et al.*	1971	$0 \leq \xi \leq 1$	$4,7$	$0,74$	$4,7$
Badgley *et al.*	1972	$0 \leq \xi \leq 1$	7	1	7
Carl *et al.*	1973	$0,08 \leq \xi$	5	$1,2$	$6,1$
Kondo in Yamamoto	1975	$0 \leq \xi \leq 0,3$	6	1	6
Hicks	1976	$0 \leq \xi \leq 3$	5	1	5
Sethurama & Brown	1976	$0,25 \leq Ri$ / $Ri \leq 0,25$	$1,6$ / $5,2$	1 / 1	$1,6$ / $5,2$
Yelagina *et al.*	1978	$0 \leq \xi$	$7,8$	1	$7,8$
Munro & Davis	1978	$0 \leq \xi$	$4,5$	1	$4,3$
Wieringa	1980a	$0 \leq \xi \leq 1$	$6,9$	1	$9,2$
Schotz & Panofsky	1980	$0 \leq \xi \leq 0,5$	$5 \leq \beta \leq 15$		

2.1.1 Universal Functions ϕ_m and ϕ_h

During the last twenty years, numerous researchers have derived relationships for ϕ_m and ϕ_h for different stability conditions and set out the limitations of these functions.

Since Monin and Obukhov (1954) introduced the form

$$\phi_m = 1 + \beta(\frac{z}{L}) \qquad (2.13)$$

for stable conditions, various workers have sought to establish a value for the constant β.

A summary of the proposed β values and equations other than the above form for ϕ_m and ϕ_h, is given in Table 2.1. When direct measurement of eddy fluxes (e.g. eddy fluxes of x-momentum $-\overline{\rho u'u'}$, $-\overline{\rho u'v'}$, and $-\overline{\rho u'w'}$ (Section 2.2.1)) are unavailable, these relationships are expressed in terms of the Richardson number, Ri. Pruitt *et al.* (1973) proposed

$$\phi_m = 0,8(1 + 18Ri)^{\frac{1}{3}} \qquad (2.14)$$

for $0 \leq Ri \leq 0,3$ where the definition of Ri is

$$Ri = \frac{g}{T} \frac{(\partial\theta/\partial z)}{(\partial u/\partial z)^2} \qquad (2.15)$$

The universal function of the potential temperature profile was suggested to be

$$\phi_h(\frac{z}{L}) = \phi_m(\frac{z}{L}) \qquad (2.16)$$

for stable conditions. Equation (2.16) is only true for the ratio $K_h/K_m = 1$ (Dyer and Hicks 1970), where K_h and K_m are the eddy diffusivity terms for heat and momentum respectively (Section 2.2.1.). Other workers, notably Businger *et al.* (1971),

10

have found that $K_h/K_m = 1,35$ and proposed

$$\phi_h(\tfrac{z}{L}) \;=\; \alpha \;+\; \beta_2(\tfrac{z}{L}) \tag{2.17}$$

where $\alpha = 0.74$. For very stable conditions Webb (1970) proposed

$$\phi_m \;=\; \phi_h \;=\; 1 + \beta \qquad \text{for} \quad 1 \leq \tfrac{z}{L} < (1 + \beta) \tag{2.18}$$

which is a deviation to the log-linear prediction postulated in equation (2.13). According to Yamada (1979) up to 10 per cent or more of the PBL may be represented by log-linear profiles. A more recent study by Skibin and Businger (1985) showed that deviations from log-linear profiles occurred at about $\beta(\tfrac{z}{L}) \cong 5$, and for $\beta(\tfrac{z}{L}) > 15$ all the profiles deviated from the log-linear profile. The transition from turbulent to laminar flow in this range is still poorly understood. Carson and Richards (1978) approximated the transition regime by

$$\phi_m \;=\; 8 \;-\; \frac{4,25}{(\tfrac{z}{L})} \;+\; \frac{1}{(\tfrac{z}{L})^2} \;\;,\;\; \text{for} \;\; 0,5 \leq \tfrac{z}{L} \leq 10 \tag{2.19}$$

Garrat (1983) describes the transition layer by

$$\phi_m \;=\; \left\{ 1 + \beta(\tfrac{z}{L}) \right\} \exp \left\{ -\alpha_2 (1 - \tfrac{z}{z_*}) \right\} \;\;,\;\; z \leq z_* \tag{2.20}$$

where $\qquad \alpha_2 \;=\; 0,7$

$\qquad\qquad\quad z_* \;=\;$ transition height

Various forms exist for ϕ_m and ϕ_h under unstable conditions ($\tfrac{z}{L} < 0$), but generally

$$\phi_m(\tfrac{z}{L}) \;=\; (1 - \gamma(\tfrac{z}{L}))^P \tag{2.21}$$

and either ($K_h/K_m = 1$, Dyer (1974))

$$\phi_h(\tfrac{z}{L}) \;=\; \phi_m^2(\tfrac{z}{L}) \tag{2.22}$$

or ($K_h/K_m = 1{,}35$, Businger *et al.* (1971))

$$\phi_h(\tfrac{z}{L}) = \gamma_1(1 - \gamma_2(\tfrac{z}{L}))^q \qquad (2.23)$$

where typical values for γ, γ_1, γ_2, p and q are given in Table 2.2. These forms predict the velocity profile well for moderately unstable conditions, *i.e.* $0 > \tfrac{z}{L} > -1$. For very unstable (convective) conditions the friction velocity, u_*, is expected to be less important and the regime of "forced convection" will give way to a regime of "free convection".

TABLE 2.2. A summary of universal functions for unstable conditions

CONTRIBUTOR	YEAR	LIMITS ($\xi=\tfrac{z}{L}$)	MOMENTUM, ϕ_m	HEAT, ϕ_h
Swinbank	1964	$\xi < 0$	$\xi\{1-\exp|\xi|\}^{-1}$	
Pandolfo	1966	$-0{,}04 < \xi$	$0{,}25(-\xi)^{-\frac{1}{6}}$	$0{,}25(-\xi)^{-\frac{1}{3}}$
Swinbank	1968	$-2 < \xi < -0{,}1$	$0{,}613(-\xi)^{-\frac{1}{6}}$	$0{,}227(-\xi)^{-\frac{11}{26}}$
Businger *et al.*	1971	$-2 < \xi < 0$	$\phi_m^4 - 9\xi\phi_m^2 = 1$	$0{,}74(1+4|\xi|^{\frac{3}{4}})^{-\frac{2}{3}}$
Pruit *et al.*	1973	$Ri < 0$	$(1-16Ri)^{-\frac{1}{2}}$	$0{,}86(1-16Ri)^{-\frac{1}{3}}$
THE FORM :			$(1 - \gamma\xi)^p$	$\gamma_1(1-\gamma_2\xi)^q$

CONTRIBUTOR	YEAR	LIMITS ($\xi=\tfrac{z}{L}$)	γ	p	γ_1	γ_2	q
Webb	1970	$-0{,}03 < \xi < 0$	4,5	1	1	4,5	1
Dyer & Hicks	1970	$-1 < \xi < 0$	16	-1/4	1	16	-1/2
Businger *et al.*	1971	$-2 \leq \xi$	15	-1/4	0,74	9	-1/2
Carl *et al.*	1973	$-10 \leq \xi < -1$	16	-1/3			
Kondo in Yamamoto	1975	$-10 < \xi$	16	-1/4	1	16	-1/2
Lettau	1979	$-2{,}5 < \xi$	15	-1/4	1	22,5	-1/3
Dyer & Bradley	1982	$-4 < \xi < 0{,}004$	28	-1/4	1	14	-1/2

The KEYPS equation (an acronym derived from the names of the scientists who, in different ways, formulated the equation : Kazinzki and Monin (1956), Ellison (1957), Yamamoto (1959), Panofsky (1961) and Sellers (1962)) is essentially an interpolation scheme for the known behaviour of equation (2.3) in free convection.. The equation is

$$\phi_m^4 - 18\xi'\phi_m^3 = 1 \qquad (2.24)$$

where $\qquad \xi' = \frac{z}{L}(K_m/K_h)$

Similarity theory predicts that for free convection (Egan and Mahoney 1972 and Pandolfo 1966) the non-dimensional universal functions can be expressed by

$$\phi_h(\frac{z}{L}) = \frac{c}{3}(|\frac{z}{L}|)^{-\frac{1}{3}} \qquad (2.25)$$

where Pandolfo (1966) estimated $c \simeq 0.75$, and

$$\phi_m(\frac{z}{L}) = \phi_h(\frac{z}{L})^{\frac{1}{2}}$$

Pandolfo shows that this is true for $\frac{z}{L} \leq -0,04$. Egan and Mahoney (1972) used the above equations for $-3 < \frac{z}{L} < -0,8$, although Businger *et al.* (1971) suggested that the relation (2.23), for values of $\frac{z}{L}$ as small as -2, fits the data more accurately.

Carl *et al.* (1973) used

$$\phi_m = (1-16\frac{z}{L})^{-\frac{1}{3}}, \qquad -10 \leq \frac{z}{L} \leq -1 \qquad (2.26)$$

for unstable conditions. This formulation agrees well with the KEYPS form and approaches the free convection limit for $\frac{z}{L} \to -\infty$ (Lumley and Panofsky 1964). Reporting on the findings of the analysis done on the 1976 International Turbulence Comparison Experiment, Dyer and Bradley (1982) found that in an unstable atmosphere the

relationships.

$$\phi_m(\tfrac{Z}{L}) = (1-28(\tfrac{Z}{L}))^{-\frac{1}{4}} \qquad (2.27)$$

and

$$\phi_h(\tfrac{Z}{L}) = (1-14\tfrac{Z}{L})^{-\frac{1}{2}} \qquad (2.28)$$

fit the average observations to within a few per cent for $-4 < \tfrac{Z}{L} < -0,004$.

Webb (1982) extended the flux-gradient profile relationships to the superadiabatic (unstable) surface layer and presented relations for Ψ_m and Ψ_h (the integral forms of ϕ_m and ϕ_h) to fit four defined regions

region 1 : A,B $\leq$ 1

$$\Psi_m = \ln\tfrac{A}{B} - (\tfrac{A}{7})(\tfrac{B}{A} - 1)$$
$$\Psi_h = \Psi_m$$

region 2 : 1 < A,B $\leq$ 8,505

$$\Psi_m = 3A^{-\frac{1}{3}}\left[\left\{1 - (\tfrac{A}{B})^{\frac{1}{3}}\right\} - (28A)^{-1}\left\{1 - (\tfrac{A}{B})^{\frac{4}{3}}\right\}\right]$$
$$\Psi_h = \Psi_m$$

region 3 : 8,505 < A,B $\leq$ 17,01

$$\Psi_m = 6,068A^{-\frac{1}{10}}\left[\left\{1 - (\tfrac{A}{B})^{\frac{1}{10}}\right\} - (77A)^{-1}\left\{1 - (\tfrac{A}{B})^{\frac{11}{10}}\right\}\right]$$
$$\Psi_h = 2,52A^{-\frac{1}{3}}\left[\left\{1 - (\tfrac{A}{B})^{\frac{1}{3}}\right\} - (28A)^{-1}\left\{1 - (\tfrac{A}{B})^{\frac{4}{3}}\right\}\right]$$

region 4 : A,B > 17,01

$$\Psi_m = 3,5266A^{-\frac{1}{3}}\left[\left\{1 - (\tfrac{A}{B})^{\frac{1}{3}}\right\} - (28A)^{-1}\left\{1 - (\tfrac{A}{B})^{\frac{4}{3}}\right\}\right]$$
$$\Psi_h = 1,92A^{-\frac{1}{3}}\left[\left\{1 - (\tfrac{A}{B})^{\frac{1}{3}}\right\} - (28A)^{-1}\left\{1 - (\tfrac{A}{B})^{\frac{4}{3}}\right\}\right]$$

$$(2.29)$$

where $\quad A = \dfrac{z_0}{z_m}$

$$\quad B = \dfrac{z}{z_m}$$

and $\qquad z_m = \dfrac{|L|}{7a}$ (the transition height)

with $\qquad a = 4,5$

The gradient profiles of velocity and temperature described in equation (2.29) initially pass from z^{-1} dependence, through a smooth transition at $\dfrac{z}{L} \approx -0,03$, towards $z^{-\frac{4}{3}}$ dependence.

Reviews of these functions can be found in Dyer (1974) and Yaglom (1977). Garatt and Brost (1981) give a summary of β values, with the suggestion that these may be influenced by radiative cooling effects. Viswanadham (1982) examined the curvature of the profiles, proposed by Swinbank (1964, 1968), Webb (1970), Dyer and Hicks (1970), Businger *et al.* (1971), Kondo (Yamamoto 1975), Lettau (1979) and Hicks (1976). The curvatures were compared with the Richardson number and the limiting forms for the curvatures were determined. Viswanadham (1982) proposed that the forms given by Webb (1970), Businger *et al.* (1971), and Kondo (Yamamoto 1975) for stable conditions, and Dyer and Hicks (1970), Businger *et al.* (1971), Kondo (Yamamoto 1975), and Lettau (1979) for unstable conditions, were the most realistic. Lo and McBean (1978) considered the relative errors in determining the flux relations from data. Significant differences between flux estimates computed using the flux-gradient relationships proposed by Businger *et al.* (1971), Dyer and Hicks (1970), and Pruitt *et al.* (1973) were observed. For unstable conditions, the differences were calculated to be between 20 and 40 per cent and considerably larger for stable conditions. The following possible sources of errors were proposed

(a) the uncertainty in the von Kármén constant; a difference between k = 0,35 and 0,42 resulted in a difference of 17% in the value of u_*

(b) that turbulence under stable conditions is greatly suppressed which results in a shallow surface layer, consequently neglected effects such as radiative flux divergence, nonstationarity and inhomogeneity, become more important

(c) the relative simplicity of the theory

(d) the imperfections in the measurement sites or equipment.

Lo and McBean (1978) also found a wide deviation of the relationships

proposed by Pruitt *et al.* (1973) from the Businger *et al.* (1971) and the Dyer and Hicks (1970) forms and suggested that the latter two proposals be used.

Solutions for the functions Ψ_m and Ψ_h for the forms

$$\phi_m = 1 + \beta\xi \qquad\qquad (2.13)$$

$$\phi_h = \alpha + \beta_2\xi \qquad\qquad (2.17)$$

under stable conditions, and for

$$\phi_m = (1 + \gamma\xi)^p \qquad\qquad (2.21)$$

$$\phi_h = \gamma_1(1 - \gamma_2\xi)^q \qquad\qquad (2.23)$$

under unstable conditions, are presented in Table 2.3.

TABLE 2.3. A summary of the universal functions Ψ_m and Ψ_h as defined by equations (2.9) and (2.10) using the forms given by equations (2.13), (2.17), (2.21) and (2.23).

STABLE	NEUTRAL	UNSTABLE
Momentum : $\ln\left\{\dfrac{z}{z_0}\right\} + \dfrac{\beta}{L}(z-z_0)$	$\ln\left\{\dfrac{z}{z_0}\right\}$	$2(\tan^{-1}b - \tan^{-1}b_0) - \ln\left\{\dfrac{b+1}{b-1} \cdot \dfrac{b_0-1}{b_0+1}\right\}$
Heat : $\alpha\ln\left\{\dfrac{z}{z_1}\right\} + \dfrac{\beta_2}{L}(z-z_1)$	$\alpha\ln\left\{\dfrac{z}{z_1}\right\}$	$\gamma_1\ln\left\{\dfrac{b_2-1}{b_2+1}\dfrac{b_1+1}{b_1-1}\right\}$
where for momentum $\begin{cases} b = (1-\frac{\gamma}{L}z)^{\frac{1}{4}} \\ b_0 = (1-\frac{\gamma}{L}z_0)^{\frac{1}{4}} \end{cases}$	and heat $\begin{cases} b_1 = (1-\frac{\gamma_2}{L}z_1)^{\frac{1}{2}} \\ b_2 = (1-\frac{\gamma_2}{L}z)^{\frac{1}{2}} \end{cases}$	

Source : McRae *et al* (1982)

16

2.1.2. Effect of Tall, Dense Vegetation and Closely-Spaced Buildings

The effect of dense vegetation or closely-spaced buildings has been observed to impose an upward-displacement on the characteristic profiles. This is accounted for by introducing a zero-plane displacement, d, which is characteristic of the surface. This zero-plane displacement is incorporated into the previous set of equations describing the wind and temperature profiles by replacing "z" with "(z - d)". The boundary condition then becomes $\bar{u}(z) = 0$ for $z \leq d$. So, for instance, the neutral velocity profile will be described by

$$\bar{u}(z) \quad = \quad \frac{u_*}{k}\ln(\frac{z - d}{z_0}) \qquad\qquad (2.30)$$

The dependance of z_0 and d on wind speed above forests is uncertain; Allen (1968), Belt (1969) and Leonard and Federer (1973), however, found little dependance between these variables and wind speed.

Various analytical least-square error methods (e.g., Lo 1977) have been used to determine d and z_0. Molion and Moore (1983) have described a method using a "mass conservation technique" mentioned by Tajchman (1981). With this technique, the zero-plane displacement could be associated with the upward displacement in the mean airflow trajectory as the flow responds to the transition from short to tall vegetation.

In recent years, with the recognition of anomalies in the flux-gradient relationships, controversy has begun to surround the interpretation of the zero-plane displacement height and its physical significance (Raupach 1979, Garrat 1980).

2.2 THE OUTER LAYER

Outside the surface-stress layer the shape of the wind profile is affected by the pressure gradient, the Coriolis effect (rotation of the earth), and gravitational forces. The earliest attempt to develop an analytical solution for the mean PBL flow was by Ekman (1905), who solved a simplified version of the Navier-Stokes equations for the balance between geostrophic pressure gradient, Coriolis forces and eddy viscous forces.

2.2.1. Analytical Approaches

Treatment of the Navier-Stokes equations for incompressible fluids is given in texts such as Sutton (1953) and Seinfeld (1975). The equations of motion of an incompressible viscous fluid are of the form:

$$\rho(\frac{\partial u}{\partial t}+u\frac{\partial u}{\partial x}+v\frac{\partial u}{\partial y}+w\frac{\partial u}{\partial z}) \quad = \quad \mu(\frac{\partial^2 u}{\partial x^2}+\frac{\partial^2 u}{\partial y^2}+\frac{\partial^2 u}{\partial z^2}) - \frac{\partial p}{\partial x} + \rho X$$

$$[\text{inertia forces}] \qquad\qquad [\text{viscous terms}] \quad [\text{forces}]$$

where
ρ = density

μ = dynamic viscosity

p = pressure

X = x-component of external acceleration per unit mass

The three equations of this form (x, y and z components) are the Navier-Stokes equations of motion. The wind components u, v, w and the temperature θ can be represented as

$$\bar{u} = u - u'$$

$$\bar{v} = v - v'$$

$$\bar{w} = w - w' \qquad\qquad (2.31)$$

$$\bar{\theta} = \theta - \theta'$$

where $\bar{u}$, $\bar{v}$, $\bar{w}$ and $\bar{\theta}$ are the mean values while u, v, w, and θ are the instantaneous measurements (deterministic) and u', v', w' and θ', the fluctuating (stochastic) components. The averaging period must be large relative to the periods of turbulent fluctuations and small relative to the variations of the mean motion. Furthermore, it can be shown that $\bar{u'} = \bar{v'} = \bar{w'} = 0$. By substituting these into the Navier-Stokes equations and introducing the Coriolis force terms, four sets of equations result. After some simplifications and averaging we get

$$\rho \frac{du}{dt} = \frac{\partial p}{\partial x} + \rho f v + \frac{\partial}{\partial x}(-\rho\overline{u'u'}) + \frac{\partial}{\partial y}(-\rho\overline{u'v'}) + \frac{\partial}{\partial z}(-\rho\overline{u'w'})$$

and similar equations for the y- and z-directions. Here f is the Coriolis parameter, given by $2\Omega\sin\lambda$, where Ω is the angular velocity of rotation of the earth $(7,29\times10^{-5}s^{-1})$, and λ the latitude of the observation site. The covariances $-\rho\overline{u'^2}$, $-\rho\overline{u'v'}$, and $-\rho\overline{u'w'}$ (and those for the y- and z-directions) constitute the Reynold stresses. Similar covariances arise when treating the energy equation. These stress terms are additional dependent variables, and the so-called *closure-problem* is concerned with establishing a closed system of equations, either by expressing the fluctuations directly in terms of the average flow variables (*first-order closure*), or by providing additional equations for the fluctuations derived from equations of motion (*second order closure*). It can be shown (Sutton 1953, Seinfeld 1975) that the covariances $-\rho\overline{u'^2}$, $-\rho\overline{v'^2}$, $-\rho\overline{u'v'}$, $-\rho\overline{u'\theta'}$ and $-\rho C_p \overline{v'\theta'}$ are negligible compared with the covariances $-\rho\overline{u'w'}$, $-\rho\overline{u'w'}$ and $-\rho C_p \overline{w'\theta'}$. It therefore remains only to specify the latter covariances. Following the notation used by Seinfeld (1975), the Reynold stresses are denoted by

$$-\rho\overline{u'w'} = \tau_{zx}$$
$$-\rho\overline{v'w'} = \tau_{zy}$$

According to the first-order closure assumption, the shearing stress components can be substituted by the K-theory forms

$$\tau_{zx} = \rho K_m \frac{\partial \bar{u}}{\partial z} \tag{2.32a}$$

19

and

$$\tau_{zy} = \rho K_m \frac{\partial \overline{v}}{\partial z} \qquad (2.32b)$$

where K_m is the eddy viscosity of momentum.

Taking $\frac{d\overline{u}}{dt} = \frac{d\overline{v}}{dt} = 0$ the Navier–Stokes equations can be simplified to :

$$\rho \frac{d\overline{u}}{dt} - \rho f\overline{v} = -\frac{\partial \rho}{\partial x} + \frac{\partial}{\partial z}(\tau_{zx})$$

$$\qquad (2.33)$$

$$\rho \frac{d\overline{v}}{dt} + \rho f\overline{u} = -\frac{\partial \rho}{\partial y} + \frac{\partial}{\partial z}(\tau_{zy})$$

Analytical solutions of the above equations are scarce. The cases of $K = $ constant (Ekman spiral solution) and $K \propto z^m$ with $0 \leq m \leq 1$ have been solved and the results are given in Sutton (1953). More recently the cases $K = cu_*z(1 - \frac{z}{h})$ and $K = cu_*z(1 - \frac{z}{h})^2$ have been treated by Nieuwstadt (1983).

Solutions using the "two-layer" approach (Haltiner and Williams 1980) are obtained by matching the surface layer with known profiles, to the upper layer solution of equation (2.33). This was developed by Rossby and Montgomery (1935) for neutral cases, and only recently applied by Yardanov (1975) to nonneutral cases.

2.2.2. Power-Law Profiles

The complicated behaviour of the outer layer is difficult to predict. However, it is often approximated by empirical models.

Power-law profiles have been used in many air pollutant diffusion studies. Although power-law profiles are empirical in formulation,

numerous experimental studies have shown them to be effective in covering a wide range of conditions when the parameters are correctly evaluated. The velocity profile is given as

$$u = u_r \left(\frac{z}{z_r}\right)^p \qquad (2.34)$$

where u_r and z_r are the reference velocity and elevation selected for the particular application. The value of p generally increases with stability and surface roughness. De Marrais (1959) and Jones *et al.* (1971) have shown variation in p to reverse at high instabilities. For neutral conditions, the "one—seventh law", namely $p = \frac{1}{7}$, is often quoted. The stability limits of p in equation (2.34) are (Seinfeld 1975) :

$$p = \begin{cases} 0,83 & \text{very stable} \\ 1/7 & \text{neutral} \\ 0,02 & \text{very unstable} \end{cases}$$

Gee (1965) developed a method by which the Monin—Obukhov length is incorporated in the exponent p:

$$p = 0,1340 + 0,244L^{-1} + 0,22L^{-2}$$

for $-0,2 < \frac{1}{L} < 0,2$. Gee (1965) pointed out that, rather than be treated as quantitatively accurate, this equation should be viewed as a qualitative approximation. De Marrais (1959) completed an extensive study on the effect of averaging time and the dependence of p on elevation range over which it was evaluated.

Values for the exponent p listed for a range of conditions, collected from several sources, are given in Table 2.4. Quite often the reference height is the planetary boundary layer height, and the reference velocity, the geostrophic wind speed (Davenport 1965).

Ragland (1973) and Ragland and Dennis (1975) deviated from equation (2.34), representing only the outer layer with a power-law profile. The velocity profile in the surface layer is described by the Monin—Obukhov similarity functions. In the outer layer, on the other

TABLE 2.4. p – values for the exponential velocity profile given by

$$u = u_r \left(\frac{z}{z_r}\right)^p \quad \text{(equation (2.34) in text)}$$

for different surfaces and stability conditions.

SURFACE CONFIGURATION & STABILITY	p	SOURCE
Smooth open country :		
Unstable	0,11	
Neutral	0,14	Sutton (1953)
Moderately stable	0,20	
Rural – varying roughness & terrain : Daytime	0,1 – 0,3	De Marrais (1959)
Nighttime	0,2 – 0,8	
Urban (Liverpool) :		
Unstable, $\Delta\theta < 0$	0,20	
Neutral, $\Delta\theta = 0$	0,21	Jones et al.(1971)
Stable, $0<\Delta\theta<0,75$	$0,21 + 0,33\Delta\theta$	$\Delta\theta = \theta(162m)-\theta(9m)$
Geostrophic wind form :(neutral)		
Flat open country, h_p = 274m	0,16	
Woodland forest, h_p = 396m	0,28	Davenport (1965)
Urban erea, h_p = 518m	0,40	

hand, it is described by a modified power-law relationship :

$$\bar{u}(z) = (u_g - \bar{u}(h_s)) \left[\frac{z - h_s}{h_p - h_s}\right]^q + \bar{u}(h_s) \qquad (2.35)$$

with
u_g = geostrophic wind

$\bar{u}(h_s)$ = windspeed at the surface layer height

h_s = top of the surface layer

h_p = top of the boundary layer

q = function of atmospheric stability

Ragland (1973) used $q = 0,20$ for unstable and neutral conditions, $q = 0,35$ for slightly stable conditions, and $q = 0,5$ for stable conditions.

2.2.3. Parametric Relationships

Several different schemes have been used for parametrising the boundary layer. The simplest scheme employs the bulk transfer relationship with all transfer coefficients assumed equal and prescribed *a priori*. These parameterisation schemes are very crude and are normally used only in global weather forecasting models. Better schemes have been formulated from similarity considerations of the PBL. Arya and Sundarajan (1976) give a detailed and critical review of various similarity theories.

The present discussion will be confined to parameterisations on the matching of surface and outer layer similarity theories. The basic assumptions underlying all similarity theories are that the PBL flow is (a) horizontally homogeneous and (b) quasi-stationary. These assumptions are obviously restrictive when applied to many real situations, but they provide, nonetheless, a basis for further work.

As Arya (1977) indicated, the drag and transfer relationships, based on matching of surface and outer layer theories, can be stated in three different ways:

$$
\begin{aligned}
\frac{ku(h_p)}{u_*} &= \ln \hat{z}_0 - A \\
\frac{kv(h_p)}{u_*} &= -B \ \text{sign} \ f
\end{aligned}
$$

or

$$
\begin{aligned}
\frac{ku_g}{u_*} &= \ln \hat{z}_0 - A_0 \\
\frac{kv_g}{u_*} &= -B_0 \ \text{sign} \ f
\end{aligned}
\qquad (2.36)
$$

or

$$
\begin{aligned}
\frac{ku_m}{u_*} &= \ln \hat{z}_0 - A_m \\
\frac{kv_m}{u_*} &= -B_m \ \text{sign} \ f
\end{aligned}
$$

where $\hat{z}_0$ = normalised roughness parameter, and $\hat{z}_0 = \dfrac{h}{z_0}$ or $z_0 = \dfrac{u_*}{|f| z_0}$.

A, A_0, A_m and B, B_0, B_m are the well-known similarity functions corresponding to the relationship based on the velocity components at the boundary layer height ($u(h_p)$, $v(h_p)$), the (surface) geostrophic wind components (u_g, v_g) and layer averaged wind components (u_m, v_m), respectively.

Two similarity theories most often used are the Kazanski-Monin, or the Rossby number, similarity theory (Kazanski and Monin 1960), and the generalized similarity theory (Deardorff 1972). The two theories differ in the formulation of the PBL height, h_p. In the Kazinski-Monin model, h_p is determined by u_*, f, and L, whereas in the generalized model it is considered as an independent variable. Similarity theories, however, do not give actual forms for A and B. Various attempts at deriving A and B were made (Yamada 1976, Brown 1982, Garrat *et al.* 1982). Arya (1977) provide a review of empirical forms for the similarity functions. These functions vary greatly, even when re-analysed using the same technique. Less scatter occurs when layer averaged velocity components (u_m, v_m) are used (Arya 1977; 1984, Hess *et al.* 1981).

The functions become universal constants in neutral conditions. As reported by Hess *et al.* (1981) for neutral conditions,

$$
\begin{aligned}
A_m &\approx 1{,}1 \pm 0{,}5 \\
B_m &\approx 4{,}3 \pm 0{,}7
\end{aligned}
\tag{2.37}
$$

Under non-neutral conditions the following suggestions (Yamada 1976) based on layer averaged wind components, provide reasonably accurate results.

STABLE

$$
\left.
\begin{aligned}
A_m &= 1{,}855 - 0{,}380\frac{h_p}{L} \\[2em]
B_m &= 3{,}020 + 0{,}300\frac{h_p}{L}
\end{aligned}
\right\} \quad \text{for } 0 \leq \frac{h_p}{L} \leq 35
$$

$$A_m = -2,94\left\{\frac{h_p}{L} - 19,94\right\}^{\frac{1}{2}}$$

$$B_m = 2,85\left\{\frac{h_p}{L} - 12,47\right\}^{-\frac{1}{2}} \quad\Bigg\} \quad \text{for } 35 < \frac{h_p}{L}$$

UNSTABLE

$$A_m = 10,0 - 8,145\left\{1,0 - 0,008376\frac{h_p}{L}\right\}^{-\frac{1}{2}}$$

$$B_m = 3,020\left\{1,0 - 3,290\frac{h_p}{L}\right\}^{-\frac{1}{2}}$$

(2.38)

Here $\hat{z}_0 = \dfrac{h_p}{z_0}$ and hence

$$u_m = \frac{u_*}{k}\left(\ln\frac{h_p}{z_0} - A_m\right)$$

$$v_m = -\frac{u_*}{k} B_m (\text{sign } f)$$

For stable conditions, Arya (1984) recommended a linear interpolation between the surface layer wind and the geostrophic wind. Observational evidence supports this type of profile (Wetzel 1982, (Figure 2.2(a))).

Under unstable and convective conditions the velocity profile is considered to be more or less uniform, independant of height and with negligible directional change. Under these conditions the outer boundary layer is usually divided into two layers: a mixed layer beneath an entrainment layer (Figure 2.2(b)). Garratt *et al.* (1982) suggested the relationships

$$\bar{u}_m = \frac{u_*}{k}\left\{\ln(\frac{h_m}{z_0}) - \frac{1}{2}\ln\left|\frac{h_m}{L}\right| - 2,3\right\} , \quad -1 > \frac{h_m}{L} \geq -200$$

(2.39)

and $\qquad\qquad \bar{v}_m \cong 0$

where $\bar{u}_m$ and $\bar{v}_m$ are the layer-averaged velocity components, and h_m = mixing layer height. For $\dfrac{h_m}{L} < -1000$, Wyngaard *et al.* (1974) and

STABLE CONDITIONS

hₚ

OUTER LAYER

hₛ

SURFACE LAYER
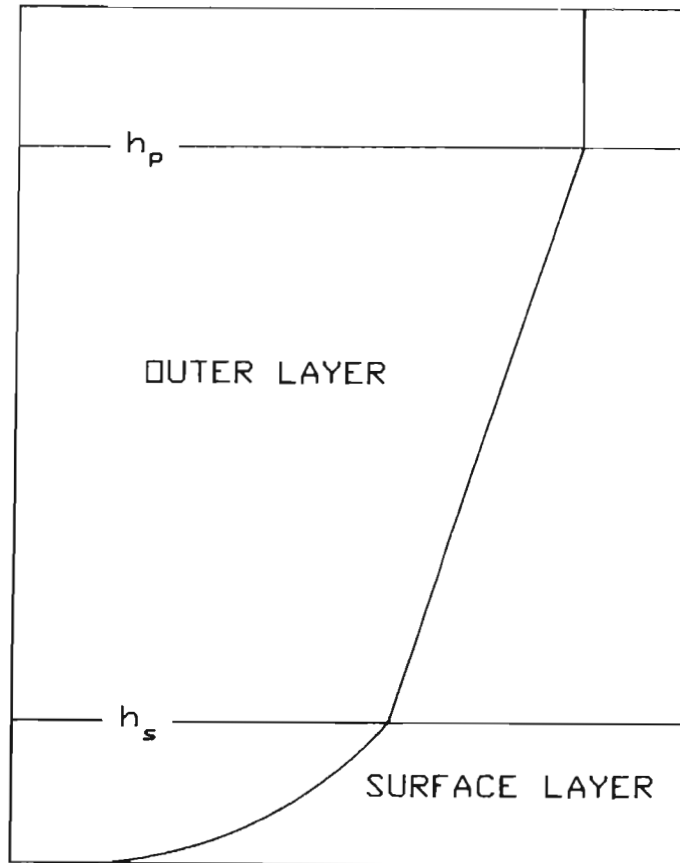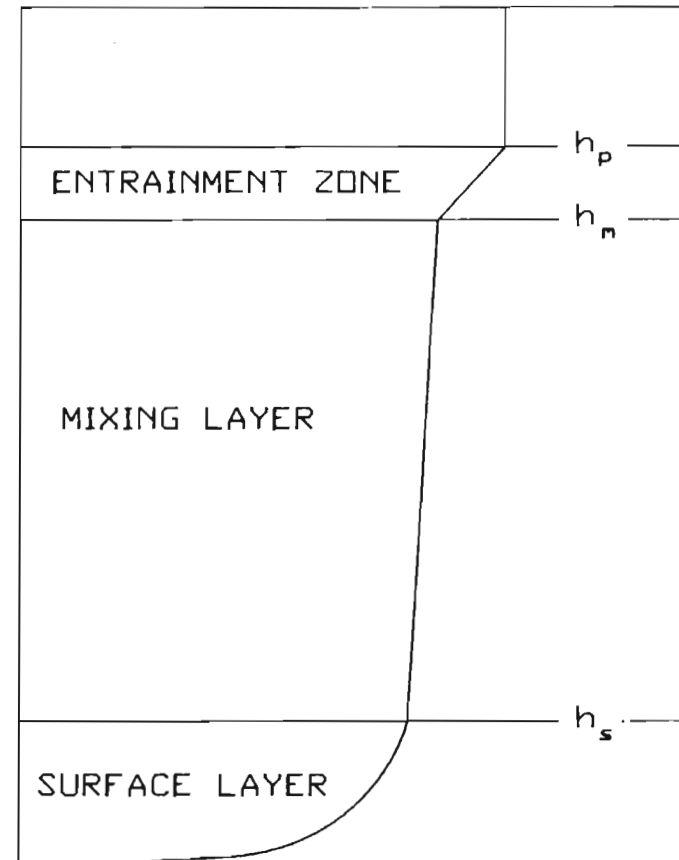
Figure 2.2(a) Wind profile for stable conditions
as suggested by Arya (1984) and
Wetzel (1982).

UNSTABLE CONDITIONS

hₚ

hₘ

ENTRAINMENT ZONE

MIXING LAYER

hₛ

SURFACE LAYER

Figure 2.2.(b) Wind profile for unstable cases as
suggested by Garratt et al (1982),
Arya (1978) and Wyngaars et al (1974).

Arya (1978) obtained a similar set of equations

$$\overline{u}_m \cong \frac{u_*}{k} \ln\left|\frac{L}{z_0}\right| + a$$

$$\overline{v}_m = 0$$

(2.40)

where the constant $a \cong 0$

The mean profiles in the entrainment layer are often assumed to be linear between the mixed layer values and the geostrophic winds at the top of the layer (Garrat *et al.* 1982). The entrainment layer extends up from h_m to h_p and generally $h_p \cong 1,3h_m$.

2.2.4. Boundary Layer Height

Various forms exist for the definition of the boundary layer height. These definitions also differ for different stability categories. So, for instance, during stable conditions, the boundary layer height is the top of the surface temperature inversion, or it is the height of the lowest discontinuity in the temperature profile, or the height to which significant cooling extends. During unstable and neutral conditions, on the other hand, it is the height at which the momentum flux has reached a minimum or the height of the low-level wind speed maximum.

Early estimates of the boundary layer height include the methods suggested by Davenport (1965) (Seinfeld 1975)), where h_p is presented as a function of z_0 (h_p proportional to log z_0); *e.g.*,

$$h_p = \begin{cases} 300m & \text{for } z_0 \cong 0,03m \\ 425m & \text{for } z_0 \cong 0,3m \\ 550m & \text{for } z_0 \cong 3m \end{cases}$$

Alternatively, the PBL height is often expressed in terms of the scaling heights $\frac{u_*}{f}$ and $\left\{\frac{u_* L}{|f|}\right\}^{\frac{1}{2}}$. It is widely accepted that the

boundary layer height during neutral stratification can be described by the diagnostic equation suggested by Zilitinkevich (1972),

$$h_p = \frac{a_1 u_*}{|f|}$$ (2.41)

where usually $a_1 = k$ (von Kármén's constant). Zilitinkevich (1972) also proposed an equation for the stable boundary layer height,

$$h_p = a_2 \left\{ \frac{u_* L}{|f|} \right\}^{\frac{1}{2}}$$ (2.42)

where $a_2 = 0,37$. Brost and Wyngaard (1978), and Garrat (1982) recommend $a_2 = 0,4$. In general, equations (2.41) and (2.42) agree well with observations. Correlation coefficients are often of the order of 0,7.

Based on the analysis of data collected during the Prairie Grass, Kansas and Minnesota experiments, Venkatram (1980) proposed an empirical relationship for stable conditions,

$$L = 1100 u_*^2$$ (2.43)

Substituting this relationship into equation (2.42) (Zilitinkevich 1972), Venkatram (1980) obtained

$$h_p = 2400 u_*^{\frac{3}{2}}$$ (2.44)

Predictions by the more complex prognostic equations are often worse than those obtained by diagnostic equations (Yu 1978). This is generally only true for stable and neutral cases. The height of the boundary layer during unstable conditions changes fairly rapidly, and prognostic equations should then be used.

Maul (1980) developed the following prognostic model to estimate the mixing layer height at time $t+\Delta t$, given the height at time t, in a

stepwise manner:

$$h_p(t+\Delta t) = \left[h_p^2(t) + \frac{2Q(1+C')\Delta t}{\Gamma \rho c_p} - \frac{2\Delta\theta(t)h_p(t)}{\Gamma} \right]^{\frac{1}{2}} + \frac{\Delta\theta(t+\Delta t)}{\Gamma}$$

$$(2.45)$$

where

$$\Delta\theta(t) = \left\{ \frac{2\Gamma C'Q\Delta t}{\rho c_p} \right\}^{\frac{1}{2}}$$

and

Γ = potential temperature lapse rate above h_p

$\quad \geq$ 0,0001 Km^{-1}

Δt = time step

C' = constant $\approx$ 0,15

Q = sensible heat flux

$\Delta\theta$ = temperature discontinuity at the top of the mixing layer

Van Dop *et al.* (1982) proposed the following approximate solution

$$h_p(t+\Delta t) = \left[\frac{Q}{\rho c_p} \right] \left[\frac{1+2C_1+2k^2\frac{C_2^2}{C_1}\frac{L}{h_p(t)})}{g\,h_p(t)\left[1-k\frac{C_2}{C_1}\frac{L}{h_p(t)}\right]} \right]^2 \Delta t + h_p(t)$$

$$(2.46)$$

where

C_1 = constant $\approx$ 0,2

C_2 = constant $\approx$ 2,5

Both these diagnostic forms assume horizontally homogeneous conditions. Consequently, large errors might occur in situations near the coast.

Other methods for determining the boundary layer height include measurements of the temperature profile, using radiosonde, or from the intensity of the vertical signal from acoustic soundings. Studies have shown that an acoustic sounding system is capable of providing information about the temperature profile and the inversion height (Wyckoff *et al.* 1973, Parry *et al.* 1975, Hall *et al.* 1975,

Goroch 1976, Prater and Colls 1981). The inversion height is that height at which the maximum return of the vertical signal occurs.

2.3. DETERMINING THE PARAMETERS z_0, d, u_*, AND L

2.3.1. Establishing the Roughness Length, z_0 and Zero-Plane Displacement Height, d

There are three acceptable methods for determining the roughness length.

(a) From tabulated values of z_0, for known surface configurations,

(b) from empirical equations, and

(c) from measurements of wind speed at various heights.

The literature is replete with tabulated values for aerodynamic roughness lengths. Figure 2.3. is an attempt to summarise most of these published values.

Cowan (1968) derived a relationship between the zero-plane displacement level, d, and vegetation height, h_*,

$$d = 0,64 \; h_* \qquad\qquad (2.47)$$

This relationship is similar to the one suggested by Thom (1971),

$$d = 0,76 \; h_* \qquad\qquad (2.48)$$

Stanhill (1969) derived a slightly different relationship using nineteen different vegetation types (mainly agricultural crops) at different stages of growth. A linear regression of the observed zero-plane displacement distance gave the expression (standard

ROUGHNESS LENGTH z_0 (m)
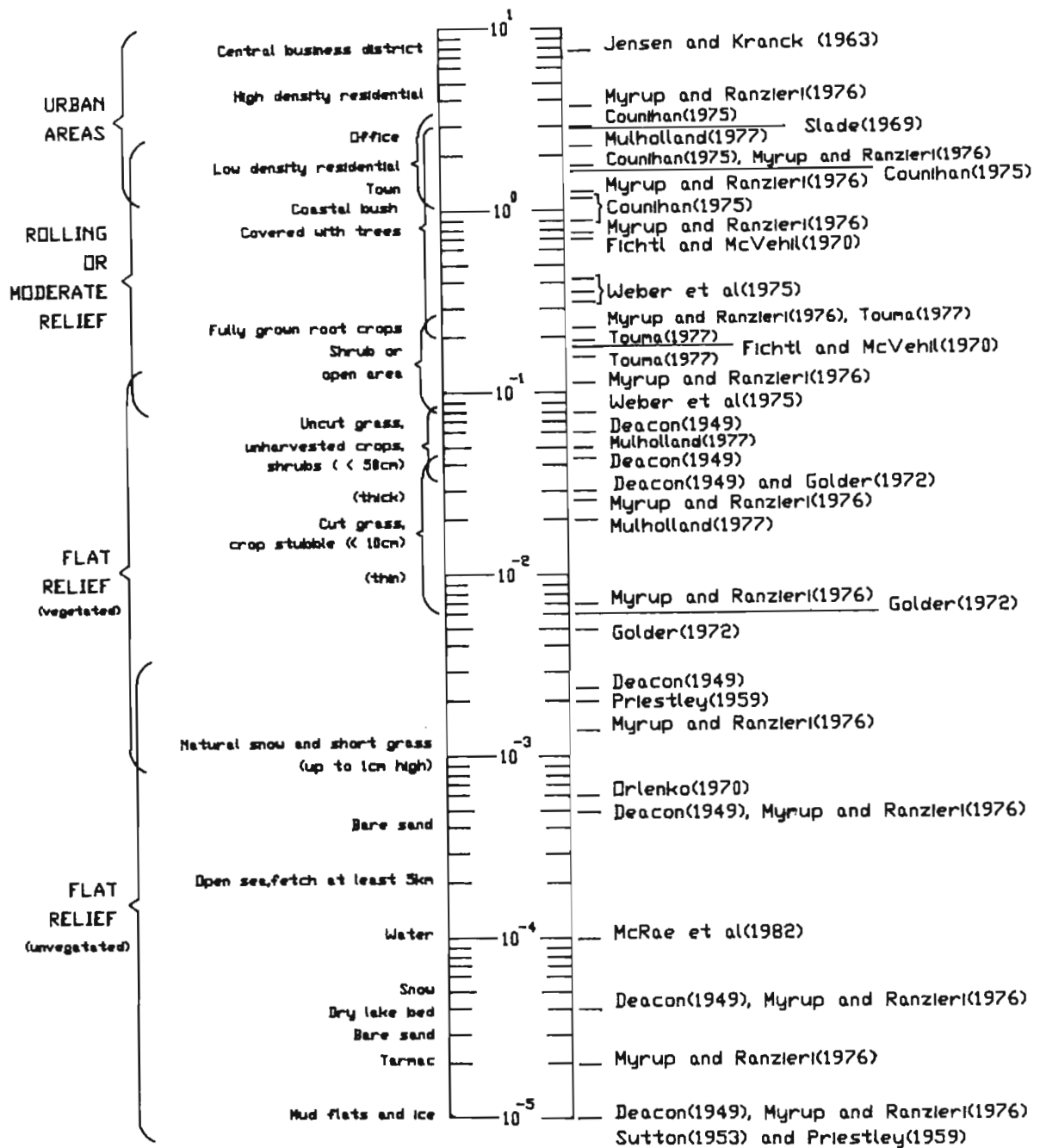
Figure 2.3. Roughness lengths for different surface configuration

categories as estimated by various researchers.

deviation of 0,06 and correlation coefficient of r = 0,97)

$$d = 0,702 \ h_*{}^{0,0799} \qquad (2.49)$$

where both d and h_* are in centimetres.

Hicks *et al.* (1975) inferred roughness lengths and zero-plane displacement data collected over a plantation of pine trees (*Pinus radiata*).

For trees with average height of 12,4m,
$$d = 0,8 \ h_*$$
$$z_0 = 0,13 \ (h_*-d)$$

For trees with average height of 13,3m,
$$d = 0,9 \ h_*$$
$$z_0 = 0,39 \ (h_*-d) \qquad (2.50)$$

According to Hicks *et al.* (1975), the second prediction is the more reliable one.

Relationships of the form

$$z_0 = a \ h_*{}^{b} \qquad (2.51)$$

are numerous; Table 2.5. summarizes some of the values for a and b that have been published.

Lettau (1969) deviated slightly from the above forms when he proposed the following expression,

$$z_0 = 0,5 \ h_* \ \frac{A_s}{A} \qquad (2.52)$$

where A_s = silhouette area (*i.e.* the area measured in the vertical-crosswind-lateral plane seen by the wind in its approach towards the obstacles)

A = total plan area

TABLE 2.5. Some well known empirical formulations for predicting the roughness length z_0 and zero-plane displacement height, d

ESTIMATION	REFERENCE

$$z_0 = 0,014 \frac{u_*^2}{g} \quad \text{(ocean surface)}$$ Charnock (1955)

$$z_0 = 0,5 \frac{A_s}{A} h_*$$ Lettau (1969)

$$z_0 = 0,5 \frac{A_0}{A} h_*$$ Davis (1970)

$$z_0 = \left(1,08 \frac{A_0}{A} - 0,08\right) h_*$$ Counihan (1971)

The general form of $z_e = a\, h_*^b$ where,

a	b		
0,0575	1,19		Kung (1963)
0,1047	1,0		Sceicz *et al.* (1969)
0,0864	1,0		Thom (1971)
0,15	1,0		Plate (1971)
0,0397	1,0		Hicks *et al.* (1975)
0,25	1,0	(rural)	Kondo & Yamazawa (1986)
0,025-0,15	1,0	(uniform forests)	

The general form of $d = m\, h_*^n$ where,

m	n	
0,64	1,0	Cowan (1968)
0,7021	0,9793	Stanhill (1969) {units in cm}
0,76	1,0	Thom (1971)
0,85	1,0	Hicks *et al.* (1975)

{all units in metres unless specified otherwise}

h_* = obstacle height u_* = friction velocity
A = total plan area g = gravitational acceleration
A_s = silhouette area A_0 = obstacle plan area

Both Kung's (1963) (Sellers 1965) and Lettau's (1969) formulae compared favourably against the results from the *Pinus resinosa* plantation experiment of Leonard and Federer (1973).

In wind tunnel tests, Counihan (1971) evaluated z_0 for various distributions of roughness elements. The experimental results were represented by

$$z_0 = (1,08 \frac{A_0}{A} - 0,08) h_*$$ (2.53)

where A_0 = plan area of the roughness elements

A = total plan area

This relationship holds only for $0,10 \leq \frac{A_0}{A} \leq 0,25$. At roughness densities below 0,10, the measured z_0 is significantly dependent on the spacing, while for densities above 0,25, a linear variation is unacceptable. This expression agrees with the one formulated by Davis (1970) :

$$z_0 = 0,5 h_* \frac{A_0}{A}$$ (2.54)

for density ratios of the order of 0,15 only.

Roughness lengths for grass and water surfaces are strong functions of wind speed. As wind speeds increase, grasses bend over, resulting in a lower value for z_0. In contrast, as the wind blows stronger over sea, z_0 increases. Charnock (1955) proposed that the roughness length for the sea be described by the relationship

$$z_0 = \frac{a}{g} u_*^2$$ (2.55)

where $a \cong 0,014$

The third method for determining roughness lengths is by means of wind profile measurements. Roughness length and zero-plane displacement were calculated by Lo (1977) using an

analytical-empirical method that draws on weighted residuals. The method requires that $\bar{u}$ and $\bar{\theta}$ be measured at various heights; then, using an iterative procedure that employs the flux-profile relationships for wind and temperature described by the KEYPS formulae (Panofsky *et al.* 1960), z_0 is solved. In a subsequent paper, Lo (1979) gives an alternative approach which is based on the least-square error method (Robinson 1962, Stearns 1970, and Nieuwstadt 1978). The velocity profile is the only input. Nieuwstadt and De Bruin (1981), in a short correspondence referring to the work of Ling (1976) and Nieuwstadt (1978), pointed out that, unless the value of z_0 is specified beforehand, a profile method does not yield an accurate estimate of the surface layer parameters. Furthermore, it was shown that the confidence interval δz_0 for z_0 may be approximated by (Nieuwstadt 1978)

$$\frac{\delta z_0}{z_0} \sim \frac{\overline{\Delta u}}{u_*}$$

where Δu is the average difference between the windspeed and the profile relation. Quite often $\overline{\Delta u}$ is of the order of u_* which shows that the estimate of z_0 is inaccurate. If, on the other hand, the velocity profile is used, u_* and θ_* are obtained with fair accuracy. Nevertheless, Lo's (1979) method is a helpful alternative when only one of the profiles is available.

A mass conservation technique that uses wind profiles for estimating the zero-plane displacement is described by Molion and Moore (1983). It was found that, in contrast to the traditional least-square methods, this technique is far less sensitive to instrumental errors.

Wieringa (1976; 1980) discussed the practical difficulties that accrue from determining roughness lengths with an extensive network of stations. A model, which relates the surface roughness length to the normalised standard deviation of wind speed, is proposed;

$$\ln(z_0) = \ln(z) - f_T E / (\langle G_T \rangle - f_T) \tag{2.56}$$

where,
$$f_T = \begin{cases} 1{,}00 & \text{sampling period of } T = 10 \text{ min} \\ 1{,}10 & \text{sampling period of } T = 1 \text{ hr} \end{cases}$$

$\langle G_T \rangle = $ gust factor $\equiv u_{max}/U_T$

where, $U_T = $ average wind speed

$u_{max} = $ maximum gust of duration t

$E \cong 1{,}42 + 0{,}30\ln([1000/U_T t] - 4)$

$z = $ height of measurement

2.3.2. Techniques for Calculating the Friction Velocity, u_*, Temperature Scale, θ_*, and the Monin-Obukhov Length, L

Just how accurately flux profile parameters can be calculated depends on the number of meteorological measurements taken at the time. Hence, a profile method (*i.e.*, wind and temperature measurements at different heights) will give better results than a method requiring one wind measurement, a temperature measurement, and cloud cover.

2.3.2.1. Given : Wind Velocity at One Height, Cloud Cover, and Roughness Length

A now widely used method for determining u_*, θ_*, and L from the Pasquill stability classification scheme (Pasquill 1962) is attributed to the work of Golder (1972). Golder (1972) proposed the relationships between the Pasquill stability classes, the Monin-Obukhov length, and the surface roughness. Wind speed at low levels (within the surface layer) and cloud cover are used to establish the stability class (Table 2.6.). Shir and Shieh (1974) represented the discrete function of this scheme (stability classes A to B) by stability classes -3, -2, -1, 0, 1, 2, and interpolated with respect to wind speed to get a continuous function (Table 2.6.). Golder's (1972) data were then approximated by the expression

$$\frac{1}{L} = \text{sign}(s) \left[d \ln(1,2 + \frac{10}{z_0}) \right] 10^{f(s)} \qquad (2.57)$$

where $\qquad f(s) = \dfrac{-a}{(1 + b|s|^c)}$

and $\qquad\qquad s$ = stability class as determined in Table 2.6

$\qquad\qquad\qquad a$ = constant = 4

$\qquad\qquad\qquad b$ = constant = 1,3

$\qquad\qquad\qquad c$ = constant = 0,85

$\qquad\qquad\qquad d$ = constant = 0,216586

Goodin and McRae (1980) represented Golder's (1972) nomogram by straight-line approximations using Pasquill's stability classification scheme :

$$\frac{1}{L} = a + b \log_{10}(z_0) \qquad (2.58)$$

where the coefficients a and b are described in Table 2.7.

Various other methods exist for classifying the atmosphere into different Pasquill classes (Sedefian and Bennett 1980). Table 2.8. is a description of a method using the wind direction (azimuth) standard deviation (σ_θ) measurements at 10m and 50m heights (U.S. Nuclear Regulatory Commission 1974).

The azimuth standard deviation decreases with height (Slade 1968). Sedefian and Bennett (1980) introduced the correction formula

$$\sigma_\theta(z_2) = \sigma_\theta(z_1) \left\{ \frac{z_2}{z_1} \right\}^{P_\theta} \qquad (2.59)$$

where $\qquad\qquad z_1$ = 10m

$\qquad\qquad\qquad z_2$ = 50m

$\qquad\qquad\qquad P_\theta$ = -0,06; -0,17; -0,23; -0,38; -0,53 for classes
$\qquad\qquad\qquad\qquad$ A to F, respectively.

TABLE 2.6. Estimation of the Pasquill stability classes and the corresponding values for the Shir and Shieh parameter s

Mean wind speed (m/s)	DAYTIME Incoming solar radiation					
	Strong		Moderate		Weak	
	Pasquill	s	Pasquill	s	Pasquill	s
< 2	A	−3,5~−3,0	A ~ B	−3,0~−2,2	B	−2,5~−2,0
2 ~ 3	A ~ B	−3,0~−2,2	B	−2,2~−2,0	C	−2,0~−1,0
3 ~ 5	B	−2,2~−1,5	B ~ C	−2,0~−1,0	C	−1,0~−0,5
5 ~ 6	C	−1,5~−1,0	C ~ D	−1,0~−0,3	D	−0,5~−0,2
6 ~ 8	C	−1,0~−0,3	D	−0,3~−0,1	D	−0,2~ 0,0
8 <	C	−0,3	D	−0,1	D	0,0

Mean wind speed (m/s)	TRANSITION PERIOD			
	Daytime to nighttime		Nighttime to daytime	
	Pasquill	s	Pasquill	s
< 2	C	−1,5~−0,5	E ~ F	0,5~1,5
2 ~ 3	C	−1,0~−0,3	E	0,5~1,0
3 ~ 5	C ~ D	−1,0~−0,3	D ~ E	0,3~0,5
5 ~ 6	C ~ D	−0,4~−0,2	D ~ E	0,2~0,4
6 ~ 8	C ~ D	−0,3~−0,1	D ~ E	0,1~0,2
8 <	D	0,0	D	0,0

Mean wind speed (m/s)	NIGHTTIME			
	Cloud fraction > 5/10		Cloud fraction ≤ 4/10	
	Pasquill	s	Pasquill	s
< 2		1,5		2,5
2 ~ 3	E	1,5~0,6	F	2,5~1,6
3 ~ 5	D	0,6~0,3	E	1,6~0,5
5 ~ 6	D	0,3~0,1	D	0,5~0,3
6 ~ 8	D	0,1~0,0	D	0,3~0,1
8 <	D	0,0	D	0,1

TABLE 2.7. Coefficients for the straight line approximations of Goodin and McRae (1980), equation (2.58)

Pasquill classification	Class	Coefficients a	b
Extremely unstable	A	−0,096	0,029
Moderately unstable	B	−0,037	0,029
Slightly unstable	C	−0,002	0,018
Neutral	D	0	0
Slightly stable	E	0,004	−0,018
Moderately stable	F	0,035	−0,036

TABLE 2.8. Determining the Pasquill stability classes using azimuth (wind direction) standard deviation

Pasquill classification	Class	Azimuth standard deviation at heights 10 and 50m (deg)
Extremely unstable	A	$22,5 < \sigma_\theta$
Moderately unstable	B	$17,5 < \sigma_\theta \leq 22,5$
Slightly unstable	C	$12,5 < \sigma_\theta \leq 17,5$
Neutral	D	$7,5 < \sigma_\theta \leq 12,5$
Slightly stable	E	$3,75 < \sigma_\theta \leq 7,5$
Moderately stable	F	$2,0 < \sigma_\theta \leq 3,75$
Extremely stable	G	$\sigma_\theta \leq 2,0$

2.3.2.2. The Energy Budget Method

Various attempts have been made to estimate the sensible heat flux H. Maul (1980) estimated H for daylight hours, with the following equation,

$$H = l_1 R + H_0 \qquad (2.60)$$

where
$$l_1 = \text{land use constant} \approx 0,3$$
$$R = \text{incoming solar radiation}$$
$$= 950 \, r_c \sin\nu$$
with
$$r_c = \text{radiation reduction factor due to the presence of clouds (Appendix B.1)}$$
$$\nu = \text{solar elevation angle (Appendix A)}$$
$$H_0 = \text{the heat flux in the absence of incoming solar radiation}$$
$$= 2,4N - 25,5$$
where
$$N = \text{opaque cloud cover fraction}$$

De Bruin and Holtslag (1982) derived an expression that includes the surface temperature for determining the sensible heat flux;

$$H = \frac{(1 - l_2)S + \gamma}{S + \gamma}(H^* - G) - l_3 \qquad (2.61)$$

where γ and S are empirical temperature dependent functions, l_2 and l_3 are constants that dependens on terrain type, and G is the soil heat flux (= $0,1H^*$). H^* is the net radiation; it is a function of temperature, cloud cover, and solar elevation. These parameters are discussed in more detail in Appendix B.2.

Venkatram (1980) observed that during stable conditions H can be approximated by

$$H = -93u_* \qquad (2.62)$$

Once the sensible heat flux is known, u_* and L can be calculated iteratively using the universal functions for wind and temperature

profiles, together with the definition of L (equation (2.4)).

2.3.2.3. Using the Richardson Number to Estimate Flux Parameters

The Ricardson number is defined by equation (2.15) and is approximated by (Paulson 1970)

$$Ri = \frac{g}{\theta_1} \frac{\dfrac{\Delta\theta \, \ln(z_{\theta_2}/z_{\theta_1})}{\sqrt{z_{\theta_1} z_{\theta_2}}}}{\left[\dfrac{\Delta u \, \ln(z_{u_2}/z_{u_1})}{\sqrt{z_{u_1} z_{u_2}}}\right]^2} \qquad (2.63)$$

where
$$\Delta\theta = \theta_2 - \theta_1$$
$$\Delta u = u_2 - u_1$$

and θ_1, θ_2 = mean potential temperature at heights $z_{\theta 1}$ and $z_{\theta 2}$, respectively

u_1, u_2 = mean wind speed at heights z_{u1} and z_{u2}, respectively

Following Businger *et al.* (1971) the Ricardson number is related to the Monin–Obukhov length by

$$\frac{\bar{z}}{L} = \frac{\phi_m^2}{\phi_h} Ri \qquad (2.64)$$

where $\bar{z} = \sqrt{z_1 z_2}$ (*i.e.*, the geometric mean height of z_1 and z_2).

L is then obtained by iteration of equation (2.64). Berkowicz and Prahm (1982) proved that for unstable conditions, the iteration procedure is always convergent, whereas for stable conditions, non-trivial solutions exist only for

$$Ri < 0,215$$

when the Businger *et al.*(1971) forms for ϕ were used. Other forms

for ϕ may result in different criteria.

By basing his work on the results of Businger *et al.* (1971), Binkowski (1975) obtained the approximations

$$\frac{z}{L} = \frac{1,35Ri}{1 - 4,7Ri} \tag{2.65}$$

for stable conditions, with an error less than 2 per cent in the range $0 \leq Ri \leq 0,19$, and

$$\frac{z}{L} = 1,35Ri\left[\frac{1 - 9Ri}{1 - 15Ri}\right]^{\frac{1}{2}} \tag{2.66}$$

for unstable conditions, with an error less than 1 per cent for the entire unstable range.

The *bulk* Ricardson number is defined as

$$Ri_B = \frac{g}{\theta} \frac{\Delta\theta}{u^2} \frac{z^2}{\Delta z} \tag{2.67a}$$

which, when the wind speed and the top temperature are measured at the same height z_2, becomes

$$Ri_B = \frac{g}{\theta_2} \frac{z_2}{u_2{}^2} \Delta\theta \tag{2.67b}$$

The relationship between the Monin-Obukhov length and Ri_B is

$$\frac{z}{L} = \frac{\phi^2{}_m}{\phi_h} Ri_B \tag{2.68}$$

Joynt and Blackman (1976) suggested a useful alternative to solving equation (2.68). Using the data of Lumley and Panofsky (1964), the following approximations were obtained :

$$\frac{z}{L} = \frac{Ri_B}{1 - 5,8Ri_B} \tag{2.69}$$

for stable conditions, and

$$\frac{\overline{z}}{L} = \frac{Ri_B}{(1 - 18Ri_B)^{0,25}} \qquad (2.70)$$

for unstable conditions.

The solution of L follows by substituting the appropriate forms for Ψ_m and Ψ_h into equation (2.68), and solving by iteration. For unstable conditions, Schultz (1979) suggested the following approximated forms:

$$\Psi_m = \ln(z/z_0) - X \qquad \underline{\text{Error for } \frac{z}{z_0} = 500 \text{ to } 5}$$

$$X = -0,472\xi^2 - 1,64\xi \qquad\qquad 3 \text{ to } 10\%$$

$$X = -0,352\xi^3 - 1,43\xi^2 - 2,22\xi \qquad\qquad 1 \text{ to } 5\%$$

$$X = -0,312\xi^4 - 1,54\xi^3 - 2,81\xi^2 - 2,69\xi \qquad 0,5 \text{ to } 3\%$$

$$(2.71)$$

Barker and Baxter (1975) discussed how the bulk Richardson number can be related to the Monin-Obukhov length using the integral forms of Paulson (1970). The derived expressions are :

$$\frac{z_2}{L} = \frac{kC_N\left[Ri_B - \left\{\frac{\gamma_1}{2\alpha}\right\} + \left\{\frac{(1-\gamma_1)}{\alpha}Ri_B + \frac{\gamma_1^2}{4\alpha}\right\}^{\frac{1}{2}}\right]}{1 - \alpha Ri_B} \qquad (2.72)$$

where $\qquad C_N = $ drag coefficient for neutral conditions

$$= \frac{1}{k}\ln(z_2/z_0)$$

for stable conditions, and the approximation

$$\frac{z_2}{L} = Ri_B \, f(C_N) \qquad (2.73)$$

for unstable conditions, where

$$f(C_N) = 0,471C_N - 1,045 \quad \text{for } \frac{z_2}{L} \leq -0,05 \text{ and } C_N \geq 10$$

43

The error in calculating u_* by this approximation is less than 2 per cent, and decreases with higher values of C_N. For the interval $-0,05 < \frac{z_i}{L} < 0$, equation (2.72) may be used.

In a technical note, Irwin and Binkowski (1981) showed how the inherent restrictions in the expressions of Barker and Baxter (1975) can be removed when the exact integral forms of Benoit (1977) is used.

2.3.2.4. Flux Parameters from Wind and Temperature Profiles

By fitting measured wind and temperature profiles to the empirical profile relationships discussed in the previous sections, an estimate is obtained for the surface layer flux parameters u_*, and L. Klug (1967) found the surface layer parameters from a least-square fit of only the wind profile to the KEYPS equation for unstable conditions with a pre-specified value of z_0. Lo (1978) developed a similar method for determing the flux parameters in the absence of temperature profiles. His predicted values of u_* and L agree well with the values obtained from measurement. Details of this method are discussed in Appendix C. In a subsequent paper, Lo (1979) extended this idea and proposed a method whereby the parameters are evaluated without, beforehand, specifying a roughness length. The results were reasonably accurate when tested.

Paulson (1970) used both the wind and temperature profiles to estimate the surface-layer parameters. The friction velocity is derived primarily from the wind profile; and the temperature scale is derived primarily from the temperature profile. Nieuwstadt (1978) presented a least-square method which uses both profiles simultaneously to estimate these parameters. He found that, by incorporating the roughness length into the procedure beforehand, the quality of the estimates is improved.

2.4. AIR MOVEMENTS OVER COMPLEX TERRAIN

2.4.1. Theoretical Background

In recent years, the modelling of mesoscale flows over complex terrain has received considerable attention. Three principal avenues have been pursued :

- Diagnostic models (Anderson 1971, Dickerson 1978, Sherman 1978, Yocke *et al.* 1978, Endlich *et al.* 1982) generally consider mass conservation or other simplifications of the equations of motion while optimising towards a minimum error between the computed and observed wind values. Interpolation methods are used to interpolate sparse measurements to the horizontal grid locations in order to provide the initial guess for the wind field (Goodin *et al.* 1979). Several objective analyses have been proposed (Endlich 1967, Sasaki 1970) to minimise anomalous divergence resulting from the interpolation methods.

- Prognostic models predict wind flow based on a mathematical representation of relevant physical processes such as the air flow over hills (Hunt and Richards 1984), land and sea breezes (Estoque 1961, Neumann and Mahrer 1971), or the development of mountain and valley winds (Manins and Sawford 1979, Rao and Snodgrass 1981, Yamada 1981). The two main computational methods are the *hydrostatic model* of Mahrer and Pielke (1975) and the method by which the full dynamical equations are solved.

- A compromise between the hydrodynamic model and objective wind model, such as the that proposed by Lee and Kau (1984), forms the third group.

The present review is restricted to diagnostic models only. In an analysis by Anderson (1971) of mesocale influences on ground level wind fields, it was indicated that the topography and the thermal cells associated with mesoscale ground temperature anomalies (*e.g.*,

urban heat islands and land-water contrasts) were the major causes of horizontal trajectory perturbations on the scales appropriate for air pollution studies.

Anderson (1971) proposed a simple two-dimensional surface wind field model which included the perturbations in the wind field due to topographic relief and surface temperature anomalies. His adjustment procedure involves the solution of Poisson's equation

$$\nabla^2\phi \;=\; \frac{\partial^2\phi}{\partial x^2} + \frac{\partial^2\phi}{\partial y^2} \;=\; \mathcal{P}(x,y) \tag{2.74}$$

where the *potential function*, ϕ, is defined in $u = \frac{\partial\phi}{\partial x}$ and $v = \frac{\partial\phi}{\partial y}$. For this application, the potential function is the sum of the *velocity potentials* due to topography, lake, heat island, and mean wind, respectively, *i.e.*,

$$\phi \;=\; \phi_{\text{topography}} + \phi_{\text{lake}} + \phi_{\text{heat island}} + \phi_{\text{mean wind}}$$

and $\mathcal{P}(x,y)$ is the *forcing function* based on the layer thickness, terrain gradients, and temperature anomolies, *i.e.*,

$$\mathcal{P}(x,y) \;=\; \frac{1}{h}\, U\cdot\nabla h_t + \frac{A(T_g - \overline{T})}{h} \tag{2.75}$$

where
$$h \;=\; \text{upper bound of the perturbed air}$$
$$U \;=\; \text{unperturbed mean velocity vector}$$
$$h_t \;=\; \text{local surface altitude}$$
$$A \;=\; \text{experimentally determined proportionality constant}$$
$$T_g \;=\; \text{ground temperature}$$
$$\overline{T} \;=\; \text{spatial mean ground temperature}$$

The net wind field is calculated by

$$V \;=\; \nabla\phi \; U \;=\; (i\frac{\partial u}{\partial x} + j\frac{\partial v}{\partial y})U \tag{2.76}$$

where V is the total perturbed velocity vector in the horizontal plane, averaged over the depth $h - h_t$, and U is the mean unperturbed

wind speed.

In order to accommodate topography, Anderson (1971) made the following assumptions :

(a) $(h - h_t)$ $\cong$ h
(b) $w(h)$ $\cong$ 0, (vertical wind speed at height h),

in other words, topography effect is not felt above the height h, and,

(c) $w(h_t)$ $\cong$ $U.\triangledown h_t$

Scholtz and Brouckaert (1978) argued that the above assumptions were applicable only to unstable atmospheric conditions $(h_t \ll h)$; they modified Anderson's (1971) method for stable conditions. In their approach, the continuity equation was averaged through the surface layer thickness; the following assumption was then made :

$$w(h_s) - w(h_t) = U.\triangledown(h_s - h_t)$$

It was therefore assumed that the stable surface air is constrained to flow between the topography and surface layer height, h_s. The resulting forcing function is then given by

$$\mathbf{F}(x,y) = \left[\frac{1}{h_s - h_t}\right] U.\triangledown(h_t - h_s) + \frac{A(T_g - \overline{T})}{h_i} \qquad (2.77)$$

where h_i is the temperature inversion height.

Determining appropriate boundary conditions for solving Poisson's equation make it difficult to apply these methods. These difficulties are discussed in Anderson (1971) and Scholtz and Brouckaert (1978).

The wind field in three dimensions has to satisfy the continuity equation. Mass-consistent wind field models, such as those proposed by Sherman (1978) and Goodin et al. (1980), solve the continuity equation. For an incompressible fluid, the continuity equation in

three dimensions is

$$\frac{\partial(u\Delta h)}{\partial x} + \frac{\partial(v\Delta h)}{\partial y} + \frac{\partial(w\Delta h)}{\partial z} = 0 \qquad (2.78)$$

where
$$\Delta h = h_m(x,y,t) - h_t(x,y)$$
$$h_m(x,y,t) = \text{mixing depth (boundary layer height)}$$
$$u, v, w = \text{velocity components in the x, y, z}$$
$$\text{directions}$$

Introducing terrain-following coordinates (Goodin *et al.* 1980), the continuity equation is rewritten as

$$\frac{\partial(u\Delta h)}{\partial x} + \frac{\partial(v\Delta h)}{\partial y} + \frac{\partial W}{\partial \rho} = 0 \qquad (2.79)$$

where W, the vertical velocity in the new coordinates, is given by

$$W = w - u\left[\frac{\partial h_t}{\partial x} + \rho\frac{\partial \Delta h}{\partial x}\right] - v\left[\frac{\partial h_t}{\partial y} + \rho\frac{\partial \Delta h}{\partial y}\right] - \rho\frac{\partial \Delta h}{\partial y}$$

and
$$\rho = \frac{z - h_t(x,y)}{h_m(x,y,t) - h_t(x,y)}$$

Solving either equation (2.78) or (2.79), then, gives a mass-consistent wind field.

2.4.2. Numerical Methods

2.4.2.1. Interpolation Schemes

Numerical computations involving data from randomly spaced meteorological stations may be conveniently done by applying an objective interpolation scheme to obtain meteorological parameters on a regularly spaced grid. The *inverse square weighting* method (Wendell 1972) is the most widely used technique for interpolating

velocity components;

$$\bar{u}_{ij} = \frac{\displaystyle\sum_{k=1}^{N} \frac{u_k}{r_{k,ij}^2}}{\displaystyle\sum_{k=1}^{N} \frac{1}{r_{k,ij}^2}} \qquad (2.80)$$

The formula takes the same form for the v-component. Here u_k is the x-component of the wind at station k and at a distance $r_{k,ij}$ away from grid point (i,j). N is the number of stations. This type of interpolation technique belongs to the so-called *weighted interpolation methods* where the weighting function $W(r)$ in this instance, is

$$W(r) = \frac{1}{r^2} \qquad (2.81)$$

Equation (2.80) can in general be rewritten in the form

$$\bar{u}_{ij} = \frac{\displaystyle\sum_{k=1}^{N} u_k W(r_{k,ij})}{\displaystyle\sum_{k=1}^{N} W(r_{k,ij})} \qquad (2.82)$$

Goodin *et al.* (1979) summarised the most frequently used weighting functions. A slightly different form to the one used by Wendell (1972) was proposed by Cressman (1959). Cressman (1959) defined the *radius of influence*, R, as that distance at which the following weighting factor becomes zero;

$$W(r) = \frac{R^2 - r^2}{R^2 + r^2} \qquad (2.83)$$

For a two-dimensional domain of area A with N stations randomly distributed over the plane, the average separation between stations is given by $d = \sqrt{A/N}$. Stephens and Stitt (1970) have shown that the optimum radius R for large signal-to-noise ratios is R = 1,6d.

An interpolation function frequently cited in the literature is the Gaussian weighting scheme that was applied by MacCracken and Sauter (1975). This scheme eliminates the complete dominance of a measuring station near a grid point;

$$W(r) = \exp(-0,1r^2) \qquad (2.84)$$

Draxler (1979) introduced a modification for any directional influence at a grid point:

$$W(r) = \frac{\alpha_s}{r^2} \qquad (2.85)$$

where α_s = alignment weighting factor

= $1 - 0,5|\sin\phi_s|$

and ϕ_s = the angle between the observed wind direction and the line from the surface station to the grid point (i,j).

Goodin *et al.* (1979) reviews two additional interpolation techniques; these are the *least-squares polynomial interpolation technique* (Gilchrist and Cressman 1954) and the *optimum interpolation technique* (Gandin 1963). These methods are complex to implement and most often not more accurate than the more simplistic approaches discussed above.

2.4.2.2. Divergence Reduction Techniques

A wind field interpolated from a limited supply of observed data often implies a specific field of divergence, in other words, a violation of the conservation of mass. To minimise this divergence, several objective analyses have been proposed. The three most important are

(a) the variational formulation of Sasaki (1970), in which the residual error in the continuity equation is minimised. This method has been used successfully by Dickerson (1978)

50

and Sherman (1978);

(b) the fixed vorticity method, where divergence is minimised, but the original vorticity is kept the same, and,

(c) the fixed station method, where measured winds are held fixed while winds at adjacent points are adjusted in order to minimise divergence.

These methods are briefly discussed below.

2.4.2.2.1. Variational formulation (Sasaki 1970)

Consider the vertically integrated continuity equation

$$\frac{\partial h}{\partial t} + \frac{\partial(uh)}{\partial x} + \frac{\partial(vh)}{\partial y} = 0 \qquad (2.86)$$

where h is the mixing depth or boundary layer height. This equation holds only for a mass-conservative wind field. If the initial wind field, obtained from observation, is denoted by the subscripts "$_0$", then the continuity equation is

$$\frac{\partial h_0}{\partial t} + \frac{\partial(u_0 h_0)}{\partial x} + \frac{\partial(v_0 h_0)}{\partial y} = \epsilon \qquad (2.87)$$

where ϵ is the residual error. The residual error has to be minimized. Sasaki's (1970) method, which estimates the adjusted wind field with equation (2.86) as the strong constraint, is based on minimisation of the functional, I:

$$I(u,v,\lambda) = \int\int_S [\alpha_1{}^2(u-u_0)^2 + \alpha_2{}^2(v-v_0)^2$$

$$+ \lambda\left[\frac{\partial h}{\partial t} + \frac{\partial(uh)}{\partial x} + \frac{\partial(vh)}{\partial y} - \epsilon\right]]dS \qquad (2.88)$$

where λ is the Lagrange multiplier and α_1 and α_2 are weighting parameters related to the scales of the standard deviation of the respective velocity components. Sherman (1978) suggested that for real wind fields $\alpha_1/\alpha_2 = 0,01$. Under the constraint that $\epsilon = 0$,

51

Sasaki (1970) found that for the condition $\lambda = 0$ at the boundary

$$\nabla^2 \lambda = -\left[\frac{\partial h_0}{\partial t} + \frac{\partial(u_0 h_0)}{\partial x} + \frac{\partial(v_0 h_0)}{\partial y}\right] \tag{2.89}$$

Once λ is calculated in equation (2.89), the adjusted values of uh and vh are obtained from

$$uh = u_0 h_0 + \frac{\partial \lambda}{\partial x}$$

$$\tag{2.90}$$

$$vh = v_0 h_0 + \frac{\partial \lambda}{\partial y}$$

2.4.2.2.2. Fixed vorticity technique (Endlich 1967)

Endlich (1967) gives an iterative method for constructing the wind field on a regular net from corresponding arrays of divergence and vorticity values. The desired wind fields are obtained by a point iterative method, analogous to the well-known Gauss-Seidel method for solving elliptical partial differential equations, applied to the two simultaneous linear partial differential equations

$$\frac{\partial u}{\partial x} + \frac{\partial v}{\partial y} = D(x,y) \tag{2.91a}$$

$$\frac{\partial v}{\partial x} - \frac{\partial u}{\partial y} = \xi(x,y) \tag{2.91b}$$

where $D(x,y)$ is the divergence, and $\xi(x,y)$ the relative vorticity. The solution begins with a guess of the values u and v. Improved values are then obtained by iteration to converge on $D(x,y)$ and $\xi(x,y)$.

Writing the above two equations in finite forms with columns denoted by i and rows by j, Endlich (1967) proceeded to show that the new adjusted wind components are given by

52

$$u''_{ND}(i,j-1) = u'_{ND}(i,j-1) - u_{RR}(i,j)$$
$$u''_{ND}(i,j+1) = u'_{ND}(i,j+1) + u_{RR}(i,j)$$
$$v''_{ND}(i+1,j) = v'_{ND}(i+1,j) + v_{RR}(i,j)$$
$$v''_{ND}(i-1,j) = v'_{ND}(i-1,j) - v_{RR}(i,j) \tag{2.92}$$

where

$$u'_{ND}(i+1,j) = u_0(i+1,j) + u_{RD}(i,j)$$
$$u'_{ND}(i-1,j) = u_0(i-1,j) - u_{RD}(i,j)$$
$$v'_{ND}(i,j+1) = v_0(i,j+1) - v_{RD}(i,j)$$
$$v'_{ND}(i,j-1) = v_0(i,j-1) + v_{RD}(i,j)$$

This reduces the divergence $D(i,j)$ at grid point (i,j) to zero with

$$u_{RD}(i,j) = -\frac{1}{2}(\Delta x)\, D(i,j)$$
$$v_{RD}(i,j) = -\frac{1}{2}(\Delta y)\, D(i,j) \tag{2.93}$$

These changes alter the vorticity to new values $\xi_t(i,j)$, and in order to restore the original vorticity at point (i,j), the components u_{RR} and v_{RR} are applied to the neighbouring points, where

$$u_{RR}(i,j) = -\frac{1}{2}(\Delta y)\left[\xi_t(i,j) - \xi(i,j)\right]$$
$$v_{RR}(i,j) = -\frac{1}{2}(\Delta x)\left[\xi_t(i,j) - \xi(i,j)\right] \tag{2.94}$$

Stephens (1967) examined the Endlich method through discrete Fourier transforms of the error fields and showed that this method always converges.

2.4.2.2.3. Fixed station velocity (Liu and Goodin 1976)

The fixed station velocity method differs slightly from the fixed vorticity method; here the wind components at the grid point closest to the observed wind, are held fixed. The divergence, $D(x,y)$, of the wind field is

$$\frac{\partial(uh)}{\partial x} + \frac{\partial(vh)}{\partial y} = D(x,y)) \tag{2.95}$$

53

Applying a finite difference approximation to this equation in a four-point grid system, the divergence is expressed by

$$D^n(i,j) = [u^n(i+1,j)h(i+1,j) - u^n(i-1,j)h(i-1,j)]/2\Delta x$$
$$+ [v^n(i,j+1)h(i,j+1) - v^n(i,j-1)h(i,j-1)]/2\Delta y$$

(2.96)

(Liu and Goodin (1976) also considered the divergence in an eight-point grid system.)

Velocities at the $(n+1)^{th}$ iteration (Endlich 1967) are obtained from the following set of equations,

$$u^{n+1}(i+1,j) = u^n(i+1,j) + f(i+1,j)\widetilde{u}^n(i,j)h(i+1,j)$$
$$u^{n+1}(i-1,j) = u^n(i-1,j) - f(i-1,j)\widetilde{u}^n(i,j)h(i-1,j)$$
$$v^{n+1}(i,j+1) = v^n(i,j+1) + f(i,j+1)\widetilde{v}^n(i,j)h(i,j+1)$$
$$v^{n+1}(i,j-1) = v^n(i,j-1) - f(i,j-1)\widetilde{v}^n(i,j)h(i,j-1)$$

(2.97)

where

$$\widetilde{u}^n(i,j) = -D^n(i,j)\Delta x/[f(i+1,j) + f(i-1,j)]$$
$$\widetilde{v}^n(i,j) = -D^n(i,j)\Delta y/[f(i,j+1) + f(i,j-1)]$$

The parameter $f(i,j)$, which defines whether or not the grid point (i,j) is the location of a wind station, assumes the following values :

$$f(i,j) = 0 \quad \text{at a station grid point}$$
$$= 1 \quad \text{at a non-station grid point} \quad (2.98)$$

Rather than keeping wind measurements fixed, Liu and Goodin (1976) suggested that a more realistic approach would be to allow wind-station velocities to vary within prescribed limits, in order to

account for uncertainties in the wind measurements.

The methods derived by Endlich (1967) and Liu and Goodin (1976) are satisfactory for the objective reduction of wind divergence. Enlich's method yields the smoother wind field of the two. The strong constraint method of Sasaki (1970) fails to reduce the divergence to the extent that the other methods do. Sasaki's (1970) method also fails to hold the station wind vectors reasonably constant, whereas the fixed station velocity method allows wind vectors at measuring points to be altered.

2.4.2.3 Constructing Three-Dimensional Wind Fields

Goodin *et al.* (1980) proposed a method of constructing a three-dimensional urban-scale objective wind model. The algorithm employs terrain-following coordinates and variable vertical grid spacing. Initial estimates of the velocity field are developed by interpolating surface and upper level wind measurements. Anderson's (1971) terrain adjustment method (Section 2.4.1) is used to establish the horizontal components of the surface layer wind field. The technique of Liu and Goodin (1976) (Section 2.4.2.2) is applied to remove divergence which exists within each layer. Using the terrain-following coordinate system and equation (2.79), the divergence, given by

$$\frac{\partial(u\Delta h)}{\partial x} + \frac{\partial(v\Delta h)}{\partial y} + \frac{\partial W}{\partial \rho} = D(x,y) \tag{2.99}$$

$D(x,y)$ is minimized. Vertical velocities, W, are developed from successive solutions of the continuity equation. This is followed by an iterative procedure which reduces the anomalous divergence of the complete field. The reduction of the divergence follows after an initial smoothing using an empirically-determined number of smoothing passes. These smoothing passes are based on the local atmospheric stability. Goodin *et al.* (1980) assumed a simple five-point filter

55

for smoothing, *viz.*,

$$u_{i,j}^{n+1} = 0,20(u_{i,j}^{n}+u_{i+1,j}^{n}+u_{i-1,j}^{n}+u_{i,j+1}^{n}+u_{i,j-1}^{n})(1-a_k)$$
$$+a_k u_{i,j}^{n} \qquad\qquad (2.100)$$

where a_k is a parameter which keeps the measured velocity at station k fixed ($a_k = 1$), or lets the velocity retain only some of its original influence ($a_k < 1$). Interpolated wind fields are smoothed 5, 10 and 20 times corresponding approximately to the Pasquill stability classes B, D and E.

A comparison of the Goodin *et al.* (1980) model with the models of Sherman (1978) [MATHEW] and Dickerson (1978) [MASCON], which are based on the Sasaki's (1970) variational method, shows that in the former model boundary values need not be specified *a priori*, and in contrast to MATHEW and MASCON, boundary values are allowed to adjust in response to interior flow.

CHAPTER 3

3. MODELS FOR DESCRIBING THE DISPERSION OF GASES IN THE ATMOSPHERE

Most models that depict the dispersion of air pollutants in the atmosphere can be classed into one of three main groups :

    Eulerian grid models
    Lagrangian trajectory models
    Statistical trajectory models

The Eulerian grid models express the geographical location in a two- or three-dimensional array of grid cells. In each grid cell, the advection, diffusion, transformation (chemical decay), and the removal (deposition, washout in rain) of pollutants are simulated by a set of mathematical expressions. Few analytical solutions are available, and then these few are generally derived for conditions which are not always realised. Instead some sort of finite-differencing technique is used in the numerical solution of these equations. A novel solution introduces a series of one-dimensional, time variant, differential equations describing the moments of the probability density function (Saffman 1962) (Section 3.1.1.2.). The complex three-dimensional, time variant, partial differential advection-diffusion equation need not be solved in this approach .

The deterministic approach to turbulence, via the Navier–Stokes equations (Section 2.2.1) of motion, leads to the classical closure problem. A similar problem arises when diffusion, in terms of the advection–diffusion model, is treated. To circumvent this problem, suggested semi–empirical closure approximations have been summarised by Monin and Yaglom (1965). First–order closure is based on the analogy between turbulence and molecular diffusion, and it leads to an eddy diffusivity (Section 3.1.1.1.). Attempts have also been made to include higher–moment statistical interactions of turbulence (higher–order closure methods; Wyngaard 1982), but these forms are not often used.

Prandtl (1925) introduced a mixing length that represents the mean distance a turbulent eddy with excess momentum travels before blending with the environment, and therefore also the average scale of motion in turbulent flow. Mixing–length theory forms the basis of many local closure models (Section 3.1.1.3.).

More recently, methods treating the entire spectrum of scales of motion have been considered. These are known as non-local closure methods and cover large–eddy (Deardorff 1972), integral (Spiegel 1963), spectral (Berkowicz and Prahm 1979), and transilient (Stull 1984) approaches. The basic concepts underlying the above ideas are covered in Section 3.1.2.

An important consideration in the numerical treatment of the advection–diffusion equation is the artificial (pseudo-) diffusion effect inherent in conventional finite–differencing techniques for the advection part of the equation. This has led to the development of various methods for minimising this effect. A summary of the numerical methods approximating the advection–diffusion equation is given in Section 3.1.3.

The frame of reference distinguishes the Lagrangian approach from the Eulerian approach. In the Lagrangian approach, calculations are performed in a moving frame of reference in accordance with an observed or calculated wind field (Section 3.2). Continuous or instantaneous pollutant emissions are simulated by a serially–released sequence of puffs or segments, superposition of

these puffs approaches the simulation of a continuous plume. The segmented plume representation is disadvantagous because convolute plume geometries may result during calm conditions, or under variable wind fields. In contrast to the Eulerian approach, the Lagrangian trajectory approach is well suited to determining contributions from individual sources. It is also relatively inexpensive to run on computer. On the other hand, nonlinear chemistry is difficult to incorporate. Horizontal and vertical diffusion are represented by empirically determined coefficients (Section 3.2.2.) which could give erroneous results.

In the third group of models, a statistical trajectory approach is taken. This model requires large quantities of simultaneous emission data, climatological wind data, and air quality measurements. Air trajectories are calculated, and the results are statistically analysed to give, amoung other things, average pollutant contributions and horizontal diffusion. Dispersion and transformation processes are usually empirical. This approach will not be discussed further in this review.

The formulation of a descriptive and predictive mechanism for chemical reactions in air pollution studies requires an identification of all the important reactions contributing to the chemical dynamics. Air pollution chemistry is difficult to investigate experimentally because a large number of reactions take place in the atmosphere. Where possible, these reactions are linearised for ease of usage in the dispersion models. Wet and dry deposition also plays an important role and can affect the distribution over large distances. The Eulerian grid approach, in contrast to the Lagrangian approach, handles nonlinear chemistry, and it is capable of sophisticated three-dimensional physical treatments. On the other hand, considerable amounts of computer time and storage are required. A quantitative treatment follows in section 3.1.4.

Section 3.2.6 deals with buoyant plumes. To ensure that gases emitted from the stack will rise above the top of the stack, gases are often released at temperatures higher than the ambient air and at a high efflux velocity. Prediction of the effective height of the plume due to buoyancy is obviously very important. Analytical

treatments exist, but because of the numerous assumptions made during the derivation, these forms are seldom any better than empirical relationships.

3.1. EULERIAN GRID MODELS

With the Eulerian grid models, the behaviour of a species is described relative to a fixed coordinate system. The concentration of a species must satisfy the diffusion equation

$$\frac{\partial C}{\partial t} + \frac{\partial}{\partial x_j} u_j C = D \frac{\partial^2 C}{\partial x_j \partial x_j} + R(C,T) + S(x,y,z,t) \qquad (3.1)$$

where $\qquad \frac{\partial}{\partial x_j} u_j C = \frac{\partial u_1 C}{\partial x_1} + \frac{\partial u_2 C}{\partial x_2} + \frac{\partial u_3 C}{\partial x_3}$

and $\qquad u_j$ = the j-th component of the fluid velocity
$\qquad\qquad\qquad$ (j=1,2,3)

$\qquad\qquad D$ = the molecular diffusivity

$\qquad\qquad R$ = the rate of generation or removal by chemical reaction

$\qquad\qquad T$ = the fluid temperature

$\qquad\qquad S$ = the rate of addition at the location x,y,z and at time t.

As the fluid is turbulent, fluid velocities, u_j, are random variables in space and time. As demonstrated Chapter 2, it is customary to represent wind velocities, u_j, as $\bar{u}_j + u'_j$. The same idea is adopted for concentration, and C is expressed as $\langle C \rangle + C'$, where, by definition, the mean of the stochastic term $\langle C' \rangle = 0$. Substituting these forms into equation (3.1) yields, after averaging over an infinite ensemble of realisations,

$$\frac{\partial \langle C \rangle}{\partial t} + \frac{\partial}{\partial x_j}(\bar{u}_j \langle C \rangle) + \frac{\partial}{\partial x_j} \langle u'_j C' \rangle = D \frac{\partial^2 \langle C \rangle}{\partial x_j \partial x_j} + \langle R(\langle C \rangle + C', T) \rangle + S(x,y,z,t)$$

$$(3.2)$$

The term $\frac{\partial}{\partial x_j}(\bar{u}_j \langle C \rangle)$ is known as the *advection* part and $\frac{\partial}{\partial x_j}\langle u_j'C' \rangle$ as the *turbulent diffusion* part. By introducing the fluctuating terms u_j' and C', a new set of dependent variables $\langle u_j'C' \rangle$ is generated, leading to a closure problem. Some of the more valued attempts to solve this problem are discussed in the next few sections.

3.1.1. Local Closure Models

3.1.1.1. K - Theory (First-Order Closure)

In first-order closure, the solution sets out to relate the variables $\langle u_j'C' \rangle$ to $\langle C \rangle$. The most common method (summary in Pasquill (1974)) is based on the mixing length model, as for heat and momentum fluxes (Section 2.2.1.)

$$\langle u_j'C' \rangle = -K_k \frac{\partial \langle C \rangle}{\partial x_k} \qquad (3.3)$$

where K_k is the eddy diffusivity. This quantity is essentially a 3 by 3 tensor (Calder 1965, Seinfeld 1975), *i.e.*,

$$\langle u_j'C' \rangle = -K_{xx} \frac{\partial \langle C \rangle}{\partial x} - K_{xy} \frac{\partial \langle C \rangle}{\partial y} - K_{xz} \frac{\partial \langle C \rangle}{\partial z} \qquad (3.4)$$

The other co-ordinates are expressed in similar forms. The terms K_{xy} and K_{xz} may only be neglected if there is no correlation between the horizontal and vertical components of turbulence. In such instances the expression can be simplified to

$$\langle u_j'C' \rangle = -K_j \frac{\partial \langle C \rangle}{\partial x_j} \qquad (3.5)$$

i.e., the coordinate axes x,y,z coincide with the principle axes of the eddy diffusivity tensor. In addition, three more assumptions, or approximations, are introduced,

(a) molecular diffusion is negligible compared to turbulent diffusion,

$$D\frac{\partial^2 \langle C \rangle}{\partial x_j^2} \ll \frac{\partial}{\partial x_j}\langle u_j' C' \rangle$$

(b) the atmosphere is incompressible,

$$\frac{\partial \overline{u_1}}{\partial x_1} + \frac{\partial \overline{u_2}}{\partial x_2} + \frac{\partial \overline{u_3}}{\partial x_3} = 0$$

(c) the reaction rate is not influenced by the concentration fluctuation,

$$\langle R(\langle C \rangle + C', T) \rangle = R(\langle C \rangle, T)$$

On substituting these approximations into the modified advection-diffusion equation (3.2), the following is obtained

$$\frac{\partial \langle C \rangle}{\partial t} + \overline{u}_j \frac{\partial \langle C \rangle}{\partial x_j} = \frac{\partial}{\partial x_j}\left\{ K_j \frac{\partial \langle C \rangle}{\partial x_j} \right\} + R(\langle C \rangle, T) + S(x, y, z, t) \qquad (3.6)$$

Two basic conditions must be satisfied for the application of the above equation (Lamb 1973, Seinfeld 1975);

(a) that temporal variations of $S(x, y, z, t)$ and R be gradual
(b) that spatial variations of $S(x, y, z, t)$ be gradual

For convenience, C will be used instead of $\langle C \rangle$. Various analytical forms exist for special cases of the diffusion equation. A summary of some important investigations is given in Table 3.1. Yardanov (1968) obtained asymptotic formulae describing the diffusion in the surface layer; results from the similarity theory of Monin and Obukhov (1954) were used as diffusion coefficients. The investigation of asymptotic representations provided an opportunity for estimating the range of applicability of the approximated formulae of Roberts (1923) and others.

Three parameters must be specified when solving the diffusion

equation

(a) The nature of the source (*i.e.*, physical properties, such as point, line, area and height), and whether the source is instantaneous or continuous.

(b) Specific forms for the diffusion coefficients

(c) Velocity profiles

In addition to the above specifications, the boundary conditions must be specified (elevated inversion, reflection or retention at ground level). The specification of the source type often leads to a simplification of the diffusion equation. So, for example, Walters (1969) considered the case of a continuous, ground-level, cross-wind, line source with a constant mean wind speed independent of height, and the diffusion coefficients defined by $K_H = K_0 z$ and $K_v = K_1 x$. Assuming that diffusion is horizontally homogeneous, the diffusion equation reduces to

$$\overline{u}\frac{\partial C}{\partial x} = K_H \frac{\partial^2 C}{\partial x^2} + \frac{\partial}{\partial z}\left(K_v \frac{\partial C}{\partial z}\right) \tag{3.7}$$

and the solution for this case is

$$C(x,z) = \frac{q_1}{K_1(1-e^{-\lambda\pi})} \frac{\exp[-\lambda\tan^{-1}(\mu z/x)]}{\sqrt{x^2 + \mu^2 z^2}} \tag{3.8}$$

where

q_1 = pollutant flux for a continuous line source $(g\ m^{-1}s^{-1})$

λ = $\overline{u}/\sqrt{K_0 K_1}$

μ = $\sqrt{K_0/K_1}$

Liu and Seinfeld (1975) used this equation to show that when dealing with a line source, horizontal diffusion may be neglected with little error.

Dilley and Yen (1971) considered a continuous, ground level, cross-wind line source including vertical winds. The two-dimensional advection-diffusion equation was solved, ignoring horizontal

diffusion

$$\overline{u}\frac{\partial C}{\partial x} + \overline{w}\frac{\partial C}{\partial z} = \frac{\partial}{\partial z}(K_v \frac{\partial C}{\partial z}) \qquad (3.9)$$

with
$$\overline{u} = (u_1 - ax)(\frac{z}{z_1})^m$$
$$\overline{w} = \frac{az}{m+1}(\frac{z}{z_1})^m$$
$$K_v = K_1(\frac{z}{z_1})^n$$

Liu and Seinfield (1975) used this equation to study the effect of vertical winds occurring typically in urban environments and concluded that the neglect of vertical winds can grossly distort predictions of pollutant concentrations.

Quesada (1971) considered the conditions for an instantaneous point source and solved the three-dimensional, time-dependent, diffusion-advection equation in unbounded shear flow for $u = u_0 + az$ and K_i = constant (i = x, y, z).

Liu and Seinfield (1975) considered the effect of wind shear for a cross-wind, continous line source and a continuous area source using $\overline{u} = u_1(\frac{z}{z_1})^m$ and $K_v = K_1(\frac{z}{z_1})^m$ and found that neglect of shear could result in errors over 50%.

Peters and Klinzing (1971) investigated the dispersion of pollutants from both an infinite line source and a point source under the condition of a diffusion coefficient expressed as a function of the downwind position of the source (*i.e.* $\overline{u} = u_0 z^m$ and $K_v = K_0 x^n$). These forms were introduced to account for the effect of larger eddies as the cloud expands in its travel downwind. The relationships were developed for sources located at ground and elevated levels.

More recently, Nieuwstadt (1980) indicated that, since K must approach zero both at the surface and at the top of the boundary layer, conventional power-law forms for the K-coefficient were not realistic. An analytical solution of the time-dependant, one-dimensional, diffusion equation for the profile $K_v = cu_* z(1-z/h_p)$ was presented. In a comparison with the more classic forms for K, it

was found that large differences occur only in the upper region of the ABL. Important differences were however also found in the ground level concentration.

TABLE 3.1 References to some important analytical expressions derived for the wind profile ($\bar{u}$), the horizontal diffusivity profile (K_H) and the vertical diffusivity profiles (K_V) as given in the table.

Reference	$\bar{u}$	K_H	K_V	Source configuration
Roberts (1923)	$u_0 z^m$	0	$K_1 z^n$	ground level release continuous point source
Smith (1957)	$u_0 z^m$	0	$K_1 z^n$	elevated release continuous point source
Walters (1969)	u_0	$K_0 z$	$K_1 z$	ground level release continuous cross-wind line source
Peters and Klinzing (1971)	$u_0 z^m$	0	$K_0 x^n$	ground level and elevated line and point source
Quesada (1971)	$u_0 + \alpha z$	K_0	K_1	instantaneous point source in an unbounded atmosphere
Liu and Seinfeld (1975)	$u_1 \left\{ \dfrac{z}{z_1} \right\}^m$	0	$K_1 \left\{ \dfrac{z}{z_1} \right\}^m$	continuous cross-wind line and area source
Heines and Peters (1973)	u_0	0	$K_1 x^m$	continuous point source in inversion capped atmosphere
Demuth (1978)	0	0	$cu_* z^m$	instantaneous release bounded by ground and boundary layer height
Nieuwstadt (1980)	0	0	$cu_* z(1 - \dfrac{z}{h_p})$	instantaneous area source bounded by ground and boundary layer height

3.1.1.2. The Method of Moments

A change in the wind vector with height has a marked effect on the diffusion of tracers (Tyldesley and Wallington 1965). Pasquill (1969) concluded that wind-shear effects were insignificant at distances below 12km, and dominated diffusion at distances beyond 25km diffusion. Csanady (1972) found that during a medium range (about 30km) experiment, wind-shear effects were significant at distances of 15km and more. Corrsin (1953), Saffman (1962) and Hogstrom (1964) have shown that at large distances from the source the along-wind spread of the cloud varies with time according to $t^{\frac{3}{2}}$, compared with the normal prediction of $t^{\frac{1}{2}}$. Early attempts to model the diffusion in shear flow include the model of Barad and Fuquay (1962) in which the tracer dosage at a point downwind from a source is given by the normal frequency function of the lateral and vertical co-ordinates and the correlation coefficient between the lateral and vertical co-ordinates of the tracer particles. The model predicted the experimental results reasonably well.

Taylor (1953; 1954) introduced the idea of shear-diffusion when he studied dispersion in both laminar and turbulent flow in a tube; he clearly demonstrated the importance of the shear effect. An important relationship resulted from Taylor's analysis: the longitudinal dispersion due to the shear effect is inversely proportional to the rate of the lateral diffusion. The flow in pipes was also treated by Aris (1956) using the "concentration moment" method. By this method of moments, Saffman (1962) derived some important results for the expansion of an instantaneous ground level source in bounded and unbounded atmospheres. The horizontal moments of the concentration at a level z are defined by

$$C_{mn}(z,t) \quad = \quad \iint_{-\infty}^{+\infty} x^m y^n C(x,y,z,t) dx dy \qquad (3.10)$$

($n \geq 0$ and $m \geq 0$). The equations describing the moments of an instantaneous puff were found by multyipling equation (3.3) by $x^m y^n$ and integrating by parts (Saffman 1962). Assuming $\bar{w} = 0$ and applying

the initial condition

$$\lim_{\substack{x \to \pm\infty \\ y \to \pm\infty}} x^m y^n C = 0$$

and the boundary conditions

$$\lim_{\substack{x \to \pm\infty \\ y \to \pm\infty}} x^m y^n \frac{\partial C}{\partial x} = 0$$

$$\lim_{\substack{x \to \pm\infty \\ y \to \pm\infty}} x^m y^n \frac{\partial C}{\partial y} = 0$$

($m = 1,2$ and $n = 0$) the following expressions were derived

$$\left.\begin{array}{rcl}
\dfrac{\partial C_{00}}{\partial t} & = & \dfrac{\partial}{\partial z}\left[K_v \dfrac{\partial C_{00}}{\partial z}\right] \\[3mm]
\dfrac{\partial C_{10}}{\partial t} & = & \dfrac{\partial}{\partial z}\left[K_v \dfrac{\partial C_{10}}{\partial z}\right] + \bar{u}C_{00} \\[3mm]
\dfrac{\partial C_{20}}{\partial t} & = & \dfrac{\partial}{\partial z}\left[K_v \dfrac{\partial C_{20}}{\partial z}\right] + 2\bar{u}C_{10} + 2K_H C_{00}
\end{array}\right\} \qquad (3.11)$$

where C_{00} is the zero-order moment, C_{10} the first order moment and, C_{20} the second order moment. C_{00} is the total mass per unit height at height z. Similar relationships are obtained by multiplying equation (3.3) by y, xy, and y^2, before integration. Lupini and Tirabassi (1983) derived the general form

$$\frac{\partial C_{mn}}{\partial t} = \frac{\partial}{\partial z}\left[K_v \frac{\partial C_{mn}}{\partial z}\right] + m\bar{u}C_{m-1,n} + n\bar{v}C_{m,n-1}$$

$$+ K_H\{m(m-1)C_{m-2,n} + n(n-1)C_{m,n-2}\} \qquad (3.12)$$

for $m + n \neq 0$ and $m-1, m-2, n-1, n-2 \geq 0$.

It follows that the centroid of the material at height z lies at

$$[\mu_x(t), \mu_y(t)] = \left[\frac{C_{10}(z,t)}{C_{00}(z,t)}, \frac{C_{01}(z,t)}{C_{00}(z,t)}\right] \qquad (3.13)$$

and the variances about this centroid are given by

$$\sigma_x^2(t) = \frac{C_{20}(z,t)}{C_{00}(z,t)} - \mu_x^2(t) \qquad (3.14)$$

and

$$\sigma_y^2(t) = \frac{C_{02}(z,t)}{C_{00}(z,t)} - \mu_y^2(t) \qquad (3.15)$$

The cross-correlation at this level is

$$\rho(t) = \left[\frac{C_{11}(z,t)}{C_{00}(z,t)} - \mu_x(t)\mu_y(t)\right]\left[\sigma_x(t)\sigma_y(t)\right]^{-1} \qquad (3.16)$$

Saffman (1962) solved the equations (3.11) for various forms of K_v and u. In the case of the unbounded layer with K_v constant, C_{00} is easily solved for unit release at t = 0 and z = 0 to give the well known Gaussian form

$$C_{00}(z,t) = (\pi K_v t)^{-\frac{1}{2}} \exp\left[\frac{-z^2}{4K_v t}\right] \qquad (3.17)$$

Using Laplace transforms, Saffman (1962) also solved the first moment for $\bar{u}(z) = \alpha z$ and for the two forms of K_H, (a) K_H = constant and (b) $K_H = K_0 z$. He showed that the x centroid and variance of the ground level distribution are

$$\mu_x(0,t) = \frac{1}{4}\alpha(\pi K_v t^3)^{\frac{1}{2}}$$

$$\sigma_x^2(0,t) = \left[\frac{7}{30} - \frac{\pi}{16}\right]\alpha^2 K_v t^3 + \begin{cases} 2K_H t & \text{for (a)} \\ \frac{1}{2}K_0(\pi K_v t^3)^{\frac{1}{2}} & \text{for (b)} \end{cases}$$

$$(3.18)$$

Saffman (1962) showed that the asymptotic value of C_{30} (the indication of skewness) is given by $\frac{21}{256}\alpha^3 K_v t^4$ plus smaller terms involving K_H. He pointed out that, in the case of a linear wind profile, the ground level skewness approaches unity. Hence the distribution would not be asymptotically Gaussian. Saffman (1962)

68

also considered the distribution in a layer of finite height and suggested asymptotic forms for the first few moments.

Okubo (1967) derived the parameters for describing the distribution of a tracer in both a bounded and unbounded sea. In the case of an unbounded sea, the advection-diffusion equation is transformed by introducing a moment-generating function.

$$\Gamma(l,m,n,t) \;=\; \iiint_{-\infty}^{+\infty} e^{lx+my+nz} \; C(x,y,z,t) \; dxdydz$$

(3.19)

Kullenburg (1971) used this function for modelling tracer dispersion in fjords. The transformed advection-diffusion equation is

$$\frac{\partial \Gamma}{\partial t} + l\bar{u} \frac{\partial \Gamma}{\partial n} + m\bar{v} \frac{\partial \Gamma}{\partial n} \;=\; K_v n^2 \Gamma$$

(3.20)

Horizontal diffusion is neglected, and the vertical diffusivity coefficient, K_v, is taken to be constant (K_1). The initial condition is

$$R \;=\; M_0$$

where M_0 is the total amount of material introduced at time $t = 0$. Equation (3.20) was then solved by the method of characteristics. The centroid and variances are obtained from

$$
\left.
\begin{aligned}
\mu_x \;&=\; \frac{1}{M_0} \left.\frac{\partial \Gamma}{\partial l}\right|_{l=m=n=0} \\[2ex]
\mu_y \;&=\; \frac{1}{M_0} \left.\frac{\partial \Gamma}{\partial m}\right|_{l=m=n=0} \\[2ex]
\mu_z \;&=\; \frac{1}{M_0} \left.\frac{\partial \Gamma}{\partial n}\right|_{l=m=n=0}
\end{aligned}
\right\}
\qquad (3.21)
$$

and

$$\sigma_x^2 = \frac{1}{M_0} \frac{\partial^2 \Gamma}{\partial l^2}\bigg|_{l=m=n=0} - \mu_x^2$$

$$\sigma_y^2 = \frac{1}{M_0} \frac{\partial^2 \Gamma}{\partial m^2}\bigg|_{l=m=n=0} - \mu_y^2 \qquad\qquad (3.22)$$

$$\sigma_z^2 = \frac{1}{M_0} \frac{\partial^2 \Gamma}{\partial n^2}\bigg|_{l=m=n=0} - \mu_z^2$$

Mulholland (1977; 1980) used moments as high as the second order to model the horizontal "across-wind" distribution of serially-released Gaussian puffs. The numerical solution of these moments accounted for spatially- and temporally-variant velocity and diffusivity profiles. A series of field experiments showed evidence of extensive wind-shear. The proposed model (Dynamic Puff Model) provided significantly better predictions than an equivalent Gaussian puff model.

Using the moments method and taking the height and the depth of the mixing layer into account, Maul (1978) derived expressions for the ground level trajectory of a diffusing cloud. These were used to observe the effect of a change in wind direction. Lupini and Tirabassi (1983) solved the diffusivity equation on the basis of a truncated Gram–Charlier expansion of the concentration field, and derived a set of equations for moments. Fourth-order moments were applied to the case of continuous plumes.

3.1.1.3. The diffusivity profile in the boundary layer

3.1.1.3.1. Surface layer

Vertical diffusivity. Earlier treatment of the atmospheric boundary layer considered the turbulence flux of momentum, $\rho\overline{u'w'}$, to be analogous to molecular diffusion. Substituting K (eddy viscosity) for ordinary viscosity gives

$$-\rho\overline{u'w'} \;\; = \;\; \tau_{zx} \;\; = \;\; \rho K_{m,z} \frac{\partial\overline{u}}{\partial z} \tag{2.32}$$

This model yields a set of commonly used rudimentary closure relationships for the transport of heat and mass in turbulent flow. The mixing length theory was introduced by Prandtl (1925). The mixing length, l, is defined as the mean distance that a turbulent eddy, with excess momentum u', travels before integrating with the environment. Hence,

$$u' \;\; = \;\; \overline{u}(z+l) - \overline{u}(z) \;\; \simeq \;\; l\frac{d\overline{u}}{dz} \tag{3.23}$$

where z is the original level of the eddy. Furthermore, it can be written (Seinfeld 1975),

$$-\rho\overline{u'w'} \;\; = \;\; \rho l^2 \; \frac{d\overline{u}}{dz} \left|\frac{d\overline{u}}{dz}\right| \tag{3.24}$$

Comparing equation (2.32) with equation (3.24),

$$K_{m,z} \;\; = \;\; l^2\frac{\partial u}{\partial z} \tag{3.25}$$

Similar expressions hold for τ_{xy} and $K_{m,x}$. For a surface layer of neutral static stability, the mixing length may be approximated by a linear function of the distance from the surface, that is, l = kz. Hence

$$K_{m,z} \;\; = \;\; kzu_* \tag{3.26}$$

The mixing length for the non-neutral surface layer is then

$$l \;\; = \;\; kz/\phi_m(\frac{z}{L}) \tag{3.27}$$

which follows from equations (2.3) and (3.25). Thus, in a manner analogous to wind shear, for the non-neutral layer $K_{m,z}$ is modified by $\phi_m(\frac{z}{L})$:

$$K_{m,z} \;\; = \;\; ku_*z/\phi_m(\frac{z}{L}) \tag{3.28}$$

71

Similarly for the heat transfer process,

$$K_{h,z} = ku_{*}z/\phi_h(\frac{z}{L})$$

(3.29)

The vertical mass eddy diffusivity, K_v, and the eddy viscosity for heat, K_h, are often assumed to be equal. K_v in the surface layer is therefore well described by one of the suggested forms for $\phi_h(\frac{z}{L})$ discussed in Chapter 2.

Yardanov (1968) based the following models for K_v in the surface layer on the observations of Monin and Obukov (1954) :

Unstable conditions

    shear-dominated ($z \leq -0,05L$)

$$K_v(z) = K_1 z^n$$

    buoyancy-dominated ($z > -0,05$)

$$K_v(z) = K_1(-0,05L)^{n-\frac{4}{3}} z^{\frac{4}{3}}$$

(3.30a)

Stable conditions

    shear-dominated ($z \leq 0,3L$)

$$K_v(z) = K_1 z^m$$

    buoyancy-dominated ($z > 0,3L$)

$$K_v(z) = K_1(0,3L)^m$$

(3.30b)

($1 < n \leq \frac{4}{3}$, $0 < m \leq 1$). Monin and Obukhov (1954) found the following asymptotic behaviour in the surface layer:

$$K_v(z) \sim \begin{cases} z & \text{when } z \ll |L| \\ z^{4/3} & \text{when } z \gg -L \text{ for unstable cases} \\ \text{constant} & \text{when } z \gg L \text{ for stable cases} \end{cases}$$

(3.31)

The transition from shear-dominated to buoyancy-dominated sublayers occurs at $0,03 \leq -\frac{z}{L} \leq 0,05$ for unstable cases and at $0,05 < \frac{z}{L} \leq 0,3$

for stable conditions.

Horizontal diffusivity. Less research has been done on horizontal diffusivities, K_H, than vertical diffusivities. Most workers have simply assumed a constant value ($\sim 500 m^2 s^{-1}$). Sometimes the horizontal diffusivity is expressed as a function of the vertical diffusivity,

$$K_H = 2 \max_z (K_v(z)) \tag{3.32}$$

or, as used by Ragland and Dennis (1975),

$$K_H(z) = \beta K_v(z) \tag{3.33}$$

where
$$\beta = 2 \quad \text{for unstable conditions}$$
$$\beta = 5 \quad \text{for neutral conditions}$$
$$\beta = 6 \quad \text{for stable conditions}$$

Sutton (1953) gave the following relationships

$$K_H = \frac{1}{4} C_y^2 \, \bar{u}^{\,2-n} \, t^{1-n}$$

and $\hspace{8cm}$ (3.34)

$$K_v = \frac{1}{4} C_z^2 \, \bar{u}^{\,2-n} \, t^{1-n}$$

hence,

$$K_H(z) = K_v(z) \left\{ \frac{C_y}{C_z} \right\}^2 \tag{3.35}$$

provided that the ratio C_y/C_z is reasonably constant with height. Venter, Halliday, and Prinsloo (1973), in their measurement of the Sutton parameters (Sutton 1953), n, C_y, and C_z, under conditions existing on the South African Highveld, found that these parameters

are adequately described by

$$C_y = 0,57n + 0,106$$

and   (3.36)

$$C_z = 0,38n + 0,112$$

where

$$n = 0,0004 \, \bar{\theta} + 0,37 \qquad (3.37)$$

and θ = mean potential temperature gradient

$$= \frac{\Delta\theta}{\Delta z} \quad °C \ m^{-1}$$

3.1.1.3.2. Outer layer

Considerably less is known about the behaviour of $K_v(z)$ and $K_H(z)$ in the planetary boundary layer above the surface layer. Most of the empirical models, cited in literature, fall into one of four groups

(a) power-law profiles
(b) parameterisations based on surface layer theory
(c) interpolation schemes
(d) curve-fitting techniques

The simplest representation of the eddy diffusivity coefficient is the power-law form. This representation has been used often (Smith 1957, Walters 1969, Peters and Klinzing 1971, Dilley and Yen 1971, Heins and Peters 1973). One of its forms is known as Schmidt's conjugate power law,

$$K_v(z) = K_1 \left(\frac{z}{z_1}\right)^q \qquad (3.38)$$

It corresponds to the power law wind profile for q = 1-p. A more

74

theoretically sound form was proposed by Gee (1965)

$$K_v(z) = u_*^2 \, p^{-1} \, u_r^{-1} \, z_r^{\,p} \, z^{1-p} \tag{3.39}$$

where the exponent p is given by (Section 2.2.2)

$$p = 0,1340 + 0,244L^{-1} + 0,22L^{-1} \tag{3.40}$$

Ragland (1973) suggested that, above the surface layer, $K_v(z)$ be taken as a constant, equal to its value at the top of the surface layer. If the height of the surface layer is given by

$$h_s = 0,1u_*/|f| \tag{2.39}$$

then the coefficients become

$$\left.\begin{aligned}
K_v(z) &= 0,1k^2 u_*^2/|f| & \text{neutral} \\[2mm]
K_v(z) &= 6ku_* L/(1+\alpha) & \text{stable} \\[2mm]
K_v(z) &= \frac{0,1k^2 u_*^2}{|f|}\left[1 - \frac{1,5ku_*}{|f|L}\right]^{\frac{1}{4}} & \text{unstable}
\end{aligned}\right\} \tag{3.41}$$

Brost and Wyngaard (1978) adopted the following expression based on the surface layer similarity theory,

$$K_v(z) = \frac{kzu_*(1-z/h_i)^{1,5}}{\phi_h(\frac{z}{L})} \tag{3.42}$$

The Businger et al. (1971) forms for $\phi_h(\frac{z}{L})$ were used.

O'Brien (1970) proposed a simple interpolation formula based on physical reasoning. At the top of the outer layer the eddy diffusivity, $K_v(z)$, is equal to $K_v(h_p)$, and its derivative, $\left[\dfrac{\partial K_v(z)}{\partial z}\right]_{h_p}$, is taken to be zero. The eddy viscosity and its derivative are assumed to be continuous across the boundary between the surface and outer layers. A cubic polynomial is fitted to the values of $K_v(h_s)$, $K_v'(h_s)$, and $K_v(h_p)$; the form of this profile

function is given by

$$K_v(z) = K_v(h_p) + \left[\frac{z-h_p}{h_p-h_s}\right]^2 \left\{K_v(h_s)-K_v(h_p)\right.$$

$$\left.+(z-h_s)\left[K_v'(h_s)+2\frac{K_v(h_s)-K_v(h_p)}{h_p-h_s}\right]\right\} \qquad (3.43)$$

This function is simple and easy to use in calculations. It also gives satisfactory results (Pielke and Mahrer 1975, Yu 1977, McRae *et al.* 1982). Using data collected by Crane *et al.* (1977) over the Los Angeles basin, Pielke *et al.* (1983) extended the application of this formula to convective conditions. The corrections for the momentum eddy viscosity are:

$$\left[\frac{K_m(z)}{K_m(h_s)}\right]_{mod} = \left[\frac{K_m(z)}{K_m(h_s)}\right]_{orig}[28,6\alpha^2-8,572\alpha+1] \qquad (3.44a)$$

for $0,04 \leq \alpha \leq 0,3$, and

$$\left[\frac{K_m(z)}{K_m(h_s)}\right]_{mod} = \left[\frac{K_m(z)}{K_m(h_s)}\right]_{orig}[9,4\alpha^2-13,2\alpha+4,8] \qquad (3.44b)$$

for $0,4 < \alpha \leq 1$,

with $\alpha = z/h_p$ and $h_s = 0,04h_p$. No correction was required for the interval $0,3 < \alpha \leq 0,4$.

Shir (1973) developed a turbulent transport model in which nine equations describing the mean motion, turbulent stresses, and turbulence length scale were integrated numerically to account for turbulence in the ABL in the case of neutral lapse rate. Five conditions to be met by the K profiles were identified. They were

$$K = 0$$
$$K' = k \text{ (von Karman constant)} \qquad \bigg\} \quad \text{at } z = 0$$

$$K = \alpha_0 k$$
$$K' = 0 \quad (i.e. \text{ a maximum})$$
$$\text{where } a_0 \approx 0,092$$
$$\left.\rule{0pt}{60pt}\right\} \quad \text{at } z = 0,25h_p$$

$$K = \beta_0 k$$
$$\text{where } \beta_0 \approx 0,031$$
$$\left.\rule{0pt}{45pt}\right\} \quad \text{at } z = h_p$$

$$(3.45)$$

Shir (1973) found that the equation

$$K_m(z) = u_* kz \exp(-4z/h_p) \tag{3.46}$$

fitted the conditions well for $z/h \leq 0,4$, while the relationship

$$K_m(z) = 0,5u_* kz \left[\exp(-4z/h_p) + \frac{1}{1+16(z/h_p)^{1,5}} \right] \tag{3.47}$$

fitted the conditions well over the whole range. The form for h_p used was

$$h_p = 0,455u_*/|f| \tag{3.48}$$

Lamb *et al.*(1975) derived numerico-empirical expressions from the numerical planetary boundary layer model of Deardorff (1970) to predict the particle displacement probability density function. These expressions were used to assess the validity of the vertical eddy diffusion equations given by Shir (1973), equation (3.46), for neutral conditions, and Shir and Shieh's (1974) suggested interpolation form for unstable conditions,

$$K_m(z) = K_v(z_1) \frac{z}{z_1} \exp\{-4(z_1 - \tfrac{z}{p})\} \tag{3.49}$$

(z_1 = 10m within the surface layer). The assessment was done for the cases $\frac{h_i}{L} = 0$ (neutral) and $\frac{h_i}{L} = -4,5$ (unstable). Shir's (1973) relationship, assuming $K_v(z) \equiv K_m(z)$, was found to be in good agreement. Shir and Shieh's (1974) relationship produced smaller diffusivities than the optimal diffusivities, but only because the

diffusivities in the surface layer $K_v(z_1)$ were smaller.

Horizontal diffusivity coefficients are usually assumed to be constant with height, or as given by Ragland (1973),

$$K_H(z) = \beta K_v(z) \qquad (3.50)$$

where β is given in equation (3.33).

3.1.1.4. Box and multiple cell models

A convective boundary layer (very unstable conditions) generally forms over land during daytime hours when solar radiation is strong and winds are calm. The convective boundary layer (mixing layer) consists of large-scale motions associated with updrafts (thermals) and downdrafts. Convective turbulence is relatively vigorous and causes rapid vertical mixing of the boundary layer. Thus, under convective conditions pollutants emitted from an elevated source are brought down to the ground close to the stack resulting in high concentrations. Because atmospheric mixing is so vigorous, the vertical concentration distribution is assumed to be uniform within a box or cell, and it extends upward to the mixing layer (convective boundary layer) height (Ragland 1973, Lebedeff and Hameed 1975; 1976). These models are known as multiple-cell, vertical-cell or integral models, or multiple box models when more than one cell is considered. The mixing height is the height to which pollutants rise under the action of temperature inversion. Application of a single box model, including time dependency, has been discussed by Lettau (1970). An average value of the wind speed is used to calculate the flux of pollutants through the box. The single box model was extended by Reiquam (1970), who developed a model consisting of a horizontal array of interconnecting boxes along the ground. Each box extends up to the mixing height. Pollutants are carried between boxes by an average wind speed. The concentration within a cell, after a given time interval, is evaluated by balancing the input to the cell, due to emission and advection, with the outflow into

78

neighbouring cells. A similar concentration evaluation was done by Hameed (1974) in his treatment of the dispersion of SO_2 in Nashville, Tennessee. These cells were unbounded at the top and Hameed accounted for this by postulating a vertical distribution.

Leahey (1975) applied a simple advective model to the city of Edmonton, Alberta, for the prediction of ground-level NO_x concentrations. The model predicted, on the average, within 50%.

Liu and Goodin (1976) considered stationary, homogeneous, vertical cells beneath a variable-inversion-layer height. The advection-diffusion equation (equation (3.6)) was integrated vertically from the ground to the base of the temperature inversion.

$$\frac{\partial \overline{C}h}{\partial t} + \frac{\partial \overline{C}h}{\partial x} + \frac{\partial \overline{C}h}{\partial y} = \frac{\partial}{\partial x}\left[K_H \frac{\partial \overline{C}h}{\partial x}\right] + \frac{\partial}{\partial y}\left[K_H \frac{\partial \overline{C}h}{\partial y}\right] + Rh + Sh$$

(3.51)

where $\overline{C}$ is the mean concentration, and h is the layer height determined using a correlation due to Neiburger (1974). This reduction has the following advantages:

(a) a knowledge of the vertical velocity component is not required

(b) detailed modelling of all turbulent diffusivities can be avoided

(c) the time increment required for equation (3.51) in a numerical integration is generally much larger than the time increment for equation (3.6)

(d) computer storage requirements are reduced.

McRae *et al.* (1982) described a vertically integrated model along the same lines as Liu and Goodin (1976), but taking into account topography. The most critical assumption in the derivation of the governing equations is that the vertical average reaction rate, $\overline{R(C)}$, and the rate based on vertical average concentration evaluation profiles, $R(\overline{C})$, are equal. For this approximation to hold, the reaction must be first-order or the time scale of the reaction must be very much

slower than the characteristic mixing time given by (Smith *et al.* 1976)

$$\lambda = h_i/\omega_*$$ (3.52)

where ω_* is the convective velocity scale defined by (Deardorff, 1970)

$$\omega_* = \left[-\frac{1}{k} \frac{h_i}{L} \right]^{\frac{1}{3}} u_*$$ (3.53)

and h_i is the inversion height. Willis and Deardorff (1976) showed that material released at ground-level is almost well-mixed within a travel time of 3λ.

In spite of its simplicity, the multiple cell method has been found to give solutions which usually agree well with observations in a well-mixed boundary layer. Unless the meteorology and source distributions are sufficiently simple and uniform, the single box approach should not be used.

3.1.1.5. Second-Order Closure Models

It has already been indicated that an exact solution to the advection-diffusion equation does not exist because of the so-called closure problem. First order closure approximations were introduced in the previous section. Analogous to molecular diffusivity, the eddy stresses ($\overline{u'C'}$, etc.) are taken to be proportional to the product of the eddy coefficient, K, and the vertical wind shear. The eddy coefficients, in turn, are expressions of the mixing length (Prandtl 1925) and the shear. Since 1972, second-order closure of the ensemble-average moments of the fluctuating variables has received considerable attention (Donaldson *et al.* 1972, Lewellen and Teske 1973, Mellor 1973, Wyngaard *et al.* 1974, Meller and Yamada 1974, Rao *et al.* 1974, Lewellen and Teske 1976, Lumley 1978, Lumley and Mansfield 1984). The underlying principle in second-order

closure consists of deriving equations for the turbulent fluxes
($i.e.$, $\overline{u'w'}$, $\overline{v'w'}$, $\overline{u'C'}$, etc.) from the original governing equations.
The derived equations contain triple- and higher-order correlations
that are assumed to be related to the second-order, or lower, terms.
It is possible to develop equations for triple moments in an attempt
to close the system, but then fourth-order correlations appear.

Mellor (1973) and Mellor and Yamada (1974) made an important
contribution to the usage of higher-order closure models by providing
a hierarchy of closure models, ordered systematically in terms of
analytical simplifications and closure assumptions. These models are
still evolving; closure refinements are being continually made.
Wyngaard (1982) gives a review of the second-order closure modelling
done to date. These models are generally capable of giving better
estimates than the ones available from standard models.

3.1.2. Nonlocal Closure Models

The most accurate way of determining the eddy-transfer coefficients
is by direct measurement of the mean product of the eddy velocity
(concentration), $\overline{wC}$, $\overline{uw}$, etc., and the instantaneous departure of the
magnitudes of the property from its mean value, $\overline{u'w'}$, $\overline{w'C'}$, etc.. In
the absence of such measurements, either first order closure models
(K-theory) or second order models are used. Deardorff (1966) showed
that the K-theory approximation has definite limitations in the
convective boundary layer – the heat flux can be up-gradient
resulting in negative K. Wyngaard and Brost (1983) indicated that K
can even be singular. In their numerical large-eddy simulations, it
was found that the flux gradient relationship for a passive scalar
depended on the boundary from which the flux originated. It was also
shown that the diffusivity could be singular for cases where the flux
came from both boundaries. Convective boundary-layer turbulence is
one of the more difficult situations to model using local (first- or
higher-order) closure methods: the flux of a property at a given
level is difficult to relate to other properties at that level. This
difficulty has, therefore, stimulated much of the recent work in

nonlocal closure modelling. Deardorff and Willis (1975) studied dispersion in the laboratory using a water tank, while Lamb (1978; 1979) investigated particle diffusion using numerical techniques. These studies demonstrated the inapplicability of conventional modelling techniques to dispersion under convective conditions.

3.1.2.1. Large Eddy Approach

What happens during convective conditions, when matter is transported throughout the entire depth of the layer, has already been discussed : turbulent diffusion is inadequately parametrised by the mixing-length hypothesis. The numerical work of Deardorff (1970) and experimental work on diffusion (from a simulated ground-level cross-wind line source in a water-tank model of the convective mixed layer) of Deardoff and Willis (1975) showed that conventional eddy diffusivity methods cannot properly describe the mechanism of dispersion in such a layer. In view of this, investigators have suggested various parameterisations based on observations (numerical and experimental) to describe the large-scale motions occuring during convective conditions. Successful forms for the eddy diffusivity coefficient have been suggested and tested. Carl *et al.* (1973) proposed a relationship for the eddy coefficient for momentum transfer under conditions of strong convection in the surface layer,

$$K_m = a(kz)^{\frac{4}{3}} \left[\frac{gH}{c_p \rho T} \right]^{\frac{1}{3}} \tag{3.54}$$

where a = 2,5. Crane *et al.* (1977) compared equation (3.54) with the second-order closure model of Zeman and Lumley (1976) for vertical diffusion from an area source. These forms were in turn compared with observed measurements; equation (3.54) was found to agree well. Finally, Crane *et al.* (1977) suggested that, for vertical eddy diffusivity, a = 2.0.

McRae *et al.* (1982) deduced an approximate value for K_H from the

measurements of Willis and Deardorff (1976),

$$K_H \simeq 0,1\omega_* h_i \tag{3.55}$$

where ω_* is defined by equation (3.53) (h_i is the inversion height). McRae et al. (1982) identified four layers in the unstable boundary layer and fitted an appropriate diffusivity profile to each one. The surface layer thickness was taken to be $0,05 h_p$, and the similarity forms, together with the expression suggested by Carl et al. (1973) (equation 3.54), were used. For the region $0,05 \leq \frac{z}{h_p} \leq 0,6$, the diffusivity coefficient is expressed in the form of a 4th order polynomial which is scaled by the convective velocity scale, ω_*:

$$K_v(z) = \omega_* h_i \left\{ a_1 + a_2\gamma + a_3\gamma^2 + a_4\gamma^3 + a_5\gamma^4 \right\} \tag{3.56}$$

where

$$a_1 = 0,021$$
$$a_2 = 0,408$$
$$a_3 = 1,351$$
$$a_4 = -4,096$$
$$a_5 = 2,560$$

and

$$\gamma = \frac{z}{h_i} \quad (h_i \text{ is the mixing-layer height})$$

The other regions are $\quad 0,6 < \frac{z}{h_p} \leq 1,1$:

$$K_v(z) = 0,2\omega_* h_i \exp(6 - 10\gamma) \tag{3.57}$$

and $\quad \frac{z}{h_p} > 1,1$,

$$K_v(z) = 0,0013\omega_* h_i \tag{3.58}$$

3.1.2.2. Spectral Diffusivity Assumption

The rate of growth of a cloud of material is dependent on the stage of growth. Hence, for dispersion close to a source, where the size of the distribution is smaller than the most energetic turbulent eddies, the K-theory with constant diffusivity is erroneous. A time dependent K_v is difficult to treat in an Eulerian reference frame.

Berkowicz and Prahm (1979) developed a non-local closure model for $\overline{w'C'}$ by Fourier-decomposing the concentration profile to individual Fourier modes: K_v was assumed to depend on the wave-number, κ, .of the mode: $K_v = K(\kappa)$.

The value of $K(\kappa)$ decreases with an increase in the wave number of the concentration spectrum. Hence the diffusivity is effectively dependent on the actual size of the concentration distribution. This agrees qualitatively with the statistical dispersion theory of Taylor (1921) (Section 3.2.3). The K-theory appears as a small scale limit of the more general spectral diffusivity approach. A new function, the turbulent diffusivity transfer function, is introduced. For the one dimensional case,

$$D(z-z') = \frac{1}{2\pi} \int_{-\infty}^{+\infty} K(\kappa) \exp\{i\kappa(z-z')\} d\kappa \qquad (3.59)$$

where the one dimensional equation

$$\frac{\partial C(z,t)}{\partial t} = K \frac{\partial^2 C(z,t)}{\partial z^2} \qquad (3.60)$$

can be rewritten as

$$\frac{\partial C(z,t)}{\partial t} = \frac{\partial}{\partial z} \int_{-\infty}^{+\infty} D(z-z') \frac{\partial C(z',t)}{\partial z'} dz' \qquad (3.61)$$

From equation (3.61) it follows that the turbulent flux of

concentration is then.

$$\overline{wC} = -\int_{-\infty}^{+\infty} D(z-z')\frac{\partial C(z',t)}{\partial z'}dz' \qquad (3.62)$$

Equation 3.62 states that the flux of C at level z is instantaneously related to the vertical gradient of C surrounding level z. It is recalled that for first-order closure approximations,

$$\overline{wC} = -K_v \frac{\partial C}{\partial z}$$

which is the same as for the case $D(z-z') = K\delta(z-z')$ in equation (3.62) (δ being the Dirac delta function). The non-local character of the diffusion is thus entirely the consequence of the κ-dependent spectral diffusivity coefficient $K(\kappa)$, being introduced.

Various forms for $K(\kappa)$ have been proposed. From the known behaviour of an evolving cloud in a homogeneous stationary turbulent field, Berkowicz and Prahm (1979) put forward the form

$$K(\kappa) = \frac{K_0}{1+B(\kappa/\kappa_m)^{4/3}} \qquad (3.63)$$

A κ^{-1} dependence on cloud dimension ($\sigma \sim \kappa^{-1}$) was assumed. K_0 is the diffusivity of the long-term diffusion limit, κ_m is the wave number corresponding to the largest turbulent eddies, and B is a dimensionless constant (0,87). Another simple expression was suggested by Berkowicz and Prahm (1980),

$$K(\kappa) = K_0(1-\exp\{-[B(\kappa/\kappa_m)^{4/3}]^{-1}\}) \qquad (3.64)$$

The parameters are identical to the ones used in equation (3.63). More general forms for $K(\kappa)$ exist. Some of these, and the methods for deriving the spectral turbulent diffusivity functions, were reviewed by Berkowicz (1984). Hence, for the one dimensional case:

$$\frac{\partial \widetilde{C}(\kappa,t)}{\partial t} = -\kappa \ K(\kappa)\widetilde{C}(\kappa,t) \qquad (3.65)$$

where C(z,t) is given by the Fourier representation

$$C(z,t) = \int_{-\infty}^{+\infty} \tilde{C}(\kappa,t)\exp(i\kappa z)d\kappa \qquad (3.66)$$

The spectral turbulent diffusivity theory is especially easy to apply to the advection-diffusion equation when a numerical technique, based on the pseudo-spectral method (Christensen and Prahm 1976, Prahm and Christensen 1977), is used.

3.1.2.3. Integral-Closure Forms

Integral-closure forms were introduced by Spiegel (1963) who developed integral equations by analogy with radiation transfer. Estoque (1968) modelled heat flux using integral equations. Recently Fiedler (1984) derived integral-closure forms using the ideas of Berkowicz and Prahm (1979). In his treatment, Fiedler (1984) derived the flux divergence from equation (3.61),

$$\frac{\partial \overline{wC}(z,t)}{\partial t} = -\int_{-\infty}^{+\infty} R(z,z')[C(z',t)-C(z,t)]dz' \qquad (3.67)$$

where $R(z,z')$ is a weighting function that accounts for anisotropy (statistical properties are different when coordinate axes are rotated or reflected, i.e., $\overline{u'^2} \neq \overline{v'^2} \neq \overline{w'^2}$) and inhomogeneity of convective layer turbulence (i.e., statistical properties depend on the particular position). $C(z',t)$ is the mean density (concentration) and $C(z,t)$ the density at the level in question. Several trial functions were tested for $R(z,z')$. The behaviour of $R(z,z')$ is not fully understood, and at this stage can only be determined from experiment or a series of numerical simulations. Also it is not known whether a unique form for $R(z,z')$ is possible.

3.1.2.4. Transilient Turbulence Theory

This form of nonlocal closure approach was developed recently by Stull (1984). It enables large eddy effects to be explicitly included. It differs from K-theory in that it is not restricted to turbulent transfer between adjacent points. Also, mixing can occur between points separated in space. Transilient mixing can therefore deal with mixing across zero-gradient (singularities) and counter-gradient (up-gradient) situations such as are found in convective mixed layers. Nonhomogeneous and anisotropic turbulence can also be adequately described. (Large size eddies are normally nonhomogeneous and anisotropic.) Stull (1984) discussed two forms of the theory. The basic equation in discrete form, which is applicable to numerical modelling, is

$$S_i' = c_{i1}S_1 + c_{i2}S_2 + \quad + c_{ij}S_j + \quad c_{iN}S_N \qquad (3.68a)$$

for N grid points, or in matrix form

$$[S_i'] = [c_{ij}(\Delta t)][S_j] \qquad (3.68)$$

where the matrix, $[S_j]$, represents the original concentration at grid point j, and S_i' the final concentration at grid point i after a discrete time period, Δt, for mixing. The c_{ij} coefficient (transilient coefficient) represents the portion of air from box j that is mixed into box i. This form can be extented to three dimensions and made continuous in space and time. Stull (1984) then showed that the kinematic turbulent flux, F(z) of some state variable, S(z,t), at a height z_ℓ is expressed as

$$F(z_\ell) = -\int_{z=a}^{z_\ell} \int_{\xi=a-z}^{b-z} [S(z+\xi,t)-S(z,t)]\gamma(z,\xi)\,d\xi\,dz$$

$$(3.69)$$

where a and b are the heights of the bottom and top boundaries, respectively. ξ is the distance separating two levels which are being mixed. γ is the transilient rate function, defined as

$$\gamma(z,\xi) \;=\; \lim_{\Delta t \to 0} \frac{\tilde{c}(z,\xi,\Delta t)}{\Delta t} \tag{3.70}$$

and $\tilde{c}(z,\xi,\Delta t)$ is the transilient coefficient for continuous mixing (equivalent to c_{ij} in equation (3.68)). If $S \equiv C$, then $F(z_\ell) = \overline{w'C'}$. The aim of the excercise is to find appropriate forms for γ. Stull (1984) discussed some parametric forms and gave examples of how this theory is used.

3.1.3. <u>Numerical methods</u>

There are numerous methods for numerically solving the advection-diffusion equation. The finite-difference scheme is one such method. The principle considerations in choosing a finite-difference method are accuracy, stability, computation time and computer memory requirements. The advection part of the finite-difference approximation equation controls the major errors (artificial or pseudo-diffusion). Stability considerations place restrictions on the maximum time and spatial steps that can be used in the integration. Other numerical methods are the pseudospectral method, the particle-in-cell method, and the method of moments. A short description of the various numerical applications is presented below.

3.1.3.1. The Advection Equation

The advection terms in the advection-diffusion equation often lead to substantial errors when not treated properly (pseudo-diffusion). This has led several workers to develop and compare different numerical schemes to treat the advection equation.

As an introduction to the mathematical concepts involved in the finite-difference method of solving the advection equation, consider

the case where the coefficients are constant:

$$\frac{\partial C}{\partial t} + a\frac{\partial C}{\partial x} = 0, \qquad a = constant \qquad (3.71)$$

Given an initial distribution $C_0(x)$, it can be shown (Haltiner and Williams 1980, Molenkamp 1968) that

$$C(x,t) = C_0(x - at) \qquad (3.72)$$

Molenkamp (1968) tested numerical solutions of the advection equation under the above conditions. The accuracy and relative computation time of the various finite-difference approximations were investigated. It was found that forward differencing introduces a pseudo-diffusive effect of about the same order, or more, as turbulent diffusion under typical conditions. Centred-difference schemes - leap frog (Richtmyer 1963), Lax-Wendorff (Lax and Wendorff 1960) - produces an anomalous oscillation when grid spacing is too large; this leads to inaccuracy and instability. The Roberts-Weiss (Roberts and Weiss 1966) scheme approximated the advection correctly, but at the cost of computer time: 10-40 times as much computer time was needed than any of the other schemes.

Chock and Dunker (1983) compared the accuracy, speed and storage requirements of the following six numerical methods:

- Flux-corrected transport (Boris and Brook 1973; 1976)
- Multidimensional flux-correction (Zalesak 1979)
- Orthogonal-collocation (Villadsen and Stewart 1967)
- Second-moment (Egan and Mahoney 1972)
- Pseudospectral (Orszag 1971)
- Chapeau-function (Long and Pepper 1976)

For some of these, variations of the method were examined. It was found that the flux-correction and orthogonal-collocation methods are the least accurate. Although the pseudospectral method was found to be the most accurate, it requires long execution times. The second-moment method produces accurate solutions, but needs a large storage area and long execution times. The chapeau-function and multidimensional flux-correction methods are unrestricted on time

89

steps and require short to moderate execution times. These methods occupy relatively small storage areas. In a further investigation by Chock (1985), five numerical methods were compared. The schemes were:

- Chapeau-function method with mass lumping
  (Donea *et al* 1979)
- Forester method (Forester 1977)
- Filtering Remedy and Methodology (Chapman 1981)
- Hermite-cubic orthogonal-collocation (Lapidus and Pinder 1982)
- Quadratic-function (Lapidus and Pinder 1982)

Chock (1985) found that the straight-forward application of the Forester method leads to a violation of the principle of mass conservation. However, the Forester method applied to the chapeau-function solution appears to be accurate, combining short execution time with minimal memory storage. Chock (1985) noted that this method is better than any of the schemes compared by Chock and Dunker (1983).

3.1.3.2. Steady State Models

In the case of a continuous source emitting at a constant rate, in a steady atmosphere, $\frac{\partial C}{\partial t} = 0$ may be assumed. Forward-difference approximations of the steady state equation have been used by various modellers in the past. Hino (1968) used this technique to model the dispersion of smoke over complex topography.

Ito (1970) integrated the steady-state advection-diffusion equation in two dimensions by moving down-wind in finite steps, and checking, after each step, whether mass is conserved.

Ragland and Dennis (1975) investigated the Peaceman-method of successive over-relaxation (SOR) and the Peaceman-Rachford alternating-direction implicit (ADI) method. The former was found to

be slower than the latter, but required less core space. Also, the alternating-direction method was found to be unstable where the diffusion gradient is steep, such as at the source origin. A fully implicit method that cuts off higher oscillations quickly, thereby solving the problem of higher gradients near the source, was put forward.

3.1.3.3. Time-Variant Models

In most real situations, the steady-state assumption is an ideal condition seldom realised, and so the more difficult problem of solving the time-dependent advection-diffusion equation must be examined. Numerous numerical techniques exist for solving one or other form of the time-variant advection-diffusion equation. The techniques belong to one or a combination of two or more of the following groups of models

  (a) explicit integration of the advection-diffusion equation
  (b) method of fractional steps
  (c) method of moments
  (d) pseudospectral methods
  (e) vertical-cell models
  (f) two-layer models
  (g) particle-in-cell methods

Randerson (1970) used the time-variant finite difference form of the advection-diffusion equation to simulate the dispersion of SO_2 over Nashville, Tennessee. The advection-diffusion equation was integrated explicitly over time steps of 5 seconds and grid sizes of $\Delta x = \Delta y = 1$ mile. These values satisfy the von Neumann condition for stability:

$$\Delta t \leq \frac{\Delta z^2}{2K_v}$$

Such large grid sizes, however, inevitably produce a large pseudo-diffusion contribution. Shir and Shieh (1974) followed a

similar approach when modelling SO_2 distribution over St. Louis, Missouri. Horizontal intervals measured 1524m. A second-order, central, finite-difference scheme was used to integrate the advection and horizontal diffusion terms, whereas the Crank-Nicholson (Richtmyer and Morton 1967) method was used for the vertical diffusion term. Egan and Mahoney (1972) developed a model for the study of air pollution transport from urban area-type sources. The pseudo-diffusive errors were eliminated by locating the mass distribution relative to a grid element using the zero, first and second moments. Chock and Dunker (1983) emphasised the shortcomings of this method and proposed a new algorithm that removes the inherent problems of the Egan and Mahoney model.

Roffman *et al.* (1975) developed a numerical model for predicting air pollution under thermal-inversion-breakup (fumigation) conditions. To account for terrain and flow irregularities, a set of successive orthogonal transformations were performed, and these transformed partial differential equations were solved by a forward time and space scheme.

Ranca and Sardei (1975) solved the advection-diffusion equation (neglecting horizontal diffusion) by the method of fractional steps (Yanenko 1971). According to this technique, the concentration at time $t+\Delta t$ is obtained from that at time t by separating, in the following way, the contributions due to the advection and diffusion terms:

The first step solves the advection term

$$\frac{\partial c}{\partial t} + u(z)\frac{\partial c}{\partial x} = 0 \qquad (3.73)$$

over the time interval Δt with the concentration at time t as the initial condition. The second step then solves the diffusion term

$$\frac{\partial c}{\partial t} - \frac{\partial}{\partial z}(K_v(z)\frac{\partial c}{\partial z}) = 0 \qquad (3.74)$$

over the same time interval Δt, with the initial condition provided by the concentration obtained from the first step. The velocity profile is approximated by a step function, the discrete values of

which are defined as fractions of the maximum velocity. This results in an advection equation with constant coefficients and which in turn permits equation (3.73) to be solved analytically. The diffusion equation is solved with an implicit centred-space-difference scheme (implicit Crank-Nicolson method) allowing for variable grid spacing. Ranca and Sardei (1975) "seeded" the system using a Gaussian distribution at the source. Their results agree well with an analytical solution by Rounds (1955) for a continuous point source with $\bar{u} = u_1 z^m$ and $K_v(z) = z$. In their treatment of urban air pollution, McRae et al. (1982) used an operator splitting technique, similar to the one used by Yanenko (1971), but according to a sequence proposed by Marchuk (1975).

Christensen and Prahm (1976) introduced a pseudo-spectral method which has been demonstrated to eliminate numerical diffusion, and, as indicated by De Haan (1980), is highly accurate and requires only modest computation time. The gradients $\frac{\partial c}{\partial x}$ and $\frac{\partial c}{\partial y}$ are determined separately for x- and y- directions by writing

$$C(x_i) = \sum_{k=0}^{N} A(k) \exp(i2\pi \frac{k}{N\Delta x} x_i) \qquad (3.75)$$

with $A(k)$ the Fourier components for wave numbers $\frac{k}{N\Delta x}$. N is the number of grid points and Δx the space interval. The derivatives are

$$\frac{\partial C(x_i)}{\partial x} = \sum_{k=0}^{N} i2\pi \frac{k}{N\Delta x} A(k) \exp(i2\pi \frac{k}{N\Delta x} x_i) \qquad (3.76)$$

For every line of grid points $C(x)$ the spectral representation, $A(k)$, is computed by means of a Fast Fourier Transformation. The diffusion term of the advection-diffusion equation is obtained by multiplying equation (3.76) by the diffusivity coefficient, K. The space derivative of the flux can then be evaluated and the derivative profile is obtained by the inverse transformation.

Zlatev et al. (1983) applied the method of Bagrinovskii and Godunov (1975), which is an extension of the 'splitting' technique of Yanenko

(1971), to model the long-range transport of sulphur pollutants over Europe. A pseudo-spectral algorithm was used in the space discretisation phase. The process was accelerated by the use of one-dimensional Fast Fourier Transforms. The diffusivity terms were treated using the spectral diffusivity theory of Berkowicz and Prahm (1979) (Section 3.1.2.2.).

Van Egmond and Kesseboom (1983) used a model which is based on the pseudo-spectral advection scheme, to describe the air pollution over an 400km x 400km area in the Netherlands. Time integration was performed by the leap-frog scheme,

$$C_{t+1} = C_{t-1} + 2\Delta t \left[\frac{\partial C}{\partial t}\right]_t \qquad (3.77)$$

Tyldesley and Wallington (1965) solved the moment equations (Saffman 1962) numerically, thereby avoiding the restriction to the forms for K_v and u. They applied their model to an instantaneous ground-level release. The investgation confirmed the asymptotic nature of the relationships obtained by Saffman (1962) for a linear velocity profile and a constant vertical diffusion. It was pointed out, in conclusion, that significant shear effects may occur at distances and times that are shorter than expected. Although the effect of shear is significant in steady-state continuous releases, it is not as dominant as in instantaneous releases.

To solve for the moments in a set of two-dimensional, time-variant, partial differential equations, Mulholland (1977; 1980) employed a numerical method that is based on explicit finite-difference solutions. The advection terms were treated according to the method of Runca and Sardei (1975) mentioned previously. A stable *limiting value* method was developed for integrating the diffusion terms. This method required less computation than the Crank-Nicolson, Gauss-Seidel and Successive Over-Relaxation methods, employed to similar degrees of accuracy.

For the partial differential equation

$$\frac{\partial C}{\partial t} = \frac{\partial}{\partial z}(K_v(z,t)\frac{\partial C}{\partial z}) \qquad (3.78)$$

94

the limiting value method for variable stepsizes, Δz, and variable diffusivity with height, may be expressed by

$$c_k^{t+1} = c_k^t + b_k^t(1 - e^{-a_k \Delta t})$$ (3.79)

where

$$b_k^t = \frac{c_{k+1}^t - c_{k-1}^t}{\left[1 + \frac{K_{v,k-1}}{K_{v,k-1}} \frac{\Delta z_{i,k+1}}{\Delta z_{i-1,k}}\right]} + c_{k-1}^t - c_k^t$$

and

$$a_k = 2 \frac{\left[K_{v,k+1}\Delta z_{k-1,k} + K_{v,k-1}\Delta z_{k,k+1}\right]}{\Delta z_{k-1,k}\Delta z_{k,k+1}\left[\Delta z_{k-1,k} + \Delta z_{k,k+1}\right]}$$

$\Delta z_{k,k-1}$ is the grid interval between grid points k and k-1. By comparing with a series of growing Gaussian puffs, an optimum criterion was established,

$$K_v \Delta t/\Delta z^2 = 0,4$$ (3.80)

Multiple-cell models were introduced in Section 3.1.1.1.4. Using a mass-balance which included the advection of the vertical distribution through a logarithmic velocity profile, Hameed (1974) solved the ground-level concentration for each cell. Liu and Goodin (1976) examined four different finite difference schemes: Fromm's zero order average phase error (Fromm 1969), leap-frog (Roache 1972), Rubin-Burstein upwind (Rubin and Burstein 1967), and the Peaceman-Rachford alternating-direction implicit ADI method (Peaceman and Rachford 1955). These methods produced widely divergent results.

A two-layer model indicating the effects of mixing between the surface layer and the outer layer was described by Reible *et al*. (1983). The resultant fumigation process occurs during the break-up of a stable layer aloft a growing unstable layer. The model equations consisted of two coupled partial differential equations which were solved using the method of characteristics (Stoker 1957). This numerical technique is normally employed in the solution of hyperbolic partial differential equations.

Random motion, or particle-in-cell (PIC), methods have been put forward as an alternative to solving the advection-diffusion equation. They concern the positioning of serially-released particles in space according to random turbulent velocities (Thompson 1971; Knox 1974). The primary advantages are (1) that it eliminates pseudo-diffusion, and (2) that no stability restrictions exist. The main disadvantage is that computer memory must be large in order to provide sufficient resolution in cell-counts. Applications of this method are to be found in Sklarew et al. (1971) and Lange (1978) (ADPIC-model). The ADPIC code solves the three-dimensional advection-diffusion equation in its flux conservative form (pseudo-velocity technique) for a given divergent-free wind field.

3.1.4. Removal Mechanisms

3.1.4.1. Chemical Reactions

In the last two decades extensive research has been done towards explaining the chemical reactions of pollutants in the atmosphere, and towards incorporating these reactions in dispersion modelling. Despite all of this research, an understanding of the chemistry of the atmosphere is still far from complete. Seinfeld (1975) presents a complete treatise on air pollution chemistry. Consequently, it is not the aim of this review to present the chemical reaction mechanisms in detail, but only to discuss some of the more important ideas and practical results.

The most important reactions taking place are those involving the oxidation of sulphur and nitrogen oxides. Oxidation mechanisms can be classified into seven types

(1) homogeneous gas phase reactions
(2) heterogeneous (catalytic) gas phase reactions
(3) photochemical oxidation with O_2
(4) oxidation with free radicals

(5)   oxidation with molecules

(6)   catalysed and uncatalysed liquid phase oxidation

(7)   surface reactions at particles.

The last two types of reaction occur in very humid and wet conditions. In a recent review by Moller (1980) on the oxidation of SO_2, it was found that the mean reaction-rate constant for photochemical oxidation was $10^{-7}s^{-1}$, for radical reactions, $1,2 \times 10^{-6}s^{-1}$, for oxidation in water droplets in the pH range 4 to 5, between 10^{-8} and $10^{-4}s^{-1}$, and for particle reactions, about $10^{-8}s^{-1}$. Moller (1980) also reported that the removal mechanisms contribute according to

9% homogeneous oxidation

35% liquid phase oxidation

45% dry deposition

11% wet deposition

Catalysts for the heterogeneous reaction include several metal salts, such as the sulphates and chlorides of manganese and iron; metal salts are usually suspended in air as particulate matter.

Various methods have been employed to describe the rate at which SO_2 transforms to the sulphate, that is,

$$SO_2 \xrightarrow{k_1} H_2SO_4 \qquad\qquad (3.81)$$

Endlich *et al.* (1984), for example, expressed the transformation rate as the sum of the homogeneous rate, based on the work of Altshuller (1979), and the heterogeneous rate, based on the review by Moller (1980). The homogeneous rate depends on solar insolation, and hence on latitude and season. A constant conversion rate of $10^{-6}s^{-1}$ was used for the heterogenous transformation. Rate constants varied from $2,778 \times 10^{-6}s^{-1}$ in winter to $1,11 \times 10^{-8}s^{-1}$ in summer.

For the homogeneous and heterogeneous transformation rates Henry and Hidy (1981; 1982) derived expressions which are a function of

background ozone concentration. In two cities in the United States,

$$k_1 = 34[O_3] \qquad \text{for St.Louis, Missouri,}$$

and

$$k_1 = 85[O_3] \qquad \text{for Los Angeles, California,} \qquad (3.82)$$

where $[O_3]$ is in ppm and k_1 in s^{-1}.

Scire *et al.* (1984) identified all possible reaction paths, and based on a sensitivity analysis, found a suitable reaction rate constant:

$$k_1 = 10^{-4}R^{0,88}[O_3]^{0,71}S^{-1,20} \qquad (3.83)$$

where R is the total solar radiation in kW/m^2, $[O_3]$ the background ozone concentration in ppm, and S a stability index, which takes on values from 2 to 6 for the Pasquill–Gilford stability classes A to F. k_1 is in s^{-1}.

The oxidation of NO_x is far more complex than the oxidation of SO_2, and normally cannot be described by a single reaction. When hydrocarbons occur with oxides of nitrogen in the atmosphere, the well known phenomenom of photochemical smog occurs. The formation of photochemical smog takes place in an extremely complex system (Seinfeld 1975, Falls and Seinfeld 1978, Falls *et al.* 1979). Of the less complicated formulations found in the literature, two reactions describe the oxidation reaction reasonably well (Scire *et al.* (1984)):

$$NO_x \xrightarrow{k_2} HNO_3 + RNO_3,$$

$$k_2 = 3,35x10^{-3}[O_3]^{1,8}S^{-1,41}[NO_x] - 0,33 \quad s^{-1}$$

$$(3.84a)$$

and

$$NO_x \xrightarrow{k_2} HNO_3$$

$$k_2 = 3,503 \times 10^{-3}[O_3]^{1,45}S^{-1,45}[NO_x] - 0,12 \quad s^{-1}$$

$$(3.84b)$$
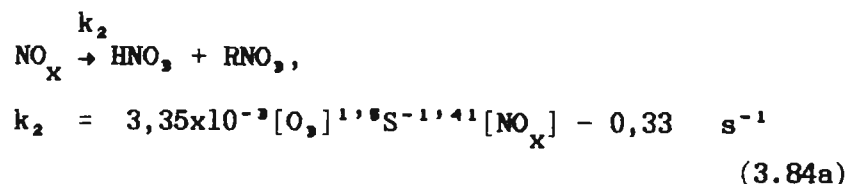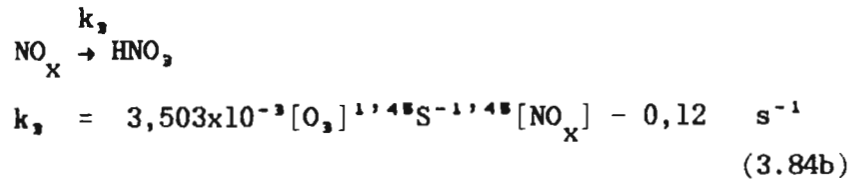
$[NO_x]$ is the background NO_x concentration in ppm (the minimum value was taken to be 10^{-4}ppm.). Only gas phase oxidation was considered.

3.1.4.2. Washout by Rain

Washout or wet deposition plays a significant role in the removal of pollutants in the atmosphere. Wet deposition is suitably described by the washout coefficient (or ratio) Λ which is defined as the fraction of particles removed in 1 second by the entire spectrum of raindrops (Pasquill 1974). In a theoretical study Chamberlain (1953) constructed curves that describe the washout of particles of varying terminal velocities as a function of the rainfall rate J (mm h^{-1}). Chamberlain (1953) assumed that the vapour pressure of a gas dissolved in the rain drop can be neglected, and he found that the washout coefficient for SO_2 and iodine lay between those for the washout of particles with terminal velocities of 0,05 and 0,1 cm/s. McMahon et al. (1976) summarised various washout coefficients for the period up to 1975, also indicating the scatter of these values.

Wet removal is a complex mechanism which includes both in-cloud and below cloud scavenging. Scott (1978; 1981) found precipitation scavenging of sulphate to be a strong function of storm type and the mechanism of precipitation formation. Scott gives the washout ratio for various cloud types. Barrie (1981) found that the washout coefficient for SO_2 was dependent on the pH and the temperature of the rain. Scire et al. (1984) used the suggested forms of Maul (1980), Garland (1978) and Levine and Schwartz (1982),

$$\Lambda_{SO_2} = 3 \times 10^{-6}J \quad s^{-1}$$

$$\Lambda_{SO_4} = 1 \times 10^{-4}J \quad s^{-1}$$

$$\Lambda_{NO_x} = 0,0 \qquad s^{-1}$$

$$\Lambda_{HNO_3} = 6 \times 10^{-6}J \quad s^{-1}$$

$$\Lambda_{NO_3} = 1 \times 10^{-4}J \quad s^{-1} \qquad (3.85)$$

wher J is the rainfall rate in mm h^{-1}. The washout ratio, then, may be conveniently included into the Lagrangian dispersion model in the form

$$M(t + \Delta t) = M(t) \exp(-\Lambda \Delta t) \qquad (3.86)$$

where $M(t)$ is the airborne mass at time t. Eulerian grid models are treated differently. Endlich *et al.* (1984) treated the washout in rain as a first order reaction mechanism

$$R_w(C) = -k_w C \qquad (3.87)$$

which effectively yields the same result as equation (3.86) on integration. It was pointed out that the removal rate constant, k_w, is proportional to the scavenging coefficient ;

$$k_w \quad \alpha \quad \Lambda(J) \qquad (3.88)$$

where J is the rainfall rate (mm h^{-1}). Endlich *et al.* (1984) used the washout ratio curves suggested by Scott (1978) for sulphate removal, and approximated them by

$$\Lambda = cJ^\beta \qquad (3.89)$$

The washout rate constant was then easily obtained :

$$k_w \quad \alpha \quad cJ^{\beta+1}$$

or

$$k_w = aJ^b \qquad (3.90)$$

and they presented values for the empirical constants a and b, assuming particular clouds to exist in a particular season. They used the work of Chamberlain (1953) with regard to SO_2.

3.1.4.3. Dry Deposition and Sedimentation

To complete the mathematical formulation of the dispersion process, the boundary conditions need to be specified. It is normally assumed that there is no flux of material through the upper boundary. However, when the plume possesses a certain degree of buoyancy (Briggs 1969), plume penetration could be allowed. The pollutant flux through the lower boundary is determined by the rate of uptake by the ground-level elements. These two boundary conditions are expressed in the mathematical forms,

$$K_v \frac{\partial C}{\partial z} = 0 \qquad \text{for the upper boundary} \qquad (3.91a)$$

$$K_v \frac{\partial C}{\partial z} = v_d(z_r)C(z_r) \qquad \text{for the lower boundary} \qquad (3.91b)$$

v_d is the deposition velocity at a reference height z_r. Various approaches have been suggested for describing the resuspension of particles (Heines and Peters 1974, Slinn 1976). These will not be discussed here.

In most numerical treatments of the advection-diffusion equation, it is necessary that the vertical concentration profile be approximated in discrete elements. $C(z_r)$ is therefore not available. The lowest grid cell is normally inside the surface layer so that the deposition velocity, $v_d(z)$, can be expressed, by means of a resistance law, in terms of the deposition velocity at a reference height; that is, $v_d(z_r)$. On integrating equation (3.91b) and rearranging the term (McRae et al. 1982),

$$v_d(z) = v_d(z_r)/[1 + v_d(z_r)R(z,z_r)] \qquad (3.92)$$

where the atmospheric (aerodynamic) resistance R is

$$R(z, z_r) = \int_{z_r}^{z} \frac{dz'}{K_v(z')} \tag{3.93}$$

The deposition velocity is often expressed as a *three-layer model*

$$v_d(z) = (r_a + r_s + r_c)^{-1} \tag{3.94}$$

where r_a is the aerodynamic resistance and is identified as $R(z, z_1)$. r_s is the surface resistance, and as given by Wesely and Hicks (1977),

$$r_s = (ku_*)^{-1} kB^{-1} \tag{3.95}$$

where B^{-1} is the surface transfer coefficient. Shephard (1974) took kB^{-1} to be equal to 2. Wesely and Hicks (1977) suggested that, for SO_2, $kB^{-1} = 2,6$. Scire *et al.* (1984) used the same value for NO_x and HNO_3, and a constant value of $r_s = 10$ s/cm for SO_4^{2-} and NO_3^-.

The surface resistance represents the resistance to transfer across the quasi-laminar layer surrounding smooth surfaces. The aerodynamic resistance is the resistance to pollutant transfer through the atmospheric surface layer. The canopy resistance is the resistance to transfer on the surface or within the plant, which will be the final resting place of the pollutant.

The rate at which pollutants are deposited depends on the state of the atmosphere, surface characteristics, and the pollutant properties. Factors influencing dry deposition removal rates have been summarised by Sehmel (1980).

Shieh *et al.* (1979) estimated the dry deposition of SO_2 as a function of land use, stability, and time of day, for the eastern parts of the United States. Scire *et al.* (1984) stated that the canopy resistance for HNO_3 could be assumed to be zero because it is very soluble and highly reactive. Canopy resistances for NO_3 were determined as a function of stability conditions: $r_c = 1,3$ s/cm for stable conditions, $r_c = 5,0$ s/cm for neutral conditions, and $r_c = 15,0$ s/cm for unstable conditions

102

Where pollutants are particles, greater than 1 μm in size, gravitational settling and particle inertia are important. A sedimentation velocity, which affects the plume as a whole, is normally introduced. So, for instance, Baron *et al.* (1949) and Overcamp (1976) in their treatment of the Gaussian plume equation, replaced z with $z + v_s x/\bar{u}$ in both the objective and image terms (see Section 3.2.1. for the definition of the objective and image terms). On the other hand, when dealing with the advection-diffusion equation, a coefficient of constant velocity can be introduced.

3.2. LAGRANGIAN TRAJECTORY MODELS

The Lagrangian approach to describing the dispersion of pollutants is concerned with the behaviour of representative fluid particles relative to the moving fluid. The fundamental Lagrangian relationship for the mean concentration of a species in a turbulent fluid in which there are sources is

$$\langle C(x,t) \rangle = \iiint_{-\infty}^{+\infty} Q(x,t|x_0,t_0) \langle C(x_0,t_0) \rangle dx_0$$
$$+ \iiint_{-\infty}^{+\infty} \int_{t_0}^{t} Q(x,t|x',t') S(x',t') dt' dx' \qquad (3.96)$$

$Q(x,t|x_0,t_0)$ is the transitional probability density defined as the probability density that a particle at x_0, at time t_0, will undergo a displacement to x, at time t. $S(x,t)$ is the spatial-temporal distribution of particle sources (units of particles per unit volume per unit time). If equation (3.96) is slightly modified

(Seinfield, 1975), a first-order chemical decay is described;

$$\langle C(x,t) \rangle = \iiint_{-\infty}^{+\infty} Q(x,t|x_0,t_0)\langle C(x_0,t_0) \rangle \exp[-\int_{t_0}^{t} k(t'')dt'']dx_0$$

$$+ \iiint_{-\infty}^{+\infty} \int_{t_0}^{t} Q(x,t|x',t')S(x',t')\exp\left[-\int_{t'}^{t} k(t)dt\right]dt'dx'$$

$$(3.97)$$

If the turbulence is stationary and homogeneous, the transition probability of a particle, Q, depends only upon the displacements in time and space, and not on where or when the particle was introduced into the flow. Under these circumstances and for special cases, in addition to empirical data, it is possible to propose forms for Q. The Gaussian puff formula and Gaussian plume formula result from the assumption of normal forms for Q.

It is also possible to express $\langle C(x,y,z,t) \rangle$, derived from the basic Lagrangian equation, as a differential equation (Seinfeld 1975). The diffusion of a particle in a turbulent fluid is considered to be a Markov process. Hence, the random component of the velocity of any particle, $v_i'(t)$ has a correlation function $R_{ij}(t;\tilde{t}) = \langle v_i'(t)v_j'(t+\tilde{t}) \rangle$ (Seinfeld 1975, Pasquill 1974), which vanishes sufficiently rapidly with increasing t so that a time scale

$$\tau_{ij} = \langle v_j'(t)v_j'(t) \rangle^{-1} \int_0^{\infty} R_{ij}(t;\tilde{t})d\tilde{t} \qquad (3.98)$$

exists for all possible values of t and all possible points of release of the particle. The motion of any particle at any time will be statistically independant of its motion prior to the time t - Δt as long as

$$\Delta t \gg \max_{i,j} \tau_{ij} \qquad (3.99)$$

Therefore, provided that Δt satisfies equation (3.99), particle diffusion in a turbulent fluid is a Markov process. Then, if the coordinate axes coincide with the principle axes of the tensor $\{\overline{K}_{jk}\}$,

where

$$K_{jk} = \langle v'_j v'_k \rangle \tau_{jk} + \langle v'_k v'_j \rangle \tau_{kj} \tag{3.100}$$

the differential equation

$$\frac{\partial \langle C \rangle}{\partial t} + \frac{\partial}{\partial x_j}(\bar{u}_j \langle C \rangle) = \frac{1}{2}\frac{\partial^2}{\partial x_j^2}(K_{jj}\langle C \rangle) - k(t)\langle C \rangle + S(x,t) \tag{3.101}$$

describes the concentration distribution. It is clear from equation (3.100), that

$$K_{jj} = 2\langle v'^2_j \rangle \tau_{jj} \tag{3.102}$$

The differential equations resulting from the Eulerian and Lagrangian approaches are essentially identical. The only difference between the two lies in their respective diffusion terms.

3.2.1. Analytical Relationships

Empirical data (Monin and Yaglom 1971) indicate that Q obeys a multidimensional normal distribution. For an inert species, substitution of such a distribution into equation (3.96) leads to the different Gaussian formulae. So, for an instantaneous point source at x_0, y_0, z_0 with a mean wind $\bar{u} = U$ and a mass of M grams, the well known Gaussian puff equation (Seinfeld 1975) is obtained,

$$\langle C(x,y,z,t) \rangle = \frac{M}{(2\pi)^{3/2}\sigma_x(t)\sigma_y(t)\sigma_z(t)}\exp\left[-\frac{(x-x_0-Ut)^2}{2\sigma_x^2(t)}-\frac{(y-y_0)^2}{2\sigma_y^2(t)}-\frac{(z-z_0)^2}{2\sigma_z^2(t)}\right] \tag{3.103}$$

where σ_x, σ_y, σ_z are the variances of the Gaussian distribution on the x, y and z axes. It is clear that the distribution from a

continuously emitting point source is the superposition of an infinite number of overlapping puffs carried along the x axis by a mean wind U; in other words, the integral of equation (3.103) over the range −∞ to t. This integration can only be performed if the turbulent velocities are assumed to be small relative to the mean velocity (Seinfeld 1975). A further assumption neglects turbulent diffusion in the x-direction. This is equivalent to assuming that the continuous plume consists of an infinite number of discs lying perpendicular to the direction of the mean velocity. The steady state solution, then, is the integration of equation (3.103) from −∞ to +∞

$$\langle C(x,y,z)\rangle = \frac{M'}{2\pi\sigma_y(x-x_0)\sigma_z(x-x_0)U}\exp\left[-\frac{(y-y_0)^2}{2\sigma_y^2(x-x_0)} - \frac{(z-z_0)^2}{2\sigma_z^2(x-x_0)}\right]$$

(3.104)

where M' is the source strength in g/sec. Equations (3.103) and (3.104) hold for an unbounded atmosphere. If pollutants do not deposit on the ground, then the ground is considered to be an impenetrable barrier to diffusion. By the method of images (Sutton 1953, Seinfeld 1975) the boundary condition is easily included in the above models. The effect of the impervious surface is accounted for by introducing an identical source (image) at $x = x_0$, $y = y_0$, $z = -z_0$, where z_0 is the height from which the pollutants are emitted. The required concentration at any point in space z > 0 is then equal to the sum of the concentrations from the two sources. For an instantaneous point source, equation (3.103) is modified to

$$\langle C(x,y,z,t)\rangle = \frac{M}{(2\pi)^{3/2}\sigma_x(t)\sigma_y(t)\sigma_z(t)}\exp\left[-\frac{(x-x_0-Ut)^2}{2\sigma_x^2(t)} - \frac{(y-y_0)^2}{2\sigma_y^2(t)}\right]$$

$$\times \left\{\exp\left[-\frac{(z-z_0)^2}{2\sigma_z^2(t)}\right] + \exp\left[-\frac{(z+z_0)^2}{2\sigma_z^2(t)}\right]\right\}$$

(3.105)

A similar expression exists for a continuous point source.

The above equations can be simplified even further for line- and area-sources. For a continuous, effectively infinite, line source extended across the wind, the pollutant distribution may be described by (Sutton (1953))

$$\langle C(x,t) \rangle = \frac{M''}{(2\pi)^{1/2} U \, \sigma_z(t)} \left(\exp\left[-\frac{(z-z_0)^2}{2\sigma_z^2(t)} \right] + \exp\left[-\frac{(z+z_0)^2}{2\sigma_z^2(t)} \right] \right)$$

(3.106)

where M" is the source strength in g/s per unit length. It is also possible to obtain the previous relationships from the differential equation form (equation 3.104) by employing the method of Green's function (Seinfeld 1975). Suggested forms for the dispersion in the case of an elevated inversion layer can be found in Seinfeld (1975). Generally, a technique similar to the ground-level reflection is employed. The sum of the reflections due to the inversion,

$$\sum_{n=1}^{\infty} \exp\left[-\frac{1}{2}\left\{ \frac{z-z_0-2nh_i}{\sigma_z} \right\}^2 \right] + \exp\left[-\frac{1}{2}\left\{ \frac{z+z_0-2nh_i}{\sigma_z} \right\}^2 \right]$$
$$+ \exp\left[-\frac{1}{2}\left\{ \frac{z-z_0+2nh_i}{\sigma_z} \right\}^2 \right] + \exp\left[-\frac{1}{2}\left\{ \frac{z+z_0+2nh_i}{\sigma_z} \right\}^2 \right]$$

is added to the exponential terms in equations (3.104) and (3.105). Seinfeld (1975) suggested that four terms are usually sufficient to approximate the summation closely enough.

3.2.2. The Diffusivity Coefficients σ_x, σ_y and σ_z

Most practical studies of the dispersion of pollutants have employed the set of empirical correlations for σ_x, σ_y and σ_z that Pasquill (1961) and Gifford (1961) used. Based on experimental observations of the dispersion of plumes, Pasquill (1961) suggested six categories of stability. Stability curves for the various stability classes provide, for a continuous plume, the diffusivity coefficients as a

107

function of downwind distances. Numerous stability classification schemes have subsequently been developed: Brookhaven (Singer *et al.* 1966), Turner stability classification (Turner 1964), and Refinery Directive Index (Raffinerieerlaß 1975). These stability classification schemes are expressed in terms of fundamental weather observations. So, for example, the Gifford, Turner, and Refinery Directive Index classification schemes employ wind-speed, cloud cover, and an estimate of the solar elevation angle. Other schemes incorporate the Richardson number (Pasquill and Smith 1971) or the standard deviation of the horizontal wind direction (Chapter 2) (Gifford 1968). Some classification schemes are compared by Sedefian and Bennett (1980), and Gifford (1976) and Weber (1976) summarize the various methods that relate the diffusion coefficients to the above stability classes.

Single functional forms have also been presented. Eimutis and Konicek (1972) used the standard deviation of wind direction fluctuations and the lapse rate to develop an expression for the diffusion coefficients. Various empirical power-law forms are also available (see Tadmor and Gur (1969) for a summary).

In recent years, attention has been directed to determining the diffusivity coefficients from Pasquill's (1971) relationships, which are

$$\sigma_x = \sigma_u f_x \left(\frac{t}{t_L} \right)$$

$$\sigma_y = \sigma_v f_y \left(\frac{t}{t_L} \right)$$ (3.107)

$$\sigma_z = \sigma_w f_z \left(\frac{t}{t_L} \right)$$

where σ_u, σ_v, and σ_w are the standard deviations in the wind components, and f_x, f_y, and f_z are universal functions. t_L is the Lagrangian time scale. The various forms for the universal functions f_x, f_y, and f_z will be discussed in the next section (Section 3.2.3.).

A workshop (Hanna *et al.* 1977) on the available stability classification schemes, and methods for determining the parameters σ_y

and σ_z, was held at the American Meteorological Society Headquaters (Boston, Massachussetts) in June 1977. No single method was preferred: only recommendations for the use of each method were given. Also, reasons were given for the unsuitability of certain methods.

3.2.3. Taylor's Statistical Analysis

An analysis of the complete statistical properties of a particle's motion for stationary, homogeneous turbulence was presented by Taylor (1921). For turbulence to be stationary and homogeneous, the relative particle distribution after an interval is independent of starting position and time. If X is the deviation, after a time T, due to the eddy velocity u', of a typical particle emitted from a continuous source, then the mean-square displacement of the particle from the axis of the plume is defined by

$$\langle X^2 \rangle = 2\langle u'^2 \rangle \int_o^T \int_o^t R_L(\xi)d\xi dt \qquad (3.107)$$

where the Lagrangian correlation coefficient, $R_L(\xi)$, is given by

$$R_L(\xi) = \frac{\langle u'(t)u'(t + \xi) \rangle}{\langle u'^2 \rangle} \qquad (3.108)$$

ξ is the lag.

The Lagrangian correlation coefficient is an indication of the correlation between the turbulent components $u'(t)$ and $u'(t+\xi)$ separated in time by ξ. As these velocities derive from the same random process, this function is known as the Lagrangian autocorrelation coefficient. By definition, correlation coefficients are unity at zero lag. Eddy sizes are reflected in the sharpness at which $R_L(\xi)$ diminishes with ξ. This can be indicated by the area under the $\xi - R_L(\xi)$ curve, i.e.,

$$t_L = \int_o^\infty R_L(\xi)d\xi \qquad (3.109)$$

provided that the integral converges. So for large T,

$$\langle X^2 \rangle = 2\langle u'^2 \rangle \, t_L T \qquad (3.110)$$

The time-scale, t_L, is known as the Lagrangian time-scale. Similar equations are found for the other coordinates. The displacements of a large number of particles can now be considered to be identical with the displacements of a single particle observed a number of times, provided that these particles do not affect the flow. The variances σ_x, σ_y, and σ_z may therefore replace $\langle X^2 \rangle$, $\langle Y^2 \rangle$, and $\langle Z^2 \rangle$, and the diffusivity coefficient can now be related to the Lagrangian autocorrelation (Seinfeld 1975, Pasquill 1974);

$$\overline{K}_x(t) = \frac{1}{2} \frac{d\langle X^2 \rangle}{dt} = \langle u'^2 \rangle \int_0^t R(\xi)d\xi \qquad (3.111)$$

or for large t,

$$\overline{K}_x = \langle u'^2 \rangle \int_0^{t_1} R_L(\xi)d\xi$$

$$= \langle u'^2 \rangle \, t_L \qquad (3.112)$$

where t_1 is the value beyond which $R_L(\xi)$ remains zero. $\overline{K}_x$ is initially zero, then increases with time, at first linearly and then more slowly, and finally tends towards the constant value given by equation (3.112).

In practice the Lagrangian fluctuations are difficult to measure. Eulerian fluctuations, on the other hand, are more easily determined. The Eulerian system refers to a particle or small element of fluid passing through a fixed point in space at time t. In an effort to relate the two correlations resulting from the different reference frames, Hay and Pasquill (1959) hypothesised that

$$R_L(\xi) = R_E(t') \text{ when } \xi = \beta t' \qquad (3.113)$$

The subscript E refers to the Eulerian autocorrelation obtained from measurements at a fixed point. β is a constant. The equivalent time

scales are related by:

$$t_L = \beta t_E \qquad (3.114)$$

Although the constants are scattered (1.1 to 8.5), Hay and Pasquill (1959) found that, on average, $\beta = 4$.

Various forms for the Lagrangian and Eulerian autocorrelations have been suggested (Sutton 1953, Pasquill 1974). These are all approximated forms as no expression has yet been found, by exact analysis, in a anisotropic field. The exponential form

$$R(\xi) = \exp\{\frac{-\xi}{t_L}\} \qquad (3.115)$$

was used by Taylor in his original discussion. The cross-wind spread of particles, using this expression, is

$$\sigma_x^2(t) = 2\sigma_u^2 t_L \{t - t_L(1 - \exp[\frac{-t}{t_L}])\} \qquad (3.116)$$

where σ_u^2 replaces $\langle u'^2 \rangle$. Neumann (1978) found this form to agree well with data in the Pasquill stability categories A to F. Explicit power-law forms of $R(\xi)$ have also been suggested. Sutton (1953) used the form,

$$R_{Lx}(\xi) = (\frac{\nu}{\nu + \sigma_u^2 \xi})^n \qquad (3.117)$$

and similar forms for the y- and z- directions, where ν is the kinematic viscosity of air. Using these relationships, Sutton (1953) showed that for an instantaneous point source,

$$C(x,y,z,t) = \frac{M}{\pi^{3/2} C_x C_y C_z (Ut)^{3/2}(2-n)} \exp\left[(Ut)^{n-2} \{\frac{x^2}{C_x^2} + \frac{y^2}{C_y^2} + \frac{z^2}{C_z^2}\}\right]$$

$$(3.118)$$

where

$$C_x^2 = \frac{4\nu^n}{(1-n)(2-n)U^n} \left[\frac{\langle u'^2 \rangle}{U^2}\right]^{1-n}$$

with similar expressions for C_y and C_z. Expressions for continuous point and line sources were also developed.

In an alternative approach, Pasquill (1971) suggested a relationship from Taylor's equation for the diffusion parameters:

$$
\begin{aligned}
\sigma_x &= \sigma_u T f_x(T/t_L) \\
\sigma_y &= \sigma_v T f_y(T/t_L) \\
\sigma_z &= \sigma_w T f_z(T/t_L)
\end{aligned}
\tag{3.119}
$$

where f_x, f_y, and f_z are universal functions. Irwin (1983) compared several proposals for these universal functions, using data from field experiments. Irwin (1983) found that Draxler's (1976) forms gave the smallest fractional error and the smallest variance of the fractional errors. The Draxler (1976) forms were based on five ground source diffusion experiments and six elevated source diffusion experiments. To illustrate, the equation for lateral dispersion in the case of elevated releases is

$$f_y = \frac{1}{1+0.90\sqrt{T/T_i}} \tag{3.120}$$

where T_i was determined from a regression fit to the experimental data. Draxler (1976) found that $T_i \approx 1,64 t_L$.

Wilson *et al.* (1981) showed that predictions from a numerical trajectory simulation method agreed closely with the Project Prairie Grass (Barad 1958) observations if the height dependence of the Lagrangian length scale was chosen to be

$$t_L = 0,5z(1 - 6\frac{z}{L})^{\frac{1}{4}} \tag{3.121}$$

for unstable conditions, and

$$t_L = 0,5z(1 + 5\frac{z}{L})^{-\frac{1}{2}} \qquad (3.122)$$

for stable conditions, where L is the Monin-Obukhov length. During neutral conditions, Reid (1979) found that

$$t_L = 0,5z \qquad (3.123)$$

This relationship was confirmed by Wilson *et al.* (1981).

Burger (1984) and Burger and Mulholland (1987) developed a continuous distribution monitor incorporating a segmented plume model. A method for estimating t_L from on-line measurement was proposed. Draxler's (1976) universal forms for *f* were used. Using a first-order running-average technique, t_{Ey} and t_{Ez} were determined directly from measurements of v' and w' respectively. An anemometer-bivane was used for this purpose. t_L was then related to t_E using equation (3.114), with β = 4 (Hay and Pasquill 1959).

3.2.4. Approximate Methods

The plume model was derived under the assumption of spatial and temporal uniformity in wind and atmospheric stability. Other important factors, such as chemical reaction, shear effects, and buoyancy of the plume, were not derived from the basic equations, and only approximate solutions exist.

In an attempt to model the effect of wind shear, Joynt and Blackman (1976) proposed a random-motion type model. The vertical root-mean-square displacement in the z-direction was approximated by

$$\sigma_z = \sqrt{2z\sigma_w \Delta t} \qquad (3.125)$$

provided that $\Delta t \geq t_L$, where Δt is the time step and t_L the Lagrangian time scale. This equation was derived from Taylor's (1921) statistical theory. The particle probability distribution was

113

assumed to be a three-dimensional normal distribution and the surfaces of equal probability are ellipsoidal. The length of the vertical axis, c, was chosen in such a way that the probability of the particle moving in the z-direction, and staying inside the ellipsoid, is 0,5;

$$i.e., \qquad c = 0,675\sigma_z \qquad\qquad (3.126)$$

The vertical-to-horizontal axis-length ratio's were estimated from observations made under differing stability conditions. Particles were then moved randomly to a point on the ellipsoidal surface. This model was applied to the steady release of SO_2 in Melbourne, Australia, and generally over-predicted.

Shieh (1978) developed a puff diffusion model which included wind shear and dynamic plume rise. Each puff was represented by a set of six tracer particles which define the shape, size, and location of the puff. Assuming a three dimensional normal distribution, the concentration distribution of each puff is determined by fitting an ellipsoid to the cluster of six particles. The particle locations are computed at each time step taking into account advection, diffusion, wind shear, and entrainment of ambient air during plume rise. In deriving the appropriate plume rise equations, the assumptions of Morton *et al.* (1956) were adopted. Application of this numerical model to typical atmospheric conditions showed that wind shear plays an important role and should not be neglected. The results indicated that the conventional puff model overestimated by a factor of 2 the concentrations at one standard deviation above the plume centre, and underestimated by the same factor, below the plume centre, at 600m downstream from the source.

The simplest way in which chemical reaction can be included in the puff model is to multiply the concentration distribution with the decay parameter (Turner 1964)

$$\exp\left(-D(t-t_0)\right) \qquad\qquad (3.127)$$

where D is a reaction constant, and $t - t_0$ the time of travel. Similarly, washout in rain may be included using a decay parameter as

indicated in equation (3.86) (Chamberlain (1953)),

$$exp \ (-\Lambda x/\bar{u})$$ (3.128)

where Λ is the washout coefficient (Section 3.1.4.2). This coefficient is a function of the rate of rainfall and the terminal velocity of the pollutant. A series of Λ-curves as a function of the these parameters can be found in Chamberlain (1953) (also Pasquill 1974).

An alternative way to include reactions in plumes is to treat the plume as a well-mixed box (Cocks, Fletcher and Kallend 1983) in a Lagrangian reference frame. Diffusion is not treated explicitly; hence the chemical equations can be included separately. A similar approach was suggested by Ludwig (1981). The model uses a gridded emission inventory and assumes that the emissions for a finite time period are introduced into an array of boxes of uniform and finite depth lying above the emission grid. The arrays of boxes are then moved after each time step according to the prevailing wind fields. Boxes are only allowed to grow in the vertical. Box-growth and inter-box transfers are determined by atmospheric stability conditions.

Random-walk (motion) theories have become very popular in recent years. Obukhov (1959) proposed that atmospheric diffusion could be represented by a continuous Markov process consisting of an air particle's coordinates and it's velocity. Lin and Reid (1963) and Monin and Yaglom (1967) summarised some of the earlier developments. Recently, Yaglom (1977a) gave a detailed review, and Sawford (1984) presented a overview on the basis and limitations of the Langevin equation in atmospheric dispersion modelling. From the statistics of the trajectories of thousands of fluid elements tracked individually through the atmosphere the Langevin models predict the concentration field downwind of a given source. Random walk theories can be stated in various forms. Langevin's equation for the velocity of Brownian motion (e.g. Gifford 1982) takes the form

$$\frac{dv}{dt} \ + \ \frac{v}{t_L} \ = \ A(t)$$ (3.129)

where v is the y component of the particle's velocity, t_L is the Lagrangian time scale, and $A(t)$ is a random acceleration given by

$$A(t) = \sigma_v \sqrt{\frac{2}{t_L}} \frac{dW_t}{dt} \qquad (3.130)$$

where dW_t is a Gaussian white-noise stochastic process, *i.e.* assuming $A(t)$ to have a flat spectrum and zero mean. Smith (1968) used a linear velocity relationship

$$v(t + \Delta t) = R_{Ly}(\Delta t)v(t) + \lambda(t+\Delta t) \qquad (3.131)$$

where $R_{Ly}(\Delta t)$ is the Lagrangian autocorrelation function with lag Δt. $\lambda(t+\Delta t)$ is a random variable, the properties of which are chosen so as to ensure that the particles move in accordance with the specified turbulence statistics and mean wind profile (Ley and Thomson 1983). A number of Monte-Carlo models based on equation (3.131) (Hanna 1979, Reid 1979, Ley 1982) have been proposed. Recently, Smith and Thompson (1984) proposed a modified form of the random walk model (integral equation method) which avoids having to inefficiently determine thousands of trajectories. This model compared very well with the more conventional random walk techniques.

Venkatram (1980a) modelled the dispersion of elevated releases in a convective boundary layer. The model compared favourably with the data of Weil (1977). Encouraged by the favourable results, Venkatram and Vet (1981) modified the model to include recent developments in dispersion occuring in convective conditions.

Differences in the surface temperature of land and sea (lake) in a littoral environment leads to the development of a thermal internal boundary layer. This boundary layer starts at the shoreline and increases in height with distance inland. The region below the internal boundary layer is unstable, whereas the region over the water and above the internal boundary layer is stable. This situation is difficult to model; conventional Gaussian models cannot be used without some modification. Several approaches at modelling this situation have been attempted (Van Dop *et al.* 1979, Misra 1980).

Practical applications for real-time usage of the Gaussian puff model are numerous. Associated with each application is a slight modification to the model. Van Egmond and Kesseboom (1983) adapted the Gaussian puff model to predict the distribution of mesoscale SO_2 distribution over the Netherlands (400km x 400km area). The model was modified to incorporate three vertical layers (surface, mixing, and reservoir layer). The concentration distribution was transformed to an Eulerian grid with a horizontal grid spacing of 15km. The resolution of the model was improved to about 1km by introducing plume segments when the puff diameters were smaller than the grid spacing.

To improve on the computation time required to add the contributions from each Gaussian puff, segmented plume models have been suggested. Gifford (1959) represented the plume as a series of discs in a plane normal to the mean wind direction. In the model proposed by Shiozawa *et al.* (1975), the discs were assumed to follow the flow of the mean wind field. Each disc was described by the plume equation. Model calculations agree well with observed data. As a result of the minimal time required in calculating the distribution, Burger (1984) used a slightly modified form of Shiozawa *et al*'s (1975) approach in an on-line prediction application. A full-scale (~10km) experiment at an industrial site gave satisfactory agreement with SO_2 measurements. The one deficiency of segmented plume and disc models is their ability to simulate calm wind conditions. Instead of segments, Smith *et al.* (1983) proposed a real-time variable trajectory model (TRAGGY), whereby the puffs are assumed to have a uniform puff concentration in the vertical. These "puffs", therefore, are vertical cylinders. This assumption reduces the computation cost and consequently the model is attractive for use in real-time accident situations.

One of the most important aspects of all puff models is the determination of the puff release rate, Δt_r. If Δt_r is too large serious errors in the plume description result, whereas if Δt_r is too small, serious problems in computer storage and computation time develop. Ludwig *et al.* (1977) proposed a reasonable solution to these problems. In their investigations, puff simulations with varying separation distances were compared with the Gaussian plume

simulation under the same conditions. It was found that, along a line parrallel to the plume, puff separation distances of less than $2\sigma_y$ caused variabilities of only a few per cent. Greater separations introduced unacceptable errors. At closer separations (less than $2\sigma_y$), puffs merged to form a single puff. Zanetti (1981) modified the application to handle non-stationary, non-homogeneous, and calm wind conditions.

3.2.5. Buoyant Plumes

As the maximum mean ground-level concentration of effluents from a source at height H is roughly inversely proportional to H^2, the amount by which a plume rises is an important factor in reducing ground level concentrations. Plume rise Δh is given by the elevation of the plume centreline above the stack outlet as a function of distance x downwind of the stack. Calculating plume rise from empirical formulae has led to much confusion because many of these formulae give different answers - often by a factor of 10 or more. This process is very complex, and understandably no complete and exact theory has emerged. Most plume rise equations were developed for uniform or smoothly-varying atmospheres. A buoyant plume rises as a result of the difference in densities between the plume and the ambient air. Plume rise is dependent on plume growth. As the plume rises, outside air will be entrained into the plume as a result of turbulence. The density deficit depends on the temperature of the entrained air. Theoretically, then, a buoyant plume in neutral and unstable conditions continues to rise indefinitely, however, in real situations the plume eventually loses its identity because of diffusion. Three types of plume are usually observed. When the initial buoyancy is much larger than the initial momentum (*i.e.* efflux velocity) the plume is known as a buoyant plume. When buoyancy and momentum are approximately equal, it is known as a forced plume, and when the initial momentum is higher than the initial buoyancy it is known as a jet.

Some analytical approaches exist (Batchelor 1954, Morton *et al.* 1956,

Slawson and Csanady 1967). A summary of these approaches is given in Seinfeld (1975). Glendening *et al.* (1984) presented an improved analytical plume-rise formulation for stable conditions with complex vertical structure. These analytical approaches normally make use of numerous assumptions, some of which are neither necessary nor physically proven. By far the majority of formulae are empirical. Summaries of these forms are given in Pasquill (1974) and Strom (1976). There exist two types of plume rise equations: (a) plume rise as a function of distance $\Delta h(x)$, and (b) final rise Δh formulae. Only the former type will be discussed. Numerous investigators have used the "2/3 law" for buoyant plume rise. This is also known as the "Briggs equation" (Briggs 1969). Briggs (1969) found the following form, for all stabilities, from his theoretical development,

$$\Delta h(x) = c_1 F_b^{1/3} u^{-1} x^{2/3} \qquad x < x_* \qquad (3.132)$$

where
$$c_1 = 1,6$$
$$F_b = g \omega_s r_s^2 (T_s - T)/T_s = \text{flux buoyancy}$$
(assuming that effluent has the same molecular weight and specific heat as air)

with
$$g = \text{acceleration due to gravity}$$
$$\omega_s = \text{effluent emission velocity at stack outlet}$$
$$r_s = \text{radius of stack outlet}$$
$$T = \text{absolute temperature of ambient air}$$
$$T_s = \text{absolute temperature of effluent at stack outlet and}$$

$$x_* = \begin{cases} 2,16 F_b^{2/5} H_s^{3/5} & H_s < 305\text{m} \\ 67 F_b^{2/5} & H_s > 305\text{m} \end{cases} \qquad (3.133)$$

where H_s is the stack height. Beyond x_*, a more accurate relationship was given :

$$\Delta h(x) = C1,6 F_b^{1/3} u^{-1} x_*^{2/3} \left[\frac{2}{5} + \frac{16}{25}\left\{\frac{x}{x_*}\right\} + \frac{11}{5}\left\{\frac{x}{x_*}\right\}^2 \right] \left(1 + \frac{4}{5}\left\{\frac{x}{x_*}\right\}\right)^{-2}$$

$$(3.134)$$

Briggs (1969) added that equation (3.132) should not be used at distances greater than $x=5x_*$. Actual plume rise can vary from calculated values by 10 per cent for flat terrain and as much as 40 per cent for complex terrain.

Rittmann (1982) found that when stack-tip downwash was unlikely to happen, plume rise (for $F_b < 100$ m^4sec^{-3}) was typically 70-75% of the value predicted by the Briggs equation for neutral and stable conditions. For sources experiencing severe downwash, plume rise was about 44% of the predicted value.

Various laws for plume penetration of an elevated inversion have been suggested. These will not, however, be discussed here.

3.3. HYBRID TRAJECTORY MODELS

There are a few hybrid approaches in which the age of the puff (as a function of distance) is introduced into the Eulerian grid models. Early attempts by Peters and Klinzing (1971) and Heines and Peters (1973) used the functional form K_0x^m for the vertical eddy diffusivity in the advection-diffusion equation. Gillani (1978) proposed a more realistic approach which included the effect of the growing cloud. The following diffusivity forms were used :

$$K_H = K_H(t)x^\gamma$$
$$K_v = K_{vm}(\frac{x}{x_r})^\gamma K_v(z,t) \qquad\qquad (1.135)$$

where
$$\gamma_0 = 0,4(1 - \frac{3}{L}) \quad , \quad |L| > 3$$
$$= 0,42 \qquad\qquad \text{near neutral cases}$$

and
$$\gamma = \begin{cases} \gamma_0 & x \leq 3h_p \\ 0 & x > 3h_p \end{cases}$$

$K_H(t)$ = the horizontal diffusivity at the time of release

K_{vm} = the maximum value of K_v during the entire duration of application of the model.

$K_v(z,t)$ = the vertical diffusivity as a function of height at the time of release.

x_r = reference distance within which the action of the entire spectrum of turbulence has been felt by the spreading plume (Gillani used $x_r = 3h_p$).

Draxler (1979) provides an alternative to the above hybrid approach. In Draxler's model, the Lagrangian trajectory is used to simulate horizontal transport and diffusion, and an Eulerian grid technique is used to simulate vertical diffusion. Puffs are advected normally and the horizontal spread is assumed to be of Gaussian form. Vertical diffusion is allowed to be a function of height as well as of time of travel. A finite difference model is run with each trajectory. Diffusion takes place in a vertical column with a horizontal area of unity and divided vertically into 20 boxes of various heights. The vertical coefficient is based upon the calculated stability at each trajectory step.

CHAPTER 4

4. <u>MODEL DEVELOPMENT</u>

The aim of the present study is to produce a high resolution pollutant distribution model for small to meso-scale simulations. The package should be self-contained, easily adaptable to include recent developments, and easy to apply to an air pollution application. Over and above these requirements, four additional areas need to be emphasised:

<u>User-friendly</u> : (i) The user must be able to choose from a wide range of meteorogical measurement input options,

(ii) The output must be clear and easily interpretable (*i.e.*, concentration isopleths instead of grid point concentrations values),

(iii) The package should run on any medium-sized computer without major modifications to the source code (*i.e.*, self-contained),

(iv) A choice of graphic terminals must be supported,

(v) Predictions must be provided at any time interval and at any height.

<u>Execution speed</u> : Execution of the model must be as fast as possible to allow on-line applications.

Memory   :   Minimal random access memory must be required

Accuracy   :   (i) Realistic simulation of the wind field and
                    hence wind and diffusivity profiles. It should
                    allow the inclusion of topography and temperature
                    anomalies.

                    (ii) It must allow spatial and temporal variations
                    of wind and temperature structure, including
                    variations of boundary layer height.

                    (iii) The model must be able to deal with
                    completely arbitrary distributions of sources with
                    variable emission rates.

                    (iv) It must adequately treat removal mechanisms
                    such as chemical reactions, washout in rain, and
                    dry deposition.

                    (v) It must permit the rise of buoyant plumes.

                    (vi) Realistic simulation of the diffusion
                    process.

The package can conveniently be subdivided into five modules: (1) the
installing module where all fixed parameters (topography, weather
station and source positions, graphics, configuration, *etc.*) are
specified, (2) the meteorological sub-module in which raw
meteorological data are manipulated into usable parameters, (3) the
three-dimensional wind field module, (4) the dispersion module, and
(5) the concentration distribution display module.

The major objective of the submeteorological module is to determine
the parameters describing the wind field, from available
measurements. Often upper air data are unavailable. In such cases,
existing parameterisations, based on surface layer similarity theory,
are used to determine the boundary layer height and outer layer
winds. Once the necessary parameters are extracted from the
measurements, the three-dimensional wind field can be constructed.

A mass consistent wind field can be obtained from sophisticated
prognostic models, but more often their complexity does not uphold
the quality of the input data. It was decided to only consider
diagnostic models. As indicated in Section 2.4, diagnostic models

123

consist of three processes:

(a) Interpolation of sparce data onto a rectangular computational grid;

(b) Reduction of anomalous divergence in the surface layer using an objective analysis procedure; and,

(c) Application of the continuity equation to construct a three-dimensional wind field.

The inverse square weighting interpolation scheme (Section 2.4.2.1.) has proved to be adequate in interpolating wind measurements (Goodin *et al.* 1979). This is the easiest and most used interpolation scheme. The divergence reduction technique of Endlich (1967) has the advantage over the variational technique of Sasaki (1970) in that the it does not require boundary conditions for the continuity equation. The former technique also reduces the divergence to much lower values. The suggestion of Liu and Goodin (1976), to keep the velocity fixed (or partially fixed) at weather station grid points, appears to be more realistic than the fixed vorticity technique of Endlich (1967). It was therefore decided to use the fixed station velocity technique for both the surface and outer layer, as applied by Goodin *et al.* (1980).

Although Lagrangian trajectory models generally require less computation effort than Eulerian grid models, they have many limitations. The Gaussian plume and puff models are derived under very strict and not always practical conditions. Modifications to include wind shear are based on intuition and are hence highly parameterised. Random motion methods, on the other hand, can accommodate wind shear, and spatial and temporal variations of characteristic parameters, but they generally require a considerable amount of computer memory and make it difficult to use for multiple sources. Grid methods allow rigorous treatment of the effects of variable boundary conditions and variations of wind and diffusivity structures. These models can also treat non-linear chemical processes. However, the few analytical expressions, derived from the advection-diffusion equation, are very limited in their usage. Most numerical approximations of the advection-diffusion equation have the disadvantage of losing accuracy as a result of time and space

124

discretisations. The moments method reduces the three-dimensional partial differential equation to two-dimensional (Mulholland 1977, 1980) or one-dimensional (Saffman 1962) equations describing the characteristic parameters of the distribution (means, variances, skewness and flatness). A suitable numerical method is used to solve these equations. The disadvantage of the K-theory is its inability to treat the eddy diffusivity properly as the cloud grows, especially during convective conditions. This is as a result of first-order closure approximations. Higher-order and non-local closure models can be used to overcome this problem. However, higher-order closure models are generally complicated and difficult to implement, resulting in greater computation time. The spectral diffusivity assumption, introduced by Berkowitz and Prahm (1979), is a promising alternative, and can be applied to the advection-diffusion equation when using a pseudo-spectral method such as proposed by Christensen and Prahm (1976). This theory and other non-local closure theories are still relatively young and developing, but deserve serious attention.

Considering the many suggestions, it remains a difficult task to choose a model, or to develop a new theory. Trajectory models are only suitable under simplified conditions. Analytical expressions based on the advection-diffusion equation suffer from too many limitations. A numerical solution of the advection-diffusion equation seems to be the only answer. Pseudo-spectral methods, applying the spectral diffusivity assumption, seem very promising. However, the moments method has two distinct advantages: (1) the reduction of a three-dimensional grid system to a two- or one-dimensional system, resulting in a reduction of storage and computational requirements; and, (2) the concentration distribution can be reconstructed using an analytical expression.

Often parts of the atmosphere will contain no pollutants, resulting in unnecessary storage of concentration values at the corresponding grid points. The moments method, on the other hand, provides the parameters _describing_ the distribution and not grid point concentrations. Storage requirements are therefore reduced considerably. Incorporating the solved moments into a suitable distribution equation (_e.g._ Gaussian), allows high resolution when

reconstructing the concentration distribution.Conventional contouring routines require values (altitude or concentration) at regular intervals in a fixed grid-matrix. The contour path is then found by interpolating between these values. This technique necessarily requires considerable memory, especially when fine resolution is required. Calculating the concentration for each grid point is also time consuming. Dayhoff (1963) described an algorithm for drawing contours of data in a two-dimensional array. This program is also explained in Monro (1983). The contouring program follows a contour from a starting point in one or two continuous movements (depending on whether the contour left the boundary of the drawing). Another routine (Monro 1983) is where four grid points, in a square, are considered in isolation. If a contour exists inside, it will be drawn from the one side to the other. Squares are traversed in rows and columns. These paths eventually combine to form the complete picture. A disadvantage of the latter technique is that line styling or smoothing is difficult to improve.

A contouring method is now proposed were the contour is followed from a starting point in one continuous movement (similar to Dayhoff (1953)), but only calculating the concentration in the neighbourhood of the contour, thus avoiding the storage of any concentrations. This also reduces the computation of unnecessary points. Line styling is easy to implement . The only disadvantage with this method is that <u>dosages cannot be accomodated</u> since concentrations are not stored.

Having identified the various aspects of the package, a summary of the proposed program is presented (Figure 4.1.). The five modules are explained in more detail in the rest of the chapter. They are :

(a) INSTAL - specification of all fixed parameters;
(b) PREMET - meteorological subprogram to determine the parameters for wind and diffusivity profiles from measurements;
(c) METPAC - construction of a three-dimensional wind field;
(d) DSPRSN - numerical treatment of the dispersion process; and,
(e) ISPLTH - isopleth drawing routine and other output from the package.

Figure 4.1. A simplified flowchart of the WIZARD package.
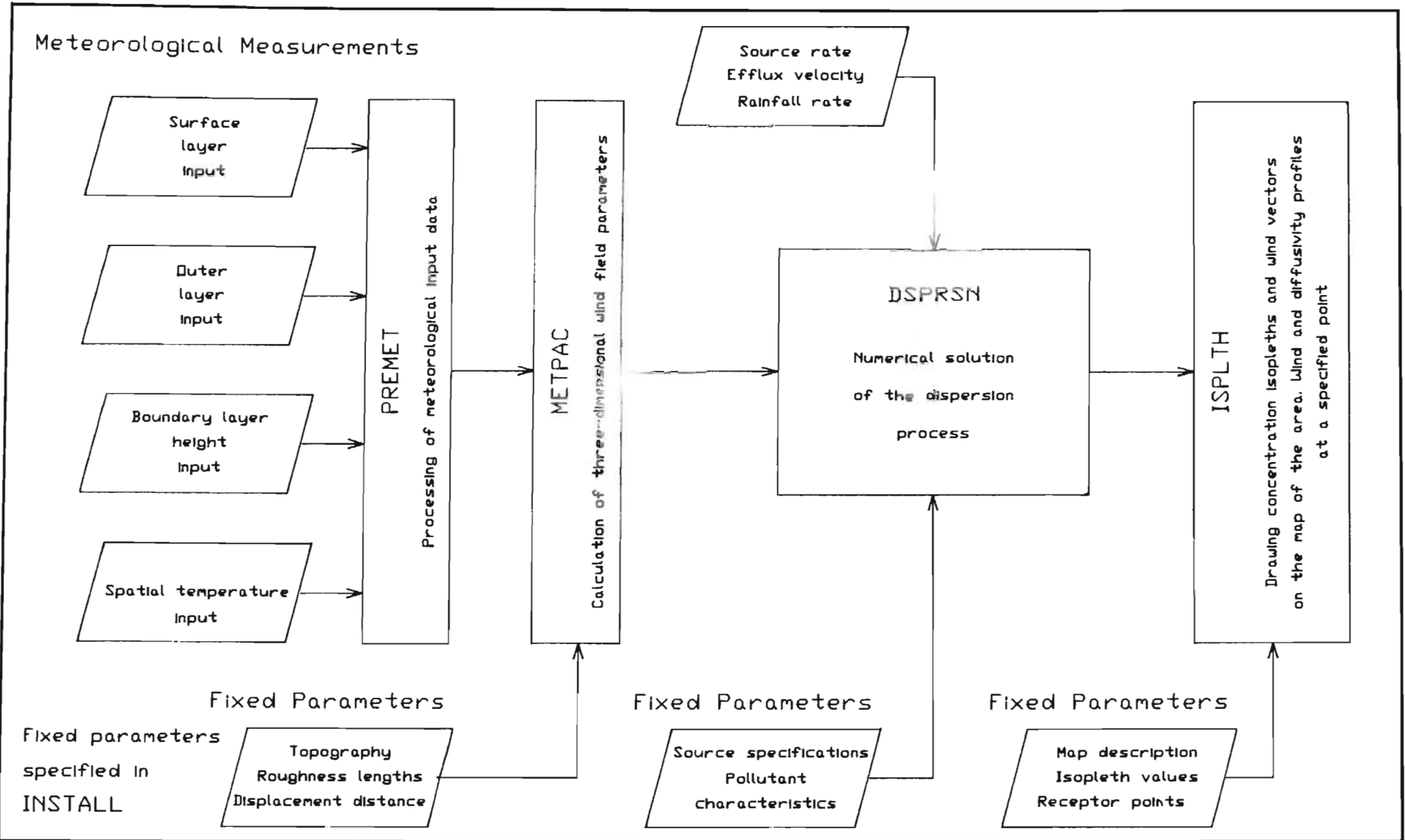
4.1. THE WIND FIELD MODEL

The planetary boundary layer is divided into three layers: the surface layer and two layers in the outer layer . The parameters describing these layers are defined in Figure 4.2. It is assumed that the surface layer depth is a tenth of the boundary layer height, as used by Jennekes and Lumley (1972) and many others, *i.e.*,

$$h_s(x,y,t) = 0,1h_p(x,y,t) \qquad (4.1)$$

Notice that the parameters h_p', h_m' and h_s' are referenced to sea level. The outer layer is divided into two layers equal in depth, Δh_0.

It is widely accepted that the similarity theory of Monin and Obukhov (1954) describes the wind and temperature profiles accurately in the surface layer. A relatively simple outer layer wind profile is assumed. This profile is based on the proposals of Arya (1984) and Wetzel (1982), for stable conditions (Figure 1.2(a)), and a modification of Garratt *et al.* (1982), Arya (1978) and Wyngaard *et al.* (1974), for unstable conditions (Figure 1.2(b)) (*i.e.*, excluding the entrainment zone). The parameters describing the wind profile are defined in Figure 4.3.

The mathematical representations for the wind and temperature profiles, in the surface layer, are according to the similarity theory. The wind profile is defined by (Section 2.1.)

$$u = \frac{u_*}{K} \Psi_m(\frac{z}{L}) \qquad (2.7)$$

and the temperature profile, by

$$\theta = \frac{\theta_*}{K} \Psi_h(\frac{z}{L}) + \theta_0 \qquad (2.8)$$

where the integral forms for the universal functions, $\phi_m(\frac{z}{L})$ and $\phi_h(\frac{z}{L})$
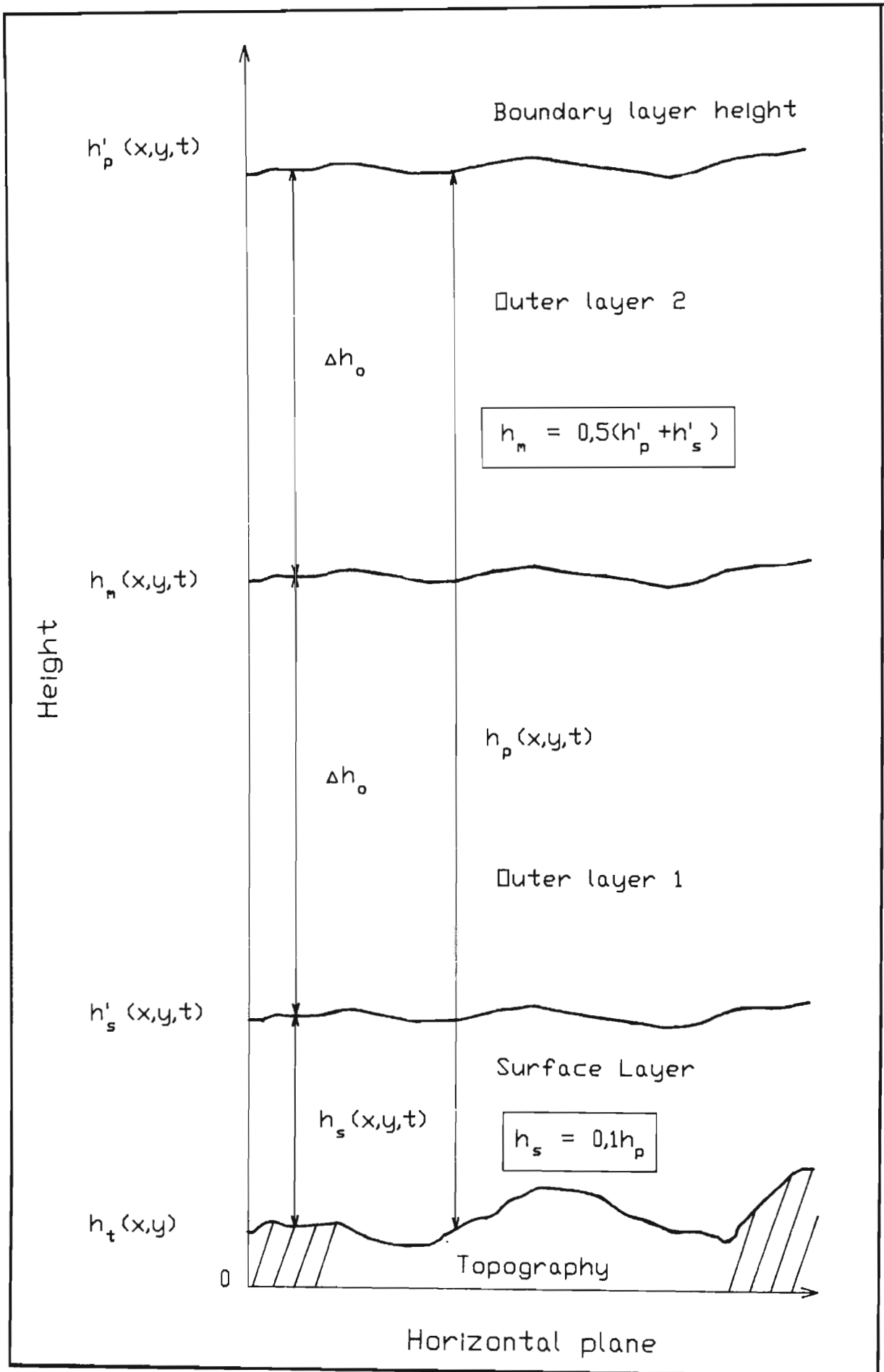
Figure 4.2. A definition of the layers in the wind field model.
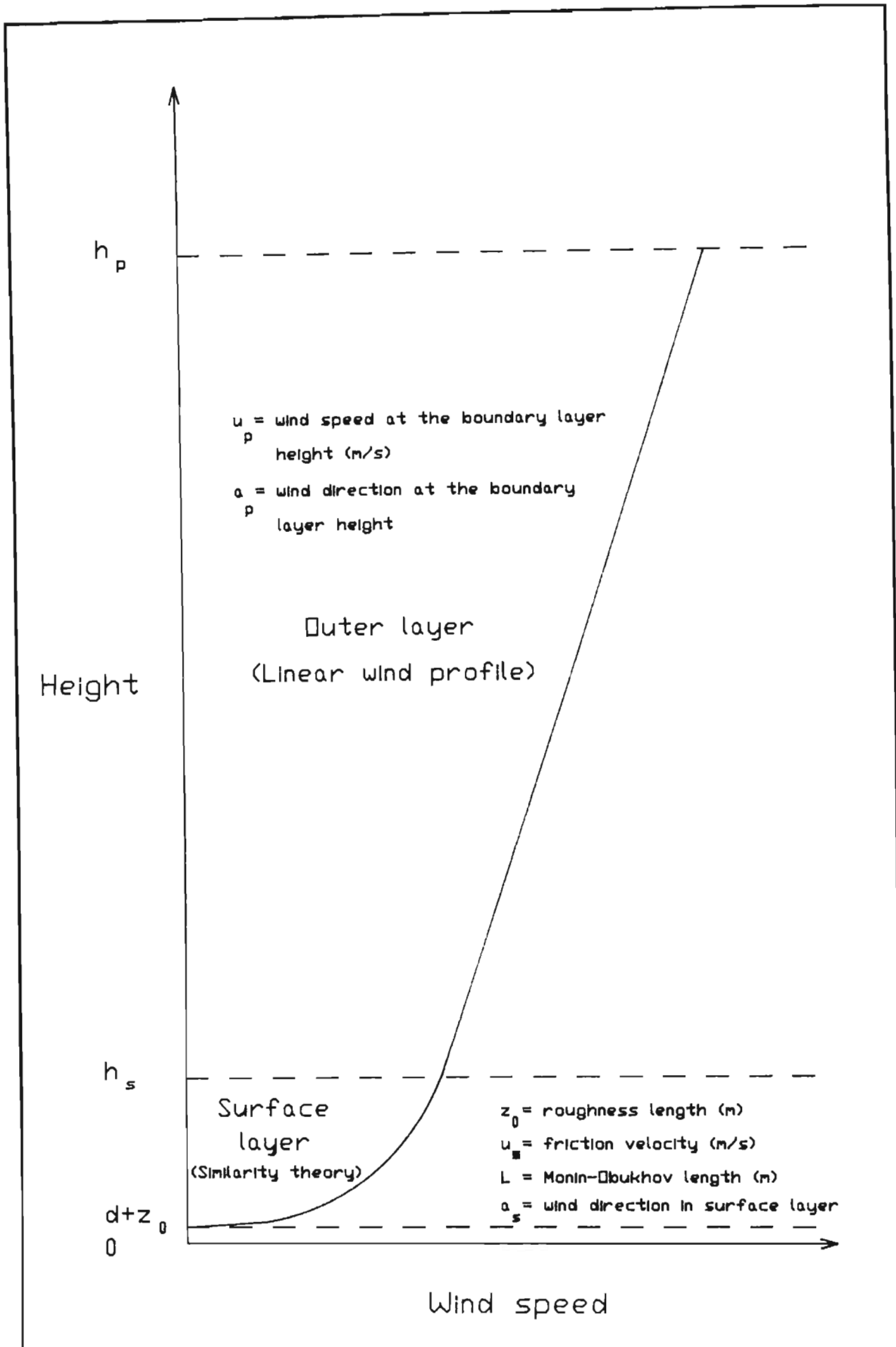
Figure 4.3. A summary of the parameters describing the wind profile in the atmospheric boundary layer.

TABLE 4.1. A summary of the universal functions and corresponding integral forms for wind and temperature profiles.

$\xi = \dfrac{z}{L}$

very stable

$$\phi_m = \phi_h = 1 + \beta \qquad \text{(Webb 1970: } \beta = 5,2)$$

$$\Psi_m = \phi_m \ln\frac{z}{z_0}$$

1

stable

$$\phi_m = \phi_h = 1 + \beta\xi \qquad \text{(Webb 1970: } \beta = 5,2)$$

$$\Psi_m = \ln(\frac{z}{z_0}) + \frac{\beta}{L}(z - z_0) \qquad \text{(Table 2.3))}$$

neutral   0

$$\phi_m = 1$$

$$\Psi_m = \ln\frac{z}{z_0}$$

moderately unstable

$$\phi_m = (1 - \gamma\xi)^{-\frac{1}{4}} \qquad \text{(Dyer and Hicks 1970: } \gamma = 16)$$

$$\phi_h = (1 - \gamma_2\xi)^{-\frac{1}{2}} \qquad \text{(Dyer and Hicks 1970: } \gamma_2 = 16)$$

$$\Psi_m = 2(\tan^{-1}p - \tan^{-1}p_0) - \ln\left\{\frac{p+1}{p-1} \cdot \frac{p_0-1}{p_0+1}\right\}$$

$$\Psi_h = \gamma_1\ln\left\{\frac{q-1}{q+1} \cdot \frac{q_T+1}{q_T-1}\right\} \qquad \text{(Table 2.3)}$$

where $p = (1-\gamma\frac{z}{L})^{-\frac{1}{4}}$ and $q = (1-\gamma_2\frac{z}{L})^{\frac{1}{2}}$

$\qquad p_0 = (1-\gamma\frac{z_0}{L})^{-\frac{1}{4}} \qquad q_T = (1-\gamma_2\frac{z_T}{L})^{\frac{1}{2}}$

−1

convective

$$\phi_m = (1 - \gamma\xi)^{-\frac{1}{3}} \qquad \text{(Carl \textit{et al.} 1973: } \gamma = 16)$$

$$\Psi_m(\xi) = \frac{1}{2}\ln\left[\left\{\frac{r-1}{r_0-1}\right\}^3 \frac{r_0{}^3-1}{r^3-1}\right]$$

$$+ 2\left[\tan^{-1}\frac{2r+1}{\sqrt{3}} - \tan^{-1}\frac{2r_0+1}{\sqrt{3}}\right]$$

where $r = (1-\gamma\frac{z}{L})^{\frac{1}{3}}$ and $r_0 = (1-\gamma\frac{z_0}{L})^{\frac{1}{3}}$

are given by $\tau_m(\frac{Z}{L})$ and $\tau_h(\frac{Z}{L})$. Some integral forms for stable, neutral and unstable conditions are given in Table 2.3. Table 4.1. contains the universal functions and the corresponding integral forms used in this study.

Above the surface layer, the wind profile follows a linear relationship. The wind speed is given by

$$u = (u_g - u_s)(\frac{z - h_s}{h_p - h_s}) + u_s \qquad (4.1a)$$

and the wind direction is given by

$$\alpha = (\alpha_p - \alpha_s)(\frac{z - h_s}{h_p - h_s}) + \alpha_s \qquad (4.1b)$$

where
u_g = wind speed at the planetary boundary layer height,

u_s = wind speed at the surface layer height,

α_p = the angle of the wind at the boundary layer height,

α_s = the angle of the wind in the surface layer

Sections 4.1.1. and 4.1.2. describe how the parameters for the wind profiles (equations (2.7) and (4.1)) are calculated from meteorological measurements.

4.1.1. PREMET - Meteorological Subprogram for Determining Wind Field Parameters

This module is considered as the "input processor". Three measurement categories are introduced:

(a) surface layer measurements

(b) outer layer wind measurements

(c) boundary layer height measurements

Each category is further subdivided to accommodate various measurement options. These options are discussed in the sections given below.

Other variables which need to be specified, include:

(a) Land/sea (lake) temperatures if necessary
(b) rainfall rates at certain points

As this is the first part of the program, all fixed parameters, such as topography, roughness lengths, weather station and source positions, and model parameters (*e.g.* grid sizes, and divergence tolerance values), are retrieved from the files created by INSTALL. It is also necessary to specify the following source variables :

(a) source strength
(b) source exit velocity
(c) temperature of source exit gases

4.1.1.1. Surface Layer Measurements.

A brief discussion of each of the measurement options is presented. Eight possibilities are identified :

(a) wind velocity at one height and cloud cover;
(b) wind velocity at one height and the variance of the azimuth;
(c) wind velocity at one height, cloud cover and the average temperature;
(d) wind velocity at one height and temperature at two heights;
(e) wind velocity at two heights and temperature at two heights;
(f) wind velocity at several heights;
(g) wind velocity at one height and temperature at several heights;
(h) wind velocity and temperature at several heights.

For an accurate description of the wind profile, the roughness length

must be specified as an independent variable. Any appropriate method described in Section 2.3.1, can be used to estimate z_0 and d.

If roughness length values and zero displacement distances are not known for every grid point, sparse values are interpolated. The logarithmic nature of the roughness length can be observed from Figure 2.3. Based on this idea, a logarithmic interpolation is used for both z_0 and d. So for the roughness length at grid point i, j and sparse values at k,

$$z_{0_{ij}} = \exp \left\{ \sum_{k=1}^{N} \frac{(\ln z_{0_k}) W(r_{k,ij})}{W(r_{k,ij})} \right\} \qquad (4.2)$$

where the inverse square weighing function is used

$$W(r_{k,ij}) = \frac{1}{r_{k,ij}^2}$$

and $r_{k,ij}$ is the distance from sparse point k to grid point (i,j). A background on the techniques for determining the parameters u_* and L is given in Section 2.3.2. and only deviations from these methods are discussed below.

4.1.1.1.1. Wind velocity and cloud cover

A slightly modified version of the Shir and Shieh (1974) method is used for this measurement option. An attempt to represent the information in Table 2.6. as linear relationships with wind speed and the appropriate weather conditions as independent variables, results in the following expressions for s :

134

<u>Daytime: (1 hour after sunrise)</u>   <u>Incoming solar radiation</u>

<u>(1 hour before sunset)</u>

$s = 0,4167u - 3,5833$ strong

$s = 0,3905u - 2,9952$ moderate

$s = 0,3357u - 2,3762$ weak

$$(4.3a)$$

<u>Transient period: 1 hour before sunset</u>

$s = 0,1213u - 1,0532$

$$(4.3b)$$

<u>Transient period: 1 hour after sunrise</u>

$s = -0,1244u + 1,0347$

$$(4.3c)$$

<u>Nighttime: sunset to sunrise</u>   <u>Cloud cover</u>

$s = -0,2167u + 1,5333$ $\leq 0,5$

$s = -0,3595u + 2,6881$ $> 0,5$

$$(4.3d)$$

The correlation coefficients for these relationships are all above 0,9. As indicated by the Pasquill stability classification, wind speeds above 8m/s result in neutral conditions. Maul's (1980) relationship for net solar radiation, R, is used to quantify the categories: "strong", "moderate" and "weak", *i.e.*,

$$R = 950 \; r_c \sin\nu \qquad (4.3e)$$

as given in equation (2.60) (r_c is a function of cloud cover, Appendix B.1. It follows that when

$634 \leq R \leq 950$ "strong"

$318 \leq R \leq 633$ "moderate" (4.4)

$0 \leq R \leq 317$ "weak"

L is obtained from equation (2.55) with the s values supplied by equation (4.3). The friction velocity is then determined from equation (2.7) using the universal functions supplied in Table 4.1.

4.1.1.1.2. Wind velocity and azimuth variance

A similar treatment to Shir and Shieh (1974) is adopted for the second type of measurement. The parameter s is defined according to the wind direction standard deviation method (Section 2.3.2., Table 2.8). This is given in Table 4.2.

TABLE 4.2. Definition of the stability parameter, s, using the azimuth standard deviation.

Stability Class	s	θ
A	-3	$22,5 < \sigma_\theta$
B	-2	$17,5 < \sigma_\theta \leq 22,5$
C	-1	$12,5 < \sigma_\theta \leq 17,5$
D	0	$7,5 < \sigma_\theta \leq 12,5$
E	+1	$3,75 < \sigma_\theta \leq 7,5$
F	+2	$2,0 < \sigma_\theta \leq 3,75$
G	+3	$\sigma_\theta \leq 2,0$

Linear interpolation between the categories gives the appropriate s-values. L is determined from equation (2.55) and u_* from equation (2.7).

4.1.1.1.3. Wind velocity, cloud cover and temperature

When the wind velocity, the cloud cover and the average temperature is known, the energy budget method of De Bruin and Holtslag (1982) is used (Section 2.3.2.2.). A detailed treatment of the necessary equations is given in Appendix B.2. The sensible heat flux is determined from equation (2.59). The friction velocity is then estimated from equation (2.7), initially taking the inverse of the Monin-Obukhov length to be zero. This calculated friction velocity is then used, together with the sensible heat flux, to determine an improved Monin-Obukhov length from equation (2.4). The iteration process proceeds until the difference in the friction velocity is less than 0,01 per cent.

4.1.1.1.4. Wind velocity and two temperature measurements

There are three possibile ways to specify two temperatures and a wind measurement, *viz*,

(a) wind velocity and top temperature at the same height
(b) wind velocity and temperatures at different heights
(c) wind velocity and temperature on different masts.

When all the measurements are on different masts, it is assumed that the temperatures vary less spatially than the wind speed. Temperatues are then assumed at the corresponding heights on the wind mast.

When the wind velocity and top temperature are at the same height, the bulk Richardson number (equation 2.67(b)) relates the Monin-Obukhov length to the measured quantities. It was decided to use the exact integral forms rather than the approximations of Joynt and Blackman (1976), Shultz (1979), or Barker and Baxter (1975) (Section 2.3.2.3.). $\frac{1}{L}$ is initially taken as zero (neutral conditions). An improved value is obtained from equation (2.68) and

the iteration proceeds until the error in the estimation of u_* is less than 0,01 per cent.

The previous method requires that the wind speed and top temperature be at the same height. This is generally not the case and the definition of the bulk Richardson number, as given by equation (2.67a), is used. The same iterative procedure as above is used to estimate $\frac{1}{L}$ and u_*.

4.1.1.1.5. Two wind and temperature measurements

The same treatment as in Section 4.1.1.1.4 is adopted when measurements of wind and temperature are on different masts. Since two wind speed and temperature measurements are available, the approximate Richardson number, as defined by equation (2.63) (Paulson 1970), can be used. The Monin-Obukhov length is related to the Richardson number according to equation (2.64). The approximations of Binkowski (1975) are used to calculate $\frac{1}{L}$.

Berkowicz and Prahm (1982) indicated that non-trivial solutions exist only when

$$Ri \ < \ 0,2$$

Above this value, neutral conditions exist.

4.1.1.1.6. Wind and temperature profiles

When more than two wind and/or temperature measurements are available at different heights, the numerical treatment of Lo (1978) is adopted (Appendix C). This treatment is based on the least-square error method. Wind and temperature measurements are treated individually, even when supplied on the same mast. The resulting Monin-Obukhov

length is then the average obtained from the two profiles. The atmospheric stability condition is easily determined from the temperature profile. The situation is more difficult when only a wind profile is available. Unstable conditions normally exist during daytime and stable conditions during nighttime. A more general method is proposed. The approximate quadratic equation for unstable conditions, given by Shultz (1979), is used to calculate an initial value for L. Lo's (1978) least square-error method, when applied to to this approximation, results in a cubic equation. The analytical solution to this cuibic equation is given in Appendix D.1. It is found that the closest root to zero gives the best initial condition. It was also discovered that stable conditions exist when this root is positive. The initial value of L, obtained from Shultz's approximation, is therefore used to establish the stability condition.

The least-square-error forms derived from the similarity forms are also given in Appendix D. An explicit equation is derived for stable conditions. The secant method was used to establish the Monin-Obukhov length during unstable conditions (Appendix D.3).

4.1.1.2. Outer Layer

Three possibilities are accounted for:

    (a) no upper air data
    (b) one wind speed at a height above the surface layer
    (c) more than one wind speed above the surface layer

When no upper air measurements are available, parametric forms, based on similarity theory, are used. The parametric forms proposed by Hess *et al.* (1981) are used for neutral conditions (equation (2.37)) and the equations proposed by Yamada (1976) for non-neutral conditions (equation (2.38)). These equations provide the average wind components in the boundary layer.

When only one measurement is available in the outer layer, a linear equation is fitted through this point and the wind speed at the surface layer height, below this point.

The outer layer wind profile is represented by equation (4.1a). With wind speeds available at different heights, a linear regression of the data points, using the method of least-squares, provides the parameters for the equation.

4.1.1.3. Boundary Layer Height

The available options to specify the boundary layer height are:

  (a) no upper-air measurement
  (b) temperature profile
  (c) Doppler acoustic sounder
  (d) user-estimates of the boundary layer height

For the case where no measurement is available and no user-supplied estimates are given, Zilitinkevich's (1972) diagnostic relationships are used. These are: equation (2.41), for neutral conditions, and equation (2.42), for stable conditions. During unstable conditions, the suggestions of Davenport (1965) (Section 2.2.4) are used.

If hourly upper air temperature measurements are available and in sufficiently small vertical intervals, the inversion height is easily inferred from the change in temperature gradient. When, however, long time intervals exist between temperature readings (*e.g*, early morning and early evening soundings) the growth of the mixing layer is calculated using the prognostic equation suggested by Van Dop *et al.* (1982) (equation (2.46)). During stable and neutral conditions, the diagnostic proposals discussed in the previous paragraph are used.

Specification of the vertical intensity signal is required when Doppler acoustic soundings are available. The height at which the

most vertical intensity signals are observed, corresponds to an inversion height (Wyckoff *et al.* 1973).

Fixed or time-variant boundary layer heights can also be supplied by the user.

4.1.2. METPAC-Construction of a Three-Dimensional Wind Field

The wind profile parameters in figure 4.1., specified at each grid point in a two dimensional matrix of m by n points, define the three-dimensional wind field. The purpose of this module is to calculate these parameters, given the parameters determined at the measuring points in PREMET. The atmospheric boundary layer is divided into three horizontal layers, (figure 4.2). The surface layer with thickness h_s, is the lowest layer. The two outer layers are of equal thickness. The first of these outer layers lies between h_s and $(\frac{h_s + h_p}{2})$. The second layer lies between $\frac{h_s + h_m}{2}$ and h_p. The following steps comprise the basic algorithm:

STEP 1.: Calculate the boundary layer height at each horizontal grid point. Interpolate from measurement points if necessary using a $\frac{1}{r}$ weighting function (inverse linear).

STEP 2.: **The surface layer wind field.**
   STEP 2.1. Calculate the average wind speed at all measuring points using the profile parameters determined in PREMET and the integrated forms of the profiles given in Table 4.1.
   STEP 2.2. Determine the initial surface wind field from the sparse averaged wind measurements employing a $\frac{1}{r^2}$ weighting function.
   STEP 2.3. Introduce topography into the forcing function, if supplied, using the method of Scholtz and Brouckaert (1978).

141

STEP 2.4. Include temperature anomalies according to the method of Anderson (1971), if necessary.

STEP 2.5. Construct the surface layer wind field and reduce the anomalous divergence using the fixed station velocity technique of Liu and Goodin (1976).

STEP 2.6. Determine the profile parameters u_* and L for each grid point.

STEP 3.: **Outer layer wind field.**

STEP 3.1. Transform the sea-level coordinate system to a coordinate system in which the vertical coordinate has its origin at the surface layer height.

STEP 3.2. Determine the average wind speed for each of the two outer layers at the upper air measuring points.

STEP 3.3. Interpolate/extrapolate the average wind speeds determined in STEP 3.2. to other grid points using a $\frac{1}{r}$ weighting function.

STEP 3.4. Follow the method of Goodin *et al*. (1980) to construct a three-dimensional wind field. Firstly, apply some smoothing to the initial wind field according to the empirical rules supplied by Goodin *et al*. (1980).

STEP 3.5. Solve the three-dimensional continuity equation.

STEP 3.6. Determine the parameters describing the outer layer profile *i.e.*, u_g and α_p.

The above steps are explained in more detail in the following sections.

4.1.2.1. The Surface Layer Wind Field.

It is assumed that the top of the boundary layer is not affected much by the topography due to the general stability of the atmosphere during stable conditions, and the fact that $h_p \gg h_t$ during unstable conditions. The boundary layer height, h_p, determined in PREMET, is

142

with reference to the ground level. The height at each grid point is interpolated from the measured heights using the following formula:

$$h_p(i,j) = \frac{\sum\limits_{k=1}^{N} (h_p + h_t)_k W(r_{k,ij})}{\sum\limits_{k=1}^{N} W(r_{k,ij})} - h_t(i,j) \qquad (4.5)$$

where $\quad W(r_{k,ij}) = \dfrac{1}{r_{k,ij}}$

The surface layer wind profiles are described by the similarity relationships given in Table 4.1. To implement the divergence reduction technique, it is necessary to calculate the average wind velocities within the surface layer. Detailed derivation of the average wind speed in the surface layer is given in Appendix F. During non-neutral conditions, the average wind speed is given by the contributions of the moderately stable (unstable) layer up to $|L|$, and the very stable (convective) layer form $|L|$ up to the surface layer height, h_s.

The average wind speed in the unstable surface layer is given by:

$$\bar{u} = \delta \bar{u}_u + (1-\delta)\bar{u}_c \qquad (4.6)$$

where $\quad \delta = \dfrac{|L|}{h_s}$

$\bar{u}_u$ = average wind speed for the layer between z_0 and $|L|$

$\bar{u}_c$ = average wind speed for the layer between $|L|$ and h_s

The average wind speed for the moderately unstable layer, $\bar{u}_u$, is given by

$$\bar{u}_u = \frac{1}{|L| - z_0} \int_{z_0}^{|L|} \frac{u_*}{k} \varphi_m(\frac{z}{L})\, dz$$

$$= \frac{u_*}{k(|L|-z_0)} \left\{ \frac{4L}{3\gamma}(b_L^3 - b_0^3) + |L| \left[2(\tan^{-1}b_L - \tan^{-1}b_0) - \ln\left(\frac{b_L+1}{b_L-1}\frac{b_0-1}{b_0+1}\right) \right] \right\}$$

(4.7)

where $\quad b_L = (1 - \gamma\frac{|L|}{L})^{\frac{1}{4}} = (1 + \gamma)^{\frac{1}{4}}$

$\quad\quad\quad b_0 = (1 - \gamma\frac{z_0}{L})^{\frac{1}{4}}$

and $\quad\quad \gamma = 16 \quad$ (Dyer and Hicks 1970)

The average wind speed for the upper, convective part of the surface layer (if any) is given by

$$\bar{u}_c = \frac{1}{h_s - |L|} \int_{|L|}^{h_s} \frac{u_*}{k} \varphi_m(\frac{z}{L}) dz$$

$$= \frac{u_*}{k(h_s - |L|)}(I(h_s) - I(|L|))$$

(4.8)

with

$$I(z) = \frac{3}{2}\left\{ \frac{L}{\gamma}(x + \frac{x^2}{2} + \frac{x^3}{3}) + z\ln(\frac{x-1}{x_0-1}) \right\}$$

$$+ \frac{z}{2}\left\{ \ln(\frac{z_0}{z}) + 1 \right\} + 2z\tan^{-1}y_0$$

$$- \frac{3\sqrt{3}}{8} \frac{L}{\gamma_1} \left\{ 2[y^3 - 2\sqrt{3}(1 + y) + 4y]\tan^{-1}y \right.$$

$$\left. - 3\ln(1 + y^2) + y(4\sqrt{3} - y) \right\}$$

where

$$x = (1 - \gamma\frac{z}{L})^{\frac{1}{3}} \quad \text{and} \quad y = \frac{2x + 1}{\sqrt{3}}$$

$$x_0 = (1 - \gamma\frac{z_0}{L})^{\frac{1}{3}} \quad\quad y_0 = \frac{2x + 1}{\sqrt{3}}$$

and $\quad\quad \gamma = 16$ (Carl *et al* 1973)

The average wind speed during stable conditions is:

$$\bar{u} = \delta\bar{u}_{st} + (1-\delta)\bar{u}_v \tag{4.9}$$

where $\quad \delta = \dfrac{L}{h_s}$

and $\quad \bar{u}_{st}$ = average wind speed in the layer z_0 to L

$\quad \bar{u}_v$ = average wind speed in the layer between L and h_s

The average wind speed for the moderately stable part is given by:

$$\bar{u}_{st} = \frac{1}{L - z_0} \int_{z_0}^{L} \frac{u_*}{k} \Psi_m\left(\frac{z}{L}\right) d_z$$

$$= \frac{u_*}{k(L - z_0)}\left\{L\left(\ln\frac{L}{z_0} - 1\right) + z_0 + \frac{\beta}{2L}(L - z_0)^2\right\} \tag{4.10}$$

where $\quad \beta = 5,2 \quad$ (Webb 1970)

The wind speed for the very stable upper part of the surface layer is given by:

$$\bar{u}_v = \frac{1}{h_s - L} \int_{L}^{h_s} \frac{u_*}{k} \Psi_m\left(\frac{z}{L}\right) d_z$$

$$= \frac{u_*(1+\beta)}{k(h_s - L)}\left\{h_s\left(\ln\frac{h_s}{z_0} - 1\right) - h_s\left(\ln\frac{h_s}{z_0} - 1\right)\right\} \tag{4.11}$$

where $\quad \beta = 5,2 \quad$ (Webb 1970)

Finally, the wind speed during neutral conditions is given by

$$\bar{u} = h_s \ln\frac{h_s}{z_0} - h_s + z_0 \tag{4.12}$$

The initial estimate of the surface layer wind field is obtained by interpolating the average wind speeds at the measuring points to the grid points according to the weighting function suggested by Cressman (1959) .

$$W(r_{k,ij}) \; = \; \frac{R^2 - r^2_{k,ij}}{R^2 + r^2_{k,ij}} \qquad R > r_{k,ij} \qquad (2.83)$$

where R, for an area A with N stations, is (Stephens and Stitt 1970)

$$R \; = \; \sqrt{A/N}$$

The forcing function is then calculated (equation (2.77)) to introduce topography (Scholtz and Brouckeart 1978) and temperature anomalies (Anderson 1971) to the surface layer wind field:

$$\Psi(x,y) \; = \; \left[\frac{1}{h_s(x,y)-h_t(x,y)}\right] U \cdot v\{h_t(x,y)-h_s(x,y)\} + \frac{A(T_g-\overline{T})}{h_s(x,y)}$$

$$= \left[\frac{1}{h_s(x,y)-h_t(x,y)}\right]\left[\overline{u}(x,y)\frac{\partial}{\partial x}\{h_t(x,y)-h_s(x,y)\} \right.$$

$$\left. - \overline{v}(x,y)\frac{\partial}{\partial y}\{h_t(x,y)-h_s(x,y)\}\right] + \frac{A(T_g-\overline{T})}{h_s(x,y)}$$

$$(4.13)$$

or in finite difference form,

$$\Psi(i,j) \; = \; \left[\frac{1}{h_s(i,j)-h_t(i,j)}\right]$$

$$\times \left[\overline{u}(i,j)\left\{\frac{h_t(i+1,j)-h_s(i+1,j)-h_t(i-1,j)+h_s(i-1,j)}{\Delta x}\right\}\right.$$

$$\left. - \overline{v}(i,j)\left\{\frac{h_t(i,j+1)-h_s(i,j+1)-h_t(i,j-1)+h_s(i,j-1)}{\Delta y}\right\}\right]$$

$$+ \frac{A(T_g-\overline{T})}{h_s(i,j)} \qquad\qquad (4.14)$$

Poisson's equation (Anderson 1971)

$$\frac{\partial^2 \phi}{\partial x^2} + \frac{\partial^2 \phi}{\partial y^2} = \phi(x,y)$$

can be solved using a numerical method such as the Successive Over-Relaxation method (S.O.R) or the Alternative Direction Implicit (A.D.I.) method. However, these methods require specification of the boundary conditions. If we now consider the definition of the potential function *i.e.*,

$$\bar{u} = \frac{\partial \phi}{\partial x}$$

and   (4.15)

$$\bar{v} = \frac{\partial \phi}{\partial y} \quad ,$$

equation (2.74) can be rewritten as

$$\frac{\partial \bar{u}(x,y)}{\partial x} + \frac{\partial \bar{v}(x,y)}{\partial x} = \Psi(x,y)$$

or in finite difference form

$$\frac{\bar{u}(i+1,j) - \bar{u}(i-1,j)}{\Delta x} + \frac{\bar{v}(i,j+1) - \bar{v}(i,j-1)}{\Delta y} = \Psi(i,j) \qquad (4.16)$$

When in this form, the numerical method first proposed by by Endlich (1967) and later modified by Liu and Goodin (1976), is used. Equation (4.16) then becomes

$$\frac{\bar{u}^n(i+1,j) - \bar{u}^n(i-1,j)}{\Delta x} + \frac{\bar{v}^n(i,j+1) - \bar{v}^n(i,j+1)}{\Delta y} - \Psi_{(ij)} = \epsilon^n_{(ij)}$$

(4.17)

where $\epsilon^n(i,j)$ is the error at grid point i,j. The improved wind velocity components are given by

147

$$\bar{u}^{n+1}(i+1,j) = \bar{u}^{n}(i+1,j) + f(i+1,j)\tilde{u}^{n}(i,j)$$

$$\bar{u}^{n+1}(i-1,j) = \bar{u}^{n}(i-1,j) - f(i-1,j)\tilde{u}^{n}(i,j)$$

$$\bar{v}^{n+1}(i,j+1) = \bar{v}^{n}(i,j+1) - f(i,j+1)\tilde{v}^{n}(i,j)$$

$$\bar{v}^{n+1}(i,j-1) = \bar{v}^{n}(i,j-1) + f(i,j-1)\tilde{v}^{n}(i,j)$$

<div align="right">(4.18)</div>

where

$$\tilde{u}^{n}(i,j) = -\epsilon^{n}(i,j)\Delta x/[f(i+1,j) + f(i-1,j)]$$

$$\tilde{v}^{n}(i,j) = -\epsilon^{n}(i,j)\Delta y/[f(i,j+1) + f(i,j-1)]$$

It was stated in equation (2.98) that

$$f(i,j) = 1 \text{ at a grid point with a measuring station;}$$

and,

$$= 0 \text{ elsewhere.}$$

$\epsilon(i,j)$ is minimised to meet the criterion specified by the user (usually 10^{-6}). It now remains to determine the profile parameters u_* and L at each grid point. The following procedure is proposed:

The stability parameter s, as defined by Shir and Shieh (1974) (equation (2.57)), is calculated for each measuring point k

$$s_k = \text{sign}(L_k)\left[\frac{1}{b}\left(\frac{a}{\log_{10}\{d|L_k|\ln(1,2 + 10/z_{0_k})\}} - 1\right)\right]^{\frac{1}{c}} \quad (4.19)$$

where
$$a = 4$$
$$b = 1,3$$
$$c = 0,85$$
$$d = 0,216586$$

It is assumed that the parameter s varies less than L. A $\frac{1}{r}$ weighting function is used to interpolate s to grid points i,j.

The Monin-Obukhov length, L(i,j), is calculated from s(i,j) and

<div align="center">148</div>

$z_0(i,j)$. From equation (2.57),

$$\frac{1}{L(i,j)} = \text{sign}(s(i,j))\left[d\ln\left\{1,2 + \frac{10}{z_0(i,j)}\right\}\right]10^{f(s(i,j))} \qquad (4.20)$$

where $\quad f(s(i,j)) = \dfrac{-a}{1 + b|s(i,j)|^c}$

The constants a to d are given in equation (4.19).

The friction velocity for each grid point, $u_*(i,j)$, is then determined from $L(i,j)$ and the average wind speed relationships given by equations (4.6) to (4.12).

4.1.2.2. Outer Layer Wind Field.

To complete the specification of the three-dimensional wind field, it is necessary to determine the parameters describing the outer layer wind velocity profiles (equation (4.2)). As with the surface layer wind field, average wind speeds are calculated for each of the two outer layers. The average wind speed in the layer $h_2 - h_1$ is given by

$$\bar{u} = \frac{1}{h_2 - h_1}\int_{h_1}^{h_2}\left\{(u_p - u_s)\left[\frac{z - h_s}{h_p - h_s}\right] + u_s\right\}dz$$

$$= \frac{1}{2}\left[\frac{u_p - u_s}{h_p - h_s}\right](h_2 + h_1 - 2h_s) + u_s \qquad (4.21)$$

The heights for layer 1 are:

$$h_1 = h_s \qquad \text{and } h_2 = \frac{1}{2}(h_p + h_s),$$

and layer 2

$$h_1 = \frac{1}{2}(h_p + h_s) \text{ and } h_2 = h_p.$$

A similar expression holds for the average wind direction, $\bar{a}$, in the outer layer. Average wind components are calculated for each of the outer layer measuring points and interpolated (or extrapolated) to the grid points according to a three-dimensional $\frac{1}{r}$ weighting function.

The initial wind field components are smoothed using the five point filter given by equation (2.100). The empirical smoothing passes of Goodin *et al* (1980) (Section 2.4.2.3.) are adopted. The next step is to transform the continuity equation from the "sea-level"-coordinate system to the "surface layer height"-coordinate system. The transformation is:

$$
\begin{aligned}
x &= x \\
y &= y \\
p &= \frac{z - h_s'}{h_p' - h_s'}
\end{aligned}
\qquad (4.22)
$$

where h_p' and h_s' are as defined in figure 4.2. This is similar to the terrain-following coordinate transformation often used (Goodin *et al* 1980) in the solution of the three-dimensional continuity equation.

The intermediate height, h_m, is given by

$$
h_m = \frac{1}{2}(h_p' + h_s')
$$

and the corresponding height in the new reference frame is

$$
\begin{aligned}
\rho_m &= \frac{h_m - h_s'}{h_p' - h_s'} \\
&= \frac{\frac{1}{2}(h_p' + h_s') - h_s'}{h_p' - h_s'} \\
&= \frac{1}{2}
\end{aligned}
$$

This is indicated in in figure 4.4(b).
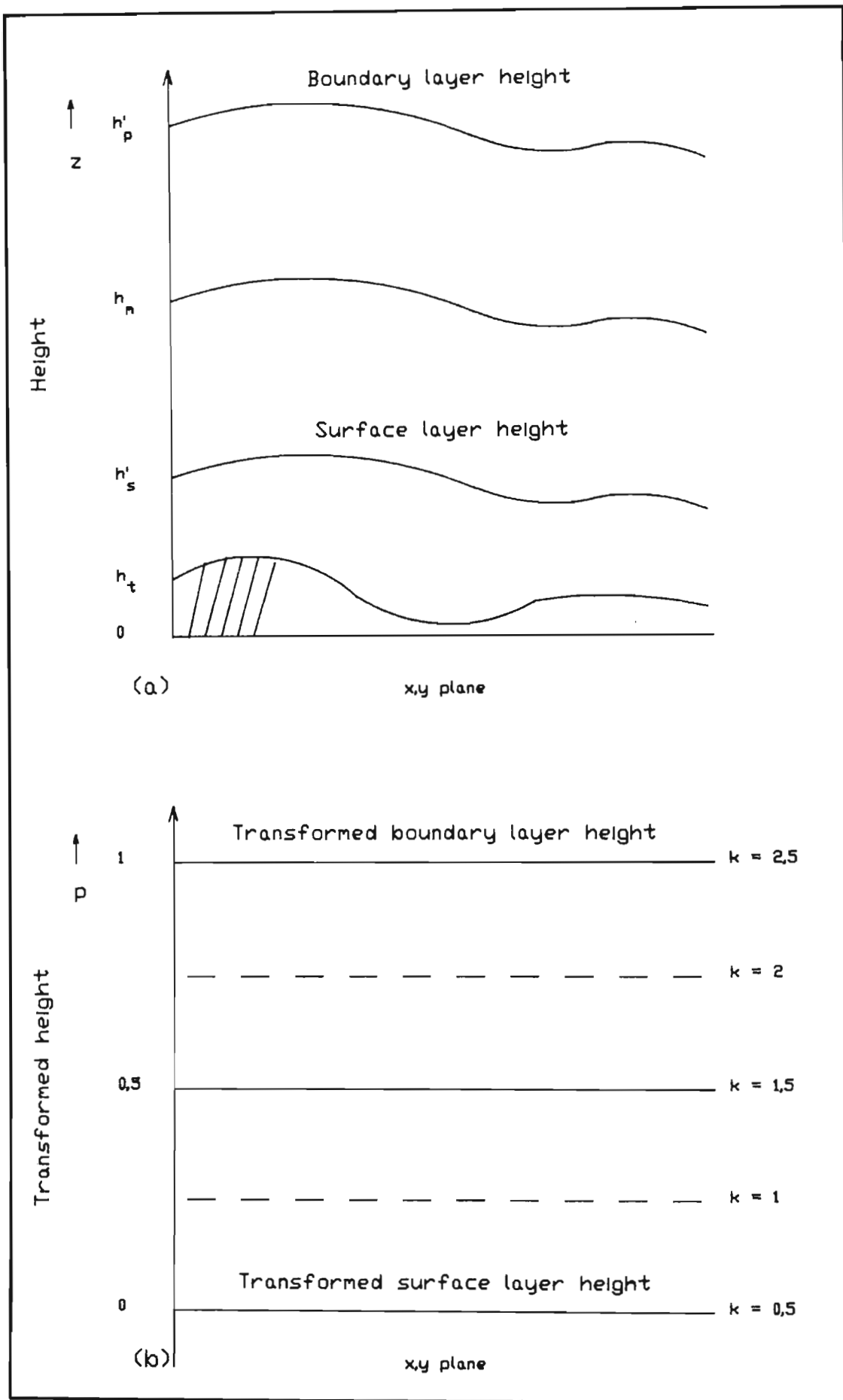
Figure 4.4. The transformation of a sea-level reference frame to a surface layer height reference frame.

If $h_p - h_s$ is denoted by Δh, the continuity equation (2.78) transforms to

$$\frac{\partial \bar{u}\Delta h}{\partial x} + \frac{\partial \bar{v}\Delta h}{\partial y} + \frac{\partial W}{\partial \rho} = 0 \qquad (4.23)$$

where the vertical velocity W, resulting from the transformation, is given by

$$W = \bar{w} - \bar{u}\left[\frac{\partial h_s}{\partial x} + \rho\frac{\partial \Delta h}{\partial x}\right] - \bar{v}\left[\frac{\partial h_s}{\partial y} + \rho\frac{\partial \Delta h}{\partial y}\right] - \rho\frac{\partial \Delta h}{\partial y} \qquad (4.24)$$

The initial estimate of $\bar{u}$ and $\bar{v}$ contain some anomalous divergence, $D(x,y,\rho)$,

$$\frac{\partial \bar{u}\Delta h}{\partial x} + \frac{\partial \bar{v}\Delta h}{\partial y} + \frac{\partial W}{\partial \rho} = D(x,y,\rho) \qquad (4.25)$$

or in discrete form

$$D(i,j,k) = \frac{W(i,j,k+\frac{1}{2}) - W(i,j,k-\frac{1}{2})}{\Delta\rho} + \frac{\bar{u}(i+1,j,k)\Delta h(i+1,j,k)}{2\Delta x}$$
$$- \frac{\bar{u}(i-1,j,k)\Delta h(i-1,j,k)}{2\Delta x} + \frac{\bar{v}(i,j+1,k)\Delta h(i,j+1,k)}{2\Delta y}$$
$$- \frac{\bar{v}(i,j-1,k)\Delta h(i,j-1,k)}{2\Delta y}$$

$$(4.26)$$

The anomalous divergence is reduced by the method of Endlich (1967) where the adjusted components at the n'th iteration, are given by:

$$\bar{u}^{\,n}(i+1,j,k) = \bar{u}^{\,n-1}(i+1,j,k) + \tilde{u}(i,j)$$
$$\bar{u}^{\,n}(i-1,j,k) = \bar{u}^{\,n-1}(i-1,j,k) - \tilde{u}(i,j)$$
$$\bar{v}^{\,n}(i,j+1,k) = \bar{v}^{\,n-1}(i,j+1,k) - \tilde{v}(i,j)$$
$$\bar{v}^{\,n}(i,j-1,k) = \bar{v}^{\,n-1}(i,j-1,k) + \tilde{v}(i,j) \qquad (4.27)$$

where

$$\tilde{u}(i,j) = -\frac{2\Delta x D^{n-1}(i,j,k)}{\Delta h(i+1,j,k) + \Delta h(i-1,j,k) + \Delta h(i,j+1,k) + \Delta h(i,j-1,k)}$$

152

and

$$\tilde{v}(i,j) = -\frac{2\Delta y D^{n-1}(i,j,k)}{\Delta h(i+1,j,k) + \Delta h(i-1,j,k) + \Delta h(i,j+1,k) + \Delta h(i,j-1,k)}$$

The transformed vertical velocities are now determined. If the transformation is applied to the surface layer, the transformed vertical velocity at $k = \frac{1}{2}$ is given as

$$W(x,y,\tfrac{1}{2}) = \bar{w}_s - \bar{u}_s\left(\frac{\partial h_s}{\partial x} + \rho\frac{\partial \Delta h}{\partial x}\right) - \bar{v}_s\left(\frac{\partial h_s}{\partial y} + \rho\frac{\partial \Delta h}{\partial y}\right) \qquad (4.28a)$$

$\bar{u}_s$, $\bar{v}_s$ and $\bar{w}_s$ are the surface layer velocities obtained from:

$$\frac{\partial \bar{u}_s}{\partial x} + \frac{\partial \bar{v}_s}{\partial y} = -\frac{\partial \bar{w}_s}{\partial z} = -D_s$$

i.e.,
$$\bar{w}_s = -D_s(h_s - h_t) \qquad (4.28b)$$

However, at the surface layer height, $\rho = 0$ and therefore, from equation (4.28a)

$$W(x,y,\tfrac{1}{2}) = \bar{w}_s - \left(\bar{u}_s\frac{\partial h_s}{\partial x} + \bar{v}_s\frac{\partial \Delta h}{\partial y}\right) \qquad (4.28c)$$

Substituting equation (4.28b) into equation (4.28c), results in the following descrete form

$$W(x,y,\tfrac{1}{2}) = -D_s(i,j)\left\{h_s(i,j) - h_t(i,j)\right\}$$

$$-\left\{\bar{u}_s(i,j)\left(\frac{h_s(i+1,j)-h_s(i-1,j)}{2\Delta x}\right)\right.$$

$$\left. + \bar{v}_s(i,j)\left(\frac{h_s(i,j+1)-h_s(i,j-1)}{2\Delta x}\right)\right\} \qquad (4.28d)$$

The procedure proposed by Goodin *et al.* (1980) is used to reduce the divergence in each of the outer layers. Initially assume $W(x,y,k-\frac{1}{2}) = 0$ and calculate $W(x,y,k+\frac{1}{2})$ from equation (4.26) *i.e.*, from the divergence within that layer. Once $W(x,y,1\frac{1}{2})$ and $W(x,y,2\frac{1}{2})$

153

are determined, $D^n(i,j,1)$ is obtained from equation (4.26), using $W(x,y,\frac{1}{2})$ from equation (4.28d). The divergence reduction technique of Endlich (1967) is employed to minimise $D(i,j,k)$. During the reduction process, the velocities $W(x,y,\frac{1}{2})$, $W(x,y,1\frac{1}{2})$ and $W(x,y,2\frac{1}{2})$, are held fixed.

Once the layer-averaged wind components are calculated, u_p can be determined from equation (4.21). The parameters $z_0(i,j)$, $u_*(i,j)$, $L(i,j)$, $\alpha_s(i,j)$, $u_p(i,j)$ and $\alpha_p(i,j)$ define the structure of the three-dimensional wind field. These parameters are stored in a temporary file for use in the dispersion module (DSPRSN).

Since spatial variations in the outer layer are less pronounced than in the surface layer, the horizontal grid spacing is twice that of the surface layer grid spacing. Wind speeds at the intermediate grid points are obtained by interpolation.

4.2. THE DISPERSION MODEL (DSPRSN)

4.2.1. <u>Solving the Advection-Diffusion Equation</u>

The distribution of the pollutant is simulated by the superpositioning of sequentially released puffs in the Eulerian reference frame. It is assumed that the wind velocity and diffusivity coefficients are constant (or reasonably constant) in the horizontal area covered by each puff. Furthermore, a puff is assumed to have a bivariate normal distribution in the horizontal. This is

given by

$$C(x,y,z,t) = \frac{C_{00}(z,t)}{2\pi\sigma_x(z,t)\sigma_y(z,t)\sqrt{1-\rho^2(z,t)}}$$

$$\times \exp\left\{-\frac{1}{2[1-\rho^2(z,t)]}\left[\left[\frac{x-\mu_x(z,t)}{\sigma_x(z,t)}\right]^2 \right.\right.$$

$$\left.\left. - 2\rho(z,t)\left[\frac{x-\mu_x(z,t)}{\sigma_x(z,t)}\right]\left[\frac{x-\mu_y(z,t)}{\sigma_y(z,t)}\right] + \left[\frac{y-\mu_y(z,t)}{\sigma_y(z,t)}\right]^2\right]\right\}$$

(4.29)

where $C_{00}(z,t)$ is the zero'th moment given by

$$C_{00}(z,t) = \iint_{-\infty}^{+\infty}C(x,y,z,t)\ dxdy$$

and

$\mu_x(z,t)$, $\mu_y(z,t)$ = coordinates of the centroid in the
horizontal plane at height z

$\sigma_x(z,t)$, $\sigma_y(z,t)$ = standard deviations about the centroid in
the x- and y- directions at height z.

$\rho(z,t)$ = correlation coefficient between the
distribution in the x and y coordinates.

The parameters μ_x, μ_y, σ_x, σ_y and ρ are obtained from equations (3.13) to (3.16). It is therefore necessary to solve the one-dimensional partial differential equations given by (3.11) and the corresponding equations for C_{01} and C_{02}. In addition, the following equation must to be solved for C_{11}:

$$\frac{\partial C_{11}(z,t)}{\partial t} = \frac{\partial}{\partial z}\left(K_v(z,t)\frac{\partial C_{11}(z,t)}{\partial z}\right) + \bar{u}(z,t)C_{01}(z,t) + \bar{v}(z,t)C_{10}(z,t)$$

(4.30)

When sedimentation and first-order chemical reactions are included, the equations become:

$$\frac{\partial C_{00}(z,t)}{\partial t} = \frac{\partial}{\partial z}(K_v(z,t)\frac{\partial C_{00}(z,t)}{\partial z}) + w_s\frac{\partial C_{00}(z,t)}{\partial z} + R(C_{00}(z,t),t)$$

$$(4.31)$$

$$\frac{\partial C_{10}(z,t)}{\partial t} = \frac{\partial}{\partial z}(K_v(z,t)\frac{\partial C_{10}(z,t)}{\partial z}) + \bar{u}(z,t)C_{00}(z,t) + w_s\frac{\partial C_{10}(z,t)}{\partial z}$$

$$+ R(C_{10}(z,t),t) \qquad (4.32)$$

$$\frac{\partial C_{20}(z,t)}{\partial t} = \frac{\partial}{\partial z}(K_v(z,t)\frac{\partial C_{20}(z,t)}{\partial z}) + 2\bar{u}(z,t)C_{10}(z,t)$$

$$+ 2K_H(z,t)C_{00}(z,t) + w_s\frac{\partial C_{10}(z,t)}{\partial z} + R(C_{20}(z,t),t)$$

$$(4.33)$$

and similar expressions for $C_{01}(z,t)$ and $C_{20}(z,t)$. Equation (4.30) becomes

$$\frac{\partial C_{11}(z,t)}{\partial z} = \frac{\partial}{\partial z}(K_v(z,t)\frac{\partial C_{11}(z,t)}{\partial z}) + \bar{u}(z,t)C_{01}(z,t)$$

$$+ \bar{v}(z,t)C_{10}(z,t) + w_s\frac{\partial C_{11}(z,t)}{\partial z} + R(C_{11}(z,t),t)$$

$$(4.34)$$

If w_b represents the resultant vertical velocity due to the buoyancy of the puff, then, as for the sedimentation velocity, w_b can be included by subtracting the term

$$w_b\frac{\partial C_{mn}(z,t)}{\partial z} \qquad (4.35)$$

from the right hand side of the equations.

The above equations are solved following the method of fractional steps (Yanenko 1971). The only difference between the proposed method and that of Yanenko (1971), is the addition of the sedimentation, buoyancy and reaction terms. The order in which the

156

equations are solved is:

        1. sedimentation and buoyancy

        2. advection

        3. reaction

        4. diffusion

The solution to the advection equation (3.71) with constant coefficients is (Section 3.1.3.1.)

$$C(x,t) = C_0(x-at)$$

where a is a constant (velocity) coefficient and C_0 the initial condition. In other words, the initial concentration is displaced by a distance, at. The sedimentation velocity can be assumed constant with time and space.

Briggs' (1969) equations for the prediction of plume rise is adopted. Instead of calculating the effective velocity due to buoyancy, the vertical displacement is used, as predicted by equation (3.132). The predicted plume rise is approximated by a step function whose discrete values are taken as the height at the start of a time step.

The first step is then to solve

$$\frac{\partial C_{mn}(z,t)}{\partial t} = (w_s - w_b) \frac{\partial C_{mn}(z,t)}{\partial z} \qquad (4.36)$$

for m = 0,2 and n = 0,2 (m = n $\neq$ 2), and the solution is simply

$$C_{mn}^{s} = C_{mn}(z+w_s\Delta t-\Delta h, t) \qquad (4.37)$$

where Δh is the plume rise due to buoyancy. The second step is to solve the advection terms with the initial condition provided by equation (4.37);

$$\frac{\partial C_{mn}(z,t)}{\partial t} = m\bar{u}(z,t)C_{m-1,n}(z,t) + n\bar{v}(z,t)C_{m,n-1}(z,t) \qquad (4.38)$$

for m+n$\neq$0, and m-1, m-2, n-1, n-2$\geq$0, and m=1,2, n=1,2, but m=n$\neq$2. It

157

is assumed that the velocity components, $\bar{u}$ and $\bar{v}$, do not change significantly during a time step, Δt. The change in the moments due to advection during the time step Δt, is now determined. By definition (equation (3.10)),

$$C_{10}(z,t) = \iint_{-\infty}^{+\infty} xC(x,y,z,t) \, dxdy$$

therefore

$$C_{10}(z,t+\Delta t) \simeq \iint_{-\infty}^{+\infty} (x + \Delta x) \, C(x,y,z,t) \, dxdy$$

where $\Delta x = \bar{u}(z,t)\Delta t$, and hence

$$C_{10}(z,t + \Delta t) \simeq \iint_{-\infty}^{+\infty} xC(x,y,z,t) \, dxdy + \iint_{-\infty}^{+\infty} \Delta xC(x,y,z,t) \, dxdy$$

$$= C_{10}(z,t) + \Delta xC_{00}(z,t)$$

The updated moment is then given by

$$C_{10}^{a} = C_{10}^{S} + \Delta xC_{00}^{S} \tag{4.40a}$$

where C_{00}^{S} and C_{10}^{S} are obtained from equation (4.37). The superscript "s" is for sedimentation and buoyancy, and "a", for advection. By similar argument it can be shown that

$$C_{01}^{a} = C_{01}^{S} + \Delta yC_{00}^{S} \tag{4.40b}$$

$$C_{20}^{a} = C_{20}^{S} + 2\Delta xC_{10}^{S} + \Delta x^{2}C_{00}^{S} \tag{4.40c}$$

$$C_{02}^{a} = C_{02}^{S} + 2\Delta yC_{01}^{S} + \Delta y^{2}C_{00}^{S} \tag{4.40d}$$

$$C_{11}^{a} = C_{11}^{S} + \Delta xC_{01}^{S} + \Delta yC_{10}^{S} + \Delta x\Delta yC_{00}^{S} \tag{4.40e}$$

where

$$\Delta x = \bar{u}(z,t)\Delta t$$

$$\Delta y = \bar{v}(z,t)\Delta t$$

For a first order reaction, we have

$$\frac{\partial C_{m,n}(z,t)}{\partial t} = -(k_r + k_w)C_{m,n}(z,t) \tag{4.41}$$

where
$$k_r = \text{reaction rate coefficient } (s^{-1})$$
$$k_w = \text{washout rate coefficient } (s^{-1})$$

The moments at time $t+\Delta t$ are then given by

$$C_{m,n}(z, t + \Delta t) = -(k_r + k_w)C_{m,n}(z,t)\Delta t + C_{m,n}(z,t)$$

or using the initial condition specified by equation (4.40),

$$C_{m,n}^r = [1 - (k_r + k_w)\Delta t]C_{m,n}^a \tag{4.42}$$

Because of the great amount of uncertainty in the specification of reaction rates, a constant value is assumed adequate. The user therefore has to supply an average reaction rate constant, suitable for most conditions. As an example: an average O_3 concentration can be assumed and the appropriate reaction rate constant for SO_2 calculated from equations (3.82). Similarly, a constant washout rate constant is assumed. A $\frac{1}{r}$ weighting function is used when more than one rainfall measurement is supplied.

The diffusion process is the final step in the calculation of the moments, $viz.$,

$$\frac{\partial C_{mn}(z,t)}{\partial t} = \frac{\partial}{\partial z}\left\{K_v(z,t)\frac{\partial C_{mn}(z,t)}{\partial z}\right\} \tag{4.43}$$

It was decided to use a slight modification of Mulholland's (1977, 1980) *limiting value method*, as stated in equation (3.79). The boundary layer is divided into horizontal layers, Δz thick. The numbering of these layers is shown in Figure 4.5 (notice, layer 1 is below ground-level and layer 2 immediately above ground level). The limiting value method, with constant Δz stepsizes and variable

Layer Number

Small K_H, K_V. Geostrophic winds

(Minimal pollutant distribution)

Boundary layer height   IH

_____

_____   IH-1

Δz

3

2

Ground level

//

1

Impervious surface, unless dry deposition and

sedimentation velocities exist
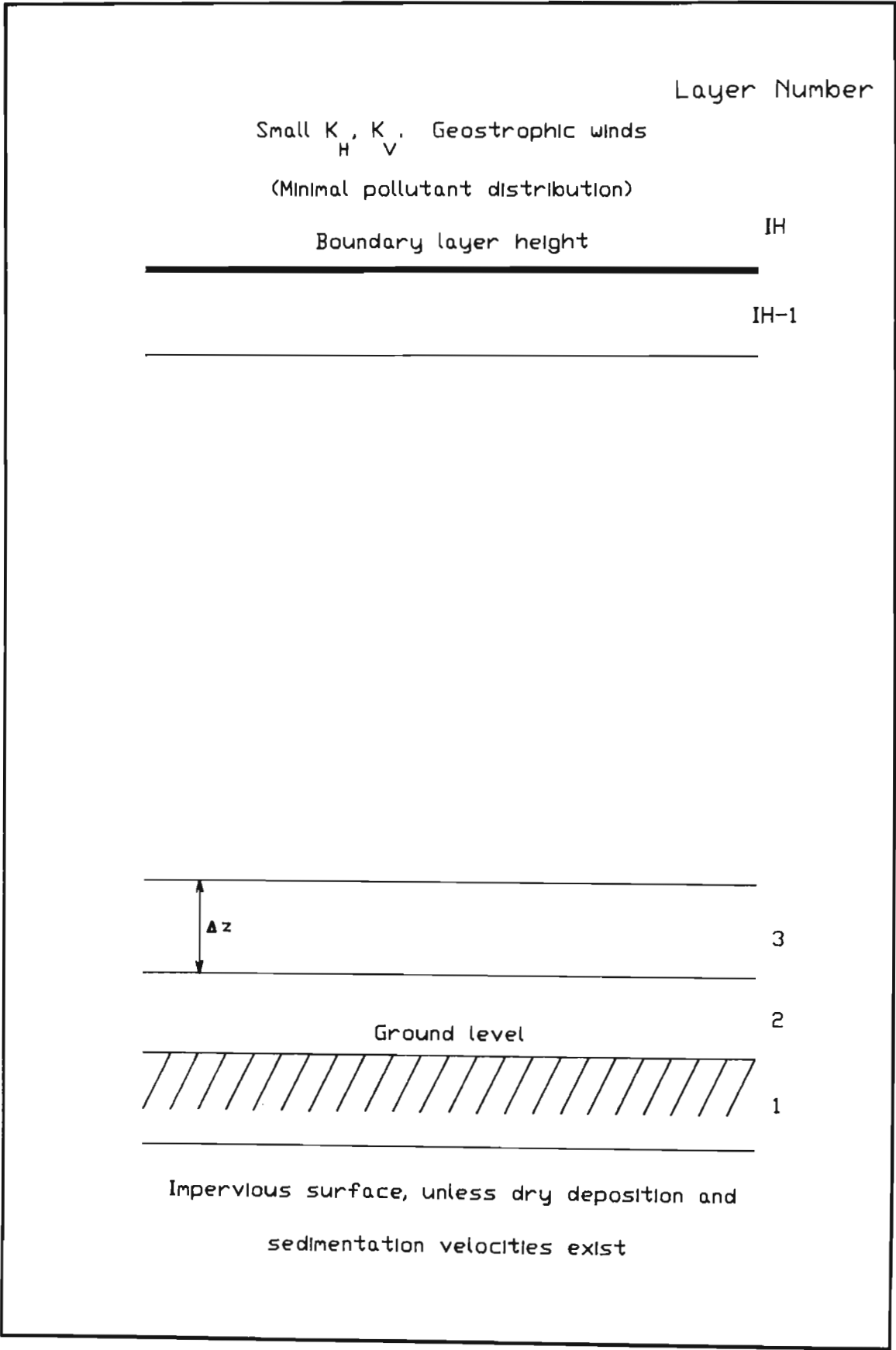
Figure 4.5. Numbering of the horizontal layers in the

dispersion model.

diffusivities, is (from equation (3.79)):

$$C_{mn}(k,t+\Delta t) = C_{mn}(k,t) + b(k,t)\{1 - \exp(-a(k)\Delta t)\} \qquad (4.44)$$

where

$$b(k,t) = \frac{C_{mn}(k+1,t) - C_{mn}(k-1,t)}{\left[1 + \dfrac{K_v(k-1)t}{K_v(k+1)t}\right]} + C_{mn}(k-1,t) - C_{mn}(k,t)$$

and

$$a(k,t) = \frac{K_v(k+1,t) + K_v(k-1,t)}{\Delta z^2}$$

with the optimum criterion given by

$$\frac{K_v \Delta t}{\Delta z^2} = 0,4$$

A modification to the limiting value theorem is now suggested that improves the optimum criterion to

$$\frac{K_v \Delta t}{\Delta z^2} = 0,8 \qquad\qquad (4.45)$$

Hence, for the same vertical spacing and vertical diffusion, a time step twice as large as the unmodified method, can be used. Derivation of this method is presented in Appendix G. It is essentially the same as equation (4.44), but applied to half the temporal and spatial stepsizes:

$$C_{mn}(k,t+\Delta t) = \{1-f(k)\}\{C_{mn}(k,t) + b(k,t)f(k)\}$$

$$+ \frac{1}{2}\left\{ g(k)\left[C_{mn}(k+1,t)+C_{mn}(k,t)+d_1(k)\{C_{mn}(k+1,t)-C_{mn}(k,t)\}\right]\right.$$

$$+ \left.[1-g(k)]\left[C_{mn}(k,t)+C_{mn}(k-1,t)+d_2(k)\{C_{mn}(k,t)-C_{mn}(k-1,t)\}\right]\right\}f(k)$$

$$(4.46)$$

where

$$f(k) = 1 - \exp\left\{ -\left[\frac{K_v(k+1) + 2K_v(k) + K_v(k-1)}{\Delta z^2} \right] \Delta t \right\}$$

$$g(k) = \frac{K_v(k+1) + K_v(k)}{K_v(k+1) + 2K_v(k) + K_v(k-1)}$$

$$d_1(k) = \left\{ 2g(k+\tfrac{1}{2}) - 1 \right\} f(k+\tfrac{1}{2})$$

$$d_2(k) = \left\{ 2g(k-\tfrac{1}{2}) - 1 \right\} f(k-\tfrac{1}{2})$$

$$b(k) = g(k)\left\{ C_{mn}(k+1,t) - C_{mn}(k-1,t) \right\} + C_{mn}(k-1,t) - C_{mn}(k+1,t)$$

and

$$g(k+\tfrac{1}{2}) = \frac{K_v(k+1)}{K_v(k+1) + K_v(k)}$$

$$g(k-\tfrac{1}{2}) = \frac{K_v(k)}{K_v(k) + K_v(k-1)}$$

$$f(k+\tfrac{1}{2}) = 1 - \exp\left\{ -2\left[\frac{K_v(k+1) + K_v(k)}{\Delta z^2} \right] \Delta t \right\}$$

$$f(k-\tfrac{1}{2}) = 1 - \exp\left\{ -2\left[\frac{K_v(k) + K_v(k-1)}{\Delta z^2} \right] \Delta t \right\}$$

The final value of $C_{mn}(k, t+\Delta t)$ is then given by equation (4.46) with C_{mn}^r as the initial condition to equation (4.46).

4.2.1.1. Initial Conditions

The system must be initialised before the equations in Section 4.2.1. can be solved. The technique of "seeding" with Gaussian puffs has been employed by Runca and Sardei (1975) in their numerical solution of the advection-diffusion equation. It was indicated in equation (3.111) that,

$$\overline{K}_x(t) \quad = \quad \frac{1}{2} \frac{d\langle x^2 \rangle}{dt} \tag{3.111}$$

or approximately,

$$\langle X^2 \rangle \quad = \quad 2\overline{K}_x(t)\Delta t$$

or for an ensemble of particles

$$\sigma_x^2 \quad = \quad 2\overline{K}_x(t)\Delta t \tag{4.47}$$

It can be assumed that, close to the source, the eddy diffusivities defined by (3.102), are approximately equal to the eddy diffusivities used in the Eulerian Grid models. The Gaussian puff model can then be written as

$$C(x,y,z,t) \quad = \quad \frac{M}{8(\pi t)^{3/2} K_H \sqrt{K_v}}$$

$$x \: \exp\left\{-\frac{1}{4t}\left[\frac{(x-U_s t)^2}{K_H} + \frac{(y-V_s t)}{K_H}\right]\right\}$$

$$x \: \left\{\exp\left[-\frac{1}{4t}\frac{(z-H)^2}{K_v}\right] + \exp\left[-\frac{1}{4t}\frac{(z+H)^2}{K_v}\right]\right\} \tag{4.48}$$

where it is assumed that $\overline{K}_x = \overline{K}_y = K_H$ and $\overline{K}_z = K_v$, with the source at H. The wind velocity components at the stack height are U_s and V_s. The moments for this distribution are determined by applying the transformation, given by equation (3.10), to equation (4.48)

(Appendix H):

$$C_{00}(z,t) = M \frac{\exp\left[-\frac{1}{4t}\left\{\frac{(z+H)^2}{K_v}\right\}\right] + \exp\left[-\frac{1}{4t}\left\{\frac{(z-H)^2}{K_v}\right\}\right]}{2(\pi K_v t)^{1/2}} \qquad (4.49a)$$

$$C_{10}(z,t) = C_{00}(z,t)U_s t \qquad (4.49b)$$

$$C_{01}(z,t) = C_{00}(z,t)V_s t \qquad (4.49c)$$

$$C_{20}(z,t) = C_{00}(z,t)\{2K_H t + (U_s t)^2\} \qquad (4.49d)$$

$$C_{02}(z,t) = C_{00}(z,t)\{2K_H t + (V_s t)^2\} \qquad (4.49e)$$

$$C_{11}(z,t) = C_{00}(z,t)U_s V_s t^2 \qquad (4.49f$$

4.4.1.2. Boundary Conditions

The boundary conditions are stated in equations (3.91a) and (3.91b), i.e.,

$$K_v(z)\frac{\partial c}{\partial z} = 0 \qquad \text{(upper boundary)} \qquad (3.91a)$$

$$K_v(z)\frac{\partial c}{\partial z} = v_d(z_r)C(z_r) \qquad \text{(lower boundary)} \qquad (3.91b)$$

where $v_d(x_r)$ is the deposition velocity at reference height z_r. In terms of moments, these become:

$$K_v(z)\frac{\partial C_{mn}}{\partial z} = 0 \qquad \text{(upper boundary)} \qquad (4.50a)$$

$$K_v(z)\frac{\partial C_{mn}}{\partial z} = v_d(z_r)C_{mn}(z_r) \qquad \text{(lower boundary)} \qquad (4.50b)$$

To prevent any dispersion across the upper boundary $z=h_p$, the concentrations above the boundary layer height are set to the values below the boundary layer height. In terms of the layers defined in figure 4.5.;

$$C_{mn}(IH + 1) = C_{mn}(IH - 2) \qquad (4.51a)$$

$$C_{mn}(IH) = C_{mn}(IH - 1) \qquad (4.51b)$$

where the boundary layer height lies between $IH - 1$ and IH.

The lower boundary is treated similarly, however ground retention must be allowed. Changing equation (4.50b) to finite difference form we get:

$$K_v(k) \left[\frac{C_{m,n}(k) - C_{m,n}(k-1)}{\Delta z} \right] = v_d(k) C_{mn}(k)$$

with $k = 2$, $i.e.$, the layer immediately above ground-level. Hence,

$$C_{mn}(k-1) = C_{mn}(k) \left[1 - \left\{ \frac{v_d(k) C_{mn}(k) \Delta z}{K_v(k)} \right\} \right] \tag{4.52}$$

with $k = 2$.

The three-layer model, discussed in Section 3.1.4.3. (equation (3.94)), is adopted.

The aerodynamic resistance is obtained from (equation 3.93)

$$r_a = \int_{z_r}^{\Delta z} \frac{dz}{K_v(z)} \tag{4.53}$$

The derivation of the r_a-values for different stability conditions is given in the next section. The surface resistance is given by the relationship (Wesely and Hicks 1977)

$$r_s = (ku_*)^{-1} kB^{-1} \tag{3.95}$$

with

$$kB^{-1} = 2,6$$

The canopy resistance r_c is supplied as a function of stability and the land usage. This is to be supplied by the user. The resulting deposition velocity is then

$$v_d(z) = (r_a + r_s + r_c)^{-1} \qquad (3.94)$$

When there is some sedimentation, $v_d(z)$ must be replaced by $v_d(z) + w_s$, where w_s is the sedimentation velocity.

4.2.2. Diffusivity Profiles

4.2.2.1. Vertical Diffusivity

The first-order closure approximation is adopted. The similarity relationships are used in the surface layer, and are given by equations (3.26) and (3.29), *i.e.*,

Neutral conditions:

$$K_v(z) = ku_*z \qquad (3.26)$$

Non-neutral conditions:

$$K_v(z) = ku_*z/\phi_h(\frac{z}{L}) \qquad (3.29)$$

The universal functions $\phi_h(\frac{z}{L})$, given in Table 4.1, are used for the different stability classes except convective conditions ($\frac{z}{L} \leq -1$). For the latter case, the vertical diffusivity is given by the large eddy approach of Crane *et al.* (1977)

$$K_v(z) = 2,0(k_z)^{\frac{4}{3}}(\frac{gH}{c_p\rho T})^{\frac{1}{3}} \qquad (3.54)$$

The above equation can be rewritten as

$$K_v(z) = 2,0\ k(-\frac{z^4}{L})^{\frac{1}{3}}u_* \qquad (4.55)$$

166

using the definition of the Monin–Obukhov length (equation 2.4).

Above the surface layer, the profile suggested by Shir (1973) is used in neutral conditions:

$$K_v(z) = 0{,}5u_*kz\left[\exp(-4z/h_p) + \frac{1}{1+16(z/h_p)^{1{,}6}}\right] \quad (3.47)$$

For stable and unstable conditions, the profile suggested by O'Brien (1970) is used. The O'Brien formula is given by

$$K_v(z) = K_v(h_p) + \left[\frac{z-h_p}{h_p-h_s}\right]^2\left\{K_v(h_s) - K_v(h_p)\right.$$

$$\left. + (z-h_s)\left[K_v'(h_s) + 2\frac{K_v(h_s) - K_v(h_p)}{h_p-h_s}\right]\right\} \quad (3.43)$$

$K_v(h_s)$ is given by equations (3.29) and (4.55) at the surface layer height, and,

$$K_v(h_p) = 0{,}01 \text{ m}^2\text{s}^{-1} \text{ stable conditions} \quad (4.56a)$$

$$= 0{,}1 \text{ m}^2\text{s}^{-1} \text{ unstable conditions} \quad (4.56b)$$

The derivatives at the surface layer height are calculated from:

Stable conditions:

$$K_v'(h_s) = \frac{-\beta\dfrac{ku_*}{L}}{\left[1+\beta\dfrac{h_s}{L}\right]^2} \quad (4.57a)$$

Very stable conditions:

$$K_v'(h_s) = \frac{ku_*}{1+\beta} \quad (4.57b)$$

167

Moderately unstable conditions:

$$K'_v(h_s) = ku_* \frac{1-\frac{3}{2}\gamma_2\frac{h_s}{L}}{\left[1-\gamma_2\frac{h_s}{L}\right]^{1/2}}$$

(4.58a)

Convective conditions:

$$K'_v(h_s) = \frac{8}{3}u_*k\left[-\frac{h_s}{L}\right]^{1/3}$$

(4.58b)

During convective conditions the correction of Pielke *et al* (1983) (equation (3.44)) is applied to the O'Brien relationship.

The aerodynamic resistance is given by equation (4.53):

$$r_a = \int_{z_r}^{\Delta z} \frac{dz}{K_v(z)}$$

(4.53)

From equations (3.26) and (3.29), r_a is calculated as:

Neutral conditions:

$$r_a = \frac{1}{ku_*}\ln\frac{\Delta z}{z_r}$$

(4.59a)

Stable conditions:

$$r_a = \frac{1}{ku_*}\left[\ln\frac{\Delta z}{z_r} + \frac{\beta_2}{L}(\Delta z - z_r)\right]$$

(4.59b)

Unstable conditions:

$$r_a = \frac{1}{ku_*}\ln\left[\frac{\Delta z}{z_r}\frac{1-\gamma_2\frac{z_r}{L}}{1-\gamma_2\frac{\Delta z}{L}}\right]$$

(4.59c)

4.2.2.2. Horizontal Diffusivity

Since very little is known about the horizontal eddy diffusivities, the suggestion of Ragland and Dennis (1974) is assumed adequate. Except for convective conditions, the horizontal diffusivity for both the surface and the outer layer is given by

$$K_H(z) = \beta K_v(z) \tag{3.33}$$

where

$\beta = 2$ for unstable conditions

$\beta = 5$ for neutral conditions

$\beta = 6$ for stable conditions

During convective conditions, a slightly different form is suggested. McRae *et al* (1982) suggested for the outer layer

$$K_H = 0,1w_* h_p \tag{3.55}$$

or

$$K_H = 0,1(-\frac{h_p^4}{kL})^{\frac{1}{3}}u_* \tag{4.60}$$

This profile is matched to the surface layer profile, at $z=h_s$ and hence, for the surface layer under convective conditions

$$K_H(z) = \beta K_v(z) \tag{3.33}$$

where

$$\beta = 5 \times 10^{-\frac{2}{3}} k^{-\frac{4}{3}} \tag{4.61}$$

to match the outer layer diffusivity.

4.2.3. Program Code and Optimising Procedures

The program package requires the specification of three time increments:

Δt_W = the time interval between updating the wind field parameters

Δt_D = the time interval between updating the advection-diffusion solution

Δt_I = the time interval between updating the concentration distribution output Δt_W is normally much larger than Δt_D.

The computer algorithm is outlined below.

STEP 1:   Seed the system with its first moments using the moments derived for a Gaussian puff of age Δt_W. Do this for all stacks, with the wind and diffusivity conditions at the stack height.

STEP 2:   Calculate the centroid positions of all the puffs.

STEP 3:   Retrieve the updated wind parameters calculated in METPAC.

STEP 4:   By using the centroids calculated in STEP 2 (initially) or STEP 6 (once the system is initialised), determine the wind and diffusivity parameters for each puff.

STEP 5:   Determine the puff rise due to buoyancy and proceed to update the moments according to the numerical methods discussed in Section 4.2.1. The time step for updating moments is given by (from equation (4.45))

$$\Delta t_D = 0,8 \frac{K_v}{\Delta t^2} \tag{4.62}$$

In order to speed the execution up, Δt_D can be limited to $\Delta t_D \geq 0,1 \Delta t_W$.

STEP 6:   Calculate the centroids of the updated puffs

STEP 7:   If the puffs are close enough, they can be merged. Ludwig *et al.*'s (1977) merging criterion is adopted

170

i.e., merge puffs if puff centres are closer than σ_y (Section 3.2.4.). The effective merging distance is determined from

$$d = \sigma = \frac{1}{2}\sqrt{\sigma_x^2 + \sigma_y^2} \qquad (4.63)$$

STEP 8: When the puffs are outside the region of interest (10% beyond the boundaries, or more than d (equation (4.63)) they are purged

STEP 9: Seed the system with the next puff. Two criteria must be met by the release interval.

(a) The release interval must not be too short, otherwise all of the material will be held in one layer only, i.e., if the puff dimension is smaller than the layer depth Δz. The vertical size of the Gaussian puff can be estimated from (Sutton 1953; 138pp)

$$\ell_z = \sqrt{8(\ln 10)K_v t}$$

If the vertical grid spacing, Δz, is substituted for ℓ_z, the criterion becomes

$$\Delta t_{release} \geq \frac{\Delta z^2}{18,421K_v} \qquad (4.64)$$

(b) The release rate should not be too large either, because then, puffs are initially too far apart. A minimum distance is specified d_c, and the release rate should satisfy

$$\Delta t_{release} \leq \frac{d_c}{\sqrt{U_s^2 + V_s^2}} \qquad (4.65)$$

where U_s, V_s, are the wind components at the stack height. To obtain good resolution close to the source, it is decided to use

$$d_c = \text{wind grid spacing} \qquad (4.66)$$

171

STEP 10: To ensure a smooth representation of the distribution, a final check is done to see whether the puffs are close enough. This is tested by using the criterion given by equation (4.63). If some puffs are too far apart, a linear interpolation of μ_x, μ_y, σ_x, σ_y and ρ is done to create intermediate puffs.

STEP 11: Ground-level distribution is then calculated by reconstructing a bivariate normal distribution as given by equation (4.29). Isopleths are drawn in ISPLTH.

STEP 12: Repeat steps 3 to 11.

The concentration distribution can be calculated at any height using the moments available for that height.

4.3. ISPLTH - CONCENTRATION ISOPLETH DRAWING ROUTINE.

Contours are drawn in one continuous movement. This can be done in two ways: once the starting point is found, either three or four immediate neighbouring "grid points" are considered to determine the next move (Figure 4.6(a) and 4.6(b)). The next point in the triangle (if points C_1, C_2 and C_3 are considered) or square (if points C_1, C_2, C_3 and C_4 are considered), is where $C_4 < C_i < C_1$ for the triangle, or $C_4 < C_i < C_3$ for the square. This will always work provided the grid spacing is small enough. A problem exists when the grid spacing is too large to show a peak or a trough in the middle of three or four grid points.

This situation is depicted in figure 4.7. It is clear from the drawing that there exists five possible moves. If three grid points were considered, this would not have been obvious. This is shown in Figure 4.8. The contour path, which in reality should pass between C_2 and C_3, will be missed (Figure 4.8(a)), and instead the contour will pass between C_1 and C_4 (Figure 4.8(b)). The remedy to this problem is therefore to consider four points at a time, and if the situation depicted in figure 4.7 should occur, the grid spacing

172
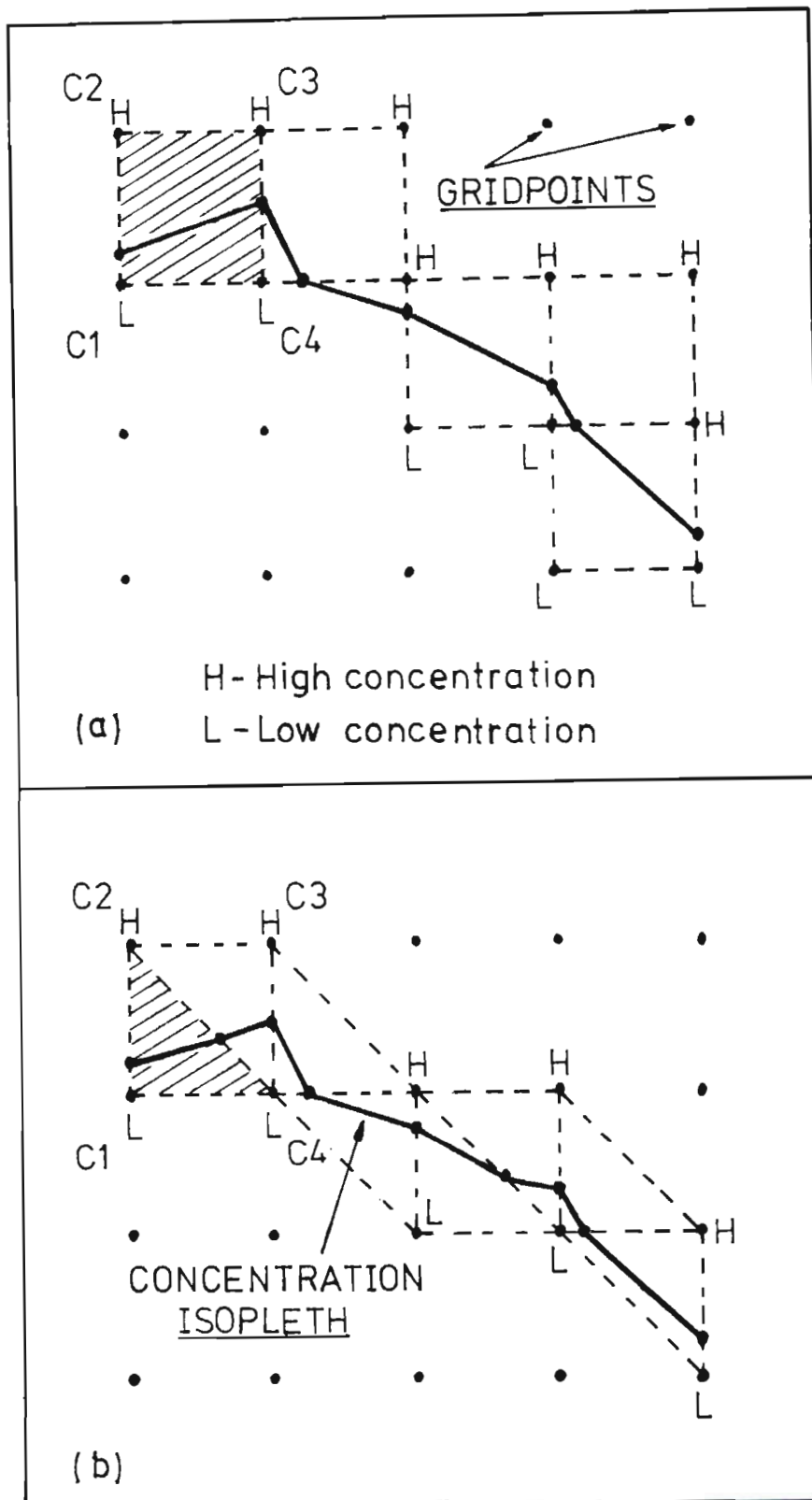
Figure 4.6. There are two ways in which the path of the contour can be determined. In figure (a), four neighbouring points are considered at the same time, whereas only three are considered in figure (b).
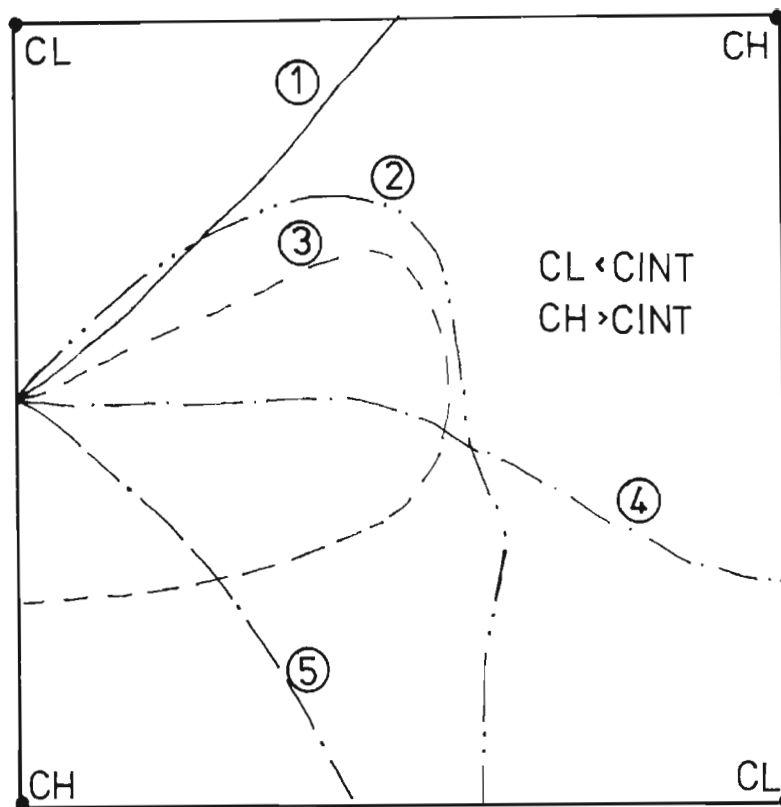
Figure 4.7.   A summary of the five different paths that a
contour can take when the grid size is too large
to indicate a peak or a trough in the middle of
the grid square.

should be reduced until it is clear where the contour should pass.
The possible paths are shown in Figure 4.9.

4.3.1. The Starting Point

To find the starting point of the contour, the two grid points
closest to the puff centre are considered firstly, as indicated in
Figure 4.10(a). If the concentration at grid points C_1 and C_2 are
higher than C_i, consider the next two points, $[C_1]$ and $[C_2]$, until a
crossing is found. If, however the concentrations at C_1 and C_2 are
lower than C_i, then change the direction of the search to the right
from the puff centre (Figure 4.10(b)). Repeat to the bottom (Figure

TWO POSSIBLE
PATHS

H
L
C2
C3
A
C1
C4
L
H
B

(a)

CONCENTRATION
ISOPLETH

TRUE
PATH

H
C2
A
C1
C4
L
H
B

(b)
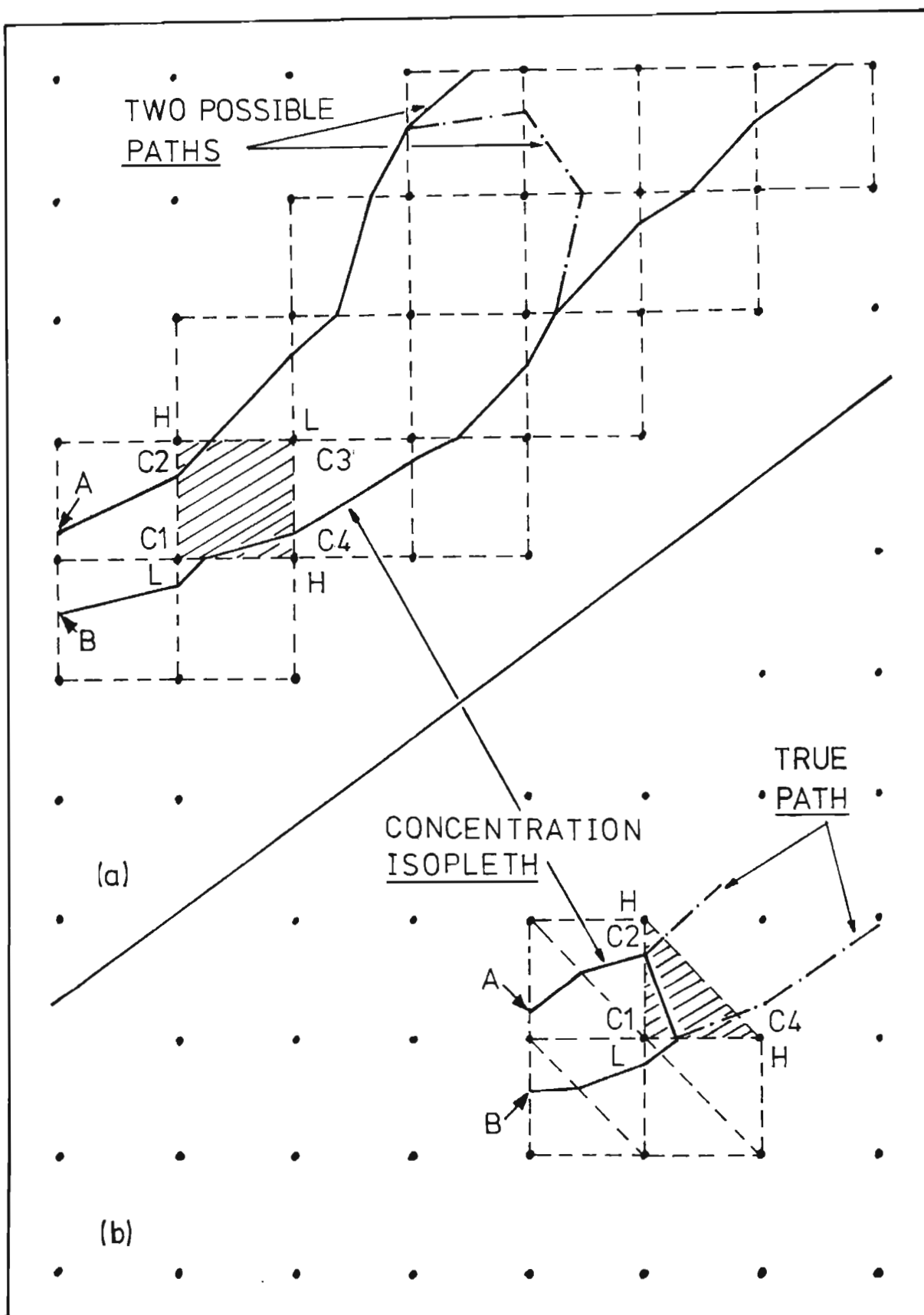
Figure 4.8. When only three grid points are used, as in figure (b), incorrect contours may result. This problem does not occur when four grid points are used.
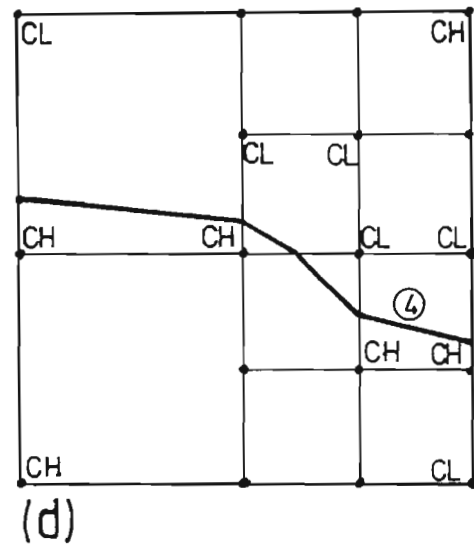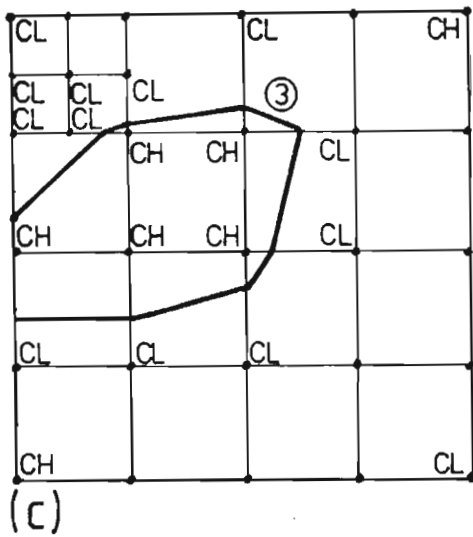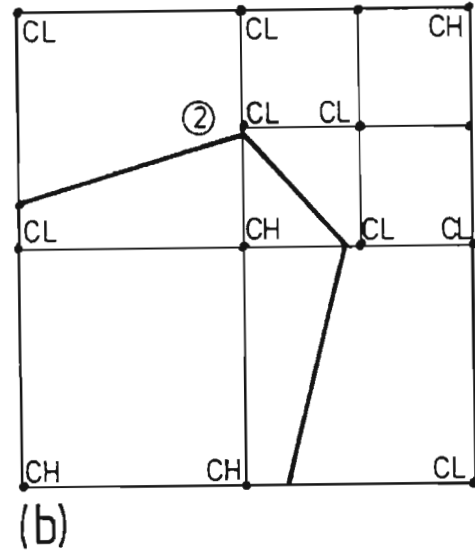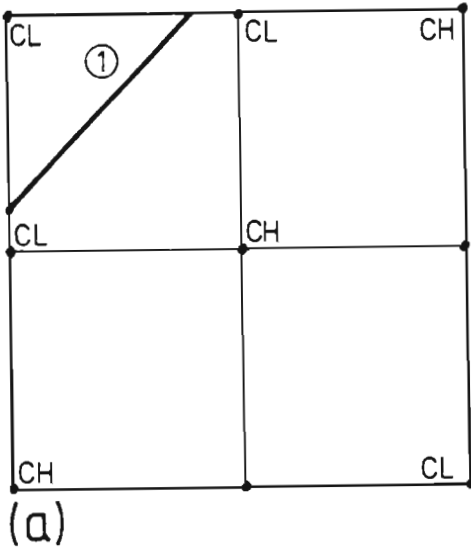
Figure 4.9. If the grid spacing is too large to indicate a peak or a trough, smaller spacings are used within the original grid square. This allows the proper path to be determined. Once the boundary of the original square is reached, the spacing changes back to the old value.
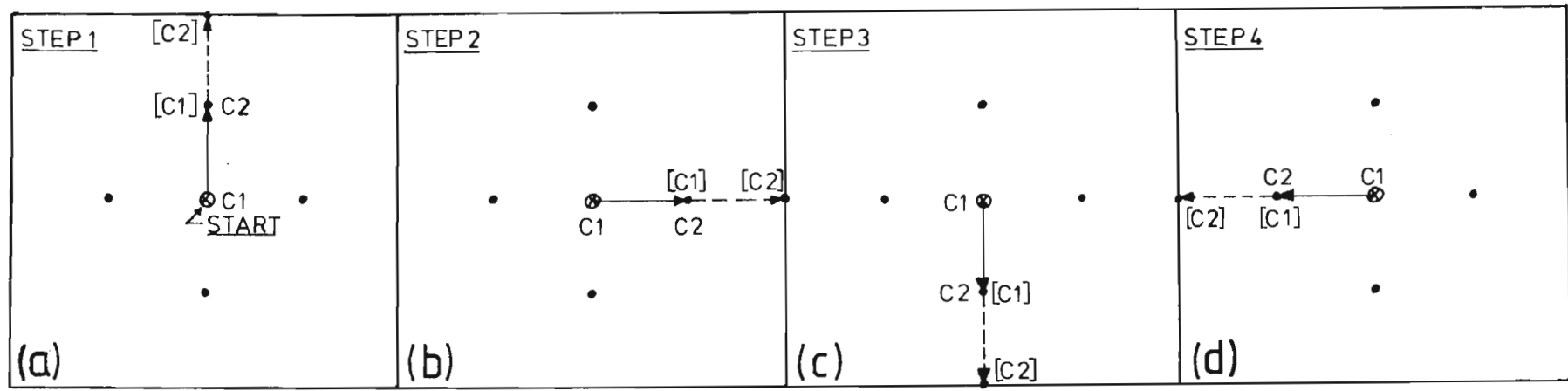
Figure 4.10.   A summary of the four directions which can be taken
from the puff centre for finding the starting point of the contour.
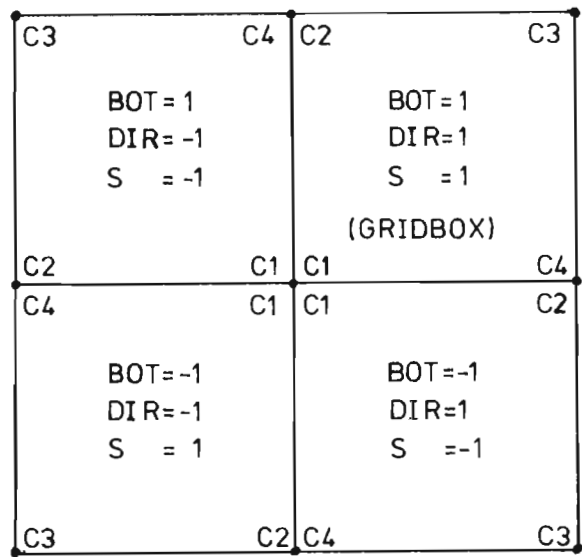
Figure 4.11.   The grid point numbering
corresponding to the different starting
configurations indicated in Figure 4.10.
The numbering in the first quadrant corresponds
to Figure 4.10(a), the numbering in the second
quadrant, to Figure 4.10(b), and so on.
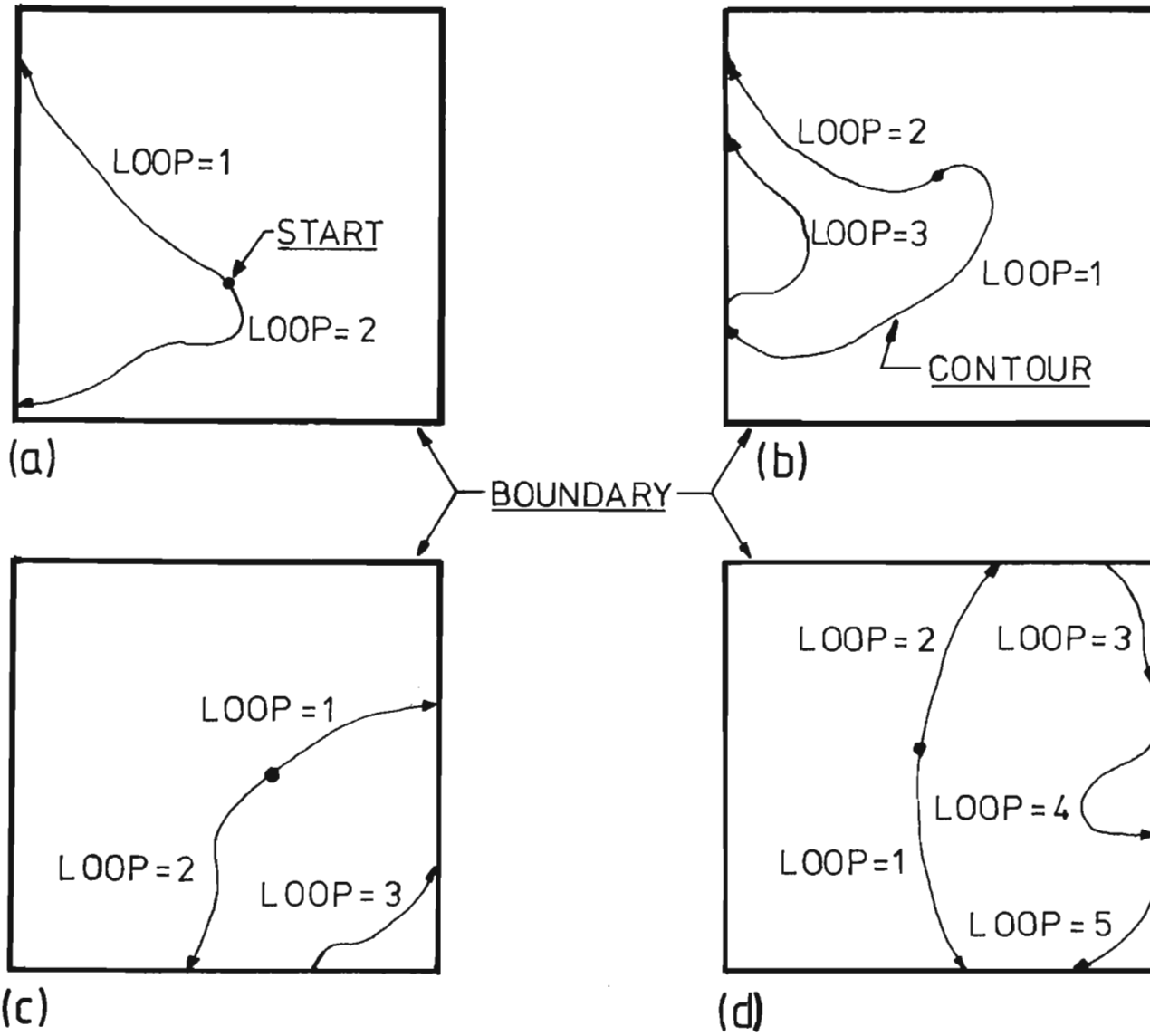
Figure 4.12. When a contour reaches the boundary of the picture, drawing commences from "START" until the boundary is reached again. The intercept where the contour enters the picture again, is then seeked by moving along the boundary.

4.10(c)), if the contour is not found to the right , and finally to the left (Figure 4.10(d)). If no contour is crossed in this process, try the next puff, and so on. The puff closest to the source is considered firstly. When the starting point is eventually found, the other two grid point concentrations (C_3 and C_4) are calculated according to the configuration in figure 4.11. The next intercept is then determined. The three parameters, BOT, DIR and S, define the direction of search.

4.3.2. The "Sniffing" Procedure and Problem Areas

The contour is "sniffed" out by comparing the concentrations at the four grid points C_1, C_2, C_3, and C_4. The contour has to pass from the one side of the square to the other. This sniffing process will continue until the starting point is reached again. The situation will arise when the contour leaves the boundary of the area (Figure 4.12(a)). When this happens, sniffing commences at the starting point and moves in the opposite direction, as indicated by the arrows. The contour is followed until the boundary is reached again and procedes along the boundary towards the point where the contour first left the boundary. During this process, the contour might loop back into the drawing again (Figure 4.12(b),(c), and (d)). The direction in which the boundary is traversed is chosen to be in the direction of the neighbouring grid point, on the boundary, with the highest concentration.

When the square is too large to indicate a peak or trough in the middle (Figure 4.9), the grid spacing is halved and the contour inside this smaller square is traced until the boundary of the original square is reached. When this happens, the grid spacing returns to its old value. If it is found that the smaller grid spacing is not adequate, the spacing is halved again, and so on (e.g., Figure 4.12(b) and (d)).

The isopleth for a particular concentration is complete once all the puffs are circled excluding those sequences on which no contour could

be found.   The next section lists all the possibilities for determining whether a puff has been circled and when the contour is closed.

4.3.3. Contour Closing Criteria and Optimisations

As soon as the starting point is reached, the contour is considered finished. A "flag" is immediately designated to the starting puff to indicate that it has been rotated.

The angle made by the starting point and each puff is also stored. At each step on the contour, the angle made by this coordinate and each puff centre is calculated. If this angle has travelled through all four quadrants around the puff centre (indicated by a "flag" for each quadrant), and the contour reached the end (starting) point, it is likely that this puff is circled completely. Puffs which don't carry the "circled flag" are then treated as if they lie within another contour.

The situation might arise where some puffs contribute very little to the overall dispersion. To optimise, the concentration is calculated at each puff centre including the contributions from all the other puffs. If the final concentration is lower than the isopleth value, the puff is given a "circled flag". This obviously saves a fair amount of computer time.

Further optimisation is done when calculating the concentration at a point. Instead of calculating the contribution from each puff at every new point on the contour, a flag is set whenever the contribution from a puff is below a certain value. This might be the case when the puff is far away or contains a small amount of material. The contribution from each puff is checked at certain intervals to see whether the situation has not changed. This is done after every second grid square.

Eastern Transvaal Highveld
SO2 distribution
(map : 123.42 x 84.15 km)

CONCENTRATION (STD UNITS/M**3)

A :   2.7 E-08
B :   2.7 E-07

TIME   08/15/84-13:30:00

WIND SPEED (M/S), DIRECTION (DEG)

KH,KZ DIFFUSIVITIES (M**2/S)

Witbank
ARNOT
WILGE
DUVHA
HENDRINA
KOMATI
Hendrina
KRIEL
MATLA
7
5
Leslie
Evander
Trichardt
Bethal
Ermelo
SASOL 2
SASOL 3
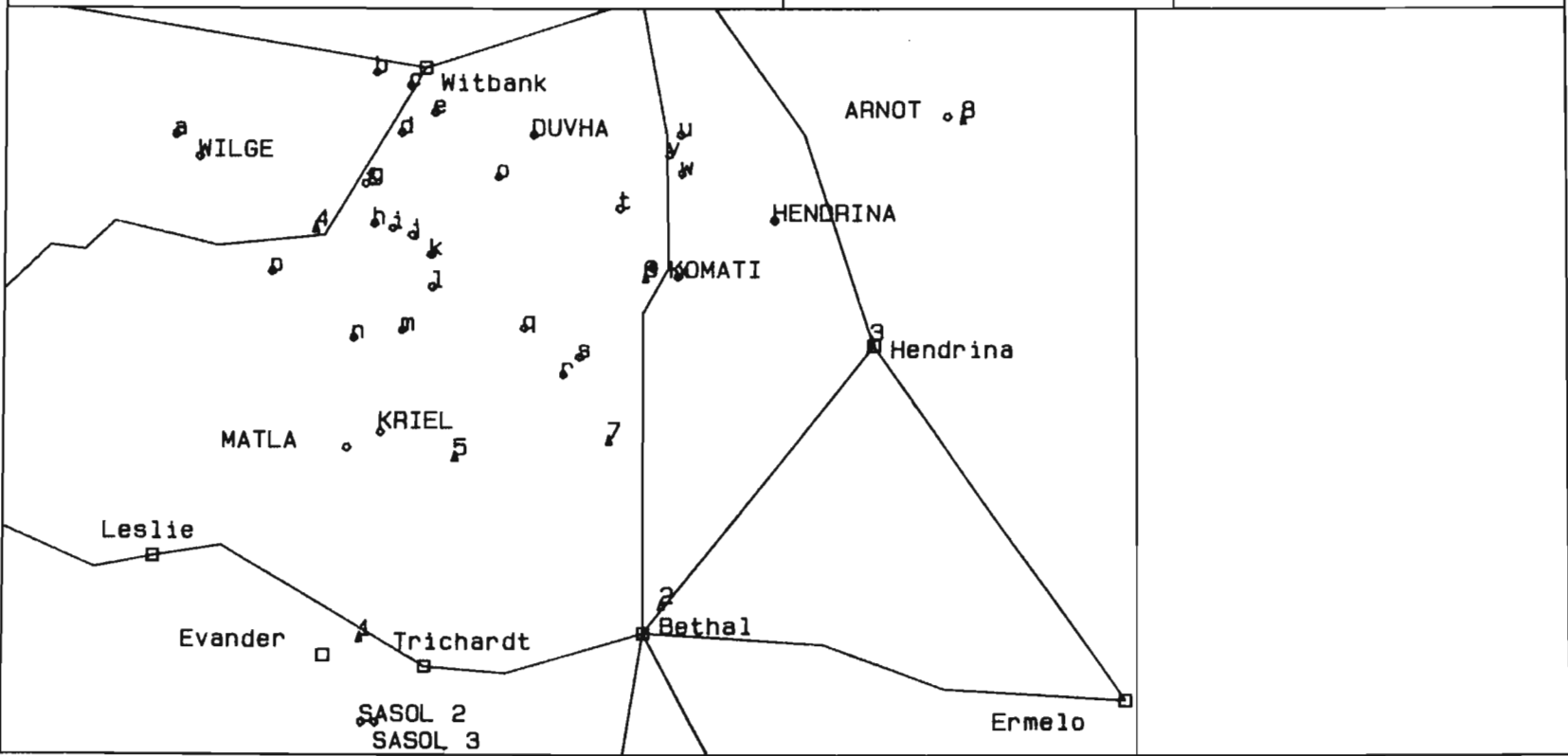
Figure 4.13   A display of the features that may appear on the
graphics screen.

4.4. SPECIAL FEATURES OF THE PACKAGE

The four models PREMET, METPAC, DSPRSN and ISPLTH are run by a master program called WIZARD. Before WIZARD is run, the user has to specify some of the fixed information such as grid sizes, topography, deposition velocity, graphics terminal, and so on. This is done by the program called INSTALL. INSTALL is "menu driven". Information for seven categories must be supplied. These categories are:

    (1) Model parameters

    (2) Source information

    (3) Terrain information

    (4) Pollutant characteristics

    (5) Meteorological measurements

    (6) Configuration of output devices

    (7) Map of prominent features.

Each of these are discussed below.

4.4.1. Model Parameters

This category is subdivided into three subheadings:

    (a) Wind field module

    (b) Dispersion module

    (c) Isopleth module

The wind field model requires specification of the following infomation:

    (1) Longitude and latitude of the area of interest (degrees)

    (2) Time difference from Greenwich mean time (hours)

    (3) Length and breadth of area of interest (meters)

    (4) Angle between North and the map reference frame (degrees)

    (5) The horizontal grid interval (metres)

(6) Anomalous divergence tolerance for each of the three wind field levels.

The dispersion module requires only the specification of the grid spacing between the vertical layers.

The output is in the form given in figure 4.13. Wind and diffusivity profiles are drawn at a specific position supplied by the user. The default position is in the middle of the map. The wind vectors and isopleths can be drawn at any height. The number of isopleth values depends on the array size in the program. It is therefore required to specify the following information:

(1) The height at which the isopleths should be calculated (metres)

(2) Grid spacing for the isopleth drawing (small for high resolution) (metres)

(3) Grid interval between wind vectors

(4) Height at which wind vectors must be drawn (metres)

(5) Position of the wind and diffusivity profiles (default: in the middle of the map) (metres)

(6) Type of wind profile required:

(a) u, v wind components

(b) wind speed and direction

(7) Number of isopleths to be drawn, and it is then necessary to choose from one of the following:

(a) fixed isopleths to be specified (g/m^3)

(b) the n isopleths scaled relative to the highest concentration prediction

(c) a combination of (a) and (b)

(8) If there are certain receptor points, then their positions should be specified. The concentrations at these points are stored in a file and continually updated on the screen.

4.4.2. Source Information

At the moment only point sources can be accomodated. Four specifications are required for each point source:

(1) Source position (metres)

(2) Source height above local ground level (metres)

(3) Radius of stack (metres)

(4) Specification of source rate. Supply one of the following

   (a) exit gas velocity and density

   (b) mass flowrate and density

   (c) volumetric flowrate and density

   (d) mass flowrate and exit gas velocity

   (e) mass and volumetric flowrates

It is important to note that when the pollutant is part of a range of gases being emitted from the stack, the density is given by

$$\rho = f_{gas}\rho_{gas}$$

where f_{gas} is the fraction of the pollutant in the gas stream.

4.4.3. Terrain Infomation

It is required to specify the altitude at each wind field grid point. If no topography is available or if it is not essential (i.e., in the case of flat terrain), only the mean altitude has to be specified. In order for the model to identify inland lakes, the height of the lake must be specified as a negative value.

The roughness length and zero displacement distance must be specified at each wind field grid point. This can be done in two ways: specification at each grid point, or, sparse values at certain points. When sparse values are supplied, a logarithmic interpolation (equation (4.3)) is used.

184

4.4.4. Pollutant Characteristics

A list of pollutants (SO_2, NO_2, HNO_3) is available for menu selection; however, if a pollutant is not on this list, the following information must be supplied:

(1) Name

(2) Reaction rate constant (s^{-1})

(3) Washout removal rate constant (s^{-1})

(4) Canopy resistance (s/m)

(5) Sedimentation velocity (m/s)

This new compound will then be added to the databank.

4.4.5. Meteorological Measurements

The user must specify whether it is an on-line or off-line execution and the following information for each of the meteorological measurement categories :

(1) Surface layer measurements

    (a) Specification of measurement type

    (b) Roughness length at the measuring point

    (c) x,y,z coordinates of measuring pointrelative to local ground level

    (d) Altitude of measuring point

(2) Outer layer measurements

    (a) Measurement type

    (b) x,y position of measuring point

    (c) The number of outer layer measuring points

    (d) If the measurements are at fixed heights, these should be supplied

(3) Boundary layer height measurements

    (a) Measurement type

    (b) Position of measurement

(4) Diffusivity profiles (at the moment only from similarity theory)

(5) Spatial temperature measurements. Positions of temperature measurements

(6) Rainfall measurements. Positions of rainmeters.

Categories 1, 2 and 3 have been discussed in Section 4.1.1. and will not be repeated here. Currently only the diffusivity profiles discussed in Section 4.2.2. are available. In case of large spatial temperature differences, such as land/sea and land/lake interfaces, average temperatures should be specified for each configuration. Positions of rainmeters should be specified, if available.

4.4.6. Output Device Configuration

At present, only graphics terminals are used. Incorporating plotters might be a possibility, but because of the slow speed of plotters it was considered wiser to have a separate program to plot the drawing. This is normally done when running a batch job. The user needs to supply the graphics terminal type. Presently only five types are supported:

(1) HP 2622A

(2) HP 2623A

(3) HP 2627A

(4) HP 150 (PC)

(5) TEKTRONIX 4105

If it is desired to add a new terminal to the list, it is required to specify the sequence of control characters for drawing to a point in the "up" or "down" position, and for writing text on the screen. These program lines have to be added to the subroutine PLOT and SYMBOL in ISPLTH. Some terminals require an initialising character string and a termination character string. The control characters for this need to be added to GRAFON and GRAFOF, respectively.

A character set can be divided into four groups :

    (1) Control characters (eg. ESCAPE, LINEFEED, RETURN, *etc.*)
    (2) Operand commands (eg. +, -, *, *etc.*)
    (3) Upper case letters
    (4) Lower case letters

These characters are accessed differently on different computers.
The two most used character set codes are ASCII and EBCDIC. There is
a choice of three at present

    (1) ASCII
    (2) EBCDIC
    (3) CYBER-6 bit ASCII

These three were used on the following three computer hosts

    (1) SPERRY UNIVAC 1100
    (2) IBM 4341
    (3) CDC CYBER 750,

respectively.

The output screen is divided into three windows: a window for the
map and concentration isopleths, a window for the wind speed and
diffusivity profiles and, a window for text (heading, subheadings,
time, *etc.*). The window for the map is obviously the most important.
The size of this window is therefore maximised. It is also possible
to specify the fraction of the screen allowed for this window.

4.4.7. Prominent Features on Map

Lines, symbols and text can be supplied on the map (Figure 4.14).
The different symbols that can be chosen are:

    (1) Triangle

187

(2) Square

(3) Circle

A triangle or square is specified by the length of a side and the position of the centre. A circle is specified by its radius and the centre. Text is specified by the position of the lower, left-hand corner of the text, and the text orientation. The user is also prompted to specify heading lines. Triangles are automatically drawn at surface layer weather stations. Sources are indicated by a circle and a name. Receptor points are numbered.

4.4.8. Data File Format

The terminology for data files is as follows:

- The data for different meteorological stations are kept in separate files
- Each file contains records for different times
- Each record contains readings which have a specific format
- Readings can be on one line or more.

The first four readings in a record are always

(1) TIME (in hours or fractions thereof)

(2) DAY (day of the month)

(3) MONTH (1-12)

(4) YEAR

These appear in the first line of a record.

The input format for all the meteorological measurement options are given in Appendix I. Appendix I also contains the format for source data specification.

188

Off-line Mode

When the simulation time is between two record times, a linear interpolation is performed. If, however, the time interval between two records is too large, the file will be ignored until the simulation time is close enough to the next record. This also applies when the data from a file stop prematurely. The readings from the last record will be used until the simulation time has gone beyond the time interval allowed between records. A warning will be printed together with the appropriate action.

On-line Mode

The option to operate the model in real-time has been incorporated in PREMET. This application has not been fully tested and will only be warranted once the situation exists, and computational power is available, to operate in this mode.

CHAPTER 5

5.1. NUMERICAL TESTS

The behaviour of the numerical dispersion model, when applied under simplified atmospheric conditions, is investigated. The predictions from the numerical model are compared to the Gaussian puff and plume models (equation (3.104), and (3.105)), which are derived under uniform wind and diffusivity profiles. When introducing an impenetrable inversion height, the Gaussian plume model can be stated as (Section 3.2.1.)

$$
\langle C(x,y,z) \rangle = \frac{M'}{2\pi\sigma_y(x-x_0)\sigma_z(x-x_0)U} \exp\left[-\frac{(y-y_0)^2}{2\sigma_y^2(x-x_0)} \right]
$$
$$
\times \left[\sum_{n=1}^{\infty} \exp\left[-\frac{1}{2}\left\{ \frac{z-H-2nh_p}{\sigma_z(x-x_0)} \right\}^2 \right] + \exp\left[-\frac{1}{2}\left\{ \frac{z+H-2nh_p}{\sigma_z(x-x_0)} \right\}^2 \right] \right.
$$
$$
\left. + \exp\left[-\frac{1}{2}\left\{ \frac{z-H+2nh_p}{\sigma_z(x-x_0)} \right\}^2 \right] + \exp\left[-\frac{1}{2}\left\{ \frac{z+H+2nh_p}{\sigma_z(x-x_0)} \right\}^2 \right] \right]
$$

(5.1)

where M' is the source strength in g/sec. The puff model is given as:

190

$$\langle C(x,y,z,t) \rangle = \frac{M}{(2\pi)^{3/2} \sigma_x(t) \sigma_y(t) \sigma_z(t)} \exp\left[-\frac{(x-x_0-Ut)^2}{2\sigma^2(t)} - \frac{(y-y_0)^2}{2\sigma_y^2(t)} \right]$$

$$\times \left[\sum_{n=1}^{\infty} \exp\left[-\frac{1}{2}\left\{\frac{z-H-2nh_p}{\sigma_z(t)}\right\}^2 \right] + \exp\left[-\frac{1}{2}\left\{\frac{z+H-2nh_p}{\sigma_z(t)}\right\}^2 \right] \right.$$

$$\left. + \exp\left[-\frac{1}{2}\left\{\frac{z-H+2nh_p}{\sigma_z(t)}\right\}^2 \right] + \exp\left[-\frac{1}{2}\left\{\frac{z+H+2nh_p}{\sigma_z(t)}\right\}^2 \right] \right]$$

$$(5.2)$$

where M is the amount of material in the puff. H is the release height and h_p, the inversion height. Seinfeld (1975) suggested that the series cut-off at n = 4 is adequate.

The modified limiting value (MLV) numerical method for solving the vertical diffusion is derived in Section 4.2.1. Firstly, the optimum criterion (Section 4.2.1.) necessary for the numerical model to produce accurate predictions, is established. The dependence of the optimum criterion on model parameters, such as diffusivities, release height, and grid spacing, is then investigated. Finally, the numerical model is run using the chosen optimum criterion and realistic wind and diffusivity profiles.

The sensitivity of the MLV numerical method to the value of the optimum criterion, f_c, is computed. f_c is given by

$$f_c = \frac{K_v \Delta t}{\Delta z^2} \qquad (5.3)$$

The conditions under which the simulation was done, were

x-component of the wind speed:	U	= 5	m/s
y-component of the wind speed:	V	= 0	m/s
horizontal diffusivity	: K_H	= 60	m²/s
vertical diffusivity	: K_v	= 30	m²/s
release height	: H	= 50	m
top of model	: h_p	= 800	m

with the wind and duffusivities constant with height. The ground-level concentration, predicted by the MLV numerical method,

Comparison of Optimum Criteria

Ground level Concentration Ratio
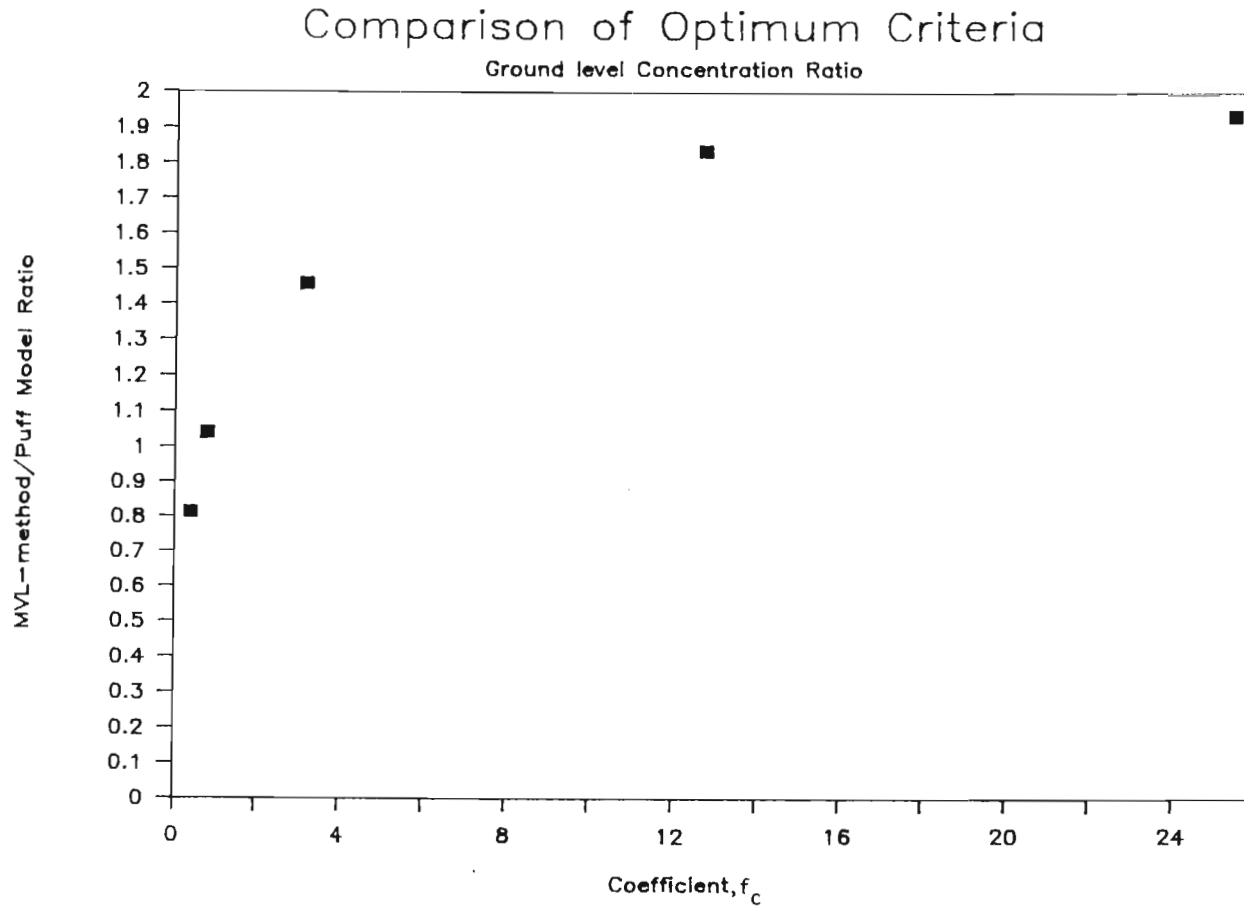
Figure 5.1. The effect on the ground level concentration predictions when using different optimum criteria in the modified limiting value (MLV) numerical method. The definition of the optimum criterion, f_c, is given in equation (5.3). The ratio, equation 5.4, of the ground level concentration predictions from the MLV and the puff model is averaged over a diatance of 40km, and plotted against f_c.

(Section 4.2.1.), and the Gaussian puff model (equation (5.2)) was compared for different values of f_c. The numerical solution was seeded with initial puffs, maintaining a maximum distance of σ_y metres between puff centres, as under normal operations. Gaussian puffs were released under the same conditions. A 12-hour simulation was done. The ground-level concentration was evaluated downwind along the centreline at intervals of 500m. The ratio:

$$\frac{\text{MLV numerical model prediction}}{\text{Gaussian puff model prediction}} \qquad (5.4)$$

was then calculated at each of these points. The averages of the ratio for various values of f_c are summarised in Figure 5.1. It is clear from the graph that the optimum criterion is very sensitive at about $f_c = 0,8$. Interestingly, one observes that at high values of f_c, the numerical model becomes less sensitive to f_c.

Figure 5.2. shows the downwind concentration ratios (up to 20km) for the two conditions: $f_c = 0,4$ and $f_c = 0,8$. The value of $f_c = 0,8$ appears to be adequate. Having chosen the optimum criterion of $f_c = 0,8$, the ground-level concentration ratios at different distances away from the centre-line are calculated. This is presented in Figure 5.3, and shows favourable comparison between the numerical solution and the Gaussian puff model.

The next test is to indicate the effect of different release heights on the predictions. The test is done for the release heights H = 50m and 100m. The corresponding ground-level concentration ratios are shown in Figure 5.4. The release height has a minimal effect on the model performance.

The sensitivity of the optimum criterion to vertical grid spacing, Δz, and vertical diffusivity, K_v, is indicated in Figure 5.5 and 5.6. On average, fair agreement between the numerical and analytical predictions exists. Some scatter occurred with $\Delta z = 30m$ and with $K_v = 15m^2/s$. However, the averages of the downwind concentration ratios are 1,026 and 0,995, respectively.

Figure 5.7 is a comparison of the numerical method with the Gaussian plume and puff models. 1g/s of material is released at a height of

Optimum Criterion for Numerical Model

Ground level Concentration Ratio

+   coefficient = 0,4   ◇   Coeficient = 0,8
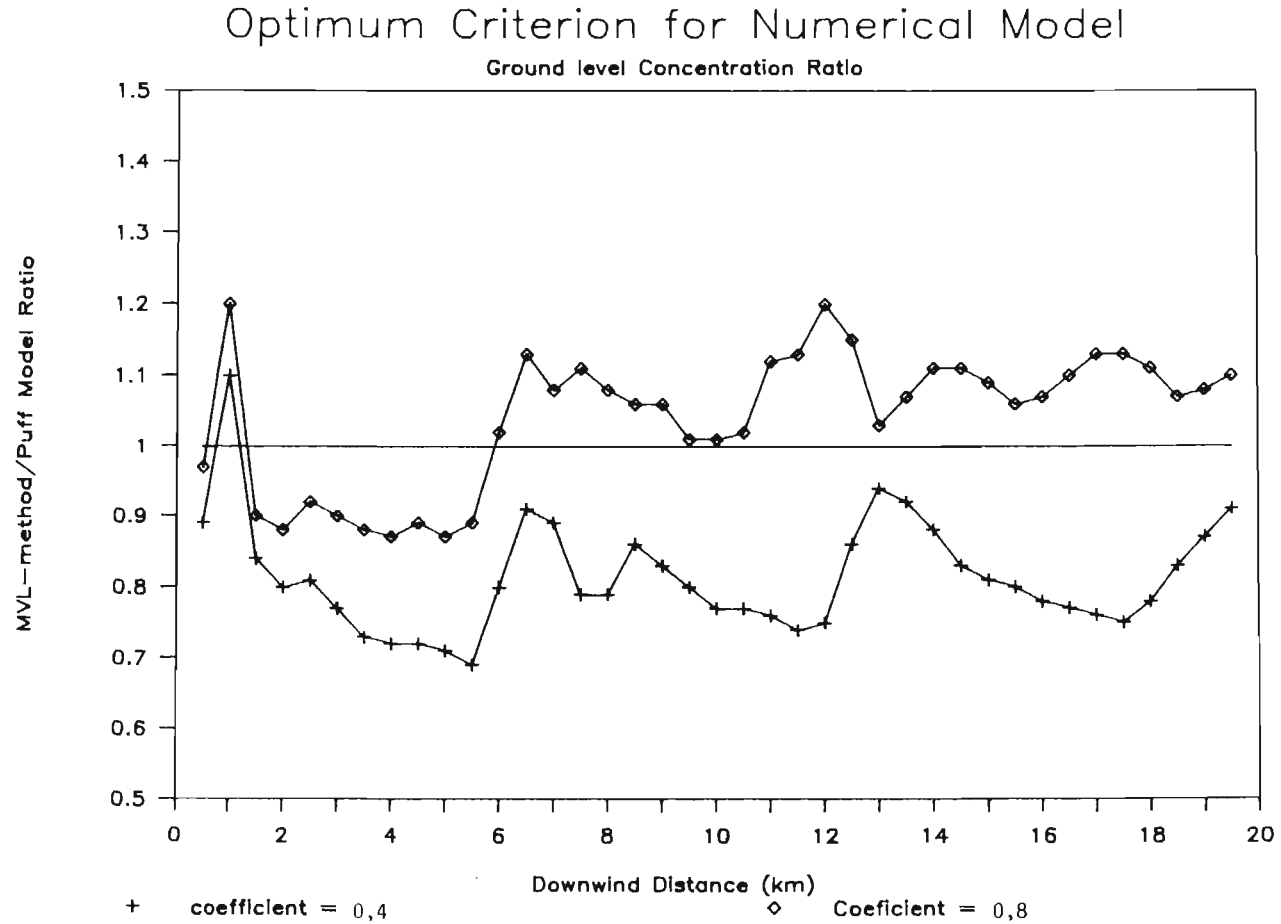
Figure 5.2. A comparison of the ratios of ground level concentrations from the MLV and the puff model when using $f_c=0,4$ and $f_c=0,8$. The ground level concentrations are evaluated at the centreline.
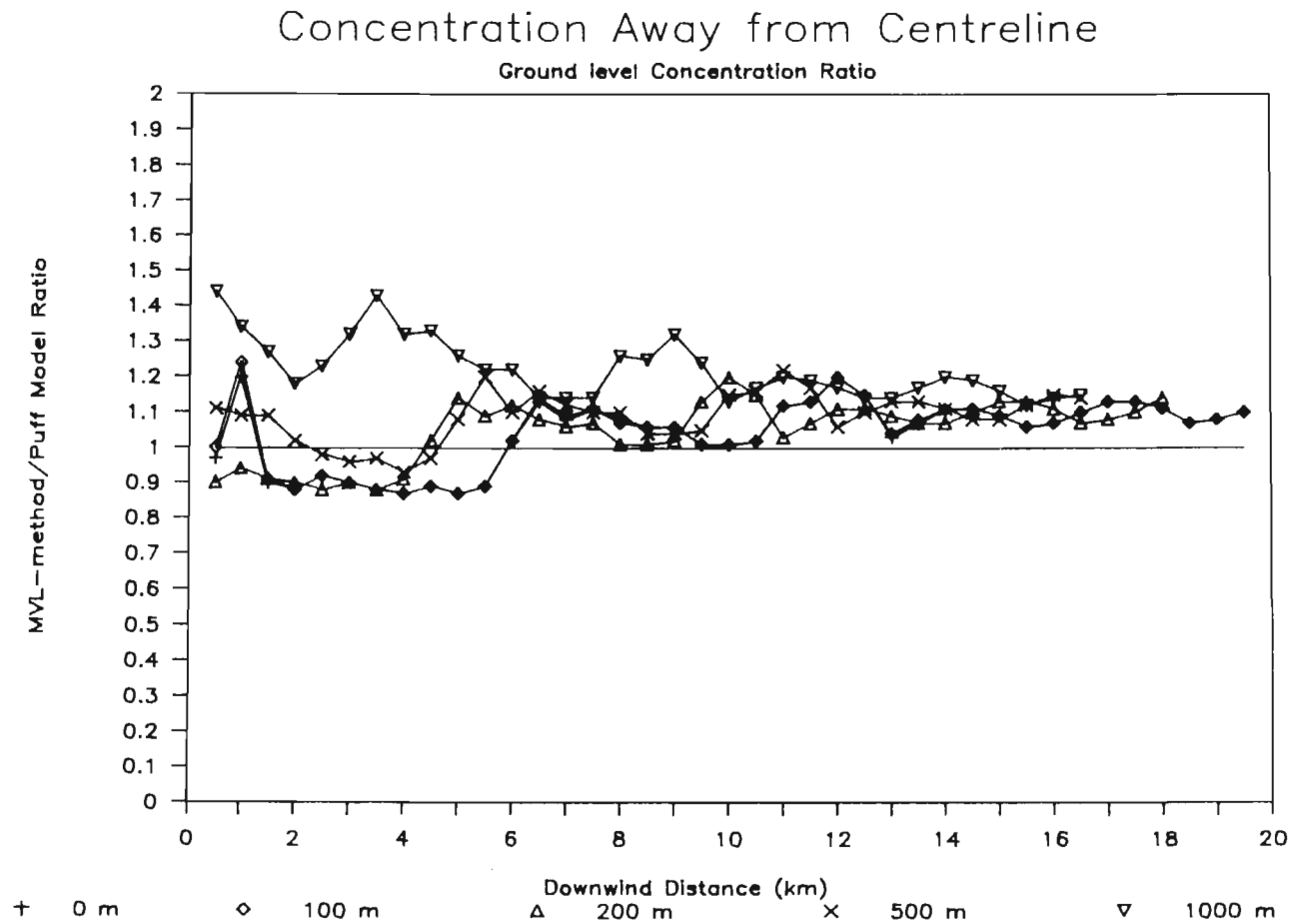
Figure 5.3. Ground level concentrations at various distances away from the centreline.

Effect of Different Release Heights
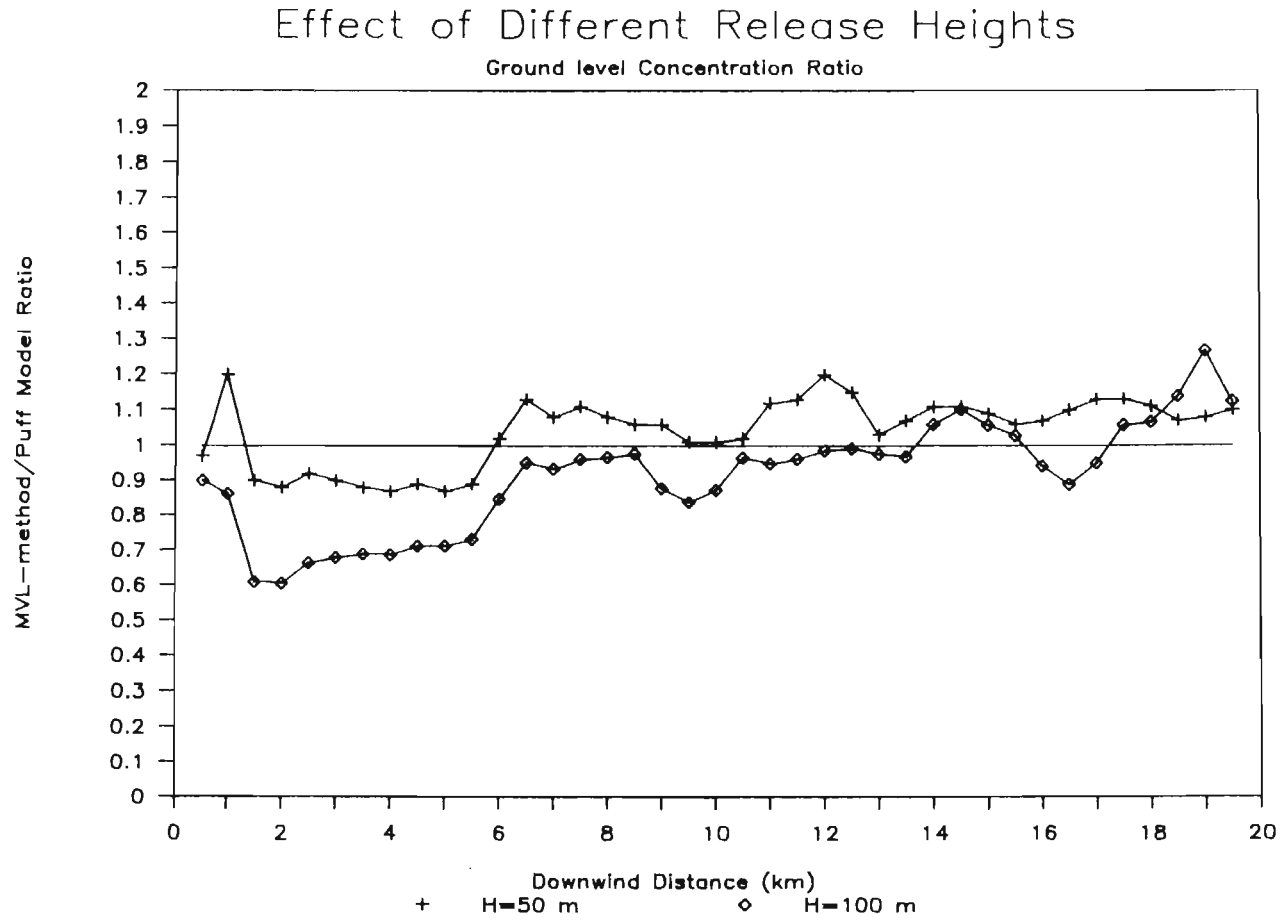
Figure 5.4. The performance of the MLV method when material is released at different heights.
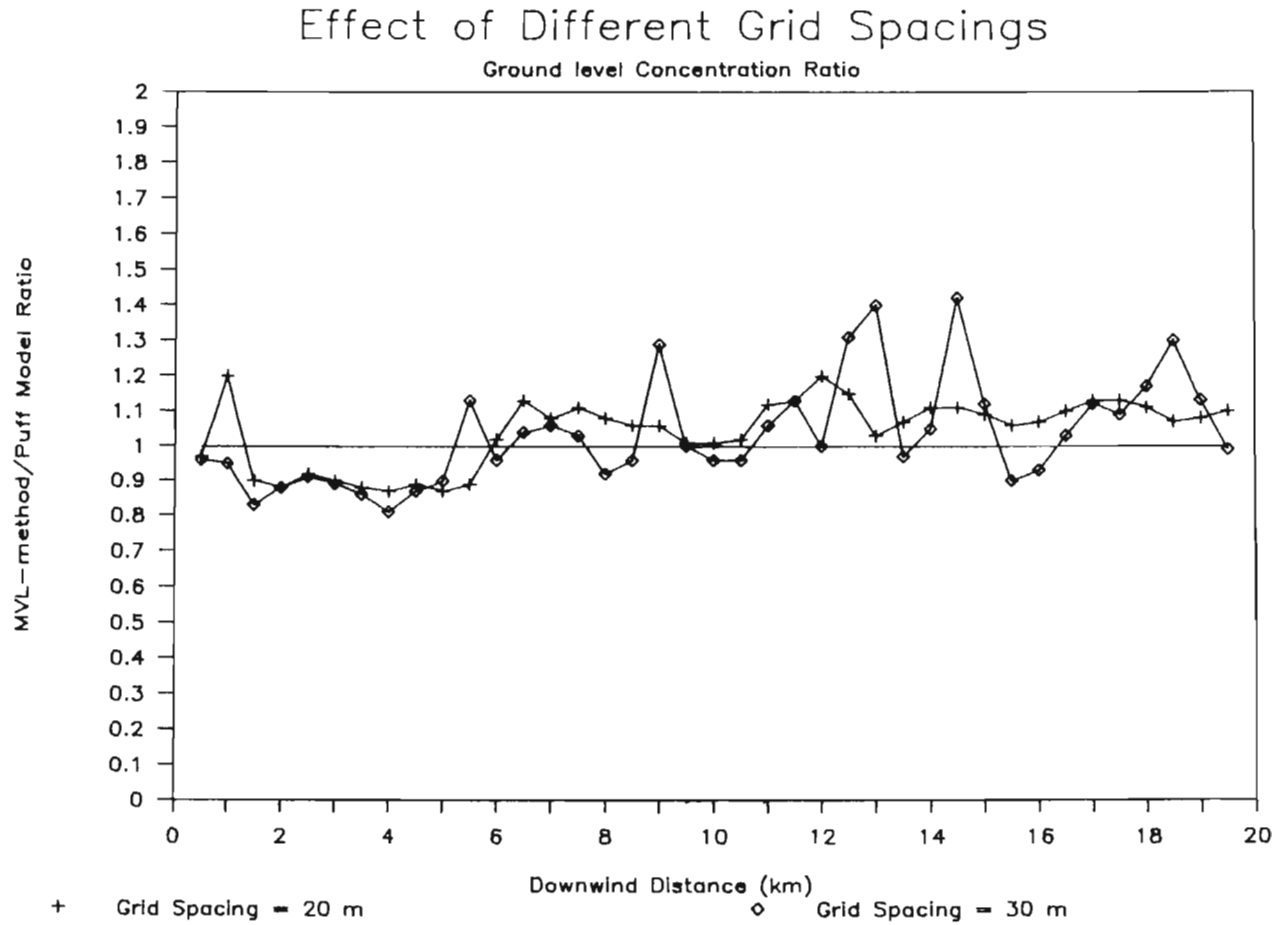
Figure 5.5. The effect on the concentration distribution when different vertical grid spacings are used in the MLV method.

Effect of Different Diffusivities

Ground level Concentration Ratio
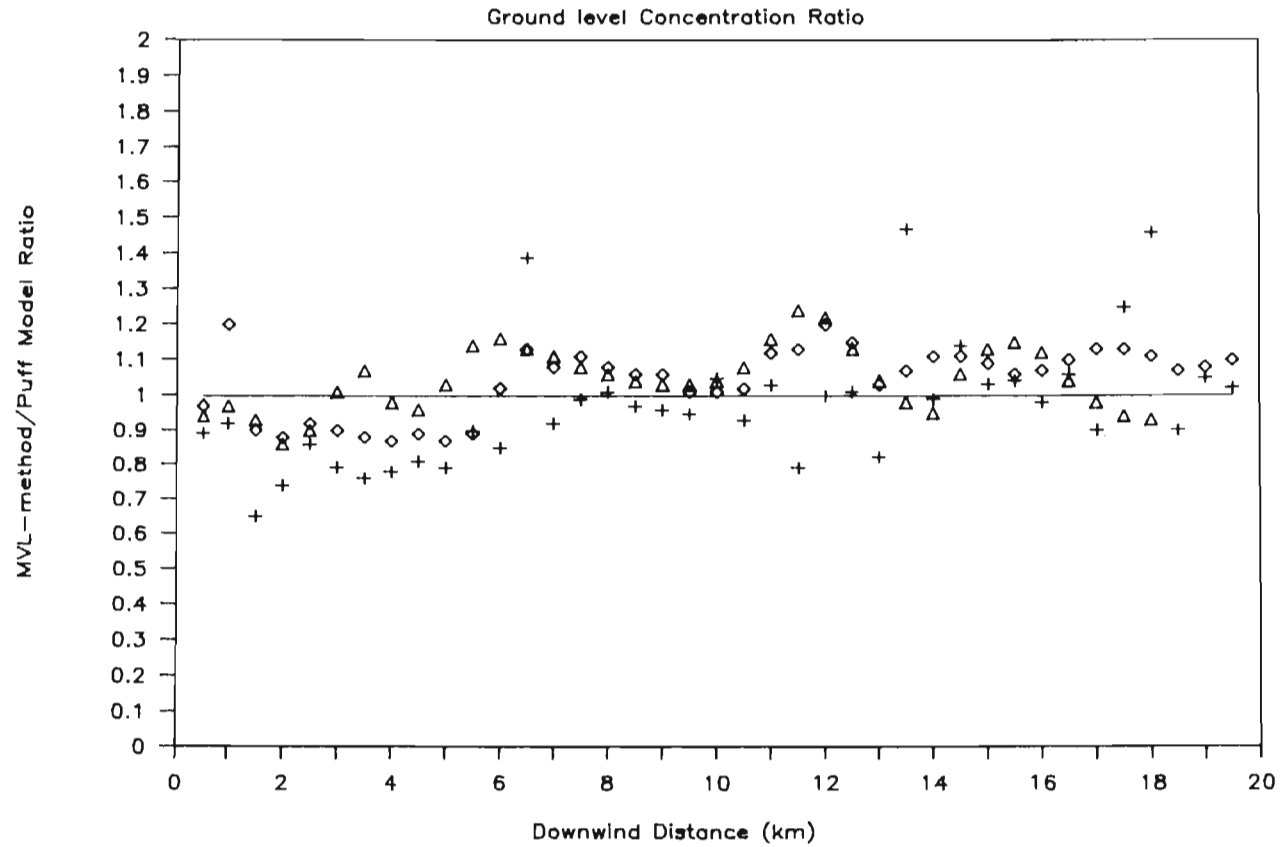
Figure 5.6. The effect different diffusivities have on the concentration distribution when using the MLV method:

$+ -- K_H = 30$ m^2/s, $K_V = 15$ m^2/s

$\Diamond -- K_H = 60$ m^2/s, $K_V = 30$ m^2/s

$\Delta -- K_H = 120$ m^2/s, $K_V = 60$ m^2/s

Analytical Compared to Numerical Model
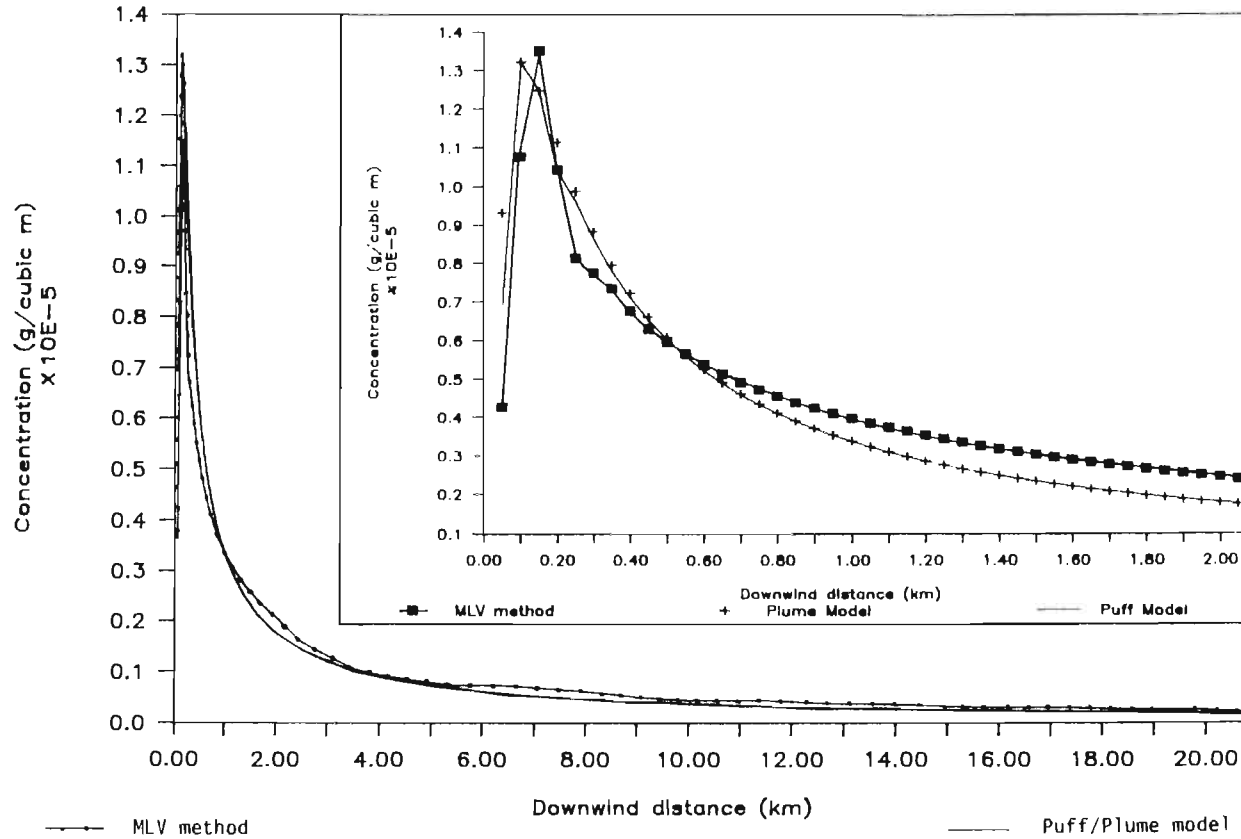
Figure 5.7. Ground level concentration as predicted by the MLV method, is compared to the predictions of the Gaussian plume and puff models. An optimum criterion of $f_c = 0,8$ is used.

50m. The other parameters are $U = 5$m/s, $V = 0$m/s, $K_H = 60$m²/s, $K_v = 30$m²/s, $h_p = 800$m, and $\Delta z = 20$m. The plume model is approximated suitably well using the Ludwig *et al.* (1978) distance criterion, *i.e.*, a maximum distance of σ_y is allowed between puff centres. When this maximum distance is increased to $2\sigma_y$, the approximation is unacceptable.

Figure 5.8 summarises the vertical distribution of the material in a puff, predicted by the numerical method, at different times. Realistic wind and diffusivity profiles are used as indicated in Figure 5.8. The parameters describing the profiles are:

$$u_* = 0,5 \quad \text{m/s}$$
$$\frac{1}{L} = -0,01 \ \text{m}^{-1}$$
$$u_p = 5 \quad \text{m/s}$$
$$z_0 = 0,01 \quad \text{m}$$
$$M' = 600 \quad \text{g}$$
$$H = 50 \quad \text{m}$$
$$h_p = 800 \quad \text{m}$$

The vertical diffusivity profile under these conditions is also shown in Figure 5.8. After 10 minutes significant diffusion has taken place in the lowest 100m. The material then gradually disperses upwards. Eventually, at times greater than 4 hours, a completely mixed and uniform distribution is achieved below 800m.
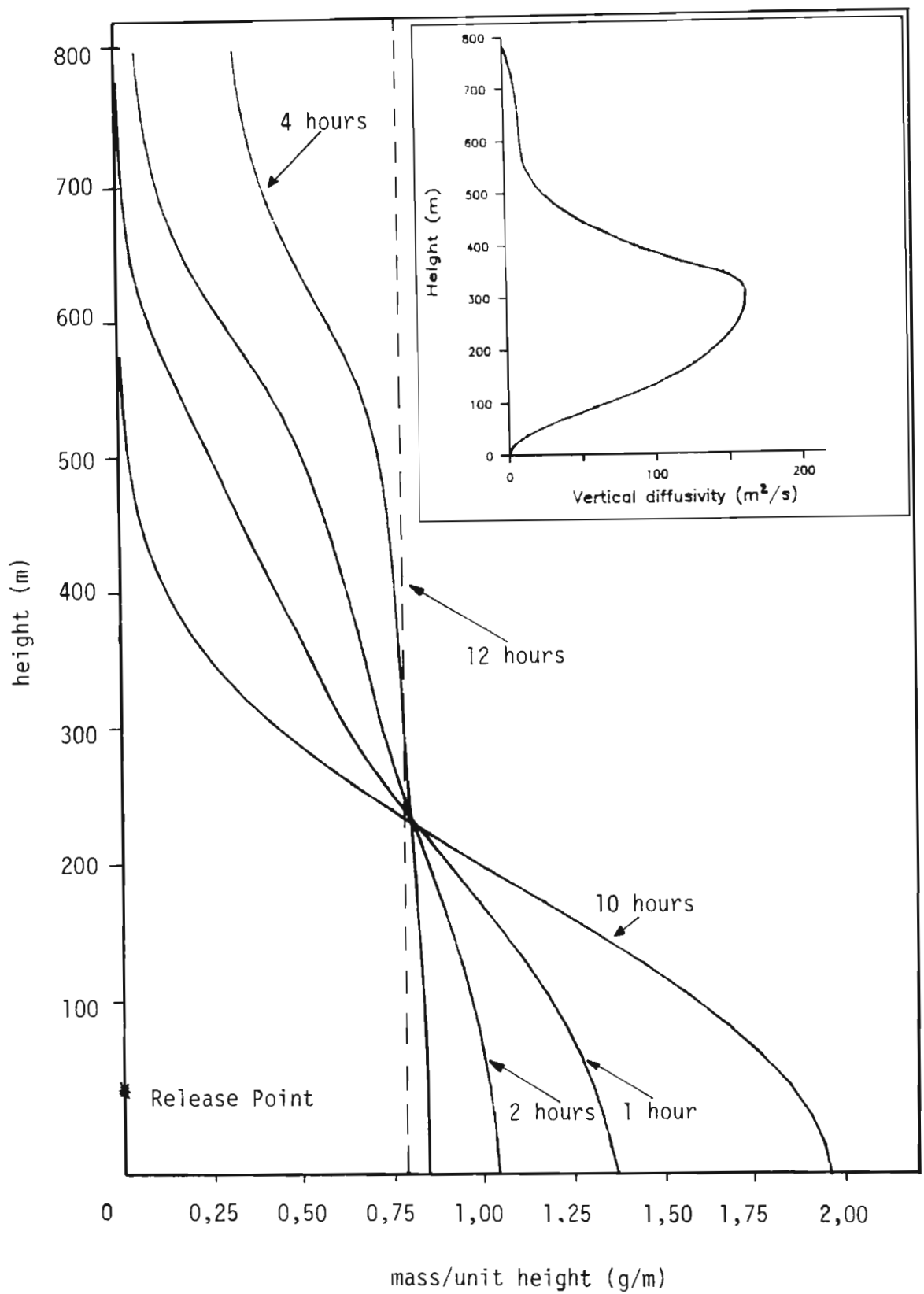
Figure 5.8. Mass profile at four downwind distances. The inset shows the diffusivity profile during the simulation. A vertical grid spacing of 20m was used.

5.2. DEMONSTRATION RUNS

The next two sections are concerned with evaluating the model under real situations. More accurate weather and source data were available for the first experiment, which was therefore used to indicate the accuracy of the model. The second case study was more to demonstrate the performance of the model when applied in a large area with multiple ground and elevated sources.

5.2.1. Durban Bluff

This study-area is characterised by moderate topography. Directly off the coastline rises an approximately 100m bluff, which descends equivalently inland. A similar, but lower hill (approximately 70m high), exists inland, parallel to the coastline bluff. Three SO_2 producing industries lie between these two hills : SAPREF, MONDI, and MOBIL. SAPREF has seven stacks, MONDI is simulated using one stack and MOBIL, two stacks. The approximate positions of these stacks are shown in Figure 5.10(a) and (b).

The bluff area is associated with north-easterly and south-westerly winds. During calm conditions, light sea and land breezes exist. A mono-vane and a cup anemometer (RM Young), on top of each of four 10m-masts (masts 1 to 4 in Figure 5.10(b)), supply the initial estimate of the surface wind field. A 12V battery-powered data acquisition station records the wind speed and direction at each mast at approximately 60 second intervals. This is stored in memory as two hexadecimal numbers. Runs lasting 36 hours, with a 1 minute sampling interval, can be stored. Data are retrieved from the station via an ordinary cassette tape-recorder to an Apple IIe microcomputer where they are converted to decimal equivalents. The converted readings are then written onto a diskette and finally transfered to a Sperry Univac 1100 mainframe computer.

Figure 5.10(a) A three-dimensional view of the Durban Bluff area.
It is important to note that the vertical scale is about 3.5 the
horizontal scale. The terrain is therefore much flatter than it is
indicated in this figure. The grid spacing is 130 m.
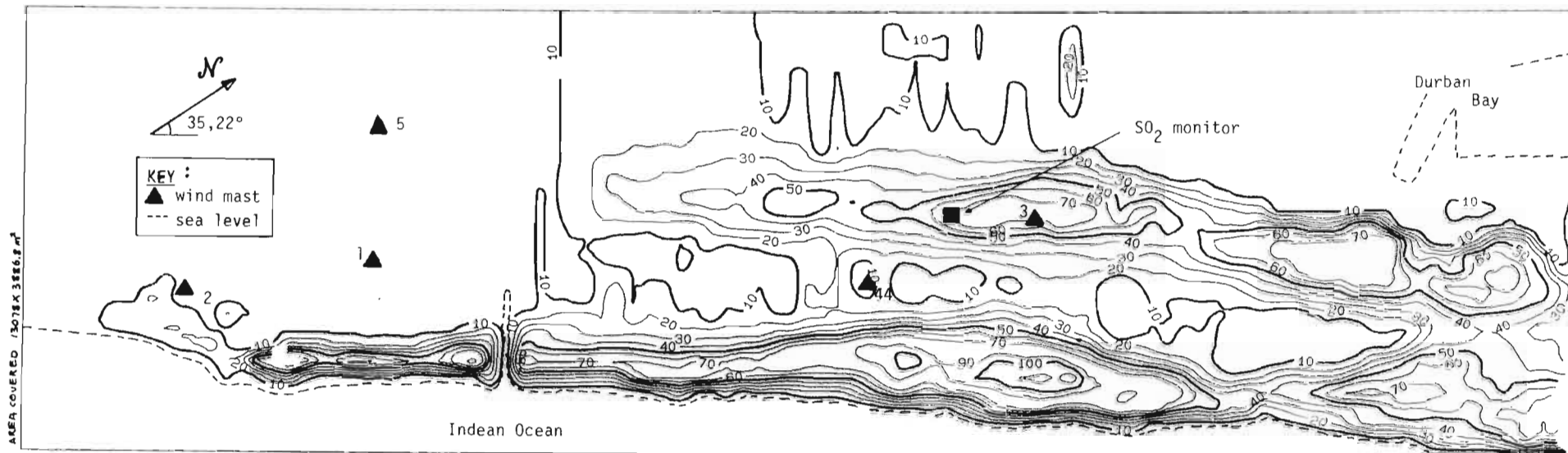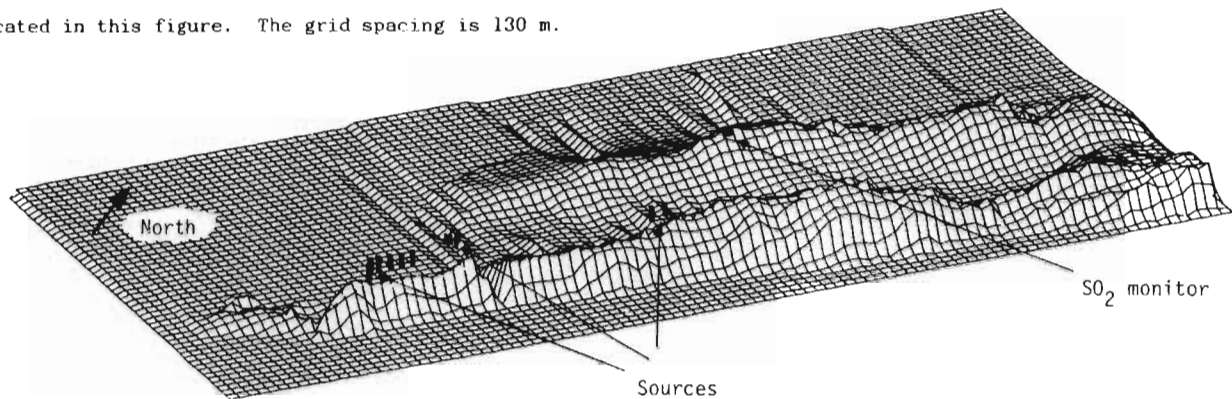
Figure 5.10(b)   Durban Bluff topography.   The positions of the masts
are also shown.

Additional hourly temperature measurements and cloud cover estimates
are available from the nearby airport (indicated as mast 5). This
allows the second surface wind option to be used (see
Section 4.1.1.), *i.e.*,

"wind velocity, cloud cover and temperature"

The airport also supplies twice-daily upper air wind and temperature
measurements.

TABLE 5.1. Site information and model parameters for the Durban
Bluff case study.

Longitude ; latitude	30,98°E ; 29,87°S
Time difference from GMT (Universal Standard Time, UST)	+ 2 hours
Dimensions of study area	13077,9m x 3830,9m
Angle between north and the x-axis of the wind field reference frame	35,22°
Wind field grid spacing	132,1m
Vertical grid spacing for dispersion model	20m
Isopleth resolution	20m
Divergence reduction criteria:	
Surface layer	$1 \times 10^{-6} \ s^{-1}$
Outer layer 1	$1 \times 10^{-5} \ s^{-1}$
Outer layer 2	$1 \times 10^{-4} \ s^{-1}$

Shrub and open area
$r_o = 0,12$ m

Vlei
$r_o = 0,2$ m

Coastal bush $r_o = 1,0$m

Sea $r_o = 0,001$ m

Industry $r_o = 1,2$ m

Coastal bush $r_o = 1,0$ m

Suburban houses
and trees $r_o = 0,5$ m
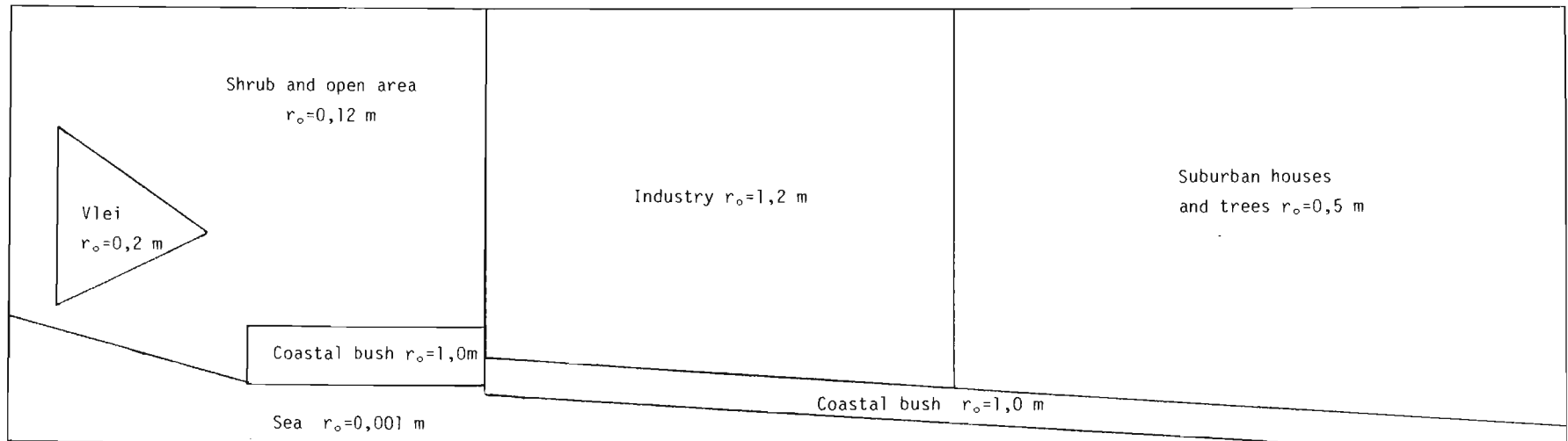
Figure 5.11   Estimates of roughness for the Durban Bluff case study
obtained from Figure 2.3.   Values are given in metres.   (Same map
area as Figure 5.10).

Hourly SO_2 concentration measurements are available. These are measured on the inland hill indicated in Figure 5.10(b).

The site position and dimensions are supplied in Table 5.1. The model parameters used during the simulation runs, are also summarised in Table 5.1. Exact source positions and dimensions are not disclosed due to security reasons. Release heights are approximately 100m.

The altitude at each wind field-grid point (132,1m intervals) is calculated using a linear interpolation between the topography contours available at 10m intervals. Six distinct surface covers were identified for evaluating roughness lengths. An average roughness length was estimated for each cover using Figure 2.3., and supplied at each wind field grid point. This is indicated in Figure 5.11. No zero-plane displacement distances are necessary (d=0).

The positions of the meteorological measuring points are indicated in Figure 5.10(b) and summarised in Table 5.2.

TABLE 5.2. Surface layer weather station information. The origin is at the lower left-hand corner of Figure 5.10(b).

Station No.	Roughness length (m)	Coordinates (m)	Height (m)	Altitude (m)
1) Bitumen	0,12	3276,0; 1824,0	10	15,00
2) Car park	0,12	1359,0; 1533,0	10	15,00
3) Wentworth	0,50	8540,4; 2146,2	10	70,00
4) Pegasus club	1,20	7160,4; 1651,2	10	17,50
5) Louis Botha	0,01	3270,0; 2940,0	10	14,00

The default values supplied by INSTALL are used for chemical reaction, dry deposition and washout rate constant of the dispersing SO_2, *viz.*,

206

Chemical reaction   : k_r = 2,878x10^{-6} s^{-1}
Canopy resistance   : Stable = 1000   s m^{-1}
                         Neutral = 300   s m^{-1}
                         Unstable = 100   s m^{-1}
Washout rate constant : k_w = 3,0x10^{-5} s^{-1}

The experiment lasted from 09h50 on 22/09/1986 to 10h00 on
23/09/1986. A fairly strong south-westerly wind (~5m/s) existed from
09h50 to about 16h00 on 22/09/1986. The wind speed then dropped to
an average of ~1m/s. This was accompanied by sporadic changes in
wind direction. These conditions are summarised in Figure
5.13, 5.14, and 5.15. A 10 minute smoothing period wa.   .ed
the wind readings. Stations 1 and 2 indicated a t   in wind
direction at about 21h00, the wind becoming an easterly wind.

TABLE 5.3. Hourly cloud cover estimates and temperature measurements
at Louis Botha Airport (mast 5).

Time	Cloud Cover	Temperature (K)	Rainfall Rate (mm/h)
9h00	0,375	299,1	0,0
10h00	0,750	298,8	0,0
11h00	0,750	297,0	0,0
12h00	0,750	296,8	0,0
13h00	0,750	296,3	0,0
14h00	0,125	298,2	0,0
15h00	0,250	296,0	0,0
16h00	0,750	296,0	0,0
17h00	0,875	297,2	0,0
18h00	1,000	297,7	0,0
19h00	1,000	297,9	0,0
20h00	1,000	298,0	0,0
21h00	1,000	298,2	3,0
22h00	1,000	298,2	3,0
23h00	1,000	298,3	0,1
24h00	0,500	298,4	0,0

Wind Bearing at Station 1
22/9/1986 (run 3)
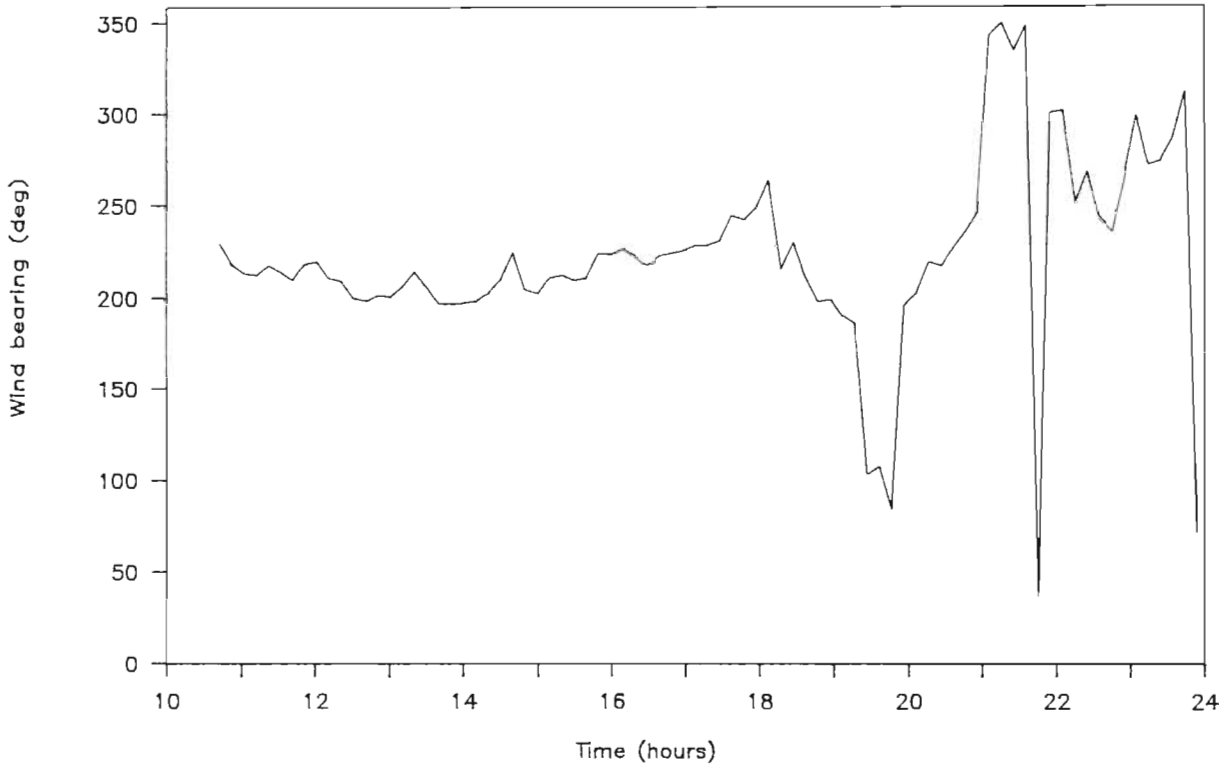
Wind Speed at Station 1
22/9/1986 (run 3)
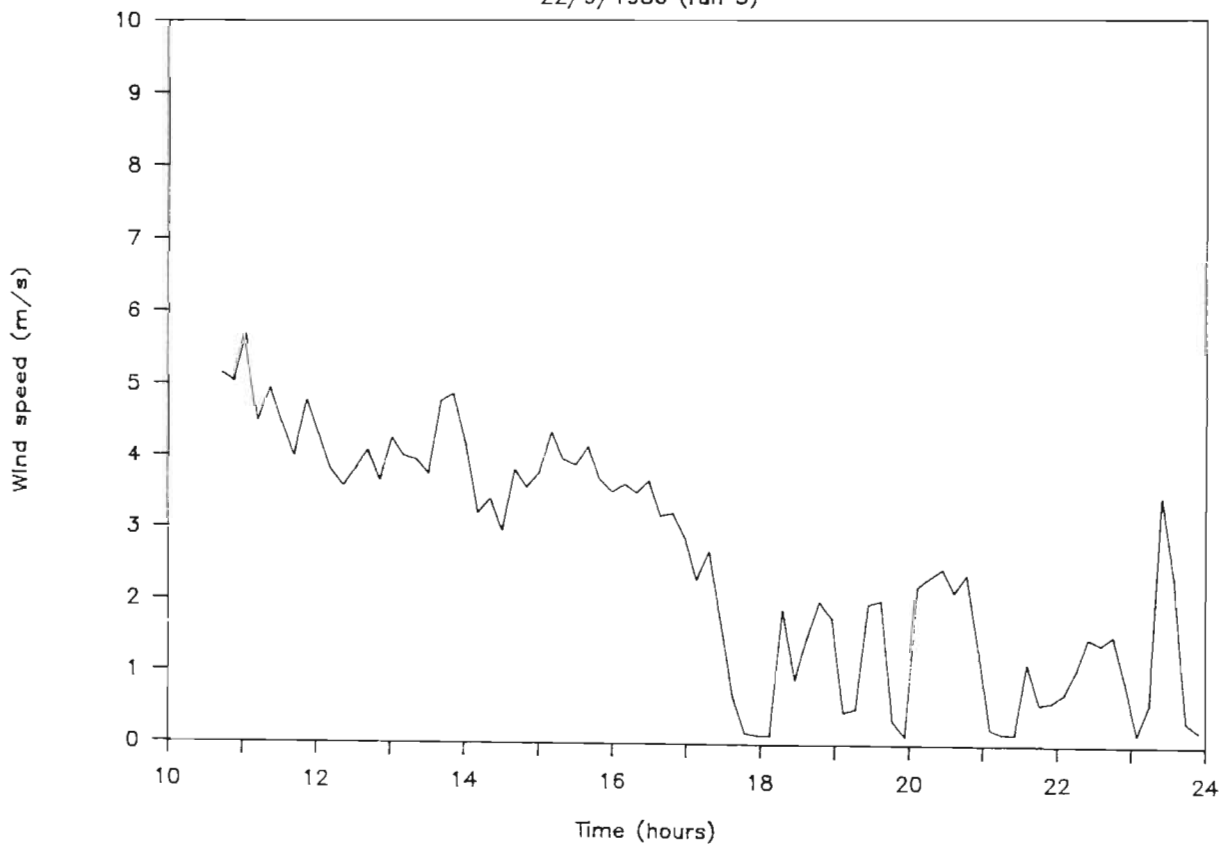
Figure 5.12   Wind speed and direction measured at 10m height at station 1 for the period 10h00 to 24h00, 22/09/1986.

Wind Bearing at Station 2
22/9/1986 (run 3)
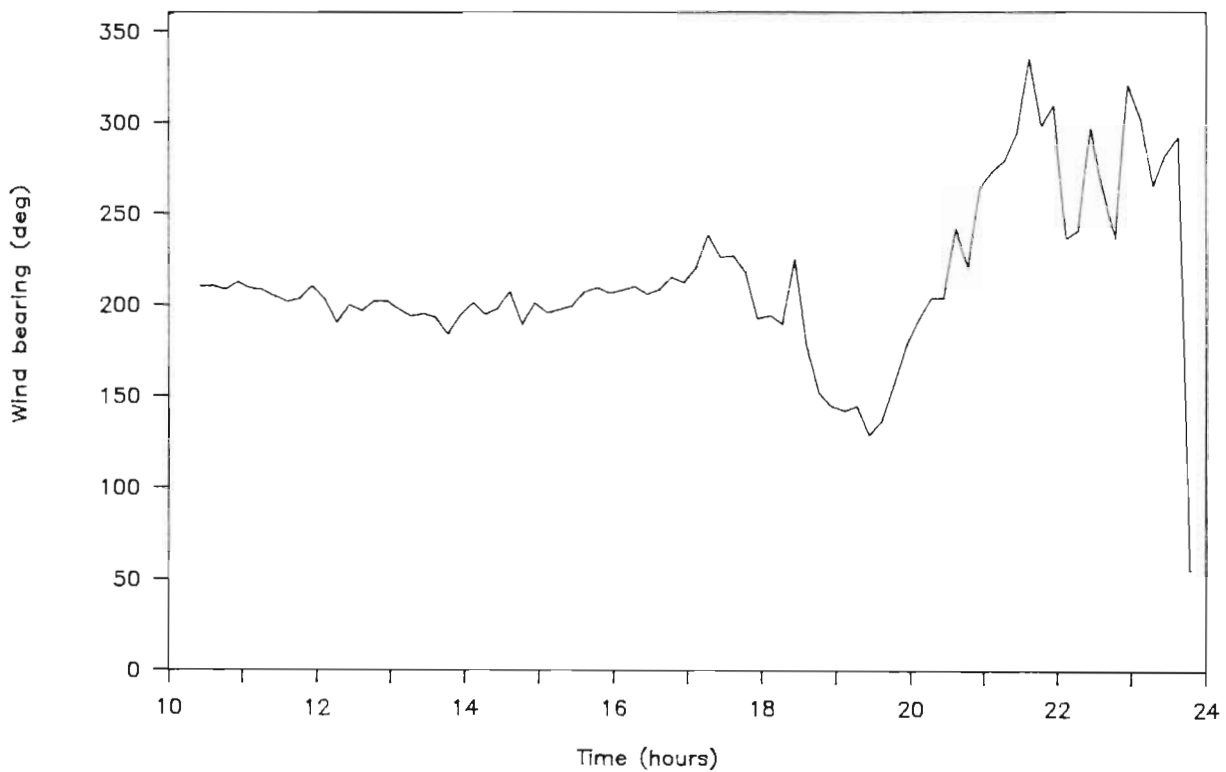
Wind Speed at Station 2
22/9/1986 (run 3)
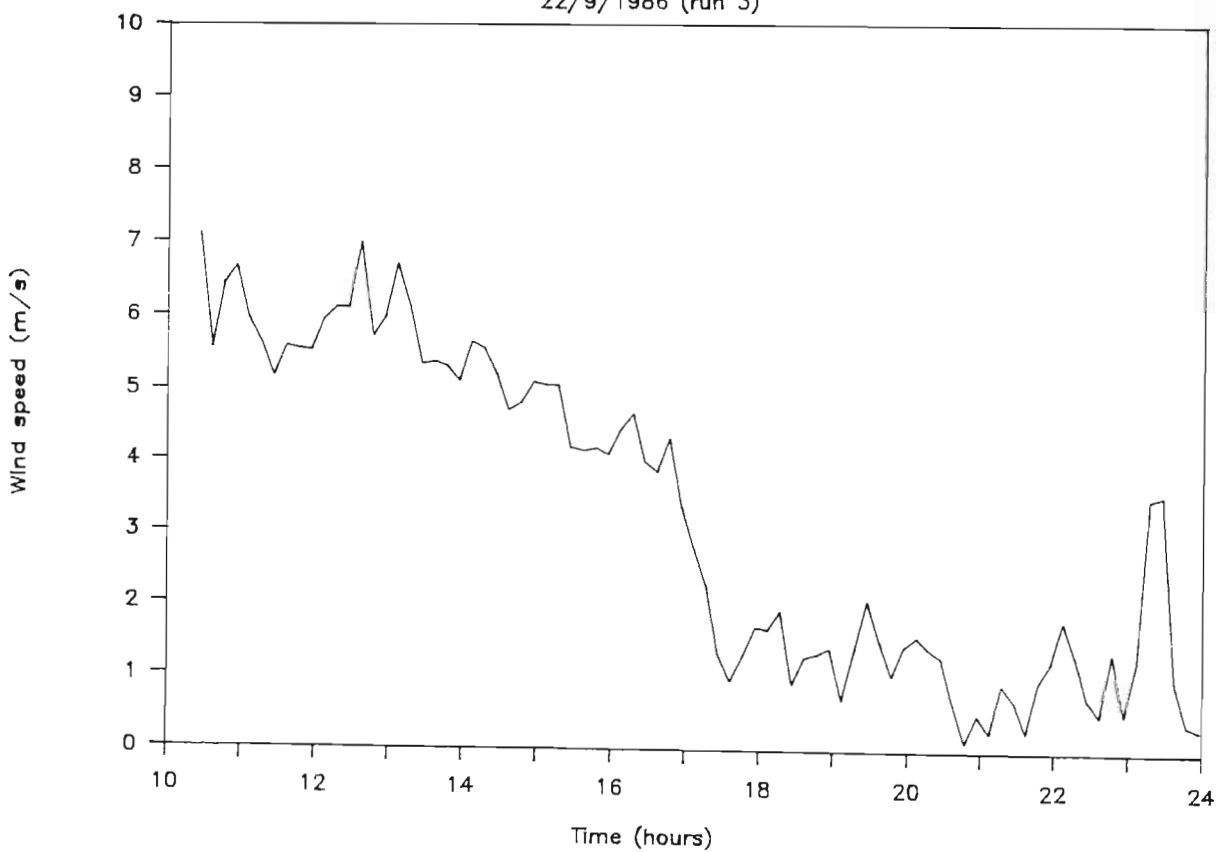
Figure 5.13   Same as for Figure 5.12, but for station 2.

Wind Bearing at Station 3
22/9/1986 (run 3)
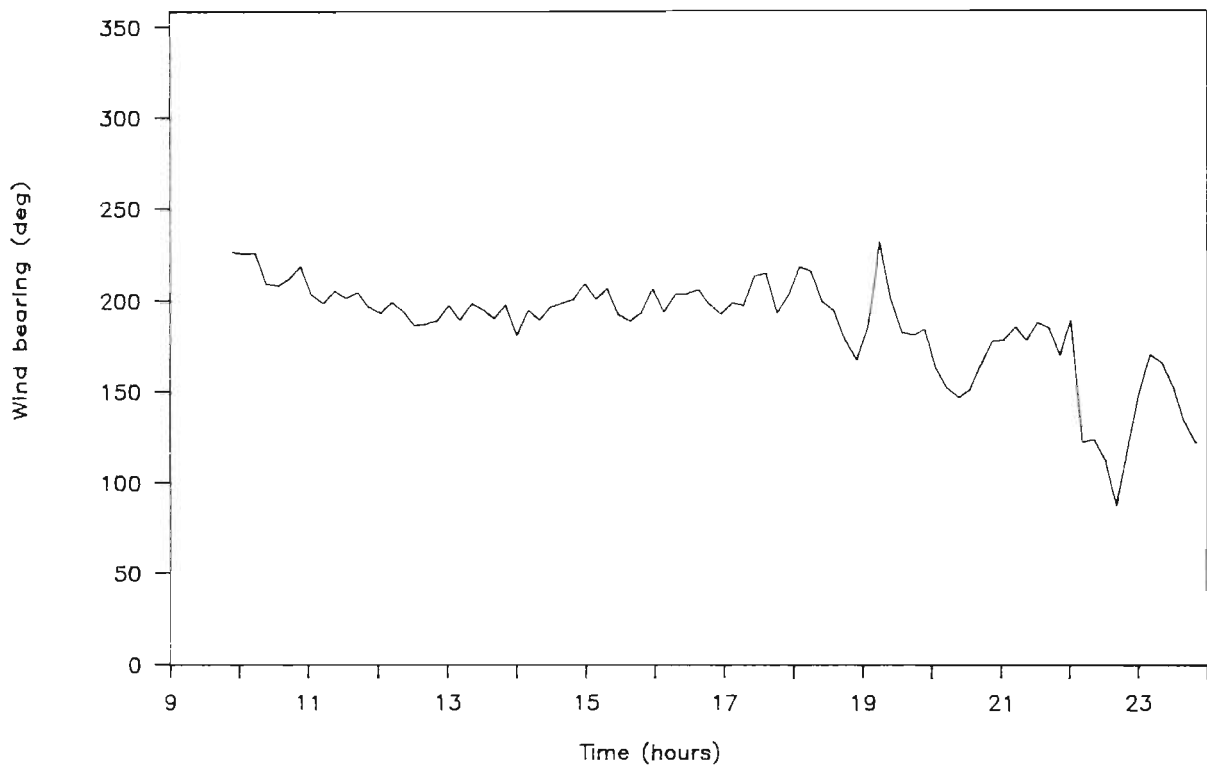
Wind Speed at Station 3
22/9/1986 (run 3)
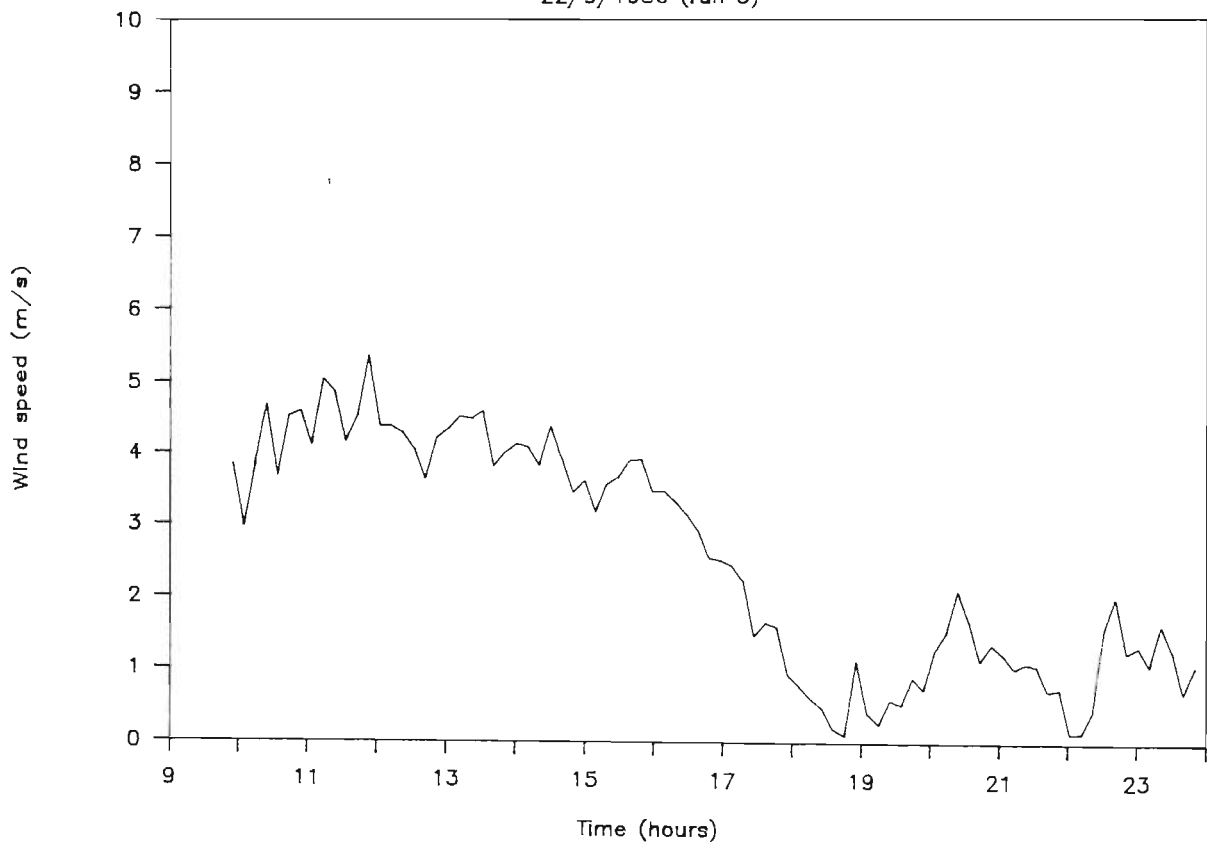
Figure 5.14 Same as Figure 5.12, but for station 3.

Wind Bearing at Station 4
22/9/1986 (run 3)
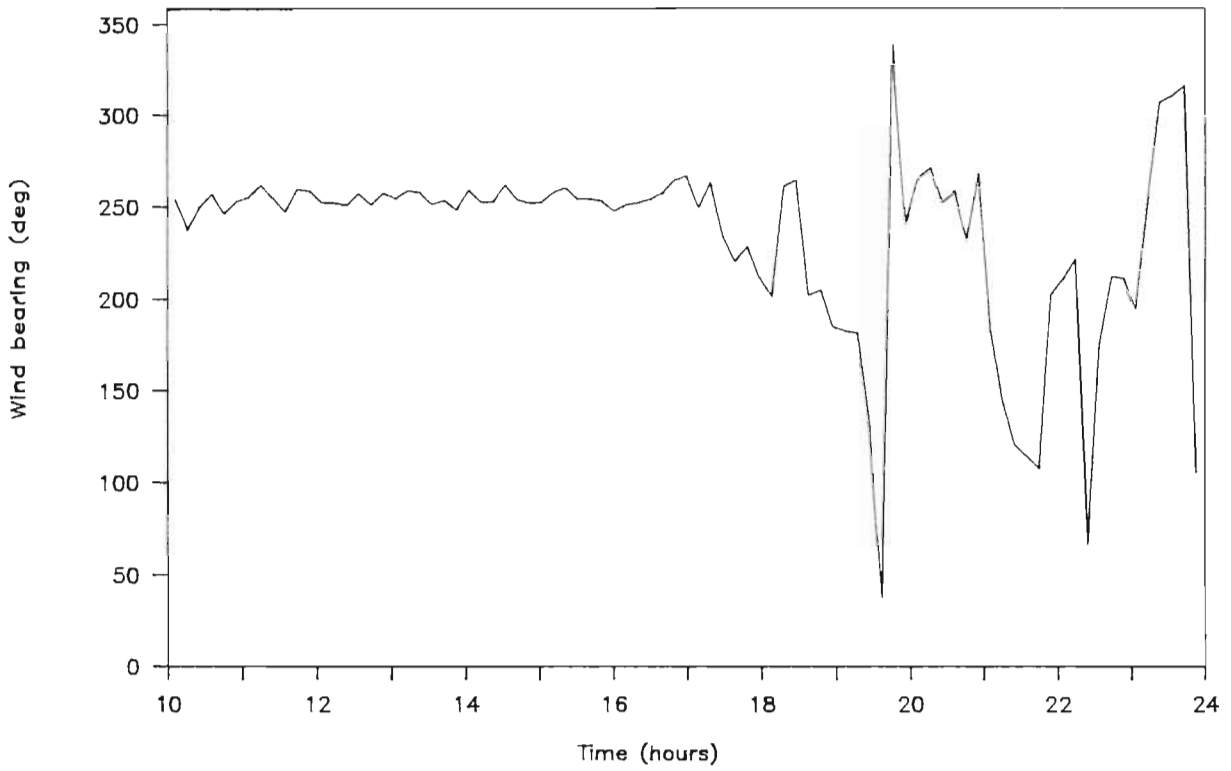
Wind Speed at Station 4
22/9/1986 (run 3)
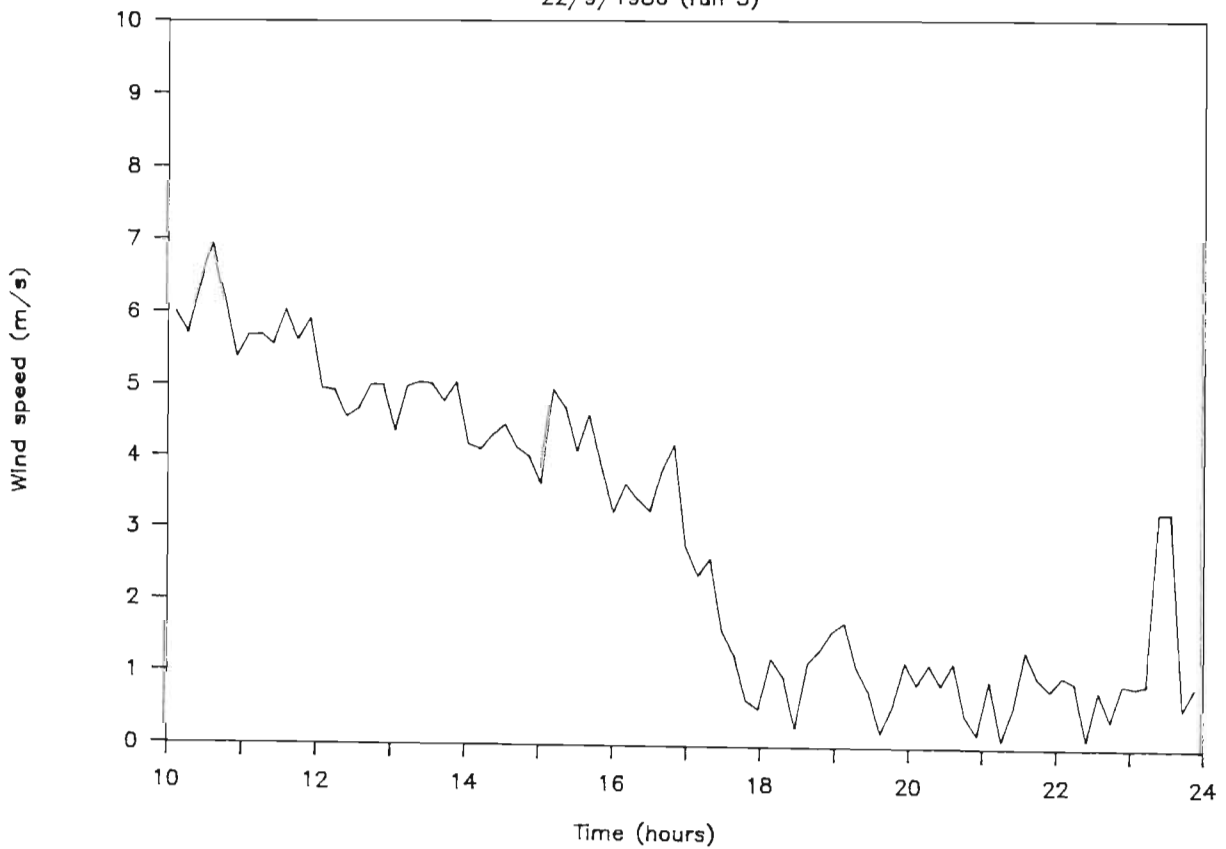
Figure 5.15 Same as for Figure 5.12, but for station 4.

Station 4 is in the lee of the bluff and, as a result of the low wind condition, indicated a fair amount of meandering. This is clear from Figure 5.15. This period also witnessed heavy rainfall (3mm/h). At approximately 01h00 (23/09/1986), the easterly wind changed to a land breeze. During these wind conditions no contribution was expected from the three industrial sites included in the simulation. Hourly cloud cover and surface temperature measurements at Louis Botha airport (mast 5) are presented in Table 5.3.

Table 5.4 contains the twice-daily upper wind measurements. Estimates of the boundary layer height are also given. Source rates, efflux velocities and outlet stack temperatures are given in Table 5.5. For security reasons, SO_2 rates are given in standard units/sec - the rate for Mobil is 100 standard units/sec.

TABLE 5.4. Upper air data measured at Louis Botha Airport.

Time	Height (m)	Wind Speed (m/s)	Direction (°)	Boundary Layer Height (m)
22/9/1986				
at 01h37 :	748	9	315	584
	991	9	315	
	1494	5	300	
at 12h31	790	11	200	800
	1022	7	215	
	1505	4	240	
23/9/1986				
at 01h03	800	6	55	800
	1032	5	305	
	1521	7	295	
at 12h01	122	2	200	800
	789	3	150	
	1021	2	145	

The Sperry Univac 1100 mainframe computer with an HP2622 graphics terminal was used for the simulation. The SO_2 predictions are shown in Figures 5.16 to 5.24. These plots were done on a HP 7580 plotter and are indentical to the graphical output on the graphics terminal. The output was given at hourly intervals. The wind field was updated every 10 minutes. Concentration isopleths were drawn for three concentration values: $2,9 \times 10^{-6}$, $2,9 \times 10^{-7}$, and $2,9 \times 10^{-8}$, standard units/m³ (with reference to Mobil 1 source rate, Table 5.5).

TABLE 5.5. Source data for 22/9/1986.

Source	SO₂ mass flowrate (standard units/sec)	Efflux velocity (m/s)	Temperature (K)
SAPREF 1	4,138	10,2	663
SAPREF 2	3,448	4,3	459
SAPREF 3	3,448	5,6	553
SAPREF 4	57,242	11,6	563
SAPREF 5	3,448	11,8	531
SAPREF 6	3,448	2,6	423
SAPREF 7	34,482	11,5	443
MONDI	29,483	2,0*	440*
MOBIL 1	100,000	7,0*	578
MOBIL 2	27,586	10,0*	633
		[*-estimated]	

Wind and diffusivity profiles are drawn for the centre of the map and the wind vectors are drawn at a height of 10m.

The concentration distribution was very similar from 10h00 to 12h00, and only the distribution at 12h00 is shown. This is due to the strong south-westerly wind. This situation was maintained until about 17h00 as indicated in Figures 5.12 to 5.15, and 5.17 to 5.20. At ~17h00 the wind calmed slightly and the wind became more westerly (Figure 5.21). The wind calmed even further and stalled conditions

```
------ DURBAN BLUFF ------
     SO2 distribution
Map    13077.9 x 3830 9 m


          CONCENTRATION (STD UNITS/M**3)

     A :    2.7 E-6
     B :    2.7 E-7
     C :    2.7 E-8


TIME   09/22/86-12 10 00



VECTOR SCALE  5 M/S        ___
```

```
WIND SPEED (M/S). DIRECTION (DEG)




              8 0              700 M

KH, KZ DIFFUSIVITIES (M**2/S)




           626           313
```
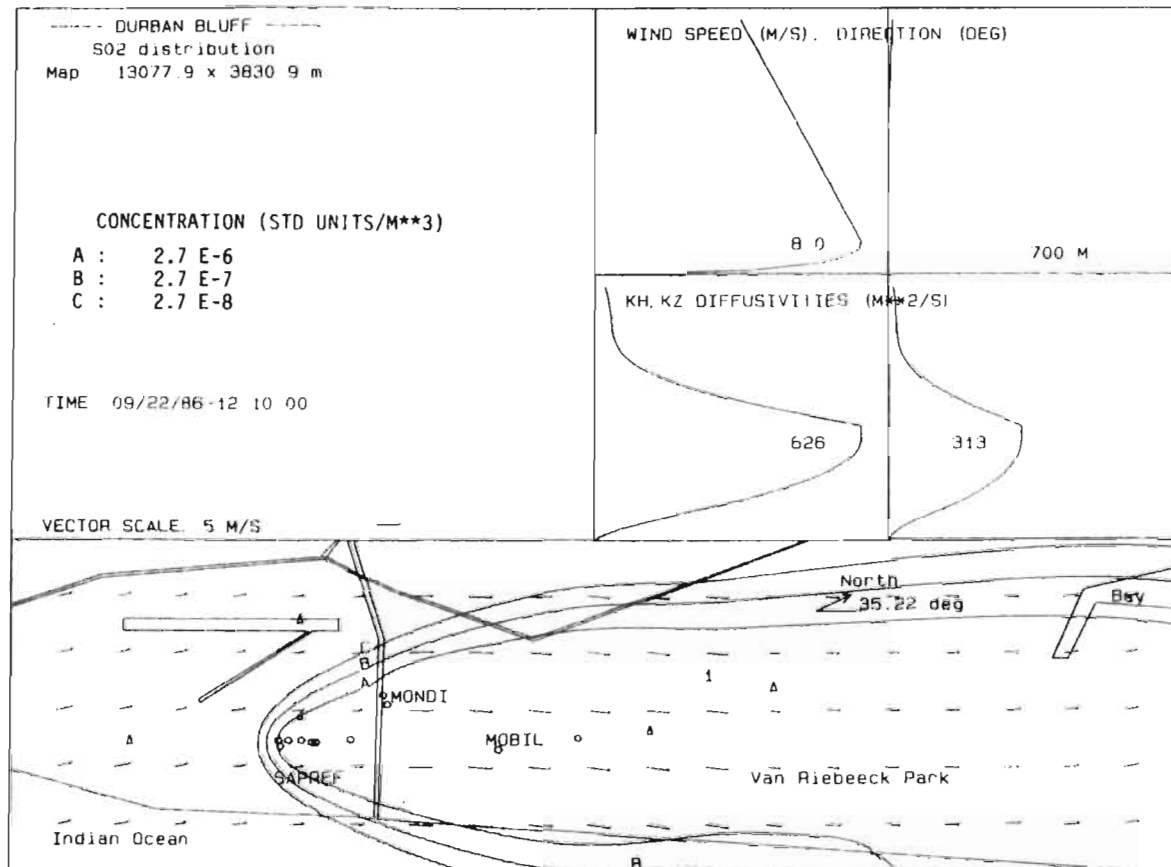
Figure 5.16   Concentration isopleths for the values 2,9 x 10^{-6}, 2,9 x 10^{-7} and 2,9 x 10^{-8} standard units /m³ are drawn (see text for definition).   Wind and diffusivity profiles represent the condition at the centre of the map.   The triangles are the five weather station positions.   The circles are the source positions.   The SO_2 monitoring point is situated at 1.   The wind vectors are drawn at 10m height.
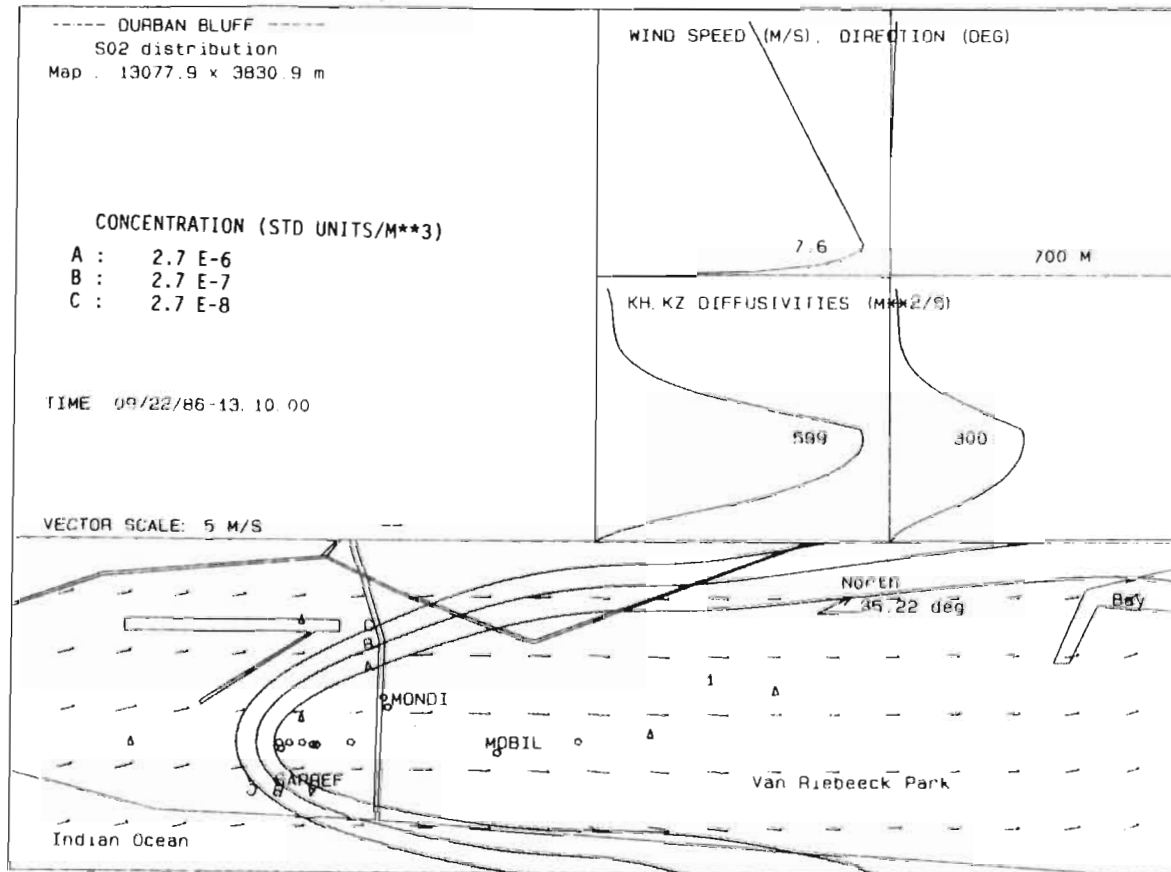
Figure 5.17 Predicted SO₂ isopleths as for Figure 5.16, But at time 13h10. A strong south-westerly wind is maintained.

```
-------  DURBAN BLUFF  -------
        SO2 distribution
Map    13077.9 x 3830 9 m



        CONCENTRATION (STD UNITS/M**3)
    A :     2.7 E-6
    B :     2.7 E-7
    C :     2.7 E-8



    TIME    09/22/86-14.10.00



VECTOR SCALE   5 M/S
```

```
WIND SPEED (M/S). DIRECTION (DEG)




                        6 3                700 M

KH, KZ DIFFUSIVITIES (M**2/S)



                                    167


            192
```

North
35.22 deg   Bay

MONDI

1

MOBIL

SAPREF   Van Riebeeck Park

Indian Ocean
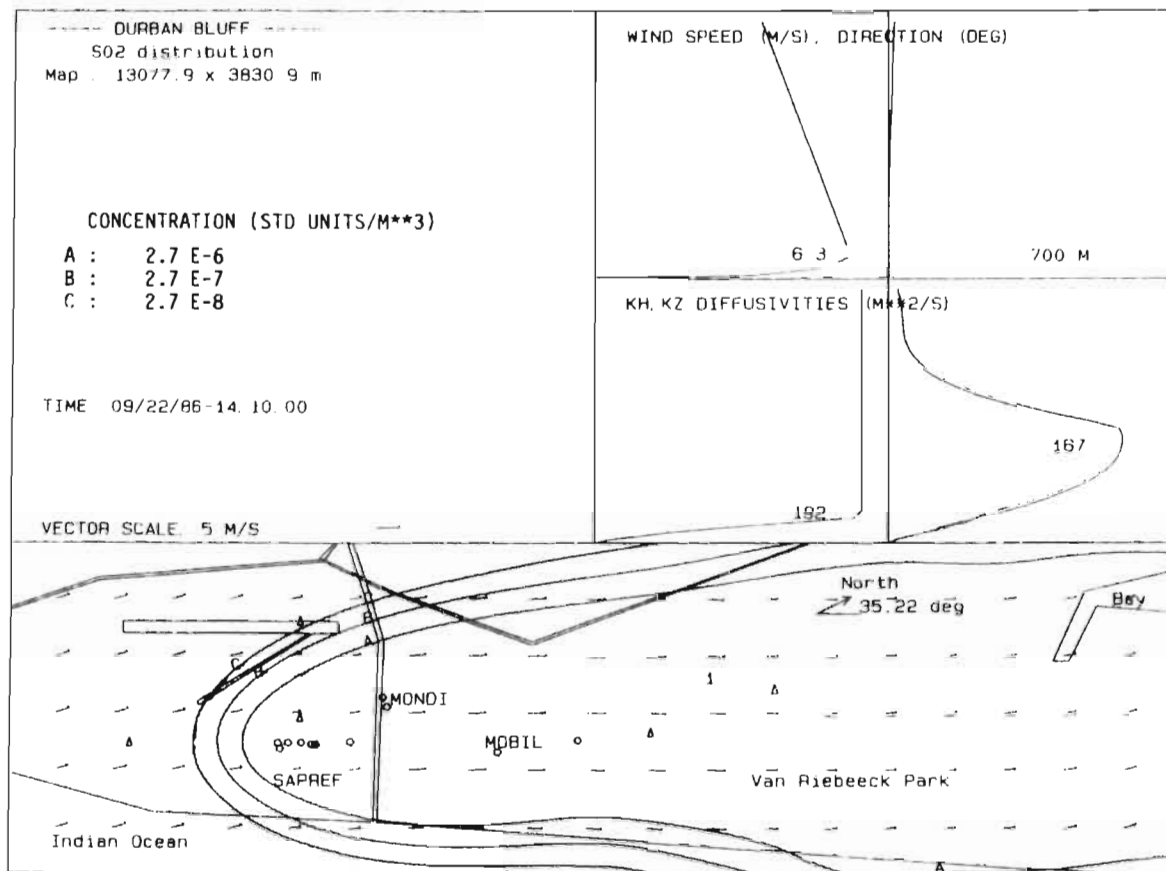
Figure 5.18   Same as for Figure 5.16, but at time 14h10.   Only a slight change in the wind direction is observed.

------ DURBAN BLUFF ------
     SO2 distribution
Map   1307/ 9 x 3830.9 m

WIND SPEED (M/S). DIRECTION (DEG)

CONCENTRATION (STD UNITS/M**3)

A :   2.7 E-6
B :   2.7 E-7
C :   2.7 E-8

7.5   700 M

KH, KZ DIFFUSIVITIES (M**2/S)

TIME   09/22/86-15.10.00

654   327

VECTOR SCALE. 5 M/S

North
35.22 deg   Bay

1   Δ

C B A   MONDI
                      MOBIL   o   Δ

SAPREF   Van Riebeeck Park

Indian Ocean
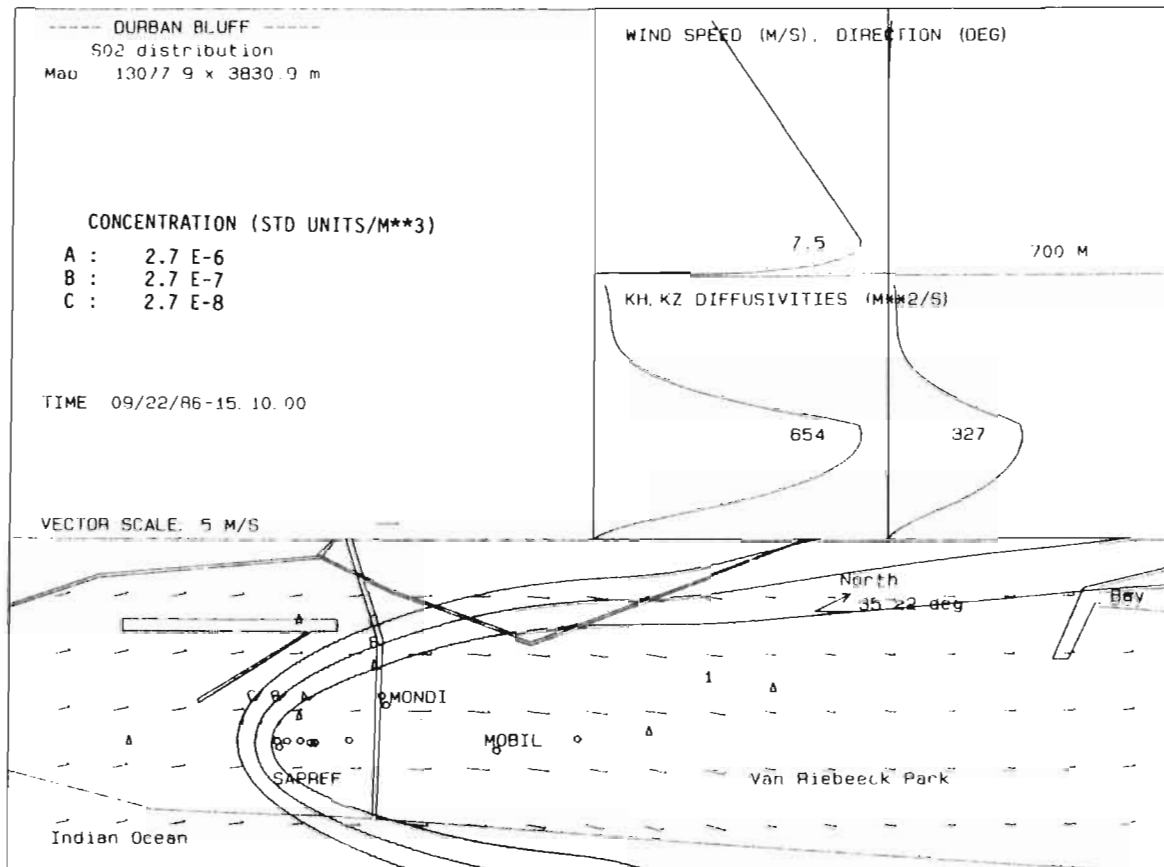
Figure 5.19   Same as for Figure 5.16, but for time 15h10.

----- DURBAN BLUFF -----
SO2 distribution
Map . 13077.9 x 3830.9 m

WIND SPEED (M/S). DIRECTION (DEG)

355

CONCENTRATION (STD UNITS/M**3)

A :   2.7 E-6
B :   2.7 E-7
C :   2.7 E-8

4.6   700 M

KH, KZ DIFFUSIVITIES (M**2/S)

TIME   09/22/86-16 10 00

142

162

VECTOR SCALE 5 M/S

North
35.22 deg

Bay

B

A

1

MONDI

MOBIL

Van Riebeeck Park

SAPREF

Indian Ocean
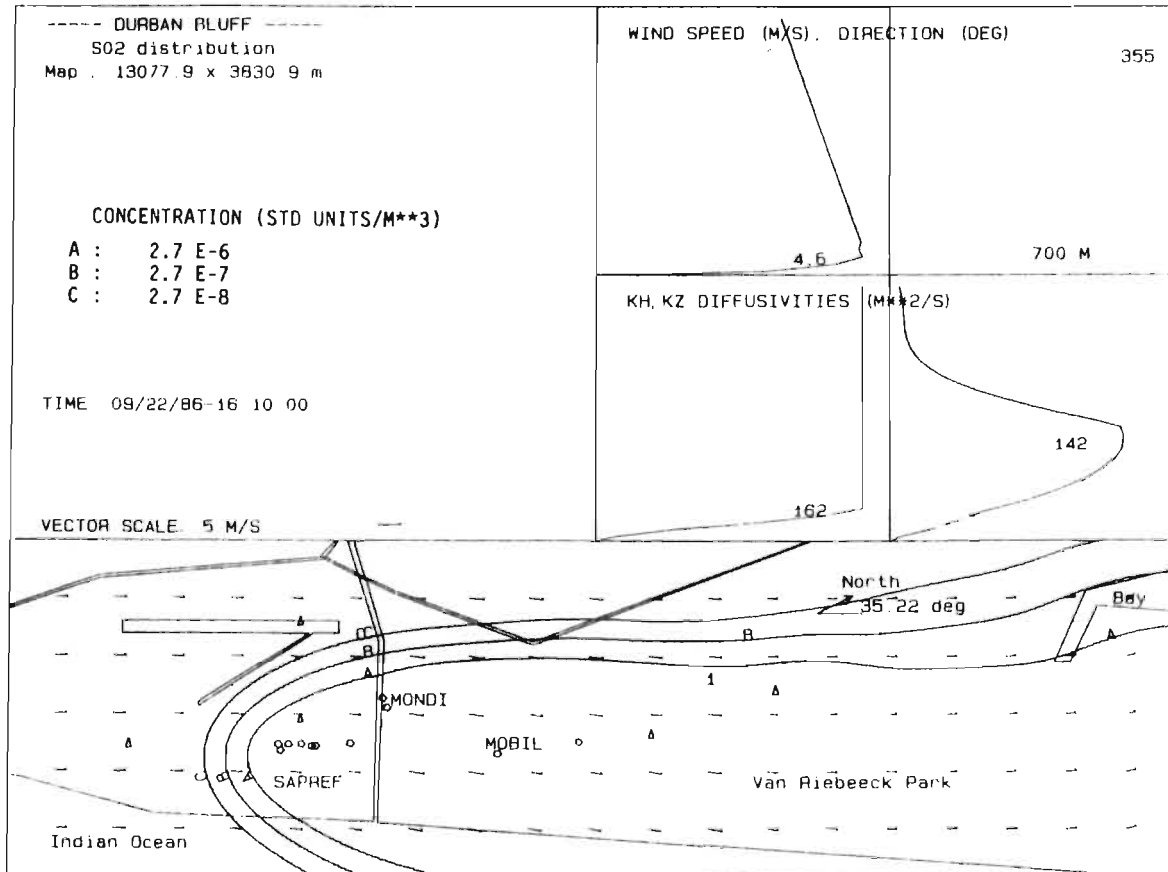
Figure 5.20   Same as Figure 5.16, at 16h10.   The wind speed is starting to decrease.   This is apparent towards the north.

----- DURBAN BLUFF -----
SO2 distribution
Map : 13077.9 x 3830.9 m

CONCENTRATION (STD UNITS/M**3)
A :   2.7 E-6
B :   2.7 E-7
C :   2.7 E-8

TIME   09/22/86-17:10.00

VECTOR SCALE: 5 M/S

WIND SPEED (M/S), DIRECTION (DEG)   347

3.8   700 M

KH,KZ DIFFUSIVITIES (M**2/S)

251   126

North
35.22 deg   Bay

MONDI
MOBIL
SAPREF   Van Riebeeck Park

Indian Ocean
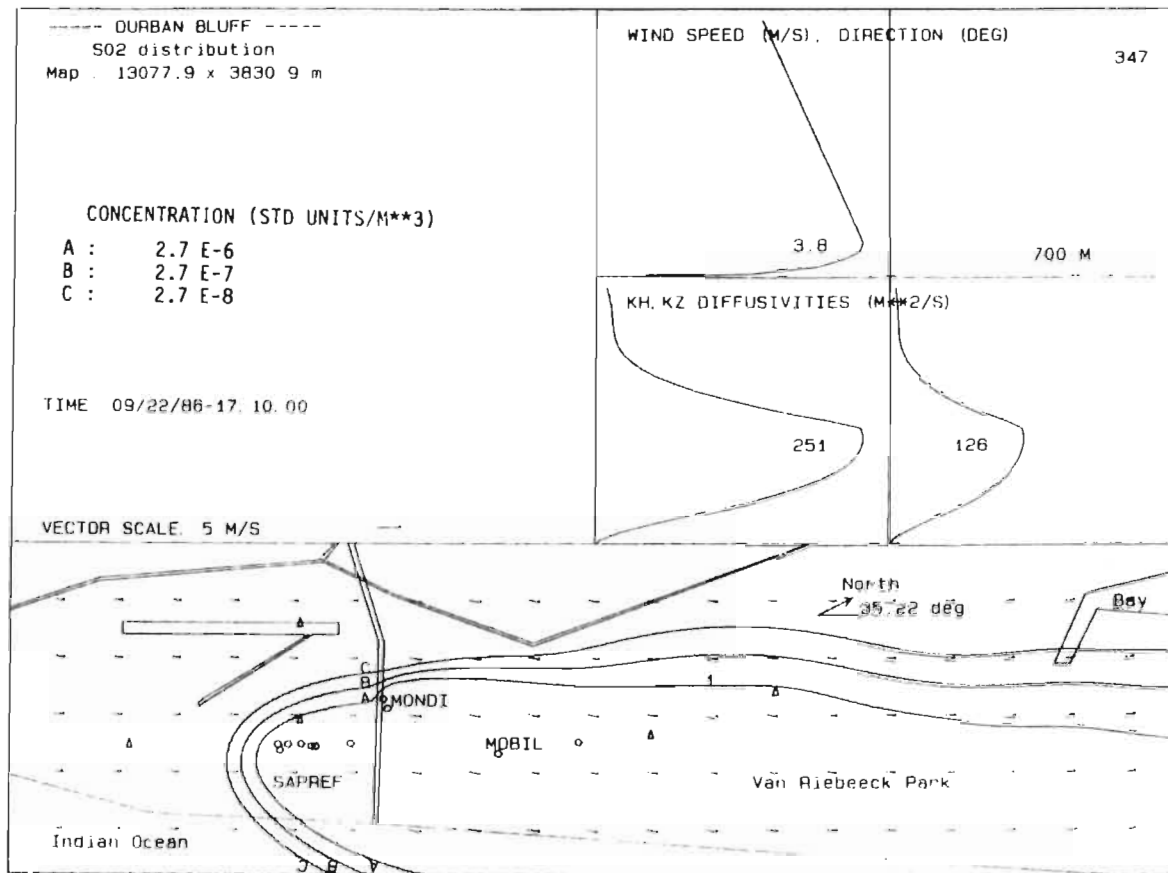
Figure 5.21   Same as Figure 5.16, but at 17h10.   The wind speed is decreasing over the whole area.

```
----- DURBAN BLUFF -----
    SO2 distribution
Map    13077.9 x 3830.9 m


        CONCENTRATION (STD UNITS/M**3)
    A :     2.7 E-6
    B :     2.7 E-7
    C :     2.7 E-8



    TIME   09/22/86-18 10 00



    VECTOR SCALE:  5 M/S        —
```

```
WIND SPEED (M/S). DIRECTION (DEG)
              2.2



                                700 M

KH, KZ DIFFUSIVITIES (M**2/S)



              59   10
```
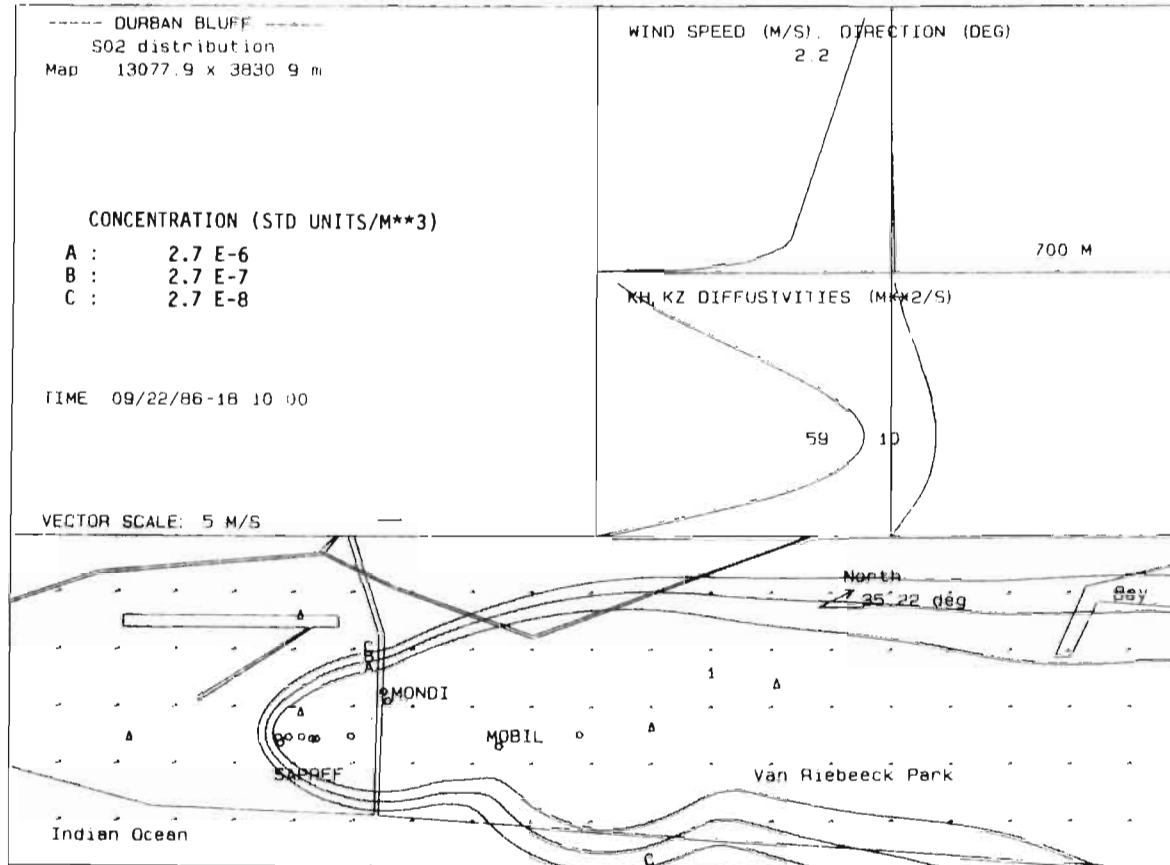
Figure 5.22   As for Figure 5.16, at 18h10.   Near-calm conditions.   A puff build-up is evident near Mobil.   The "bulge" is due to earlier advection towards the sea (see Figure 5.21).
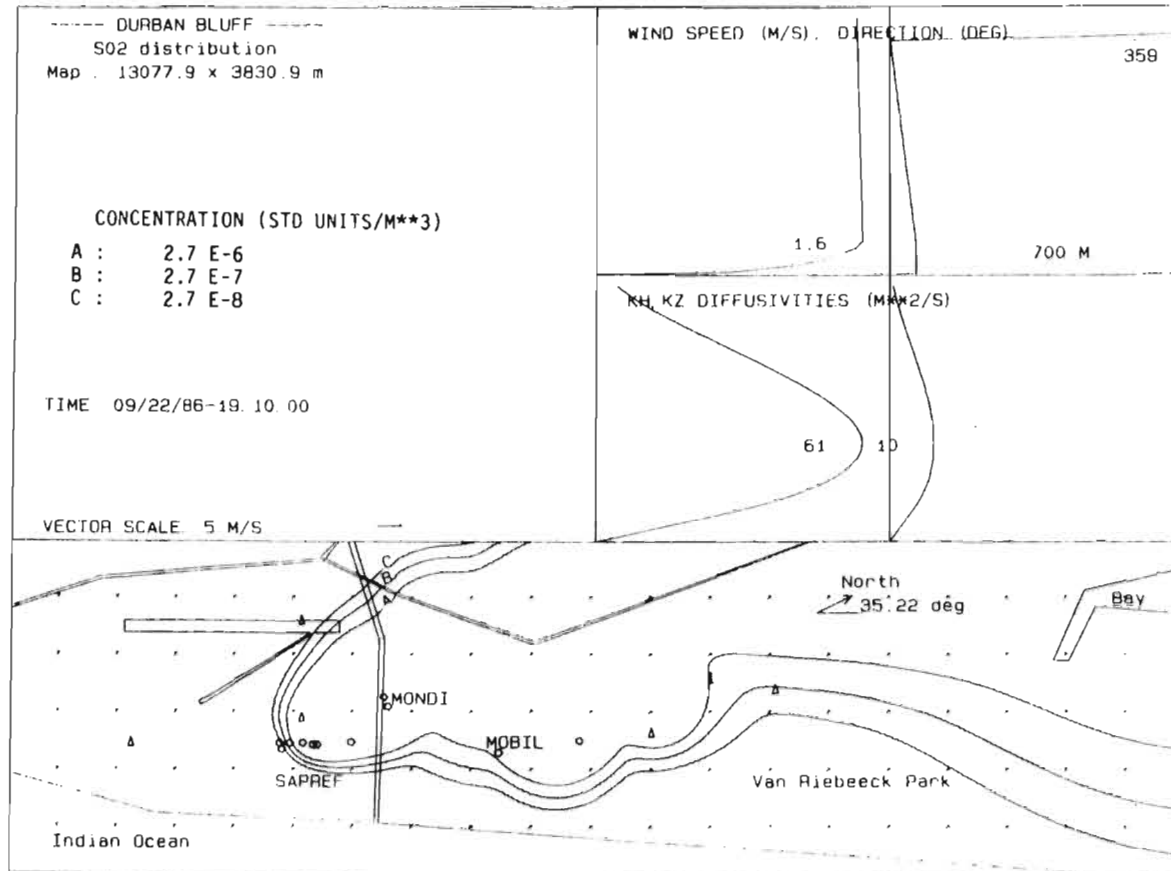
Figure 5.23 Same as for Figure 5.16, but at time 19h10. Low wind conditions still exist. A fair amount of meandering takes place. The wind is gradually changing direction to south-easterly.
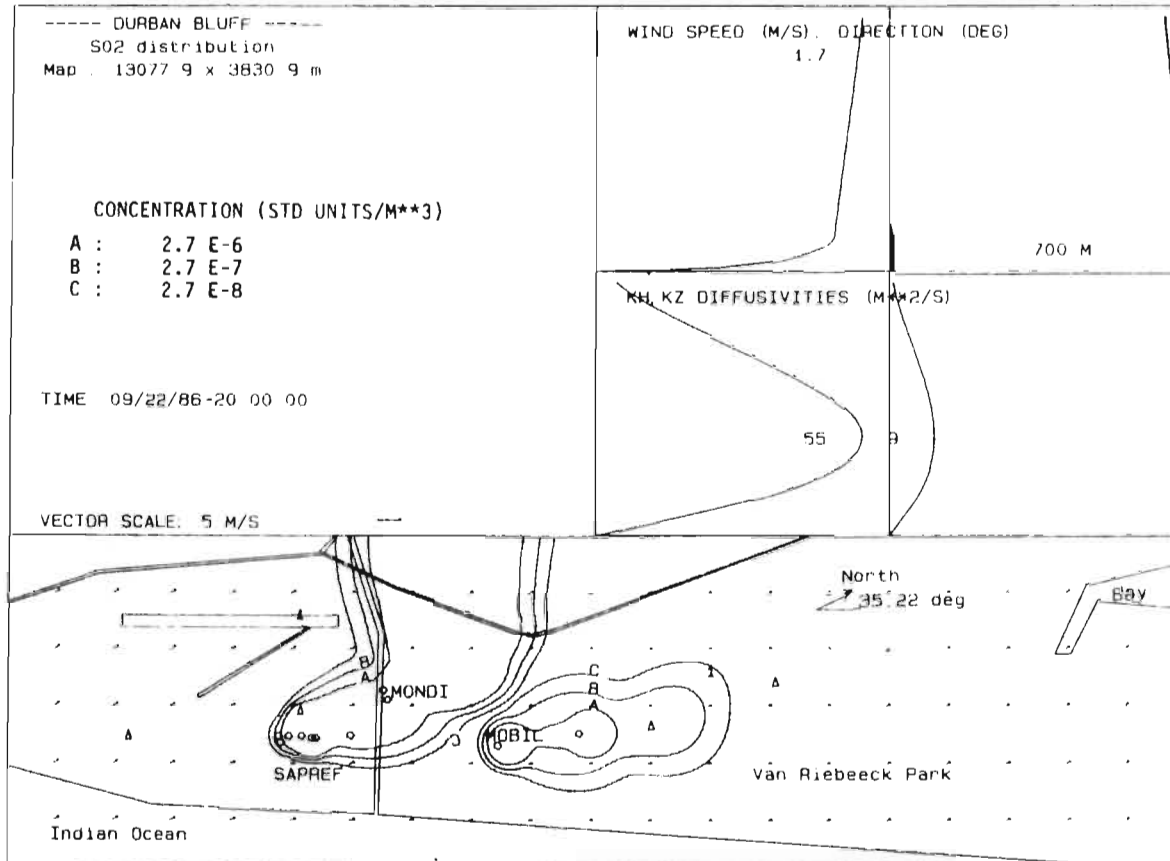
Figure 5.24 Same as for Figure 5.17, at time 20h00. Between 19h00 and 20h00, the wind blew towards the west. This situation then changed and a weak south-westerly is shown above. As a result of the low wind speeds, buoyancy of the plume caused rapid rise of the plumes emitted from MOBIL.

existed. This had the result of a puff build-up close to the sources and the very peculiar shape depicted in Figure 5.22 arose. Stable conditions, as indicated by the shape and maximum value of the diffusivity profiles, existed. As the wind changed from a southerly to a south-easterly, the whole distribution shifted anti-clockwise (Figure 5.23). At about 19h40, the wind became southerly. As a result of the low wind conditions around MOBIL, very little advection of the SO_2 took place. Considerable plume rise due to buoyancy also occurred and hence very low ground level concentrations are predicted. A fair amount of washout occurred during the period 21h00 to 22h00. This also evident in Figure 5.25. The directional shear effect is clearly demonstrated in Figure 5.2 with the plumes from SAPREF and MONDI as the wind changed to southerly from a south-easterly.

The concentrations predicted at the SO_2 monitoring point are compared with the observed concentration in Figure 5.25. On the whole, there is excellent agreement. The effect of rain on the concentration is indicated. The dotted line is the prediction excluding rainfall. An appreciable amount of washout is observed.

This 24-hour simulation took 23 hours CPU time on the Sperry Univac 1100.

223

OBSERVED AND PREDICTED CONCENTRATIONS

Run#3 (22/9/1986)
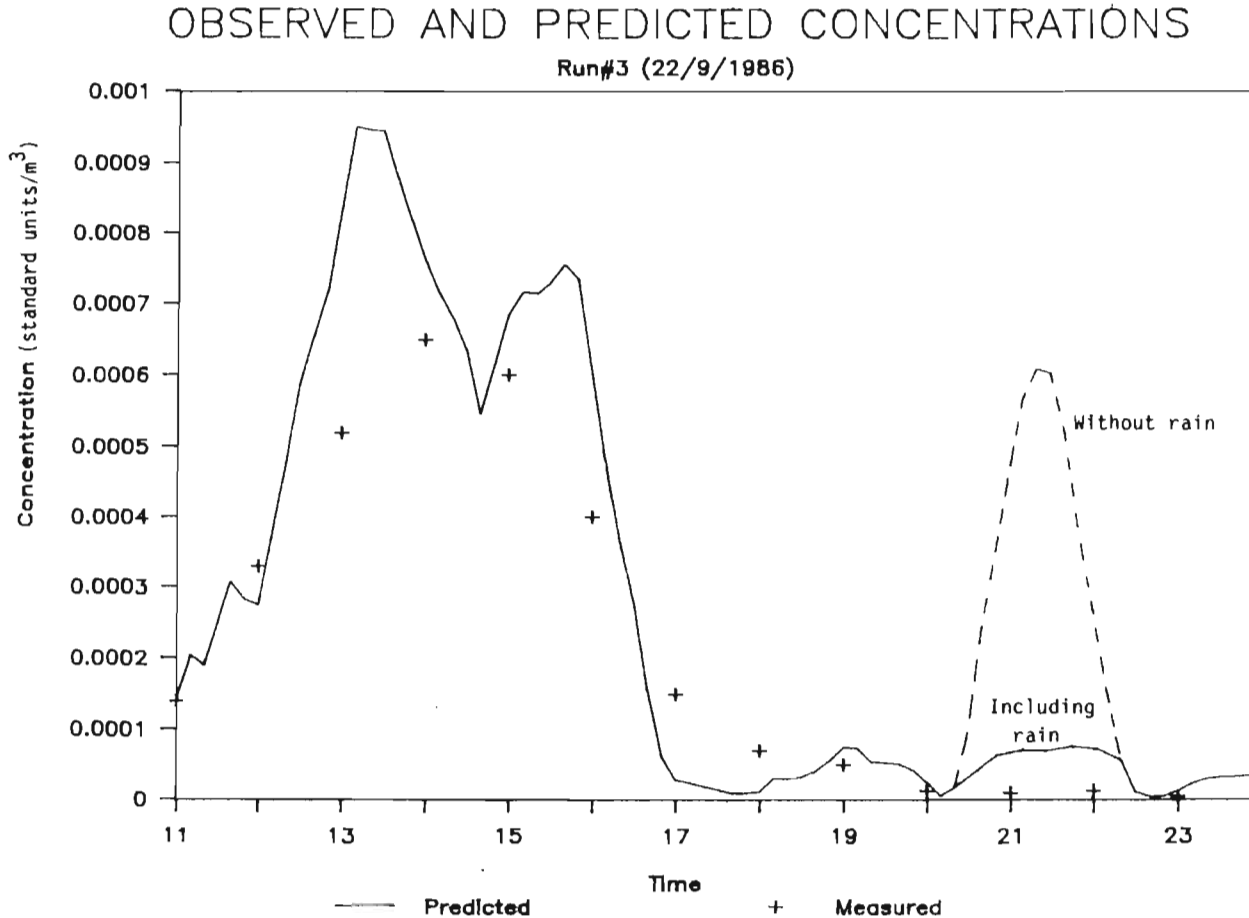
Figure 5.25.   A comparison of the numerical model prediction and the observed concentration at the SO_2 monitoring point (position 1) shown in plots, Figures 5.16 to 5.24.   The prediction curve is obtained by imposing a 60 minute running average to the 10 minute interval predictions.   The effect of rain on the ground-level concentration is clearly shown.   (See text for the definition of 'standard units/m³')

5.2.2. Eastern Transvaal Highveld

The Eastern Transvaal Highveld is essentially a flat countryside. It is therefore decided not to include topography. An average altitude of 1650m is used. As this is only a demonstration run, accurate estimation of the roughness length is not done and an average of 0,15m is chosen based on the maize crop grown in the area.

TABLE 5.6. The Eastern Transvaal Highveld case study. A summary of the model parameters.

Longitude ; latitude	29,375°E ; 26,208°S
Time difference from GMT (UST)	+ 2 hours
Dimensions of study area	123,42km x 84,15km
Angle between north and the x-axis of the wind field reference frame	90°
Wind field grid spacing	1870m
Vertical grid spacing for dispersion model	30m
Isopleth resolution	200m
Divergence reduction criteria:	
Surface layer	$1 \times 10^{-6} \ s^{-1}$
Outer layer 1	$1 \times 10^{-5} \ s^{-1}$
Outer layer 2	$1 \times 10^{-4} \ s^{-1}$

Model parameters and site dimensions are presented in Table 5.6. The positions of the eight surface weather stations (ESCOM: Electricity Supply Commission), available in the area, are presented in Table 5.7. Hourly wind and temperature measurements are taken. A Doppler Acoustic Sounder is situated at Elandsfontein (weather station number 7). Upper air wind measurements at 23 heights, equally spaced at 30 metres, starting at 90m, are available. The Doppler Acoustic Sounder also supplies estimates for the boundary layer height, using the intensity of the vertical signal as an indicator. Hourly measurements of SO_2 concentrations are taken at each of the eight weather stations.

The area is characterised by heavy industry, and as a result of the vast coal reserve, many power stations have been erected. In fact these industries are sparsely spread in a large and otherwise empty landscape The seven power stations included in the study area, can be seen in Figure 5.26. Sasol 2 and 3 produce petrol and by-products from coal, and are also included. Twenty-four smouldering discard coal dumps have been included. The approximate positions of these point sources can be seen in Figure 5.26. For security reasons, the exact positions and dimensions of the stacks may not be listed.

TABLE 5.7. Surface layer weather station information for the Eastern Transvaal Highveld case study.

Station No.	Roughness length (m)	Coordinates (m)	Height (m)	Altitude (m)
1) Wildebeest	0,15	39000; 13500	10	1600
2) Bethal	0,15	72000; 17250	10	1650
3) Hendrina	0,15	94750; 47000	10	1700
4) Grootpan	0,15	34000; 59750	10	1550
5) Kriel	0,15	49500; 34000	10	1600
6) Komati	0,15	70250; 54125	10	1600
7) Elandsfontein	0,15	66250; 35875	10	1740
8) Arnot	0,15	104750; 72000	10	1700

Source : Electricity Supply Commission

The heights of the power station and SASOL stacks range from 90m to 300m. The release heights of the smouldering coal dumps were taken as 5 metres.

The simulation lasted from 09h00 on 15/08/1984 to 09h00 on 16/08/1984. This period was characterised by clear skies. Hourly meteorological measurements are given in Appendix K. Source data for SO_2 are presented in Table 5.8. These values were based on annual averages (Boegman 1985) for 1983. A constant rate was assumed for each of the burning coal dumps. This rate was estimated in accordance with the CSIR report ATMOS/83/16 (von Gogh 1983).

The simulation was conducted on a CDC CYBER 750 mainframe computer. The 24 hour simulation required 4 hours CPU time. The wind field was updated once every 30 minutes and the concentration distribution, every 60 minutes. Examples of the output are given in Figures 5.26 to 5.31.

TABLE 5.8. Source data for the Eastern Transvaal Highveld (1983). Emission rate units are based on Mobil 1 emission (Table 5.5.).

Source	SO_2 mass flowrate (standard units/sec)	Volumetric flowrate (m^3/s)	Temperature (K)
Arnot	826,163	1174,5	398
Duvha	1224,161	3000,0	398
Hendrina	661,109	1238,0	413
Komati	348,888	1107,5	413
Kriel	755,255	2296,0	413
Matla	1901,397	1957,0	398
Wilge	156,265	199,5	445
Sasol 2	595,564	2632,0	483
Sasol 3	810,671	2646,9	482
Each burning coal dump	223,448	–	–

Source : N. Boegman 1985

Figure 5.26. A northerly wind existed at the outset of the simulation. Wind and diffusivity profiles are drawn for the centre of the map. Wind vectors are at a height of 10m. Two isopleths with concentration values of $2,7 \times 10^{-8}$ and $2,7 \times 10^{-7}$ standard units/m^3 are shown. The lower case letters are the positions of burning discard coal dumps and the numbered triangles, the position of the weather stations.

Eastern Transvaal Highveld
SO2 distribution
(map : 123.42 x 84.15 km)

CONCENTRATION (STD UNITS/M**3)

A :   2.7 E-08
B :   2.7 E-07

TIME   08/15/84-11: 30: 00

VECTOR SCALE: 5 M/S

WIND SPEED (M/S). DIRECTION (DEG)

2.8   344
                1200 M

KH, KZ DIFFUSIVITIES (M**2/S)

Figure 5.27.   Same as Figure 5.26, but at 11h30.   The northerly wind
has changed to a light westerly wind.
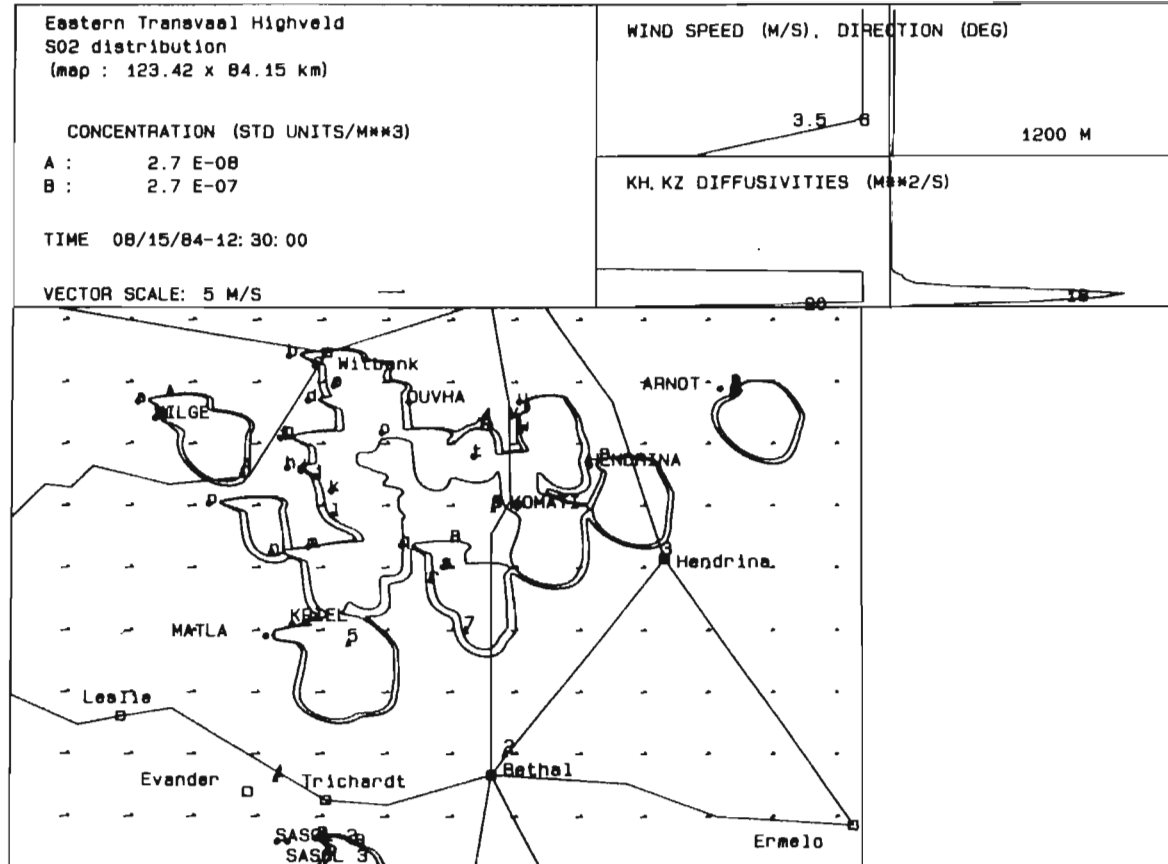
Figure 5.28. As for Figure 5.26, but at time 12h30. The shear effect, as a result of the change in wind direction from northerly to westerly, is obvious in this plot.
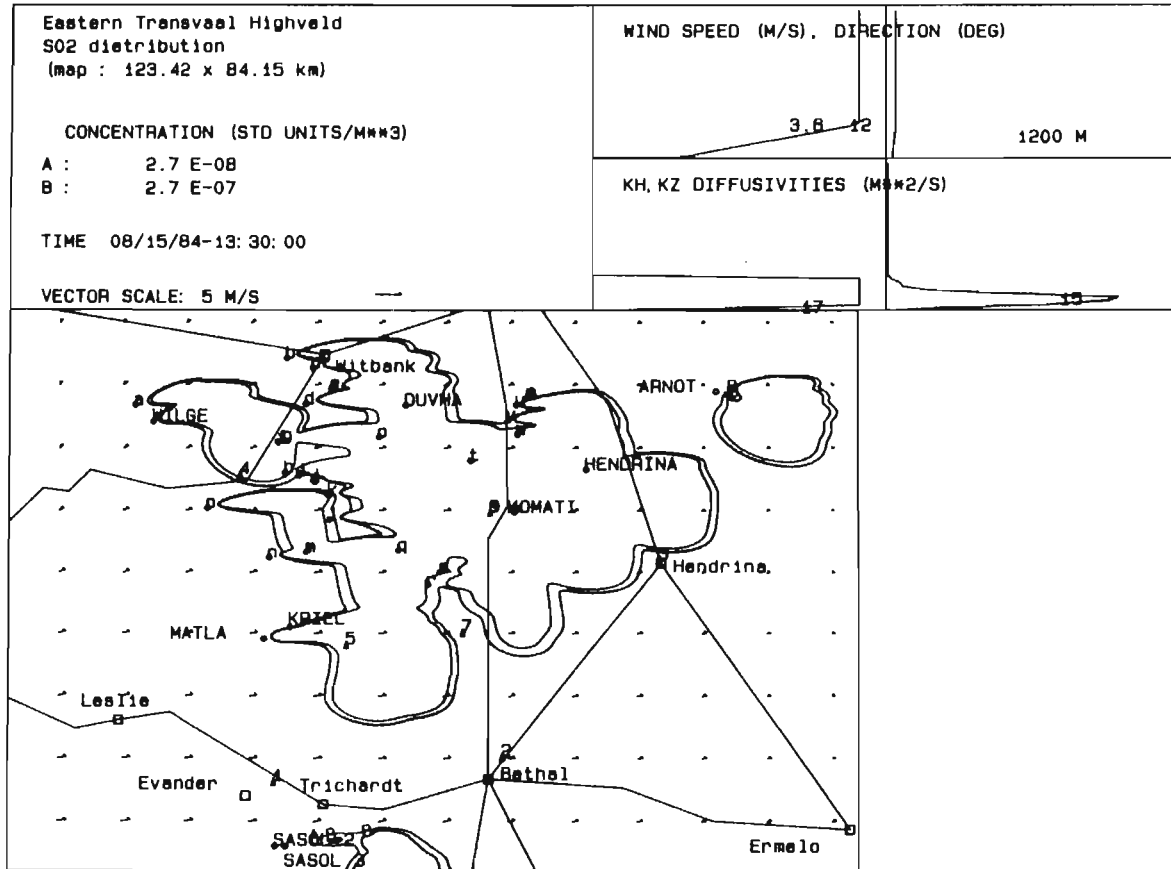
Figure 5.29. Same as Figure 5.26, but at 13h30. The wind direction is changing slightly to a south-westerly.

Eastern Transvaal Highveld
SO2 distribution
(map : 123.42 x 84.15 km)

CONCENTRATION (STD UNITS/M**3)

A :   2.7 E-08
B :   2.7 E-07

TIME   08/15/84-14: 30: 00

VECTOR SCALE: 5 M/S   —

WIND SPEED (M/S). DIRECTION (DEG)

3,8   1200 M

80

KH, KZ DIFFUSIVITIES (M**2/S)

15   13

Witbank
KILOE   DUVHA   ARNOT · B
                                              HENDRINA
                    KOMATI
                              Hendrina.

MATLA   KRIEL
Leslie
                              Bethal
Evander   Trichardt
SASOL 2
SASOL 3   Ermelo
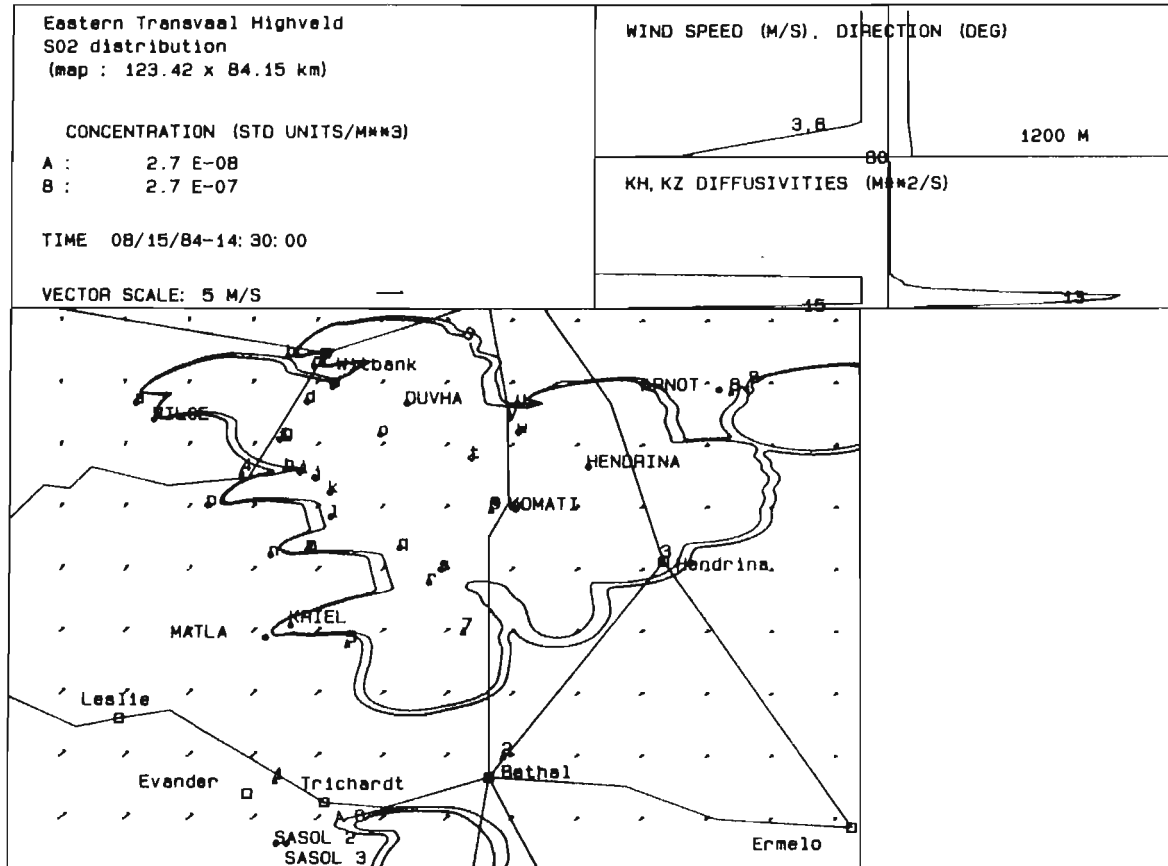
Figure 5.30.   As for Figure 5.26, but at 14h30.   The SO$_2$ distribution at a more advanced stage.

Eastern Transvaal Highveld
SO2 distribution
(map : 123.42 x 84.15 km)

CONCENTRATION (STD UNITS/M**3)

A :   2.7 E-08
B :   2.7 E-07

TIME   08/15/84-15: 30: 00

VECTOR SCALE: 5 M/S

WIND SPEED (M/S), DIRECTION (DEG)

4.2   1200 M

KH, KZ DIFFUSIVITIES (M**2/S)

Witbank

DUVHA   ARNOT

HILGE

HENDRINA

KOMATI

Hendrina

MATLA   KRIEL   5   7

Leslie

Evander   Trichardt   Bethal

SASOL 2   Ermelo
SASOL 3
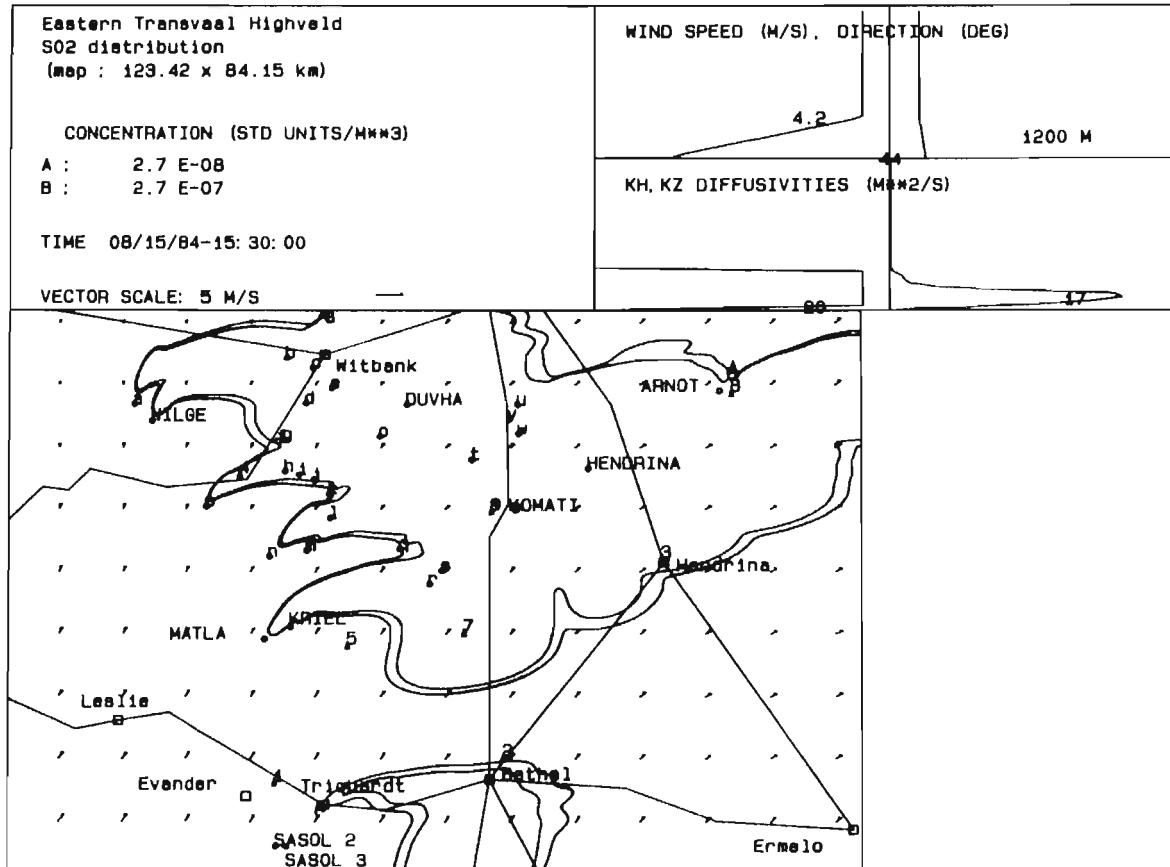
Figure 5.31.   Same as Figure 5.26 at time 15h30.

A northerly wind was blowing at the commencement of the experiment. This soon changed to a westerly, and as indicated by the plots, a shift of the plumes occurred. Caution is necessary in viewing the inital plots since emissions has been assumed to start at the beginning of the simulation, so complete plumes which would have existed, have not developed. This wind was maintained until 11h00 when it became south-westerly and finally a southerly wind. An excellent example of the shear effect is observed during the experiment. Consider the emissions from Matla and Kriel: as the wind changes from a northerly to a westerly wind, the initial part of the plume (originally moving south), clearly shears to the east.

The SO_2 concentrations observed at the eight monitoring points are compared to the predicted concentrations in Figures 5.32 to 5.39. As was indicated earlier, only crude estimates of emission rates were available and therefore accurate predictions were not expected. Furthermore, several smaller industries were excluded from the case study. However, reasonable accuracy was achieved.

Concentration at Wildebeest
15/08/1984–16/08/1984
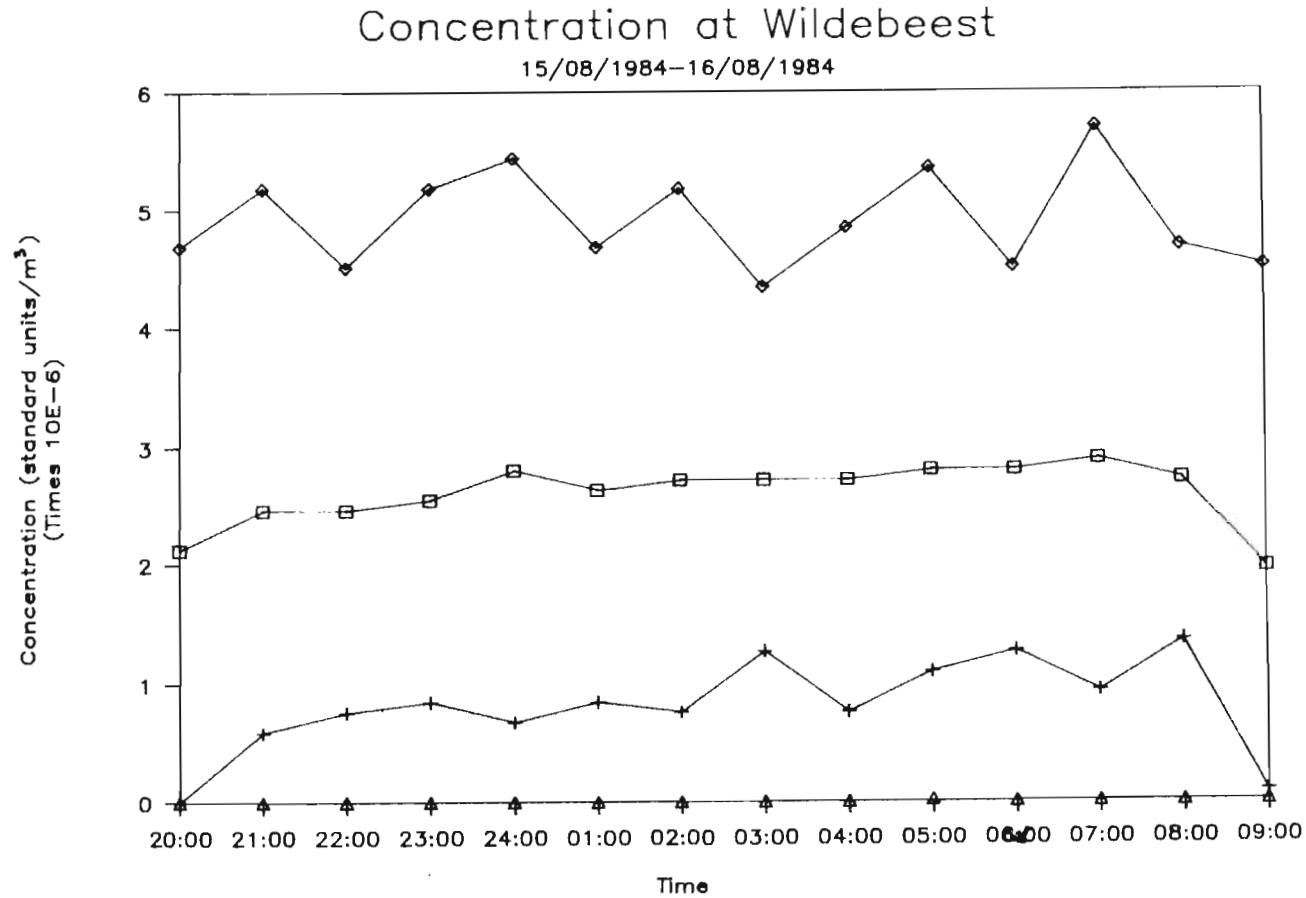
Figure 5.32. A comparison of measured and predicted concentrations at Wildebeest, where

+   Minimum measured concentration

◇   Maximum measured concentration

□   Average measured concentration

Δ   Predicted concentration

The definition of 'standard unit/m^3' is given in Section 5.2.1.: the emission rate for MOBIL (Table 5.4) is 100 standard units/m^3.

Concentration at Bethal

15/08/1984~16/08/1984

Concentration (standard units/m^3) (Times 10E-5)

Time
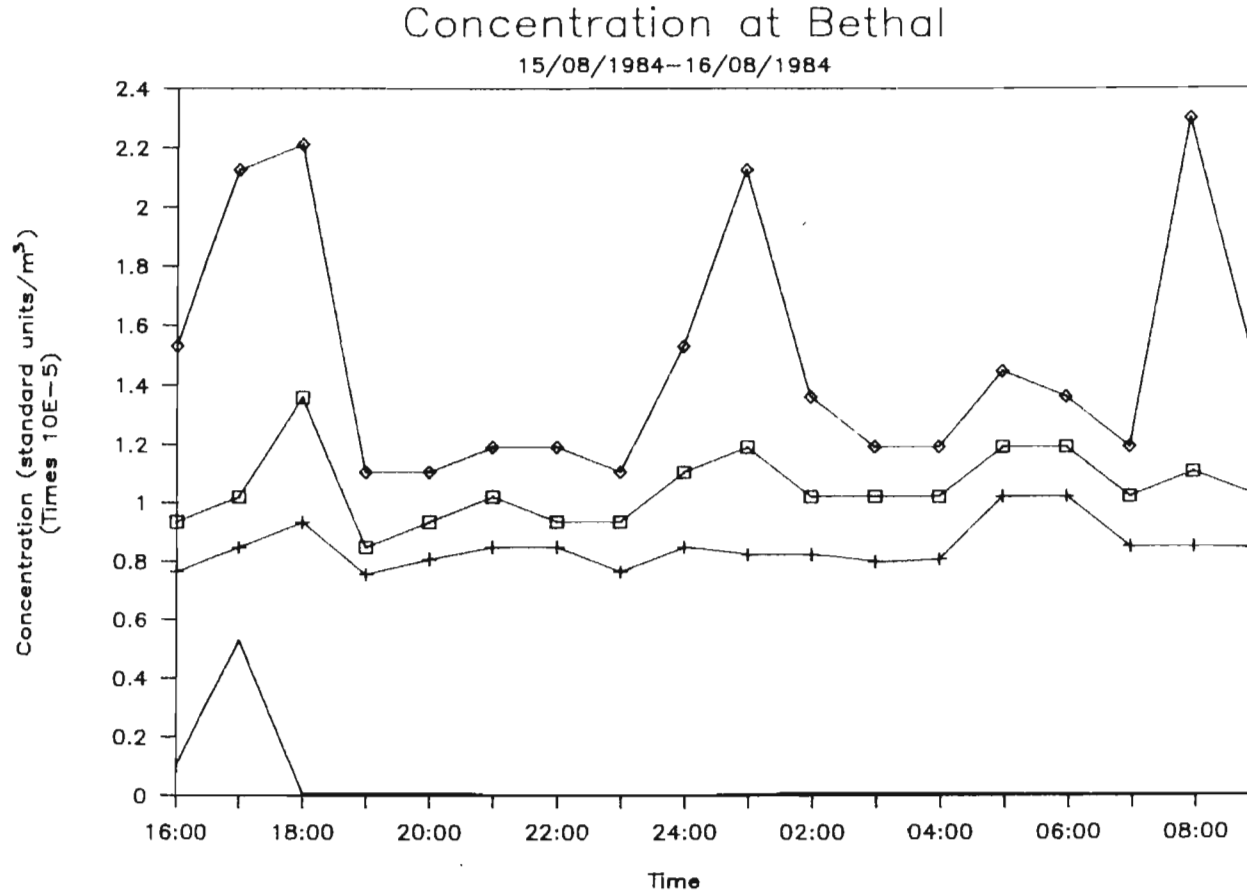
Figure 5.33.   A comparison of measured and predicted concentrations
at Bethal, where

+   Minimum measured concentration

◇   Maximum measured concentration

□   Average measured concentration

—   Predicted concentration

The definition of 'standard unit/m^3' is given in Section 5.2.1.:   the
emission rate for MOBIL (Table 5.4) is 100 standard units/m^3.

Concentration at Hendrina
15/08/1984–16/08/1984
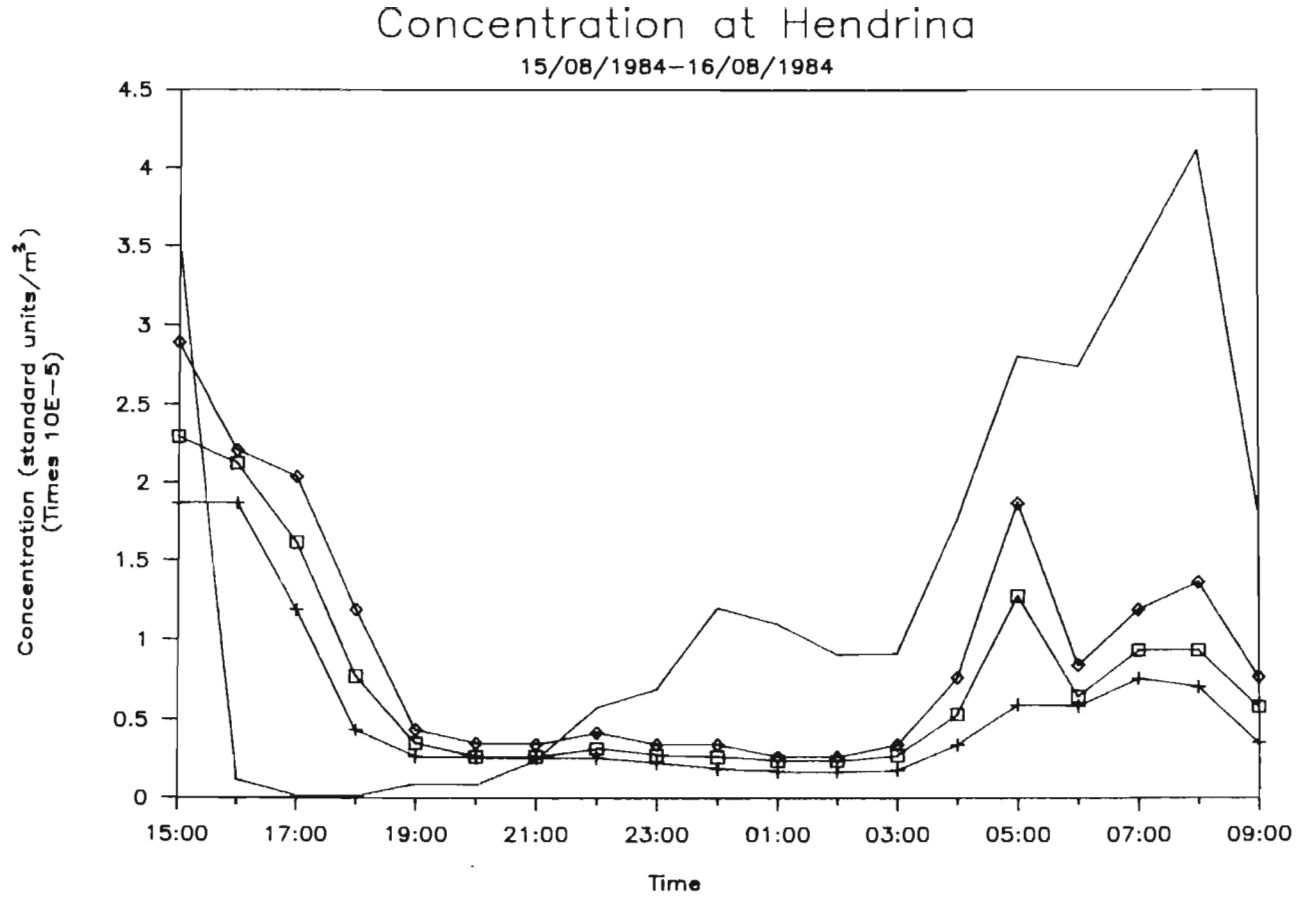
Figure 5.34.   A comparison of measured and predicted concentrations at Hendrina, where

+   Minimum measured concentration

◇   Maximum measured concentration

□   Average measured concentration

—   Predicted concentration

The definition of 'standard unit/m³' is given in Section 5.2.1.: the emission rate for MOBIL (Table 5.4) is 100 standard units/m³.

Concentration at Grootpan
15/08/1984–16/08/1984
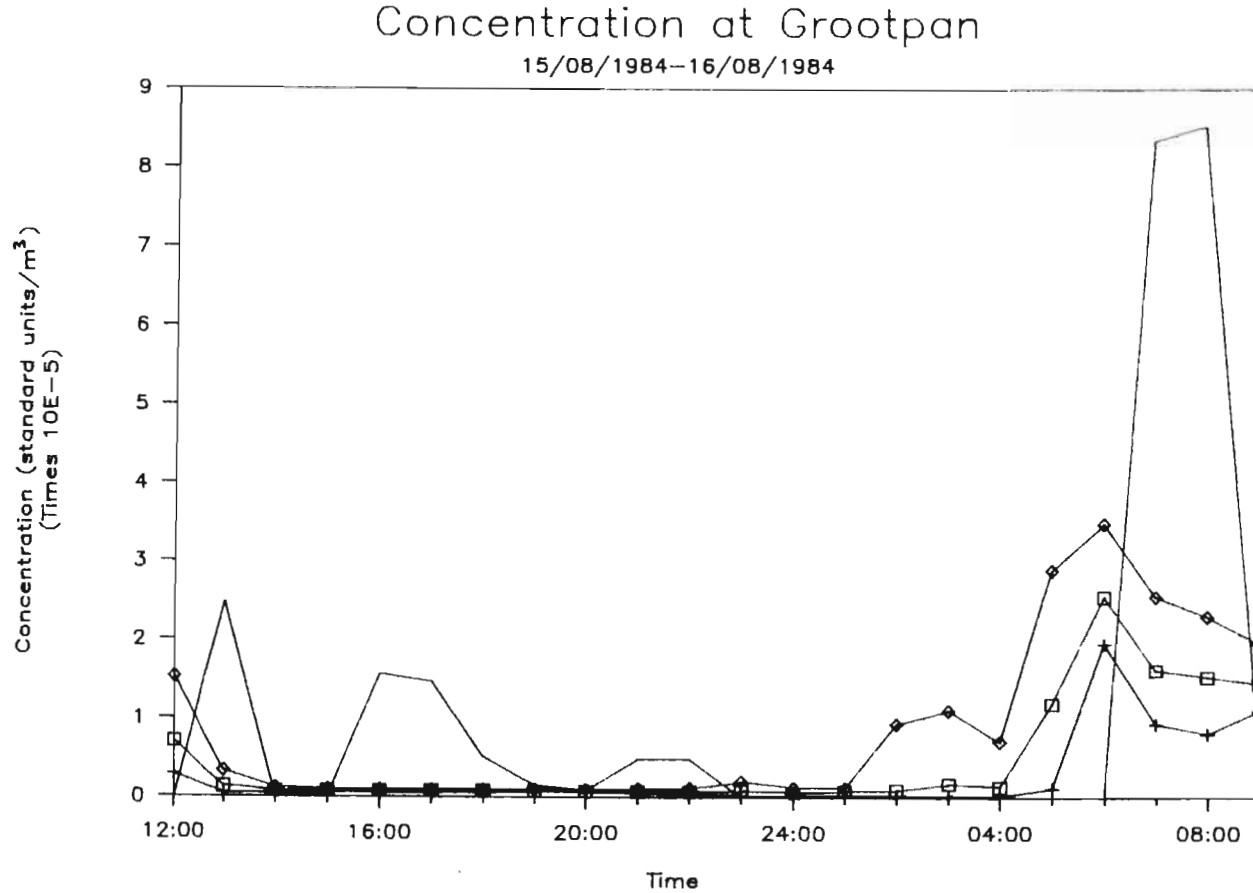
Figure 5.35. A comparison of measured and predicted concentrations at Grootpan, where

+   Minimum measured concentration

◇   Maximum measured concentration

□   Average measured concentration

—   Predicted concentration

The definition of 'standard unit/m^3' is given in Section 5.2.1.: the emission rate for MOBIL (Table 5.4) is 100 standard units/m^3.
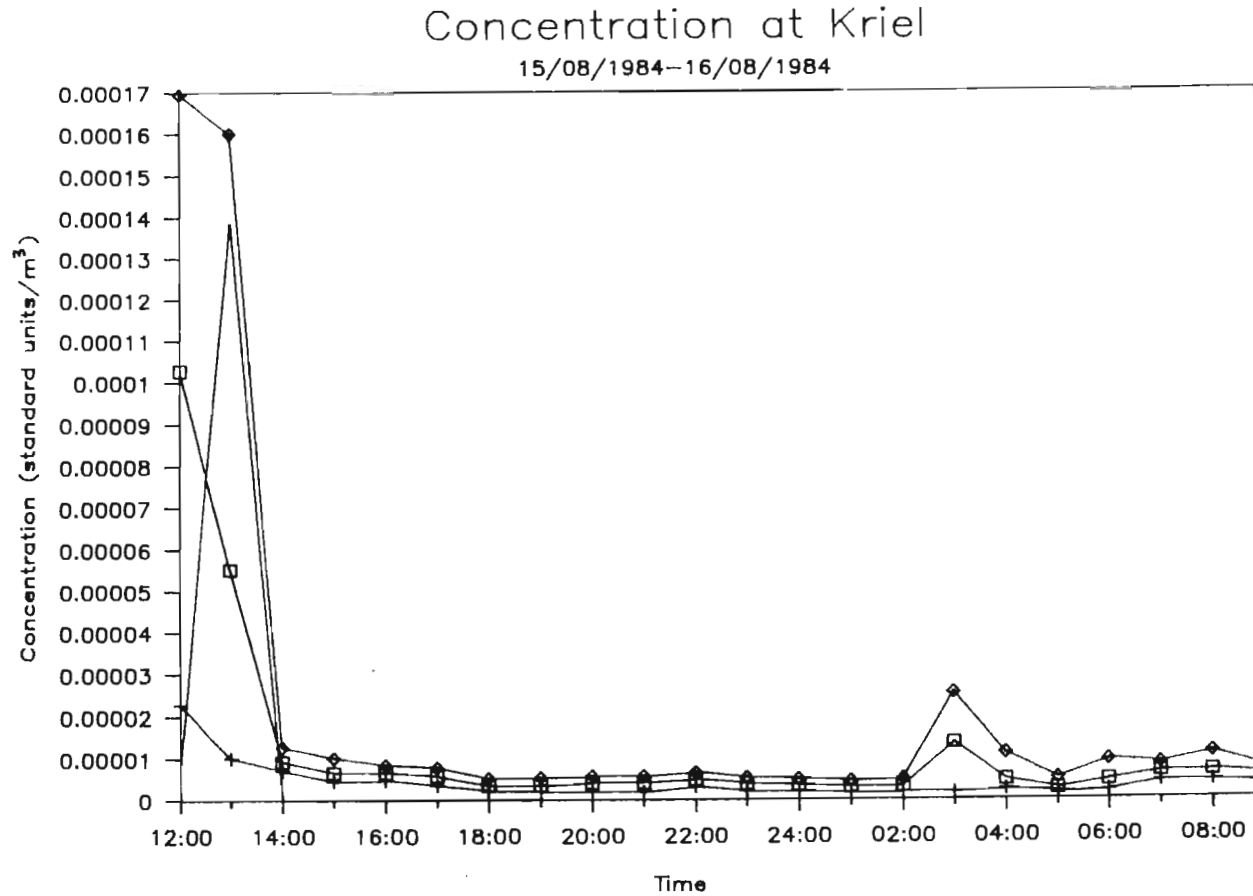
Figure 5.36.   A comparison of measured and predicted concentrations at Kriel, where

    +   Minimum measured concentration

    ◇   Maximum measured concentration

    □   Average measured concentration

    —   Predicted concentration

The definition of 'standard unit/m^3' is given in Section 5.2.1.:   the emission rate for MOBIL (Table 5.4) is 100 standard units/m^3.

Concentration at Komati
15/08/1984—16/08/1984
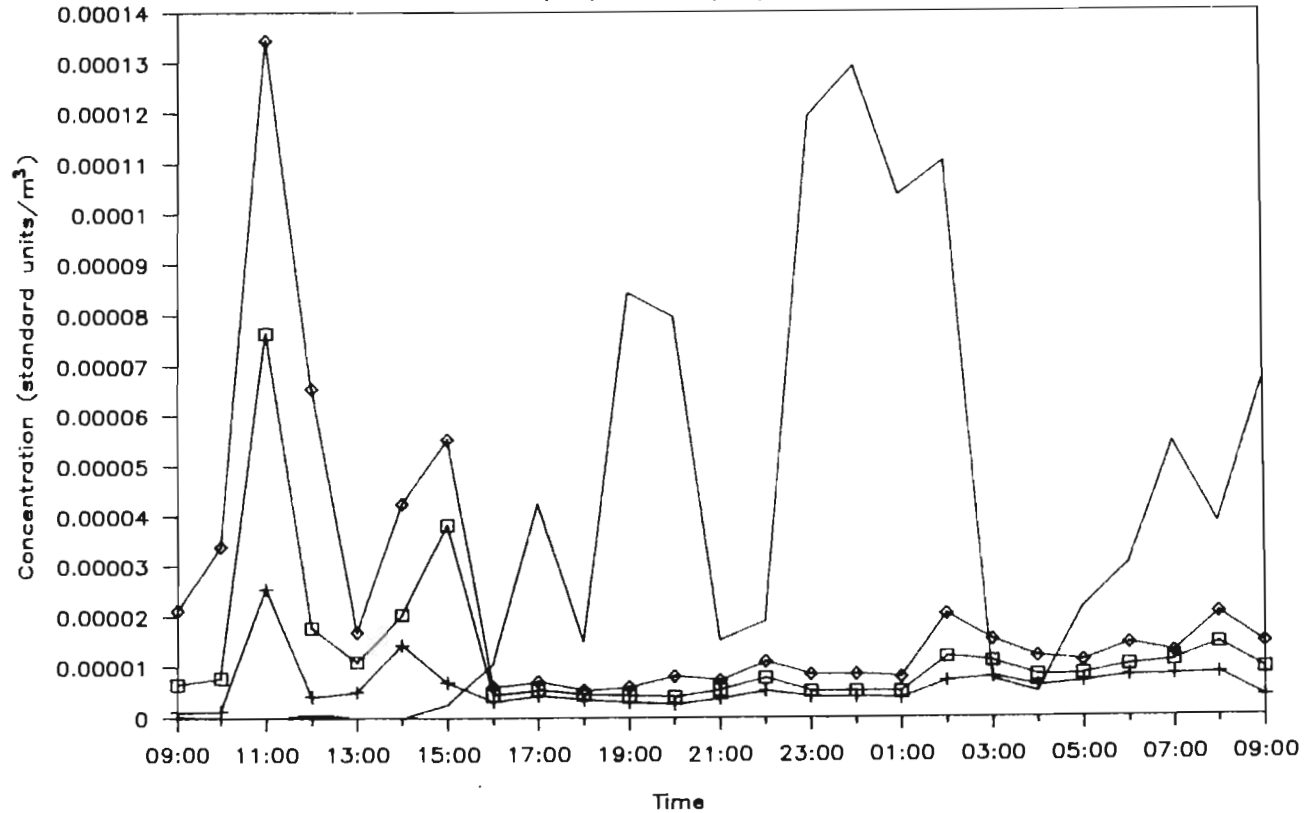
Figure 5.37. A comparison of measured and predicted concentrations
at Komati, where

+   Minimum measured concentration

◇   Maximum measured concentration

□   Average measured concentration

—   Predicted concentration

The definition of 'standard unit/m^3' is given in Section 5.2.1.: the
emission rate for MOBIL (Table 5.4) is 100 standard units/m^3.

Concentration at Elandsfontein
15/08/1984–16/08/1984
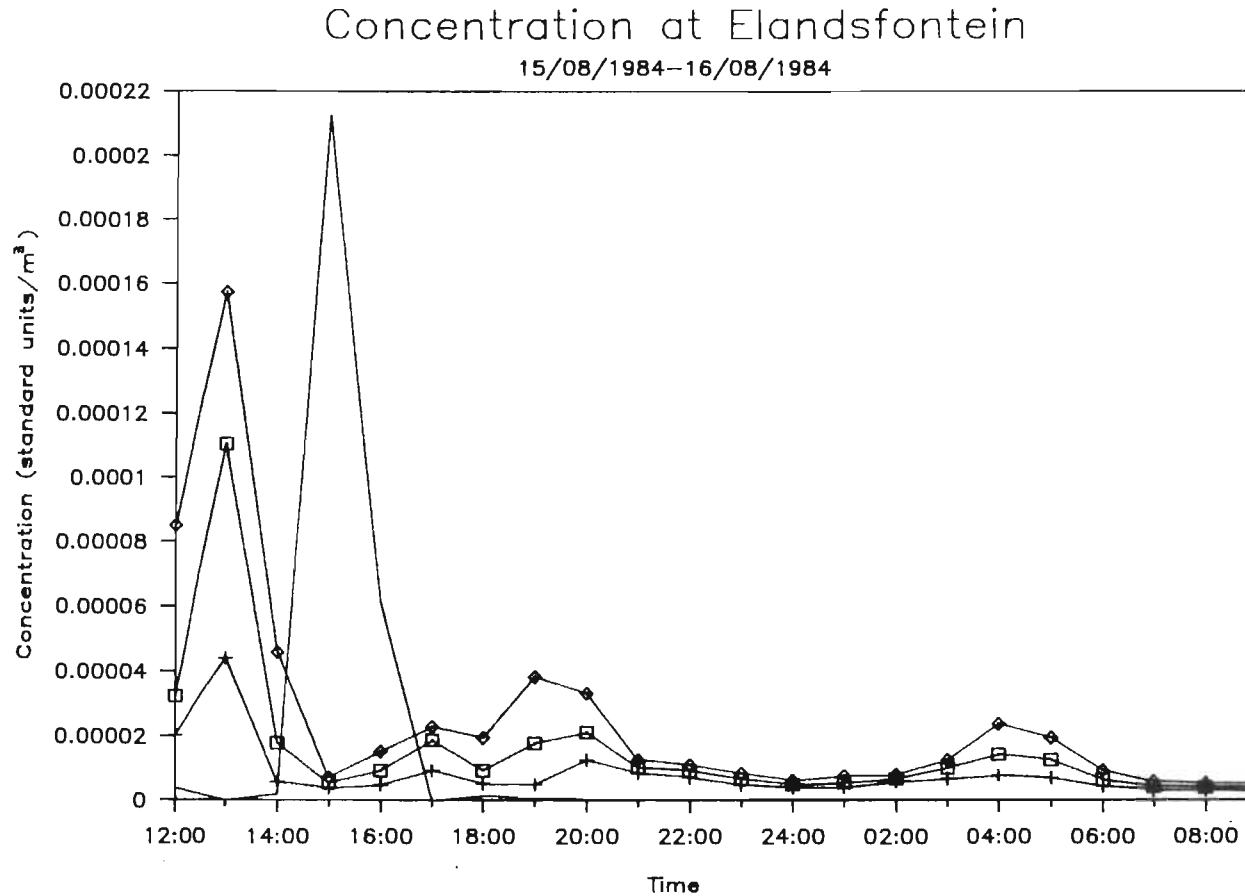
Figure 5.38. A comparison of measured and predicted concentrations at Elandsfotein, where

+   Minimum measured concentration

◇   Maximum measured concentration

□   Average measured concentration

—   Predicted concentration

The definition of 'standard unit/m^3' is given in Section 5.2.1.: the emission rate for MOBIL (Table 5.4) is 100 standard units/m^3.

Concentration at Arnot
15/08/1984–16/08/1984
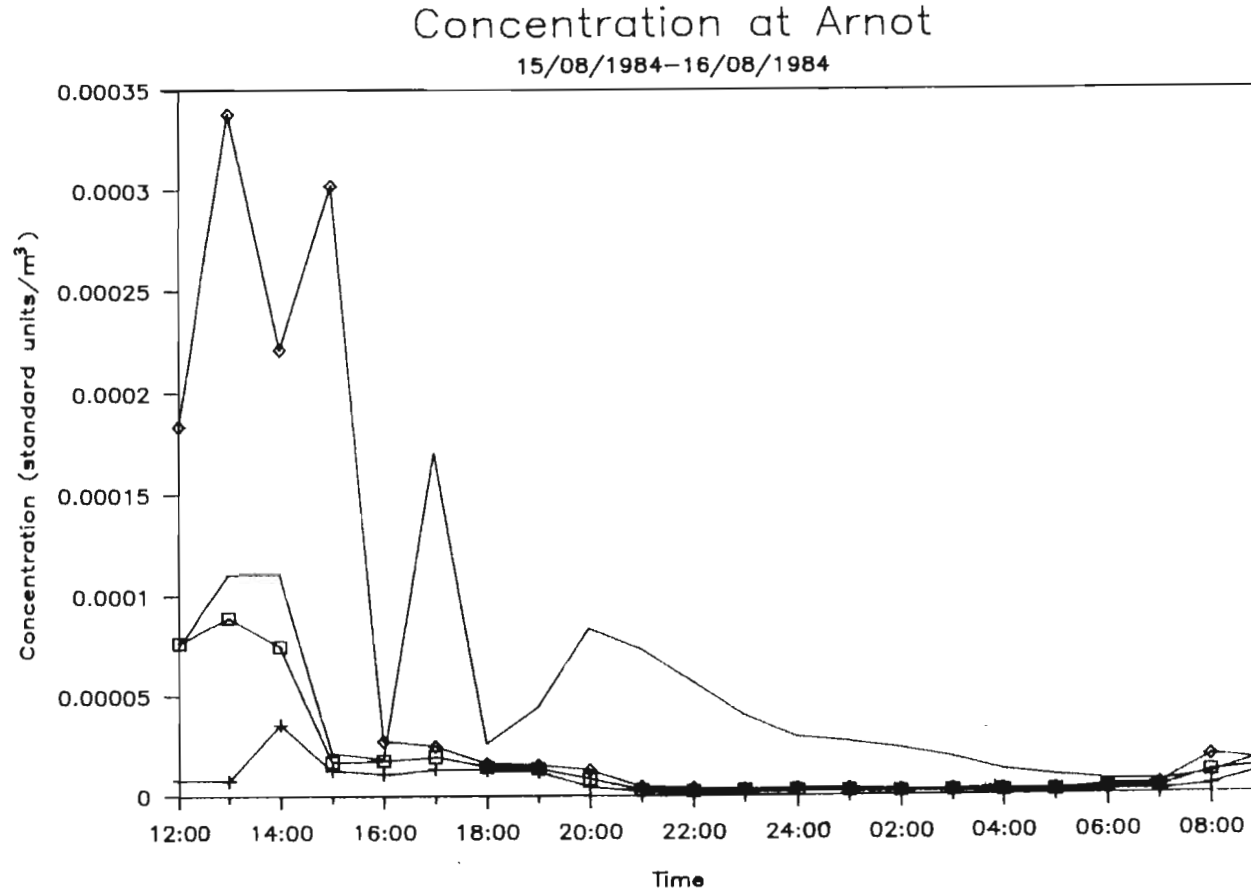
Figure 5.39.   A comparison of measured and predicted concentrations at Arnot, where

+   Minimum measured concentration

◇   Maximum measured concentration

□   Average measured concentration

—   Predicted concentration

The definition of 'standard unit/m^3' is given in Section 5.2.1.:   the emission rate for MOBIL (Table 5.4) is 100 standard units/m^3.

CHAPTER 6

DISCUSSION

The dispersion of pollutants can be described reasonably well by the advection-diffusion equation. Two processes are clearly identified: the transport (advection) and diffusion process. Generally, advection has a dominant effect, and it is thus necessary to determine the wind field affecting the pollutants as accurately as possible from routine meteorological measurements. The diffusion parameters are also deduced from meteorological measurements. To accomplish the general meteorological input structure, a submeteorological package was written to accept meteorological measurements from a wide range of options.

The Monin-Obukhov similarity theory has been widely accepted in describing the surface layer wind and diffusivity parameters (Section 2.1.). This theory has been used in the model, as discussed in Section 4.1. It assumes a constant shear layer with no turning of the wind vector with height. The surface layer is assumed to be ten per cent of the boundary layer height. Above this layer, very little is known about the behaviour of the atmosphere (Section 2.2.), and linear wind profiles are assumed (equation 4.1). A mass consistant three dimensional wind field is constructed (Section 4.1.2.) using a well known diagnostic model (Goodin *et al*. 1980, Section 2.4.2.3.). The resulting wind components were then used to determine the characteristic parameters describing the wind and diffusivity

profiles at each grid point of an array overlying the area of interest (Section 4.1.2.).

Due to the limitations imposed on analytical solutions of the advection-diffusion equation in an Eulerian reference frame (Section 3.1.1.1.), and the limitations of the Lagrangian trajectory models Section 3.2.1.), it was decided to use a numerical solution of the advection-diffusion equation (Section 4.2.1.). In this way, complex wind and diffusivity structures could be accommodated (Section 4.2.2.). First-order closure assumptions were used in the solution of the advection-diffusion equation. These assumptions cannot describe the dispersion process as accurately as higher-order closure or non-local closure assumptions since they are based on average eddy sizes (Section 3.1.1.1.3.). Smaller eddies, close to the source and larger eddies, during convective conditions, are therefore not accurately described. A large-eddy relationship (Section 3.1.2.1.) was however included in the model in an attempt to account for convective conditions.

The dispersion of pollutants is simulated by a series of sequentially released puffs in an Eulerian reference frame. The moments of the distribution of an instantaneously released puff are determined from the advection-diffusion equation by the method of fractional steps (Section 4.2.1.). A modification of the limiting value (LV) method of Mulholland (1979) is used to solve the vertical diffusion part of the equation of this puff. The modified limiting value (MLV) method is derived in Appendix G.. The conditions under which this method would produce the most accurate results were determined by Mulholland (1977) to be

$$\frac{K_v \Delta t}{\Delta z^2} = 0,4$$

The aim of the present modification to the LV method, was to allow larger time steps to be used for the same vertical spacing and diffusivity. By applying the LV method to half the space and time intervals, a modified method results which improves the optimum

criterion to (Appendix G)

$$\frac{K_v \Delta t}{\Delta z^2} = 0,8$$

This value was confirmed by numerical tests reported in Chapter 5, Section 5.1.

The release rate of "solved" instantaneous puffs is determined by a separation distance criterion. As the puffs grow, some will eventually overlap to such an extent that they can be merged. Puffs are "purged" when they leave the area of interest. In order to obtain a smooth graphical representation, puffs are interpolated between solved puffs when the distance between the solved puffs exceeds $\frac{1}{2}\sqrt{\sigma_x^2 + \sigma_y^2}$. A linear interpolation of the puff parameters is assumed. As seen in Section 3.2.2., the parameter σ_y, for example, varies non-linearly with time, so a linear variation with distance is not expected. Nevertheless, for small (100 - 500m) "solved" puff separation distances, and relatively long spatial and temporal variation scales in the wind field and diffusivity, little error is expected from the linear interpolation of the parameters μ_x, μ_y, σ_x, σ_y, ρ for each level

Chapter 5 contains two case studies which demonstrate the use of the package. The first case study was done under better documented conditions and hence produced better predictions than the second case study. The results of the Durban Bluff case study are given in Figure 6.1. It is clear from the figure that excellent comparison exists between the observed and predicted ground-level concentrations. Moderate agreement existed for the second case study on the Eastern Transvaal Highveld (Figures 5.32 to 5.39). This is acceptable in view of the approximate source data which were available for this study.

The Bluff case study was for a relatively small area: 13 x 4 km, whereas the Eastern Transvaal Highveld case study was for a much larger area (120x84km). The output resolutions were 20m and 200m, respectively. To achieve such high resolutions, a "hound-sniffing" contour drawing routine was developed (Section 4.3). With this

OBSERVED AND PREDICTED CONCENTRATIONS

Run#3 (22/9/1986)
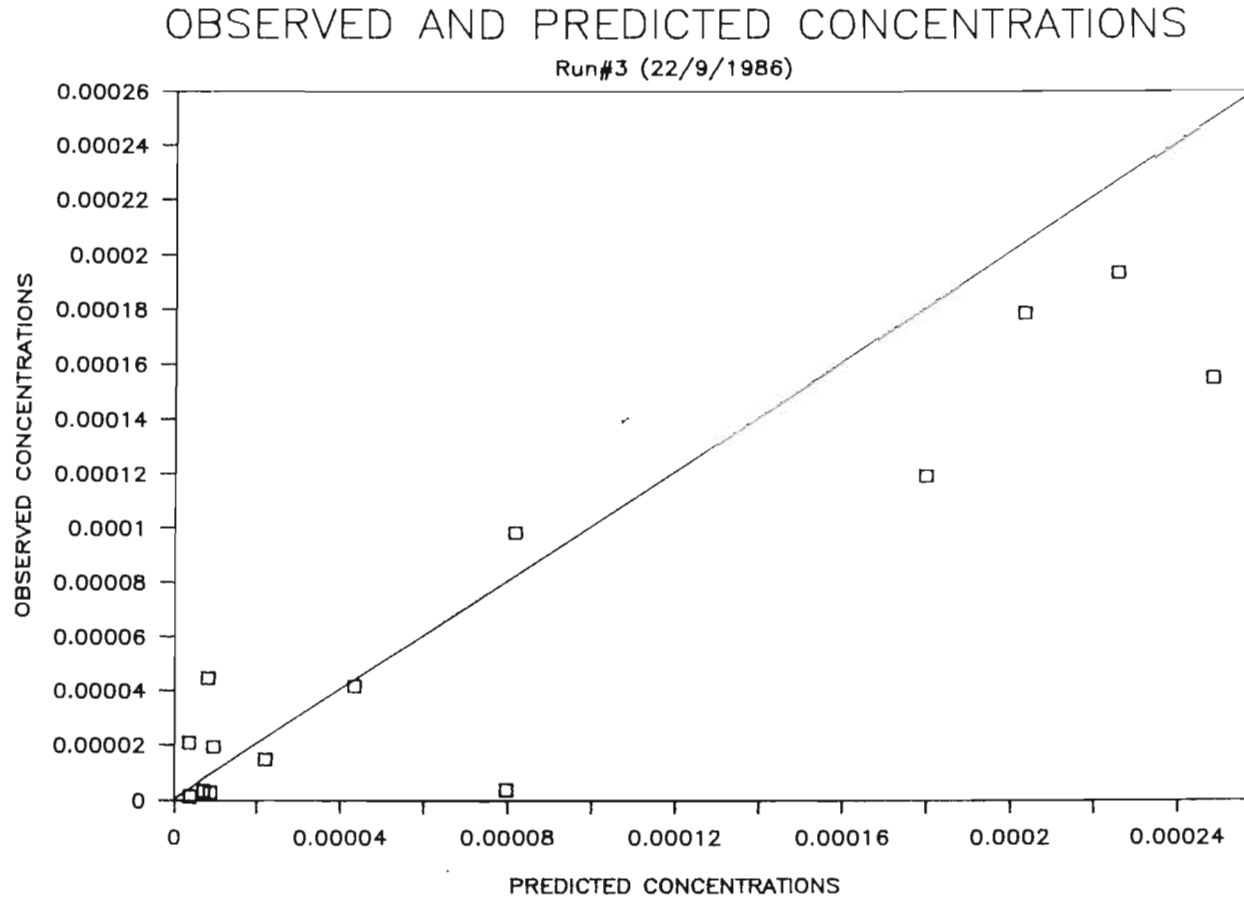
Figure 6.1. A comaparison of the measured and predicted concentrations during the Durban Bluff simulation. Concentrations are given in 'standard units/m^3', defined in Section 5.2.1.: the emission rate for MOBIL (Table 5.4) is 100 standard units/m^3.

method, a contour is followed from a starting point in one continuous movement. Each new point on the contour is calculated by considering four neighbouring points separated by a distance supplied by the user. When high resolution is required, a small value is obviously chosen. Additional information such as wind vectors in a plane, and wind and diffusivity profiles at any chosen point on the map, appear with the concentration distribution. Examples of the graphical output are given in Plates 6.1, 6.2, and 6.3.

The computer package was written to allow easy modification of the source code when new developments are desired. The different modules describing each process, *i.e.*, submeteorological module, wind field module, dispersion module and the concentration isopleth module, are well-defined units. The variables and parameters required by each module are also easily identified. The overall package is a self contained program written in standard FORTRAN 77 (Burger 1986), and requires no additional routines for graphics. A total of some 15000 statements are involved, of which about a third are "comments" The program supports Hewlett-Packard and Tektronix 4100 type graphics terminals. The addition of support for more graphics terminals is easily achieved by supplying the codes for: (a) drawing a line to a point with the pen in either the up or down position, and (b) writing text. This requires the addition of only a few lines to the source code. The package runs successfully on a Sperry Univac 1100 mainframe (Durban Bluff case study), a CDC Cyber 750 mainframe (Eastern Transvaal Highveld case study) and an IBM 4341 mainframe.

The main program, WIZARD, together with all of the subroutines, requires 93K RAM for a wind field grid of 3000 points, 10 sources with 50 solved puffs, and 40 layers for the numerical solution of the advection-diffusion equation. When the modules are chained or overlayed, only 57K RAM are required.
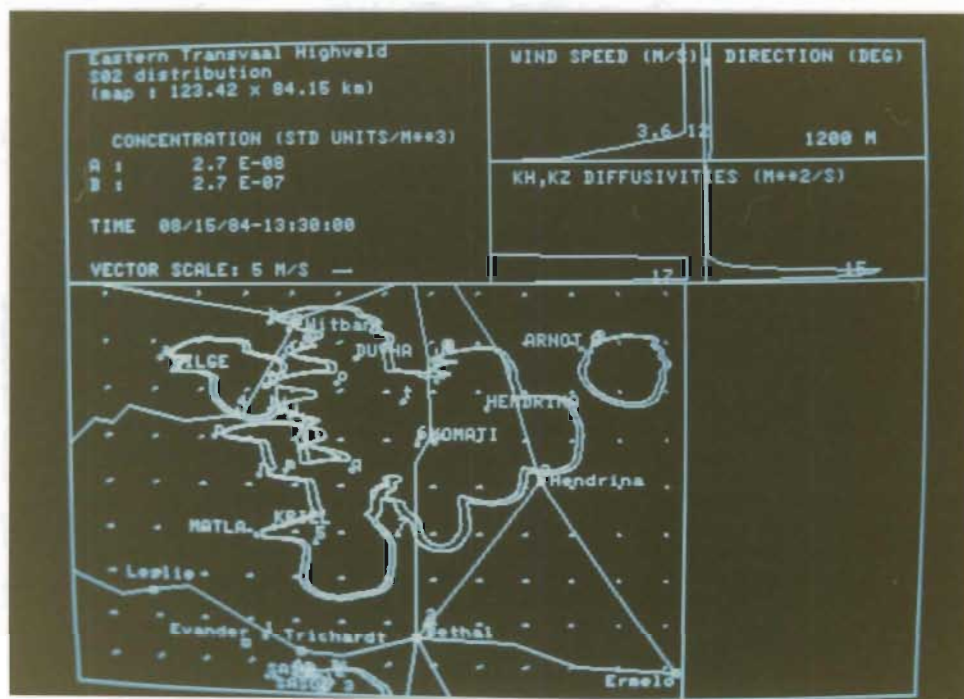
Plate 6.1. An example of the graphics output on an HP2326A terminal.
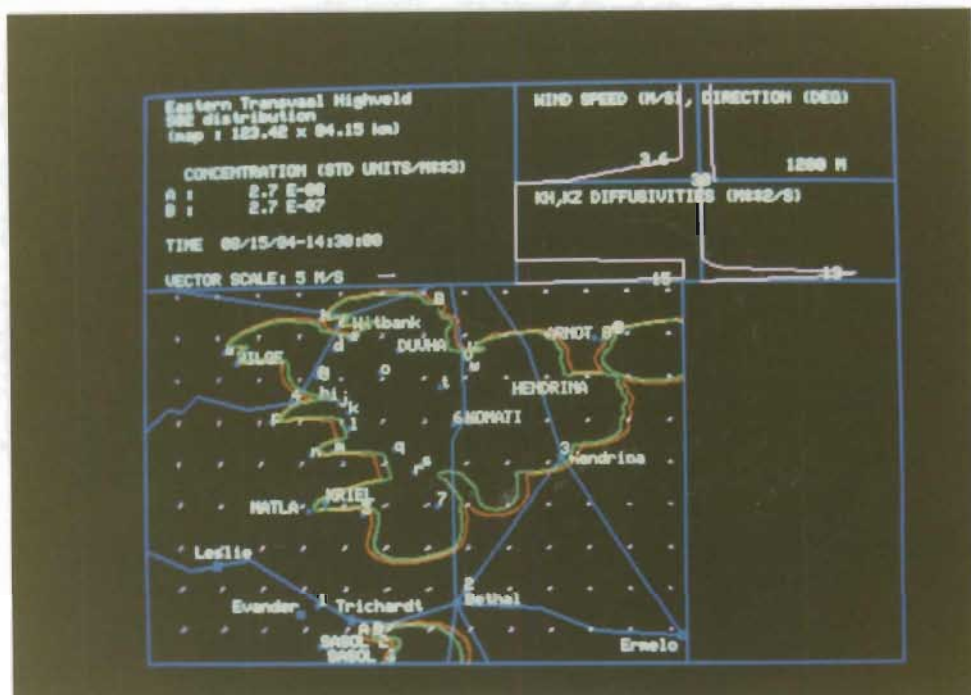
Plate 6.2.   An example of the graphics output on a Tektronix 4105 terminal.
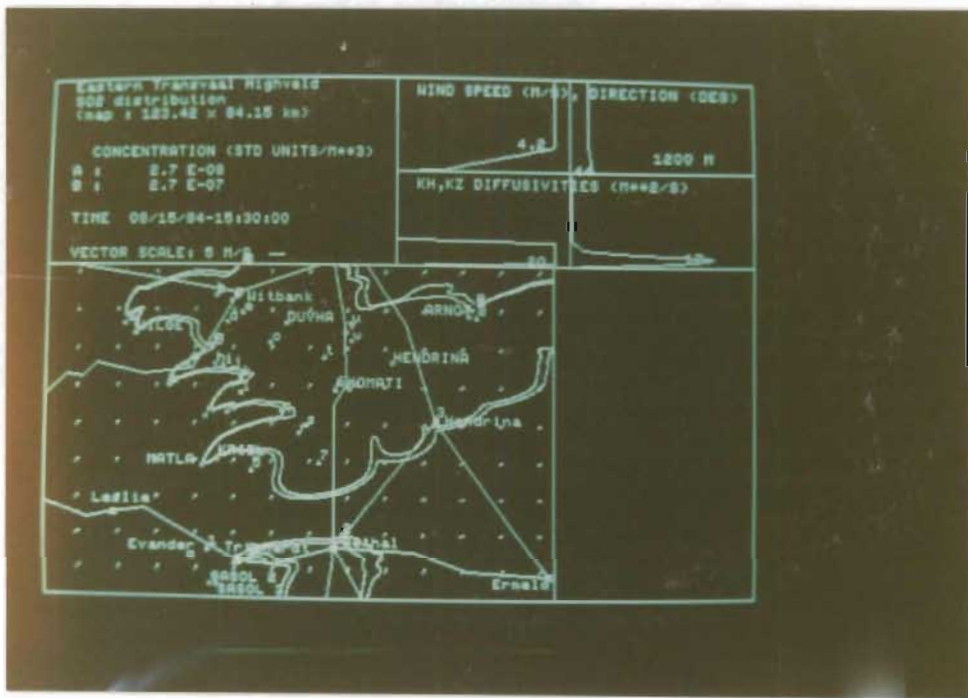
Plate 6.3.   An example of the graphics output on an HP150 Personal Computer.

CONCLUSION AND RECOMENDATIONS

A computer program has been written to predict the distribution of pollutants released from multiple sources in complex terrain with realistic wind and diffusivity profiles (Burger 1986). A particular feature is that the model allows an arbitrary variation of wind vector with height. The model includes the following removal mechanisms:

Chemical reaction/decay

Washout in rain

Sedimentation

Ground retention

Plume rise due to the thermal buoyancy is also accommodated. A high resolution, clear, and easily interpretable graphical output, describes the concentration distributions.

The construction of a mass-consistent three-dimensional wind field from routine meteorological measurements provides the wind and diffusivity profile parameters required to solve the advection-diffusion equation. The plume is simulated by a sequence of serially released puffs. The distribution within each puff is described by the moments at different heights in an Eulerian reference frame. The moments are obtained from a numerical solution of the advection-diffusion equation. A modified version of

Mulholland's (1977; 1980) limiting value method is used to solve the vertical diffusion process. Reconstruction of the puff is done by assuming a bivariate normal (Gaussian) distribution in the horizontal. This requires the solution of the zero'th, first and second-order moments of the advection-diffusion equation. The combined effect of wind shear and vertical diffusion on the horizontal dispersion is of considerable importance (Section 3.1.1.2.). Considerable enhancement of the horizontal spreads occurs as a result of a temporal variation in wind direction (e.g., Figures 5.28 to 5.31), as well as variations in wind direction with height. Both these phenomena are properly modelled by the proposed numerical solution for moments.

The numerical solution for vertical diffusion of moments (MLV : modified limiting value) is unconditionally stable. In comparison with the Gaussian plume and puff analytical models, it was observed (Section 5.1) that the MLV method produces its most accurate predictions when

$$\frac{K_v \Delta t}{\Delta z^2} = 0,8$$

The package is designed to be user-friendly. All fixed parameters, such as topography, pollutant characteristics, graphics terminal type, prominent features on output, weather station and source positions, are supplied by the menu-driven installing package, INSTALL. This program needs to be run only once. The dispersion package, WIZARD, consists of four modules : PREMET (treatment of raw meteorological measurements), METPAC (construction of a three-dimensional wind field), DSPRSN (solution of the advection-diffusion equation), and ISPLTH (construction of concentration distribution isopleths). The programs are written in standard FORTRAN 77. The package has been run successfully on the following mainframe computers: Sperry Univac 1100, CDC Cyber 750 and IBM 4341, and it supports HP and Tektronix 4100 type graphic terminals.

Two case studies demonstrate the use of the package. The Durban Bluff (13x4km) field experiment (22/09/1986-23/09/1986) was based on

more accurately recorded meteorological and source data, and was therefore used to illustrate the accuracy of the dispersion model. Excellent agreement existed (Section 5.2.1.). The second case study (Eastern Transvaal Highveld, 15/08/1984-16/08/1984) concerns a much larger area (120x84km) and many more point sources. Emission rates were based on 1983 annual averages and were therefore not considered accurate. Nevertheless, reasonable predictions were obtained (Section 5.2.2.).

A wide range of meteorological measurement types are included in INSTALL. These are assumed to cover most possibilities:

Surface Layer Measurements

(a) wind velocity at one height and cloud cover;

(b) wind velocity at one height and the variance of the azimuth;

(c) wind velocity at one height, cloud cover and the average temperature;

(d) wind velocity at one height and temperature at two heights;

(e) wind velocity at two heights and temperature at two heights;

(f) wind velocity at various heights;

(g) wind velocity at one height and temperature at various heights

(h) wind and temperature at various heights.

Outer Layer

(a) no upper air data

(b) one wind speed at a height above the surface layer

(c) more than one wind speed above the surface layer

Boundary Layer Height

(a) no upper-air measurement

(b) temperature profile

(c) Doppler acoustic sounder

(d) user-estimates of the boundary layer height

The package was designed to be easily adaptable to include future

developments in the dispersion theory. The one weakness of the package is that first-order closure was assumed in the solution of the advection-diffusion equation. When better practical solutions to the closure problem are reported, these should be included in the model. An average chemical reaction rate constant is required by the model (Section 4.2.1.). A better approach would be to have a variable rate, dependent on the season, and other chemicals in the environment. The assumption of a constant deposition velocity could lead to some error (Section 4.4.1.2.), since it depends on surface types. It would, however, not be a difficult task to allow for this: deposition velocities could be supplied at each grid point or interpolated on demand from a few positions.

The concentration distribution can be drawn for any height. The module ISPLTH was especially designed for fast, high resolution output (Section 4.3.). As demonstrated in Chapter 5, the resolution for the Durban Bluff case study (13 x 4km) was 20m, and that for the Eastern Transvaal Highveld case study (120 x 84km), 200m. Wind vectors can be drawn at any height and resolution. The wind and diffusivity profiles for a chosen position on the map are also supplied. In addition to minimising computation, it was an objective to keep the memory requirement as low as possible. The contour drawing routine requires no storage of grid point concentrations. As a result, dosages cannot be accommodated. If it is essential to supply dosages for a particular application, grid point concentrations can be stored in a file and updated accordingly. This would require additional computation, since concentrations must be calculated at each grid point for accumulation.

Though the model produced in this study demands considerable computational resources (*e.g.*, CPU time of 1 hr / hr of simulation on a Sperry Univac 1100, and 93K RAM core memory), it does represent a demonstration of a flexible, high-resolution, multiple source technique which correctly models complex atmospheric structure. The adaptable meteorology package makes optimal use of available measurement data to provide winds and diffusivity based on a comprehensive synthesis of modern-day micrometeorological results (Section 4.1.). A model which sets out to include so much detail can clearly only be proved by observations of equivalent detail.

251

Suitable measurements would require enormous investments of time and money. Nevertheless, the Durban Bluff data set, collected specifically for this simulation, and the archived Eastern Transvaal Highveld data, both provide some support for the quality of the model results.

APPENDICES

APPENDIX A

A.1 SOLAR ELEVATION ANGLE

The solar elevation angle ν is obtained from

$$\sin \nu = \sin \phi \sin \delta + \cos \phi \cos \delta \cos h_A \qquad \text{(A.1)}$$

where

$$h_A = (\pi/12)(\tau - 12 + Q_E + \Delta t_g) - \lambda \qquad \{\text{hour angle}\} \quad \text{(A.2)}$$

$$Q_E = a_1 \cos D + a_2 \cos D + a_3 \sin 2D + a_4 \cos 2D$$

$$\{\text{the equation of time}\} \quad \text{(A.3)}$$

and the constants are

$$a_1 = 0,004289$$

$$a_2 = -0,12357$$

$$a_3 = -0,153809$$

$$a_4 = -0,060783$$

$$D = d_y(360/365,242)(\pi/180)$$

$$\delta = \sin^{-1}[0,39784989 \sin(\pi\alpha/180)]$$

$$\{\text{sun declination}\}$$

$$\alpha = b_1 + b_2 D + b_3 \sin D + b_4 \cos D + b_5 \sin 2D$$

$$+ b_6 \cos 2D$$

and

$$b_1 = 279,9348$$

$$b_2 = 180/\pi$$

$$b_3 = 1,914827$$

$$b_4 = -0,079525$$

$$b_\bullet = 0,019938$$
$$b_\bullet = -0,00162$$

with

τ = time of day in hours

d_y = day of the year (*i.e.* d = 0 at 0h00 1 January)

λ = longitude (radians)

ϕ = latitude (radians)

Δt_g = time difference from Greenwich Mean Time (hrs)

A.2 SUNRISE AND SUNSET TIMES

Sunrise and sunset times are calculated from equation (A.1) by substituting for the elevation, the following

$$\nu = -(0,8° + A_\ell) \tag{A.4}$$

where $-0,8°$ is the altitude of the sun at sunrise and sunset, *i.e.* when the sun's upper limb is 32' below the horizon (for *horizontal refraction*) and 16' for the *semi-diameter* of the sun. A_ℓ is the angle correction of the average height above sea level, given as

$$A_\ell = \tan^{-1}\left[\frac{r_e}{r_e + 1,32z_t}\right] \tag{A.5}$$

where

r_e = earth's radius = $6,37 \times 10^6$ m

z_t = average height above sea level (m)

The times of sunrise and sunset are then expressed as

$$t_{SR} = (h_{SR} + \lambda)(12/\pi) + 12 - Q_E - \Delta t_g \tag{A.6a}$$
$$t_{SS} = (h_{SS} + \lambda)(12/\pi) + 12 - Q_E - \Delta t_g \tag{A.6b}$$

with Q_E given by equation (A.3) and the hour angles given by

$$h_{SR} = -\cos^{-1}\left[\frac{\sin\left\{\frac{-\pi}{225} - A_\ell\right\} - \sin\phi \sin\delta}{\cos\phi \cos\delta}\right] \quad (A.7a)$$

$$h_{SS} = -h_{SR} \quad (A.7b)$$

APPENDIX B

B.1 THE ENERGY BUDGET METHOD - MAUL'S SOLAR REDUCTION FACTOR

The solar reduction factor, r_c, for Maul's (1980) estimate of the sensible heat flux H, is given in the following table

Cloud Cover, N	Radiation Reduction Factor, r_c
0,0	1,00
0,1	0,91
0,2	0,84
0,3	0,79
0,4	0,75
0,5	0,72
0,6	0,68
0,7	0,62
0,8	0,53
0,9	0,41
1,0	0,23

B.2 THE ENERGY BUDGET METHOD OF DE BRUIN AND HOLTSLAG

The sensible heat flux H, is calculated by De Bruin and Holtslag (1982) from:

$$H = \frac{(1-l_2)S + \gamma}{S + \gamma}(H^* - G) - l, \tag{B.1}$$

where

$$\gamma = 0,646 + 6 \times 10^{-4}(T-273,1)$$

$$S = 4 \times 10^3 \frac{\epsilon(T)}{(T - 35,8)^2}$$

and

$$\epsilon(T) = 10^{\left[\frac{7,5(T - 273,1)}{T - 35,8} + 0,786\right]}$$

256

with the temperature T in Kelvin. The parameters α and β, depend on the terrain type. Holtslag *et al* (1981) suggests the following

$$\alpha = 1$$
$$\beta = 20$$

for roughness lenths in the interval $0,025 \leq z_0 \leq 0,5$ and

$$\alpha = 0$$
$$\beta = 0$$

for $z_0 > 0,5$. H^* is the net radiation calculated from (Holtslag 1984)

$$H^* = \frac{(1-a)R + c_1 T^6 - \sigma T^4 + c_2 N}{1 + c_3} \qquad (B.2)$$

where   a = albedo = 0,14 for snow-free land
                    = 0,7 for temporary snow

On average, a value of 0,25 can be assumed. c_3 also depends on surface conditions, but on average $c_3 = 0,12$ (Holtslag 1984). The other constants are :

$$c_1 = 5,31 \times 10^{-13} \text{ Wm}^{-2}\text{K}^{-6}$$
$$\sigma = 5,67 \times 10^{-8} \text{ Wm}^{-2}\text{K}^{-4}$$
$$c_2 = 60 \text{ Wm}^{-2}$$

R, the incoming solar radiation, is given by

$$R = (1041\sin \nu - 69)(1 - 0,75 N^{3,4}) \qquad (B.3)$$

with   N = cloud cover fraction
            ν = solar elevation

The soil heat flux G is estimated by

$$G \approx 0,1 H^* \qquad (B.4)$$

257

During nighttime conditions, Holtslag and Van Ulden (1982) proposed

$$H^* = - \frac{90}{1 + \dfrac{4}{u^2(10)}} (1-0,9N^2) \quad \text{for } u(10) \geq 2 \text{ m/s}$$

$$\text{(B.5)}$$

$$- 45(1-0,9N^2) \quad \text{for } u(10) < 2\text{m/s}$$

Van Dop *et al* (1982) added that if $H^* < 0$, equation (B.1) no longer applies and,

$$H = 0,4H^* \qquad \text{(B.6)}$$

C.1 THE LEAST-SQUARE ERROR METHOD OF LO (1978)

The least-square error method, as discussed by Lo (1978), is presented slightly differently. The wind velocity profile is given by (Section 2.1.)

$$u(z) = \frac{u_*}{k} \, \Psi_m(\xi) \tag{2.7}$$

where $\xi = \frac{z}{L}$ and the potential temperature profile, is given by

$$\theta(z) = \frac{\theta_*}{k} \, \Psi_h(\xi) \tag{2.8}$$

At any data height we can therefore write

$$\frac{k}{u_*} u_i = \Psi_m(\xi_i) \tag{C.1}$$

and similarly for the temperature profile. The calculation procedes by estimating a value for L and substituting it into equation (C.1). Since it is only an estimate, there exist some error :

$$\frac{k}{u_*} u_i - \Psi_m(\xi_i) = \epsilon_i \neq 0 \tag{C.2}$$

Lo (1978) applies the least-square error method to equation (C.2). This requires that $\sum_{i=1}^{N} \epsilon_i^2$ be minimised. N is the number of data points. In other words

$$\frac{\partial}{\partial L} \sum_{i=1}^{N} \epsilon_i^2 = 0 \tag{C.3a}$$

or

$$\sum_{i=1}^{N} \epsilon_i \frac{\partial \epsilon_i}{\partial L} = 0 \qquad\qquad (C.3b)$$

and when applied to (C.2) becomes

$$\sum_{i=1}^{N} \epsilon_i \left\{ ku_i \frac{\partial}{\partial L} [\frac{1}{u_*}] - \frac{\partial}{\partial L} [\Psi_m(\xi_i)] \right\} = 0 \qquad\qquad (C.4)$$

Lo (1978) then assumes an average value for u_*, and suggests

$$\frac{1}{u_*} = \frac{1}{kN} \sum_{j=1}^{N} \frac{\Psi_m(\xi_j)}{u_j} \qquad\qquad (C.5)$$

Therefore,

$$\frac{\partial}{\partial L} [\frac{1}{u_*}] = \frac{1}{kN} \sum_{j=1}^{N} \frac{1}{u_j} \frac{\partial}{\partial L} [\Psi_m(\xi_j)] \qquad\qquad (C.6)$$

Substituting (C.6) into (C.4) we get

$$\sum_{i=1}^{N} \epsilon_i \left\{ \frac{u_i}{N} \sum_{j=1}^{N} \frac{(\partial/\partial L)\Psi_m(\xi_j)}{u_j} - \frac{\partial}{\partial L} [\Psi_m(\xi_i)] \right\} = 0 \qquad\qquad (C.7)$$

The correct value of L is then determined by iteration or as shown in Appendix D.

APPENDIX D

APPLICATION OF LO's (1978) LEAST-SQUARE ERROR METHOD

D.1. Shultz's (1979) Approximate Universal Function

Consider the quadratic approximation

$$\Psi_m(\xi) = \ln \frac{z}{z_0} + a\xi^2 + b\xi \tag{D.1}$$

proposed by Shultz (1979), where

$$\xi = \frac{z}{L}$$
$$a = 0,472$$
$$b = 1,64$$

So, from equation (C.2)

$$\epsilon_i = k\frac{u_i}{u_*} - \ln \frac{z_i}{z_0} - a\xi_i^2 - b\xi_i \tag{D.2}$$

where $\xi_j = \frac{z_j}{L}$, and from (C.5)

$$\frac{1}{u_*} = \frac{1}{kN} \sum_{j=1}^{N} \frac{\ln \frac{z_j}{z_0} + a\xi_j^2 + b\xi_j}{u_j} \tag{D.3}$$

We now define the following coefficients

$$A_i = a\left[\frac{u_i}{N} \sum_{j=1}^{N} \frac{z_j^2}{u_j} - z_i^2\right] \tag{D.4a}$$

$$B_i = b\left[\frac{u_i}{N}\sum_{j=1}^{N}\frac{z_j}{u_j} - z_i\right] \qquad (D.4b)$$

$$C_i = \frac{u_i}{N}\sum_{j=1}^{N}\frac{\ln\frac{z_j}{z_0}}{u_j} - \ln\frac{z_i}{z_0} \qquad (D.4c)$$

Substituting equation (D.3) into equation (D.2) and after some simplifications, using the above three definitions (D.4a-c), we get

$$\epsilon_i = A_i\left\{\frac{1}{L}\right\}^2 + B_i\left\{\frac{1}{L}\right\} + C_i \qquad (D.5)$$

Differentiating equation (D.1) with respect to L, gives

$$\frac{\partial}{\partial L}\Psi_m(\xi_j) = \frac{\partial}{\partial L}\left[\ln\frac{z_j}{z_0} + a\xi_j^2 + b\xi_j\right]$$

$$- z_j\left\{\frac{1}{L^2}\right\}\left[2az_j\left\{\frac{1}{L}\right\} + b\right] \qquad (D.6)$$

Therefore, substituting equation (D.6) into (D.7), results in

$$\sum_{i=1}^{N}\epsilon_i\left[2A_i\left\{\frac{1}{L}\right\} + B_i\right] = 0 \qquad (D.7)$$

where A_i and B_i are defined in (D.4a) and (D.4b). Substituting equation (D.5) for ϵ_i into (D.7), gives

$$S_A\left\{\frac{1}{L}\right\}^3 + S_B\left\{\frac{1}{L}\right\}^2 + S_C\left\{\frac{1}{L}\right\} + S_D = 0 \qquad (D.8)$$

where

$$S_A = 2\sum_{i=1}^{N}A_i^2$$

$$S_B = 2\sum_{i=1}^{N}A_iB_i$$

262

$$S_C = \sum_{i=1}^{N} (2A_i C_i + B_i^2)$$

$$S_D = \sum_{i=1}^{N} B_i C_i$$

L can now be obtained by solving the cubic eqaution (D.8). Consider the equation

$$z^3 + a_2 z^2 + a_1 z + a_0 = 0 \qquad (D.9)$$

and let

$$q = \frac{1}{3}\left(a_1 - \frac{1}{3}a_2^2\right) \qquad (D.10a)$$

$$r = \frac{1}{6}(a_1 a_2 - 3a_0) - \frac{1}{27}a_2^3 \qquad (D.10b)$$

then for $q^3 + r^2 > 0$, one real root and a pair of conjugate imaginary roots exist; for $q^3 + r^2 = 0$, all roots are real and at least two are equal; and for $q^3 + r^2 < 0$, all roots are real (irreducible case). So for $q^3 + r^2 \geq 0$ the roots are (Abramowitz and Stegun 1972) :

$$z_1 = (s_1 + s_2) - \frac{a_2}{3} \qquad (D.11a)$$

$$z_2 = -\frac{1}{2}(s_1 + s_2) - \frac{a_2}{3} + i\frac{\sqrt{3}}{2}(s_1 - s_2) \qquad (D.11b)$$

$$z_3 = -\frac{1}{2}(s_1 + s_2) - \frac{a_2}{3} - i\frac{\sqrt{3}}{2}(s_1 - s_2) \qquad (D.11c)$$

with

$$s_1 = [r + \sqrt{q^3 + r^2}]^{\frac{1}{3}}$$

$$s_2 = [r - \sqrt{q^3 + r^2}]^{\frac{1}{3}}$$

Since we are only interested in the real roots, solutions z_2 and z_3 are only applicable when $s_1 = s_2$. For the irreducible case, $q^3 + r^2 < 0$ the roots are :

$$z_1 = 2\sqrt{-q}\cos\frac{\phi}{3} \qquad (D.12a)$$

$$z_2 = -2\sqrt{-q}\cos\frac{1}{3}(\phi+\pi) \qquad\qquad \text{(D.12b)}$$

$$z_3 = -2\sqrt{-q}\cos\frac{1}{3}(\phi-\pi) \qquad\qquad \text{(D.12c)}$$

with
$$\phi = \cos^{-1}\frac{3}{\sqrt{-q^3}}$$

When applied to equation (D.8), the following substitutions are made:

$$a_0 = \frac{S_D}{S_A}$$

$$a_1 = \frac{S_C}{S_A}$$

$$a_2 = \frac{S_B}{S_A}$$

D.2. Similarity Forms : Stable Conditions

D.2.1. Wind Profile

For stable conditions, the function Ψ_m may be given by :

$$\Psi_m(\xi) = \ln\frac{z}{z_0} + \frac{\beta}{L}(z-z_0) \qquad\qquad \text{(Table 2.3.)}$$

So, for $z_j > z_0$, from equation (C.5) we have

$$\frac{1}{u_*} = \frac{1}{kN}\sum_{j=1}^{N}\frac{\ln(z_j/z_0) + \frac{\beta}{L}(z_j-z_0)}{u_j} \qquad\qquad \text{(D.13)}$$

and therefore substituting Ψ_m and equation (D.13) into equation (C.2) results in

$$\epsilon_i = A_i + B_i\left\{\frac{1}{L}\right\} \qquad\qquad \text{(D.14)}$$

where we have defined the following

264

$$A_i = \frac{u_i}{N} \sum_{j=1}^{N} \frac{\ln \frac{z_j}{z_0}}{u_j} - \ln \frac{z_i}{z_0}$$

$$B_i = \beta \left[\frac{u_i}{N} \sum_{j=1}^{N} \frac{z_j - z_0}{u_j} - z_i + z_0 \right]$$

It can also be shown that

$$\frac{\partial}{\partial L} \Psi_m(\xi) = -\frac{\beta}{L^2}(z - z_0) \tag{D.15}$$

Substitution of equation (D.15) into (D.7) results in

$$\sum_{i=1}^{N} \epsilon_i \left\{ \frac{u_i}{N} \sum_{j=1}^{N} \frac{z_j - z_0}{u_j} + z_0 - z_i \right\} = 0 \tag{D.16}$$

From the definition of B_i in equation (D.14), it is clear that equation (D.16) can be rewritten as

$$\sum_{i=1}^{N} \epsilon_i B_i = 0 \tag{D.17}$$

Substitution of (D.14) into (D.17) leads to

$$\frac{1}{L} = - \frac{\displaystyle\sum_{i=1}^{N} A_i B_i}{\displaystyle\sum_{i=1}^{N} B_i^2} \tag{D.18}$$

D.2.2. Temperature Profile

The universal function for the temperature profile is given as

$$\Psi_h(\xi) \;=\; \alpha \ln \frac{z}{z_1} + \frac{\beta_2}{L}(z - z_1) \qquad \text{(Table 2.3.)}$$

It is quite obvious from the previous discussion for the wind profile, that

$$\frac{1}{L} \;=\; -\, \frac{\displaystyle\sum_{i=1}^{N} A_i' B_i'}{\displaystyle\sum_{i=1}^{N} B_i'^{\,2}} \qquad \text{(D.19)}$$

where A_i' and B_i' are defined by

$$A_i' \;=\; \alpha \left[\frac{\theta_i}{N} \sum_{j=1}^{N} \frac{\ln \dfrac{z_j}{z_1}}{\theta_j} - \ln \frac{z_i}{z_1} \right]$$

$$B_i' \;=\; \beta_2 \left[\frac{\theta_i}{N} \sum_{j=1}^{N} \frac{z_j - z_1}{\theta_j} - z_i + z_1 \right]$$

D.3. Unstable Conditions

D.3.1. Wind Profile

The Function Ψ_m is given by

$$\Psi_m(\xi) \;=\; 2(\tan^{-1} b - \tan^{-1} b_0) - \ln\left\{ \frac{b+1}{b-1}\, \frac{b_0-1}{b_0+1} \right\}$$

$$\text{(Table 2.3)}$$

266

where
$$b = (1-\gamma\xi)^{\frac{1}{4}}$$

$$b_0 = (1-\gamma\xi_0)^{\frac{1}{4}}$$

and, as before $\xi = \frac{z}{L}$ and $\xi_0 = \frac{z_0}{L}$. It now remains to determine $\frac{\partial}{\partial L}\Psi_m(\xi)$ for use in equation (C.7). This derivation was done in Lo (1979) :

$$\frac{\partial}{\partial L}\Psi_m(\xi) = \frac{1}{L}\left[\frac{\gamma}{b(1+b)(1+b^2)} - 1\right] \tag{D.20}$$

L is obtained by iteration using equations (C.2), (C.5) and (C.7) with equation (D.20) and the secant method described below (Section D.3.3).

D.3.2. Temperature Profile

From Table 2.3. :

$$\Psi_h(\xi) = \gamma_1 \ln\left\{\frac{b_2+1}{b_2-1}\frac{b_1-1}{b_1+1}\right\}$$

with
$$b_1 = (1-\gamma_2\xi_1)^{\frac{1}{2}}$$

$$b_2 = (1-\gamma_2\xi_2)^{\frac{1}{2}}$$

The derivative, $\frac{\partial}{\partial L}\Psi_h(\xi)$, is now sought.

$$\frac{\partial}{\partial L}(\ln[b_2-1]) = \frac{1}{b_2-1}\frac{\partial}{\partial L}(b_2-1)$$

$$= \frac{1}{b_2-1}\frac{\partial}{\partial L}(1-\gamma_2\xi_2)^{-\frac{1}{2}}$$

$$= \frac{\gamma_2 z}{2(b_2-1)L^2 b_2} \tag{D.21}$$

Similarly,

$$\frac{\partial}{\partial L}(\ln[b_2+1]) \;=\; \frac{\gamma_2 z}{2(b_2+1)L^2 b_2} \tag{D.22}$$

and therefore

$$\frac{\partial}{\partial L}\left\{\ln\left[\frac{b_2-1}{b_2+1}\right]\right\} \;=\; \frac{\gamma_2 z}{2L^2 b_2}\left[\frac{1}{b_2-1} - \frac{1}{b_2+1}\right]$$
$$\;=\; -\,\frac{1}{b_2 L} \tag{D.23}$$

and similarly

$$\frac{\partial}{\partial L}\left\{\ln\left[\frac{b_1+1}{b_1-1}\right]\right\} \;=\; -\,\frac{1}{b_1 L} \tag{D.24}$$

Therefore

$$\frac{\partial}{\partial L}\,\Psi_h(\xi) \;=\; \frac{\gamma_2}{L}\left[\frac{1}{b_1} - \frac{1}{b_2}\right] \tag{D.25}$$

D.3.3 Secant Method Applied to the Least-Square Error Forms for Unstable Conditions

The procedure applied during unstable conditions is described :

STEP 1 : Determine u_* from equation (C.5), *i.e.*, average friction velocity from all measurements.

STEP 2 : Determine the function to be minimised, *i.e.*, ϵ_i from equation (C.2).

STEP 3 : Calculate from equation (C.7)

$$E\left(\frac{1}{L}\right) \;=\; \sum_{i=1}^{N}\epsilon_i\left\{\frac{u_i}{N}\sum_{j=1}^{N}\frac{(\partial/\partial L)\Psi_m(\xi_j)}{u_j} - \frac{\partial}{\partial L}[\Psi_m(\xi_i)]\right\} \tag{D.26}$$

using the relationship given by equation (D.20)

268

STEP 4 : Let the two trials for ξ be denoted by s_1 and s_2, *i.e.*,

$$s_1 = \frac{1}{L_1}$$
$$s_2 = \frac{1}{L_2}$$

Calculate $E(s_1)$ and $E(s_2)$ according to STEPs 1 to 3. The improved value for s (or $\frac{1}{L}$) will then be

$$s = s_2 - E(s_2)\frac{s_2 - s_1}{E(s_2) - E(s_1)} \tag{D.28}$$

STEP 5 : Let $s_2 = s$
$$s_1 = s_2$$
$$E(s_1) = E(s_2)$$
and calculate the new $E(s_2)$ according to STEPs 1 to 3.

STEP 6 : Check if $\quad \Delta = \left| \frac{s_2(\text{new}) - s_2(\text{old})}{s_2(\text{new})} \right| \quad$ satisfies the criterion

$$\Delta \leq 1 \times 10^{-8}$$

If not, repeat STEPs 5 and 6.

A similar treatment for the temperature profile is employed.

E.1. THE UNIVERSAL FUNCTION, Ψ_m, FOR CONVECTIVE CONDITIONS

The following form for ϕ_m is adopted from Carl *et al* (1973)

$$\phi_m = (1-\gamma\xi)^{-\frac{1}{3}} \qquad \text{for } \xi = \frac{z}{L} \qquad \text{(Table 2.3)}$$

The following has to be found

$$\Psi_m = \int_{\xi_0}^{\xi} \frac{\phi_m(\xi)}{\xi} \, d\xi$$

for use in the wind profile (equation (2.7)):

$$u = \frac{u_*}{k} \Psi_m(\xi)$$

So,

$$\Psi_m(\xi) = \int_{\xi_0}^{\xi} \frac{d\xi}{\xi(1-\gamma\xi)^{1/3}} \qquad (E.1)$$

Do the following substitution

$$x = (1-\gamma\xi)^{\frac{1}{3}} \qquad \text{and} \qquad x_0 = (1-\gamma\xi_0)^{\frac{1}{3}} \qquad (E.2)$$

then, after some manipulation, equation (E.1) is rewritten as

$$\Psi_m(x) = \int_{x_0}^{x} \frac{3x \, dx}{(x-1)(x^2+x+1)} \qquad (E.3)$$

The integral (E.3) is easily solved using the method of partial

fractions:

$$\Psi_m(x) \;=\; \int_{x_0}^{x} \frac{dx}{x-1} \;+\; \int_{x_0}^{x} \frac{dx}{x^2+x+1} \;-\; \int_{x_0}^{x} \frac{x\,dx}{x^2+x+1}$$

$$=\; \left[\ln(x-1) + \frac{4}{3}\tan^{-1}\frac{2x+1}{\sqrt{3}} - \left\{ \frac{1}{2}\ln(x^2+x+1) - \frac{2}{3}\tan^{-1}\frac{2x+1}{\sqrt{3}} \right\} \right]_x^x$$

$$(E.4)$$

The integrals are found from standard integral tables. Noting that

$$(x^2+x+1) \;=\; \frac{x^3-1}{x-1}$$

and after some simplification, we obtain

$$\Psi_m(\xi) \;=\; \frac{1}{2}\ln\left[\left\{ \frac{x-1}{x_0-1} \right\}^3 \frac{x_0^3-1}{x^3-1} \right] + 2\left[\tan^{-1}\frac{2x+1}{\sqrt{3}} - \tan^{-1}\frac{2x_0+1}{\sqrt{3}} \right] \quad (E.6)$$

271

EXPRESSIONS FOR THE AVERAGE WIND SPEEDS IN THE SURFACE LAYER

To obtain the average wind speed in the surface layer, the following integral is needed

$$\bar{u} = \frac{1}{z_2 - z_1} \int_{z_1}^{z_2} u(z) \ dz$$

$$= \frac{u_*}{k(z_2 - z_1)} \int_{z_1}^{z_2} \left[\int_{\xi_0}^{\xi} \frac{\phi_m(\xi)}{\xi} \ d\xi \right] \ dz$$

$$= \frac{u_*}{k(z_2 - z_1)} \int_{z_1}^{z_2} \Psi_m(\xi) \ dz \qquad (F.1)$$

where
$$\xi = \frac{z}{L}$$
$$\xi_0 = \frac{z_0}{L}$$

F.1. Neutral Layer

For neutral conditions:

$$\Psi_m(\xi) = \ln\frac{z}{z_0}$$

and $z_1 = z_0$, and $z_2 = h_s$ (surface layer height).

Therefore,

$$\bar{u} = \frac{u_*}{k(h_s - z_0)} \int_{z_0}^{h_s} \ln \frac{z}{z_0} \, dz$$

$$= \frac{u_*}{k(h_s - z_0)} \left[z(\ln z - 1 - \ln z_0) \right]_{z_0}^{h_s}$$

$$= \frac{u_*}{k(h_s - z_0)} \left[h_s(\ln \frac{h_s}{z_0} - 1) + z_0 \right] \qquad (F.2)$$

F.2. Moderately Stable Layer

The integral function Ψ_m for this layer is:

$$\Psi_m(\xi) = \ln \frac{z}{z_0} + \frac{\beta}{L}(z - z_0)$$

For the layer $z_1 = z_0$ to $z = L$, the average wind speed is given by

$$\bar{u} = \frac{u_*}{k(L - z_0)} \int_{z_0}^{L} \left[\ln \frac{z}{z_0} + \frac{\beta}{L}(z - z_0) \right] dz$$

$$= \frac{u_*}{k(L - z_0)} \left[L(\ln \frac{L}{z_0} - 1) + z_0 + \frac{\beta}{2L}(L - z_0)^2 \right] \quad (F.3)$$

F.3. Very Stable Layer

According to Webb (1970), the following integral function is appropriate in very stable conditions

$$\Psi_m(\xi) = (1 + \beta) \ln \frac{z}{z_0}$$

273

The average wind speed in this layer, $z_1 = L$ to $z_2 = h_s$, is given by

$$\bar{u} = \frac{u_*}{k(h_s - z_0)} \int_L^{h_s} (1+\beta) \ln\frac{z}{z_0} \, dz$$

$$= \frac{u_*(1+\beta)}{k(h_s - L)} \left[h_s(\ln \frac{h_s}{z_0} - 1) - L(\ln\frac{L}{z_0} - 1) \right] \qquad (F.4)$$

F.4. Moderately Unstable Conditions

The average wind speed for the layer between $z_1 = z_0$ and $z_2 = |L|$ is given by

$$\bar{u} = \frac{u_*}{k(|L| - z_0)} \int_{z_0}^{|L|} \left\{ 2(\tan^{-1}b - \tan^{-1}b_0) - \ln(\frac{b+1}{b-1} \cdot \frac{b_0-1}{b_0+1}) \right\} \, dz$$

$$(F.5)$$

where $b = (1 - \gamma\frac{z}{L})^{\frac{1}{4}}$ and $b_0 = (1 - \gamma\frac{z_0}{L})^{\frac{1}{4}}$. Let us first consider

$$I_A = \int_{z_0}^{|L|} \left\{ 2\tan^{-1}b - \ln(\frac{b+1}{b-1}) \right\} \, dz \qquad (F.6)$$

and using the substitute $x = (1 - \gamma\frac{z}{L})^{\frac{1}{4}}$, we get

$$I_A = -\frac{4L}{\gamma} \int_{z=z_0}^{z=|L|} x^3 \left\{ 2\tan^{-1}x + \ln(\frac{x+1}{x-1}) \right\} \, dx \qquad (F.7)$$

From tables, it is found that

$$\int x^3 \tan^{-1}x \, dx = \frac{1}{4} \left\{ x^4 \tan^{-1}x - \int \frac{x^4}{1 + x^2} \, dx \right\} \qquad (F.8)$$

and

$$\int x^3 \ln(\frac{x+1}{x-1})\ dx\ =\ \frac{1}{4}\left\{(x^4-1)\ln(\frac{x+1}{x-1}) + \frac{2x}{3}(x^2+3)\right\} \qquad \text{(F.9)}$$

So, after some simplification,

$$I_A\ =\ \frac{L}{\gamma}\left[\frac{4x^3}{3} - (x^4-1)\left\{2\tan^{-1}x + \ln(\frac{x+1}{x-1})\right\}\right]_{z=z_0}^{z=|L|}$$

$$\text{(F.10)}$$

Consider now

$$I_B\ =\ \int_{z_0}^{|L|}\left\{2\tan^{-1}b_0 + \ln(\frac{b_0+1}{b_0-1})\right\}\ dz$$

$$=\ \left[-2z\tan^{-1}b_0 + z\ln(\frac{b_0+1}{b_0-1})\right]_{z_0}^{|L|} \qquad \text{(F.11)}$$

Substituting I_A and I_B into equation (F.5), we get

$$\bar{u}\ =\ \frac{u_*}{k(|L|-z_0)}\left\{\frac{L}{\gamma}\left[\frac{4}{3}(b_{|L|}^3-b_0^3) + (1-b_{|L|}^4)[2\tan^{-1}b_0 + \ln(\frac{b_{|L|}+1}{b_{|L|}-1})]\right]\right.$$

$$\left.+ \left[2\tan^{-1}b_0 + \ln(\frac{b_0+1}{b_0-1})\right]\left[z_0-|L|-\frac{L}{\gamma}(1-b_0^4)\right]\right\} \qquad \text{(F.12)}$$

But,
$$b_{|L|}\ =\ (1-\gamma\frac{|L|}{L})^{\frac{1}{4}}\ =\ (1+\gamma)^{\frac{1}{4}}$$

since L < 0 and also

$$1-b_{|L|}\ =\ -\gamma \qquad \text{(F.13)}$$

$$1-b_0\ =\ \gamma\frac{z_0}{L} \qquad \text{(F.14)}$$

The average wind speed is then

$$\bar{u} = \frac{u_*}{k(|L|-z_0)}\left\{\frac{4L}{3\gamma}(b^3_{|L|}-b_0^3) + |L|\left[2(\tan^{-1}b_{|L|} - \tan^{-1}b_0)\right.\right.$$

$$\left.\left. - \ln(\frac{b_{|L|}+1}{b_{|L|}-1}\cdot\frac{b_0-1}{b_0+1})\right]\right\} \tag{F.15}$$

F.5. Convective Layer

The integral function for convective conditions using the Carl *et al.* (1973) universal function, was derived in Appendix E. The average velocity for the layer $|L|$ to h_s is then

$$\bar{u} = \frac{u_*}{k(h_s-|L|)}\left[I_A + I_B + I_C + I_D\right]_{|L|}^{h_s} \tag{F.16}$$

where

$$I_A = \frac{3}{2}\int\ln\frac{x-1}{x_0-1}\ dz \tag{F.17a}$$

$$I_B = \frac{1}{2}\int\ln\frac{x_0^3-1}{x^3-1}\ dz \tag{F.17b}$$

$$I_C = 2\int\tan^{-1}\frac{2x+1}{\sqrt{3}}\ dz \tag{F.17c}$$

$$I_D = 2\int\tan^{-1}\frac{2x_0+1}{\sqrt{3}}\ dz \tag{F.17d}$$

and

$$x = (1-\gamma\frac{z}{L})^{\frac{1}{3}}$$

$$x_0 = (1-\gamma\frac{z_0}{L})^{\frac{1}{3}}$$

Equation (F.17a) can be written as

$$I_A = \frac{3}{2}\int\ln(x-1)\ dz - \frac{3}{2}\int\ln(x_0-1)\ dz$$

$$= \frac{3}{2}\int\ln(x-1)\ dz - \frac{3}{2}\ z\ln(x_0-1)$$

Note that

$$dz = -\frac{3L}{\gamma} x^2 dx$$

Therefore

$$I_A = \frac{3}{2}\left\{-\frac{3L}{\gamma}\int x\ln(x-1)\ dx - z\ln(x_0-1)\right\}$$

But,

$$\int x\ln(x-1)\ dx = \frac{1}{3}(x^3-1)\ln(x-1) - \frac{1}{3}(x+\frac{x^2}{2}+\frac{x^3}{3})$$

and therefore

$$I_A = \frac{3}{2}\left\{-\frac{L}{\gamma}\left[[x^3-1]\ln(x-1) - (x+\frac{x^2}{2}+\frac{x^3}{3})\right]-z\ln(x_0-1)\right\}$$

$$(F.18)$$

Equation (F.17b) can be rewritten as

$$I_B = \frac{1}{2}\int\ln(x_0{}^3-1)\ dz - \int\ln(x^3-1)\ dz$$

$$= \frac{1}{2}\left\{z\ln(x_0{}^3-1) - \int\ln(x^3-1)\ dz\right\}$$

Noting that

$$x^3-1 = -\alpha_1\frac{z}{L}$$

we get from the above equation

$$I_B = \frac{1}{2}\left\{z\ln(x_0{}^3-1) - z\ln(-\gamma\frac{z}{L}) + z\right\}$$

$$= \frac{z}{2}\left\{\ln(\frac{z_0}{z}) + 1\right\}$$

Consider now equation (F.17c). Let

$$y = \frac{2x+1}{\sqrt{3}} \tag{F.20}$$

then

$$dx = \frac{\sqrt{3}}{2} dy \tag{F.21}$$

also, note that

$$dz = -\frac{3L}{\gamma}x^2 dx \tag{F.22}$$

Substitution of equations (F.20), (F.21) and (F.22) into equation (F17.c) leads to

$$I_C = -\frac{6\sqrt{3}L}{\gamma}\int(\frac{3}{4}y^2 - \sqrt{3}y + 1)\tan^{-1}y \, dy \tag{F.23}$$

Let us now consider the integral

$$\frac{3}{4}\int y^2 \tan^{-1}y \, dy$$

$$= \frac{3}{4}\tan^{-1}y - \frac{1}{4}\int \frac{y^3}{1+y^2} \, dy \tag{F.24}$$

Using integration by parts, it can be shown that

$$\int \frac{y^3}{1+y^2} \, dy = \frac{1}{2}[y^2 - \ln(1+y^2)] \tag{F.25}$$

The following is found from standard integral tables

$$\sqrt{3}\int y \tan^{-1}y \, dy = \frac{\sqrt{3}}{2}[(1+y^2)\tan^{-1}y - y] \tag{F.26}$$

and

$$\int \tan^{-1}y \, dy = y \tan^{-1}y - \frac{1}{2}\ln(1+y^2)$$

Hence

$$
\begin{aligned}
I_C = \frac{6\sqrt{3}\,L}{\gamma}\Big\{ & \frac{3}{4}\tan^{-1}y - \frac{1}{8}[y^2 - \ln(1+y^2)] \\
& - \frac{\sqrt{3}}{2}\,[(1+y^2)\tan^{-1}y - y] + y\,\tan^{-1}y \\
& - \frac{1}{2}\ln(1+y^2)\Big\}
\end{aligned}
\tag{F.27}
$$

And, finally

$$
I_D = 2z\,\tan^{-1}y_0
\tag{F.28}
$$

The integrals given by equations (F.18), (F.19), (F.27), and (F.28) are combined and simplified to give equation (4.8) in Section 4.1.2.1..

APPENDIX G

MODIFIED LIMITING VALUE METHOD

The *limiting value* numerical method used by Mulholland (1977) states that for the horizontal layer at height k, $C(k,t+\Delta t)$ can be obtained from

$$C(k,t+\Delta t) = C(k,t) + b(k,t) \ f(k,\Delta t) \tag{G.1}$$

where

$$b(k,t) = g(k)[C(k+1,t) - C(k-1,t)] + C(k-1,t) - C(k,t) \tag{G.2}$$

with

$$g(k,t) = \left[1 + \frac{K_v(k-1,t)}{K_v(k+1,t)}\right]^{-1} \tag{G.3}$$

and

$$f(k,t) = 1 - \exp\{-a(k,t)\Delta t\} \tag{G.4}$$

where

$$a(k,t) = \frac{K_v(k+1,t) + K_v(k-1,t)}{\Delta z^2} \tag{G.5}$$

The most accurate results are give when the following situation is met

$$\frac{K_v \Delta t}{\Delta z^2} = 0,4 \qquad \text{(from equation (3.79))}$$

A modification is proposed that will improve the speed of computation. By using equation (G.1), with half intervals $\frac{1}{2}\Delta t$ and $\frac{1}{2}\Delta z$, the above equation becomes

$$\frac{K_v \Delta t}{\Delta z^2} = 0,8$$

Let us now conveniently write $K(k)$ instead of $K_v(k,t)$, and consider the situation:

$$C(k,t+\tfrac{1}{2}\Delta t) = C(k,t) + b(k,t) \; f(k,\tfrac{1}{2}\Delta t) \qquad (G.6)$$

It then follows that

$$C(k,t+\Delta t) = C(k,t+\tfrac{1}{2}\Delta t) + b(k,t+\tfrac{1}{2}\Delta t) \; f(k,\tfrac{1}{2}\Delta t) \qquad (G.7)$$

Substituting equation (G.1) into (G.7), we get

$$C(k,t+\Delta t) = A(k,t) + b(k,t+\tfrac{1}{2}\Delta t) \; f(k,\tfrac{1}{2}\Delta t) \qquad (G.8)$$

where $\qquad A(k,t) = C(k,t) + b(k,t) \; f(k,\tfrac{1}{2}\Delta t)$

Also,

$$\begin{aligned}
b(k,t+\tfrac{1}{2}\Delta t) = \; & g(k)[C(k+1,t+\tfrac{1}{2}\Delta t) - C(k-1,t+\tfrac{1}{2}\Delta t)] \\
& + C(k-1,t+\tfrac{1}{2}\Delta t) - C(k,t+\tfrac{1}{2}\Delta t)
\end{aligned}$$
$$(G.9)$$

Substituting the appropriate values for C obtained from equation (G.6) into (G.9), the following is obtained

$$\begin{aligned}
b(k,t+\tfrac{1}{2}\Delta t) = \; & g(k)[C(k+1,t) + b(k+1,t) \; f(k+1)] \\
& + [1-g(k)][C(k-1,t) + b(k-1,t) \; f(k-1)] \\
& - [C(k,t) + b(k,t) \; f(k)]
\end{aligned}$$
$$(G.10)$$

where $\tfrac{1}{2}\Delta t$ is conveniently dropped from $f(k)$. Note that

$$b(k+1,t) = g(k+1)[C(k+2,t) - C(k,t)] + C(k,t) - C(k+1,t)$$
$$(G.11)$$

and

$$b(k-1,t) = g(k-1)[C(k,t) - C(k-2,t)] + C(k-2,t) - C(k-1,t)$$
$$(G.12)$$

281

We now introduce imaginary half-space intervals and rewrite all the concentrations as

$$C(k+1,t) = C(k+\tfrac{1}{2},t)$$

and   (G.13)

$$C(k+2,t) = C(k+1,t)$$

We then assume that the concentrations at these intervals are the average of the two neighbouring layers, i.e.,

$$C(k+\tfrac{1}{2},t) = \frac{C(k+1,t)-C(k,t)}{2}$$ (G.14)

and

$$C(k-\tfrac{1}{2},t) = \frac{C(k,t)-C(k-1,t)}{2}$$ (G.15)

Introducing the above ideas into equations (G.8), (G.10), (G.11), and (G.12), the following is obtained

$$
\begin{aligned}
C(k,t+\Delta t) = \ & [1-f(k)]\ A(k,t) \\
& + \frac{1}{2}\Big[g(k)[C(k+1,t)+C(k,t)+B_1\{C(k+1,t)-C(k,t))] \ + \\
& \quad [1-g(k)][C(k,t)+C(k-1,t)+B_2\{C(k,t)-C(k-1,t))]\Big] f(k)
\end{aligned}
$$

(G.16)

where

$$B_1 = [2g(k+\tfrac{1}{2}) - 1]\ f(k+\tfrac{1}{2})$$ (G.17)

$$B_2 = [2g(k-\tfrac{1}{2}) - 1]\ f(k-\tfrac{1}{2})$$ (G.18)

As a result of the introduction of the half spatial intervals, $a(k,t)$ and $g(k,t)$ need to be re-defined:

$$a(k,t) = \frac{K(k+\tfrac{1}{2}) + K(k-\tfrac{1}{2})}{(\frac{\Delta z}{2})^2}$$ (G.19)

and

$$g(k,t) = \left[1 + \frac{K(k-\frac{1}{2})}{K(k+\frac{1}{2})}\right]^{-1} \tag{G.20}$$

Assuming the following approximations

$$K(k+\frac{1}{2}) = \frac{K(k+1) + K(k)}{2} \tag{G.21}$$

and

$$K(k-\frac{1}{2}) = \frac{K(k) + K(k-1)}{2} \quad , \tag{G.22}$$

equations (G.19) and (G.20) can be rewritten as

$$a(k,t) = 2\left[\frac{K(k+1) + 2K(k) + K(k-1)}{\Delta z^2}\right] \tag{G.23}$$

and

$$g(k,t) = \frac{K(k+1) + K(k)}{K(k+1) + 2K(k) + K(k-1)} \tag{G.24}$$

Similarly,

$$a(k+\frac{1}{2},t) = 4\left[\frac{K(k+1) + K(k)}{\Delta z^2}\right] \tag{G.25}$$

$$a(k-\frac{1}{2},t) = 4\left[\frac{K(k) + K(k-1)}{\Delta z^2}\right] \tag{G.26}$$

and finally,

$$g(k+\frac{1}{2},t) = \frac{K(k+1)}{K(k+1) + K(k)} \tag{G.27}$$

$$g(k-\frac{1}{2},t) = \frac{K(k)}{K(k) + K(k-1)} \tag{G.28}$$

And note that

$$f(k) = 1 - \exp\{-\frac{a(k,t)\Delta t}{2}\} \tag{G.29}$$

MOMENTS OF A GAUSSIAN PUFF

The concentration distribution in a Gaussian puff is described by the equation

$$C(x,y,z,t) = \frac{M}{8(\pi t)^{3/2} K_H K_V^{1/2}} \exp\left\{-\frac{1}{4t}\left[\frac{(x-ut)^2}{K_H} + \frac{(y-vt)^2}{K_H}\right]\right\}$$

$$x \left\{\exp\left[-\frac{1}{4t}\frac{(z-H)^2}{K_V}\right] + \exp\left[-\frac{1}{4t}\frac{(z+H)^2}{K_V}\right]\right\} \qquad (H.1)$$

where H is the stack height. The zero'th moment, C_{00}, is given by

$$C_{00}(z,t) = \iint_{-\infty}^{+\infty} C(x,y,z,t)\, dxdy \qquad (H.2)$$

Applying equation (H.2) to (H.1), the following is obtained

$$C_{00}(z,t) = A\iint_{-\infty}^{+\infty} \exp\left\{-\frac{1}{4t}\left[\frac{(x-ut)^2}{K_H} + \frac{(y-vt)^2}{K_H}\right]\right\} dxdy$$

$$= A\int_{-\infty}^{+\infty} \exp\left[\frac{(x-ut)^2}{4tK_H}\right]\left\{\int_{-\infty}^{+\infty} \exp\left[\frac{(y-vt)^2}{4tK_H}\right] dy\right\} dx \qquad (H.3)$$

where
$$A = \frac{M}{8(\pi t)^{3/2} K_H K_V^{1/2}} \left\{\exp\left[-\frac{(z-H)^2}{4tK_V}\right] + \exp\left[-\frac{(z+H)^2}{4tK_V}\right]\right\}$$

It is well-known that the *error-function* of "∞" is given by

$$\int_{-\infty}^{+\infty} \exp(-\lambda \xi^2)\, d\xi = \sqrt{\frac{\pi}{\lambda}} \qquad (H.4)$$

Therefore,

$$
C_{00}(z,t) = A \int_{-\infty}^{+\infty} (4\pi K_H t)^{\frac{1}{2}} \exp\left[- \frac{(x-ut)^2}{4tK_H}\right] dx
$$

$$
= A \, (4\pi K_H t)^{\frac{1}{2}} \, (4\pi K_H t)^{\frac{1}{2}}
$$

$$
= 4A\pi K_H t \tag{H.5}
$$

And hence

$$
C_{00}(z,t) = \frac{M}{2(\pi t K_V)^{1/2}} \left\{ \exp\left[- \frac{(z-H)^2}{4tK_V}\right] + \exp\left[- \frac{(z+H)^2}{4tK_V}\right] \right\}
$$

$$
\tag{H.6}
$$

The first moment is obtained in a similar fashion.

$$
C_{10}(z,t) = A \iint_{-\infty}^{+\infty} x \, \exp\left[- \frac{(x-ut)^2}{4tK_H} \, \exp \frac{(y-vt)^2}{4tK_H}\right] dx dy \tag{H.7}
$$

Introduce the following transformation

$$
X = x - ut \tag{H.8a}
$$

$$
Y = y - vt \tag{H.8b}
$$

then

$$
C_{10} = A \int_{-\infty}^{+\infty} (X+ut) \exp\left[- \frac{x^2}{4tK_H}\right] \left\{ \int_{-\infty}^{+\infty} \exp\left[- \frac{x^2}{4tK_H}\right] dy \right\} dx
$$

$$
= A(4\pi K_H t)^{\frac{1}{2}} \int_{-\infty}^{+\infty} (X+ut) \exp\left[- \frac{x^2}{4tK_H}\right] dx
$$

$$
= A(4\pi K_H t)^{\frac{1}{2}} \left[-4tK_H \, \exp\left[- \frac{x^2}{4tK_H}\right]_{-\infty}^{+\infty} + ut(4\pi K_H t)^{\frac{1}{2}} \right.
$$

$$
= A(4\pi K_H t)ut \tag{H.9}
$$

and therefore

$$
C_{10} = C_{00}ut \tag{H.10}
$$

By similar treatment, the following are obtained

$$C_{01} = C_{00}vt \tag{H.11}$$

$$C_{20} = C_{00}(2+K_H+(ut)^2) \tag{H.12}$$

$$C_{02} = C_{00}(2+K_H+(vt)^2) \tag{H.13}$$

$$C_{11} = C_{00}uvt^2 \tag{H.14}$$

DATA FILE FORMATS

A list of the record formats for the input data files is given below.
Notice that all files must be terminated by supplying "-1." for TIME.
The following dimensional units apply to the input:

TIME	–	hours, *e.g.* 11.9828
DAY	–	normal day of the month
MONTH	–	1-12
YEAR	–	*e.g.*, 1986
wind speed (components)	–	$m\ s^{-1}$
wind bearing	–	degrees
cloud cover	–	fraction
azimuth fluctuation	–	degrees
all temperatures	–	Kelvin
all heights	–	metres

The wind velocity may be supplied either as u,v components, or wind
speed and bearing. This has to be specified in INSTALL.

Surface layer measurement

Option 1:
TIME, DAY, MONTH, YEAR, U (or wind speed), V (or bearing), cloud
cover

Option 2:
TIME, DAY, MONTH, YEAR, U (or wind speed), V (or bearing), azimuth
fluctuation

Option 3:
TIME, DAY, MONTH, YEAR, U (or wind speed), V (or bearing), cloud
cover, average temperature.

Option 4:

TIME, DAY, MONTH, YEAR, U (or wind speed), V (or bearing), TEMP1,
TEMP2

Option 5:

TIME, DAY, MONTH, YEAR, U_1 (or wind speed), V_1 (or bearing), U_2 (or
wind speed), V_2 (or bearing), TEMP1, TEMP2

Option 6:

Line 1 : TIME, DAY, MONTH, YEAR

Line 2 : U (wind speed), V (or bearing)

   (a new line for each height)

A height must also be supplied when it is not constant. This must be
indicated when running INSTALL. In such cases,

Line 2 : HEIGHT, U (wind speed), V (or bearing)

   (a new line for each height)

Option 7:

Line 1 : TIME, DAY, MONTH, YEAR

Line 2 : TEMP

   (a new line for each height)

or

Line 2 : HEIGHT, TEMP

   (a new line for each height)

Option 8:

Line 1 : TIME, DAY, MONTH, YEAR

Line 2 : U (wind speed), V (or bearing)

⎡or

⎢**Line 2 :** HEIGHT, U (wind speed), V (or bearing)⎤

Line 3 : TEMP

⎡or

⎢**Line 3 :** HEIGHT, TEMP⎤

   (a set of two new lines for each height)

Outer layer measurements

Option 2:

TIME, DAY, MONTH, YEAR, U (or wind speed), V (or bearing)

Option 3:

Line 1 : TIME, DAY, MONTH, YEAR

Line 2 : U (wind speed), V (or bearing)

or

Line 2 : HEIGHT, U (wind speed), V (or bearing)

Boundary layer height

Option 2:

Line 1 : TIME, DAY, MONTH, YEAR

Line 2 : HEIGHT, TEMP

    (a new line for each height)

Option 3:

Line 1 : TIME, DAY, MONTH, YEAR

Line 2 : HEIGHT, TEMP

    (a new line for each height)

Option 4:

Line 1 : TIME, DAY, MONTH, YEAR

Line 2 : Intensity of the vertical signal

    (a new line for each height)

or

Line 2 : HEIGHT, Intensity of the vertical signal

    (a new line for each height)

Option 5:

TIME, DAY, MONTH, YEAR, Boundary layer height

Temperature

TIME, DAY, MONTH, YEAR, TEMP

Rainfall

TIME, DAY, MONTH, YEAR, Rainfall rate (m/s)

Source inventory

TIME, DAY, MONTH, YEAR, A, TSTACK, TAMBENT, B

where A, B are given in the following table:

Option	A	B
1	Density (g/m^3)	Exit gas velocity (m/s)
2	Density (g/m^3)	Mass flowrate (g/s)
3	Density (g/m^3)	Volumetric flowrate (m^3/s)
4	Exit gas velocity (m/s)	Mass flowrate (g/s)
5	Volumetric flowrate (m^3/s)	Mass flowrate (g/s)

Examples of the surface layer, outer layer and boundary layer height input   files   are   given   in   Appendix   K.

A Short Description of the Computer Program

The package has been programed in FORTRAN 77 and consists of the two driver programs, INSTALL and WIZARD, and several subroutines (Burger 1986). INSTALL generates all the files containing the fixed parameters used by WIZARD. Some important aspects of the program are discussed below.

J.1. INPUT, OUTPUT, AND TEMPORARY FILES

The following file names are used for the fixed parameters created by INSTALL:

FIXD Contains model parameters, source configuration, isopleth information and pollutant characteristics (logical unit 7)

TOPO Contains the altitude for each wind field grid point (logical unit 8)

RGH Contains zero-plane displacement heights and roughness lengths for each wind field grid point (logical unit 9)

MET Contains chosen meteorological measurement options, positions of weather stations and other measurement configuration information (logical unit 10)

CONF Graphics terminal settings (logical unit 11)

MAPS Contains the symbol names and positions used on the map. This file is only used by INSTALL. The lines and

text generated when designing the features to appear on the map are stored in a separate file (see below) (logical unit 12)

MAPD   Contains the text, and the coordinates and pen position for drawing lines on the map (logical unit 13)

The input data files required by WIZARD are given below. These must be created by the user. The data file formats are given in Appendix I.

Input data files

METD   Meteorological measurement for the first surface layer weather station (logical unit 20)

METD + m   The rest of the meteorological measurements, where m+1 is the number of meteorological measurement data files. The files are in the following order:

         (1) surface layer measurements

         (2) outer layer measurements

         (3) boundary layer height measurements

         (4) spatial temperature measurements

         (5) rainfall rate measurements

     (logical unit 20+m)

ISTK   Source rate, temperature and other data for the first source (logical unit 40)

ISTK + n   The rest of the sources, where n+1 is the number of sources (logical unit 40+n)

Temporary files

ITMP   Storage of meteorological and source data arrays (logical unit 14)

ISLG   Storage of surface layer wind profile parameters (logical unit 15)

IOLG   Storage of outer layer wind profile parameters
          (logical unit 16)

ISPARM   Storage of moments for the first source
          (logical unit 60)

ISPARM+n Storage of moments for the rest of the sources
          (logical unit 60+n)

Output files

IPLTF   Plotter file. Contains the coordinates of isopleths
          and map features (logical unit 90)

MON   Concentrations   at   monitoring   positions
          (logical unit 19)

J.2. IMPORTANT PARAMETER SETTINGS

PREMET module   :   NP1 - maximum number of surface layer
                                    measurments per option
                       NP2 - maximum number of outer layer
                               measurements per option
                       NP3 - maximum number of boundary layer
                               height measurements per option
                       NP4 - maximum number of diffusivity
                               estimates (=1, at present)
                       NP5 - maximum number of spatial
                               temperature measurement points
                       NP6 - maximum number of rainfall meters

Wind field grid size :   LM - number of horizontal grid points
                          LN - number of vertical grid points

Dispersion module   :   LS - maximum number of sources
                          LP - maximum number of solved puffs

LL - number of horizontal layers in the
numerical solution of the
advection-diffusion equation

J.3. MAIN PROGRAM, WIZARD, AND SOME OF THE SUBROUTINES

The main program prompts the user to supply the following
information:

```
*****************************************
WELCOME TO WIZARD!


PLEASE SUPPLY THE FOLLOWING INFORMATION

CHOOSE ONE OF THE FOLLOWING
     1)  INTERACTIVE GRAPHICS MODE
     2)  POINT CONCENTRATIONS ONLY
     3)  BATCH MODE GRAPHICS

SUPPLY THE INTERVAL FOR DRAWING GRAPHICS
     1)  SAME AS SIMULATION TIME INTERVAL
     2)  SPECIFIC TIME INTERVAL

STARTING TIME OF SIMULATION
     A)  STARTING TIME OF EARLIEST RECORD
     B)  SPECIFIC TIME

TERMINATION OF SIMULATION
     A)  END TIME OF LAST RECORD
     B)  SPECIFIED TIME

SIMULATION INTERVAL (SECONDS)

*****************************************
```

The "simulation time interval" is the same as the time interval between updating the wind field parameters. Once the above information is supplied, simulation starts and the modules, PREMET, METPAC, DSPRSN, and ISPLTH are called by WIZARD. A few of the important subroutines associated with each of these modules are listed below.

PREMET: Treatment of raw input data

FXDATA	reads fixed parameters created by INSTALL
READS	reads surface layer measurements
READO	reads outer layer measurements
READB	reads boundary layer height measurements
READD	(not used at present) reads diffusivity estimates
READT	reads spatial temperature measurements
READST	reads emission inventory
WARN	supplies a warning in case of errors in the input data files
SYSTIM	in <u>on-line mode</u>, the system time is read; in <u>off-line mode</u>, the time is computed from the input data records

METPAC: Construction of a three-dimensional wind field

READTP	reads topography data
PBLHT	calculates the boundary layer height at each wind field grid point
SURFS	calls the subroutines constructing the surface layer wind field
INTER	interpolate from sparse points to horizontal grid points
TOPO	includes topography into the forcing function
TEMPAN	includes temperature anomalies into the forcing function
SWIND	constructs the surface layer wind field
SPRFIL	calculates the parameters describing the wind profile in the surface layer
LAYERS	calls the subroutines which construct the outer wind field

LAYINT	interpolates wind data from sparse data points to the outer layer grid points	
SMOOTH	initial smoothing of the outer layer wind components	
GOODIN	construction of the three-dimensional wind field	
OPRFIL	calculates the parameters describing the outer layer wind profiles	

DSPRSN: Dispersion module

READW	reads the wind profile parameters that were calculated in METPAC
SPEDDY	calculates the wind velocity and diffusivity at any height
SEED	"seeds" the system with initial moments determined from a Gaussian puff model
CENTRE	determines the centroids of the solved puffs
TSTEP	updates the solution of the advection-diffusion equation
MERGE	merges puffs when they are close enough
PURGE	purges puffs when they are outside the area of interest
INTPFF	interpolates between solved puffs before drawing isopleths

ISPLTH: Concentration distribution output

FUNCTION CG	calculates the concentration at a point
ROTATE	determines whether a puff has been encircled by an isopleth
GRAFON	initialises graphics terminal
GRAFOF	terminates graphics terminal
PLOT	draws a line or moves to a point
SYMBOL	writes text on the graphics screen

Meteorological Data for the Eastern Transvaal Highveld Study

Examples of the file format for the data files, as discussed in Appendix I and J, is presented. These files are for the Eastern Transvaal Highveld demonstration run reported in Section 5.2.2.

Surface layer measurement

Only one option is used (option 1)

Option 1: Format — TIME, DAY, MONTH, YEAR, wind speed, wind bearing, cloud cover

Station No. 1. Wildebeest. File METD (logical unit 20)

9. 15. 8. 1984. 7.5 41. 0.
10. 15. 8. 1984. 4.8 .7 0.
11. 15. 8. 1984. 0.0 195. 0.
12. 15. 8. 1984. 3.9 263. 0.
13. 15. 8. 1984. 1.2 264. 0.
14. 15. 8. 1984. 3.4 260. 0.
15. 15. 8. 1984. 2.8 221. 0.
16. 15. 8. 1984. 2.5 257. 0.
17. 15. 8. 1984. 7.3 194. 0.
18. 15. 8. 1984. 5.8 220. 0.
19. 15. 8. 1984. 3.2 225. 0.
20. 15. 8. 1984. 3.1 241. 0.
21. 15. 8. 1984. 3.8 251. 0.
22. 15. 8. 1984. 3.9 259. 0.
23. 15. 8. 1984. 4.0 245. 0.
0. 16. 8. 1984. 3.7 233. 0.
1. 16. 8. 1984. 2.6 221. 0.
2. 16. 8. 1984. 0.8 271. 0.
3. 16. 8. 1984. 2.0 16. 0.
4. 16. 8. 1984. 0.1 283. 0.
5. 16. 8. 1984. 3.8 268. 0.
6. 16. 8. 1984. 4.0 273. 0.
7. 16. 8. 1984. 3.3 246. 0.
8. 16. 8. 1984. 3.1 242. 0.
9. 16. 8. 1984. 4.2 221. 0.
-1. 1. 1. 1. 1. 1. 1. 1.

Station No. 2. Bethal. File METD+1 (logical unit 21)

9. 15. 8. 1984. 4.9 41. 0.
10. 15. 8. 1984. 3.8 358. 0.
11. 15. 8. 1984. 1.5 286. 0.
12. 15. 8. 1984. 0.8 246. 0.
13. 15. 8. 1984. 3.3 267. 0.
14. 15. 8. 1984. 0.5 184. 0.
15. 15. 8. 1984. 1.3 186. 0.
16. 15. 8. 1984. 3.7 179. 0.
17. 15. 8. 1984. 4.4 184. 0.
18. 15. 8. 1984. 3.2 201. 0.
19. 15. 8. 1984. 1.9 208. 0.
20. 15. 8. 1984. 2.0 213. 0.
21. 15. 8. 1984. 2.2 216. 0.
22. 15. 8. 1984. 1.7 218. 0.
23. 15. 8. 1984. 2.2 218. 0.
0. 16. 8. 1984. 1.7 183. 0.
1. 16. 8. 1984. 0.3 127. 0.
2. 16. 8. 1984. 0.0 102. 0.
3. 16. 8. 1984. 0.0 22. 0.
4. 16. 8. 1984. 0.0 334. 0.
5. 16. 8. 1984. 0.0 312. 0.
6. 16. 8. 1984. 0.0 306. 0.
7. 16. 8. 1984. 0.0 222. 0.
8. 16. 8. 1984. 1.7 215. 0.
9. 16. 8. 1984. 2.5 206. 0.
-1. 1. 1. 1. 1. 1. 1. 1.

Station No. 3.   Hendrina.   File METD+2 (logical unit 22)

```
9. 15. 8. 1984. 2.8 96. 0.
10. 15. 8. 1984. .4 346. 0.
11. 15. 8. 1984. .2 95. 0.
12. 15. 8. 1984. .2 152. 0.
13. 15. 8. 1984. .2 221. 0.
14. 15. 8. 1984. .3 282. 0.
15. 15. 8. 1984. 1.7 278. 0.
16. 15. 8. 1984. 3.4 270. 0.
17. 15. 8. 1984. 3.7 261. 0.
18. 15. 8. 1984. 1.5 242. 0.
19. 15. 8. 1984. 2.6 232. 0.
20. 15. 8. 1984. 2.4 234. 0.
21. 15. 8. 1984. 2.2 260. 0.
22. 15. 8. 1984. 0.6 17. 0.
23. 15. 8. 1984. 0.3 41. 0.
0. 16. 8. 1984. 0.1 319. 0.
1. 16. 8. 1984. 0.0 11. 0.
2. 16. 8. 1984. 0.0 345. 0.
3. 16. 8. 1984. 0.0 292. 0.
4. 16. 8. 1984. 0.0 286. 0.
5. 16. 8. 1984. 0.3 269. 0.
6. 16. 8. 1984. 0.3 268. 0.
7. 16. 8. 1984. 0.0 316. 0.
8. 16. 8. 1984. 0.0 170. 0.
9. 16. 8. 1984. 0.9 263. 0.
-1. 1. 1. 1. 1. 1. 1. 1.
```

Station No. 4.   Grootpan.   File METD+3 (logical unit 23)

```
9. 15. 8. 1984. 2.4 88. 0.
10. 15. 8. 1984. .3 40. 0.
11. 15. 8. 1984. .4 301. 0.
12. 15. 8. 1984. 2.1 274. 0.
13. 15. 8. 1984. 1.4 237. 0.
14. 15. 8. 1984. 0.7 169. 0.
15. 15. 8. 1984. 1.2 203. 0.
16. 15. 8. 1984. 0.0 356. 0.
17. 15. 8. 1984. 4.3 220. 0.
18. 15. 8. 1984. 2.1 233. 0.
19. 15. 8. 1984. 2.6 177. 0.
20. 15. 8. 1984. 2.0 189. 0.
21. 15. 8. 1984. 5.6 80. 0.
22. 15 8. 1984. 2.3 244. 0.
23. 15. 8. 1984. 4.6 277. 0.
0. 16. 8. 1984. 4.7 274. 0.
1. 16. 8. 1984. 3.9 270. 0.
2. 16. 8. 1984. 0.6 188. 0.
3. 16. 8. 1984. 0.2 47. 0.
4. 16. 8. 1984. 0.9 196. 0.
5. 16. 8. 1984. 0.9 147. 0.
6. 16. 8. 1984. 0.9 154. 0.
7. 16. 8. 1984. 1.6 151. 0.
8. 16. 8. 1984. 1.3 144. 0.
9. 16. 8. 1984. 1.7 160. 0.
-1. 1. 1. 1. 1. 1. 1. 1.
```

Station No. 5. Kriel. File METD+4 (logical unit 24)

```
9. 15. 8. 1984. 1.7 352. 0.
10. 15. 8. 1984. 3.5 355. 0.
11. 15. 8. 1984. 0.4 285. 0.
12. 15. 8. 1984. 2.6 270. 0.
13. 15. 8. 1984. 4.0 267. 0.
14. 15. 8. 1984. 3.9 267. 0.
15. 15. 8. 1984. 4.2 183. 0.
16. 15. 8. 1984. 4.3 195. 0.
17. 15. 8. 1984. 4.8 208. 0.
18. 15. 8. 1984. 4.5 198. 0.
19. 15. 8. 1984. 4.8 181. 0.
20. 15. 8. 1984. 3.5 186. 0.
21. 15. 8. 1984. 2.5 198. 0.
22. 15. 8. 1984. 2.4 205. 0.
23. 15. 8. 1984. 4.1 187. 0.
0. 16. 8. 1984. 2.7 198. 0.
1. 16. 8. 1984. 2.0 29. 0.
2. 16. 8. 1984. 0.8 25. 0.
3. 16. 8. 1984. 0.9 79. 0.
4. 16. 8. 1984. 1.2 216. 0.
5. 16. 8. 1984. 1.8 189. 0.
6. 16. 8. 1984. 0.7 153. 0.
7. 16. 8. 1984. 0.8 81. 0.
8. 16. 8. 1984. 1.4 136. 0.
9. 16. 8. 1984. 0.9 194. 0.
-1. 1. 1. 1. 1. 1. 1. 1.
```

Station No. 6. Komati. File METD+5 (logical unit 25)

```
9. 15. 8. 1984. 6.1 47. 0.
10. 15. 8. 1984. 3.9 4.9 0.
11. 15. 8. 1984. 0.6 250. 0.
12. 15. 8. 1984. 2.7 271. 0.
13. 15. 8. 1984. 5.5 268. 0.
14. 15. 8. 1984. 1.7 244. 0.
15. 15. 8. 1984. 1.0 225. 0.
16. 15. 8. 1984. 0.6 277. 0.
17. 15. 8. 1984. 2.3 200. 0.
18. 15. 8. 1984. 2.1 195. 0.
19. 15. 8. 1984. 2.5 298. 0.
20. 15. 8. 1984. 0.2 141. 0.
21. 15. 8. 1984. 0.1 298. 0.
22. 15. 8. 1984. 0.2 334. 0.
23. 15. 8. 1984. 0.4 81. 0.
0. 16. 8. 1984. 0.7 88. 0.
1. 16. 8. 1984. 0.1 95. 0.
2. 16. 8. 1984. 0.8 93. 0.
3. 16. 8. 1984. 0.7 124. 0.
4. 16. 8. 1984. 0.4 114. 0.
5. 16. 8. 1984. 0.4 69.0 0.
6. 16. 8. 1984. 0.7 87.0 0.
7. 16. 8. 1984. 0.1 137. 0.
8. 16. 8. 1984. 0.1 61.0 0.
9. 16. 8. 1984. 0.7 206. 0.
-1. 1. 1. 1. 1. 1. 1. 1.
```

Station No. 7.   Elandsfontein.   File METD+6 (logical unit 26)

```
9. 15. 8. 1984. 7.2 91. 0.
10. 15. 8. 1984. 3.5 358. 0.
11. 15. 8. 1984. 3.5 357. 0.
12. 15. 8. 1984. 1.2 279. 0.
13. 15. 8. 1984. 0.2 250. 0.
14. 15. 8. 1984. 1.6 274. 0.
15. 15. 8. 1984. 3.9 269. 0.
16. 15. 8. 1984. 1.8 263. 0.
17. 15. 8. 1984. 7.7 232. 0.
18. 15. 8. 1984. 7.3 221. 0.
19. 15. 8. 1984. 7.9 225. 0.
20. 15. 8. 1984. 5.8 235. 0.
21. 15. 8. 1984. 4.4 259. 0.
22. 15. 8. 1984. 4.6 261. 0.
23. 15. 8. 1984. 6.0 251. 0.
0. 16. 8. 1984. 5.9 248. 0.
1. 16. 8. 1984. 0.5 281. 0.
2. 16. 8. 1984. 1.6 144. 0.
3. 16. 8. 1984. 2.0 337. 0.
4. 16. 8. 1984. 3.1 352. 0.
5. 16. 8. 1984. 3.4 271. 0.
6. 16. 8. 1984. 1.8 270. 0.
7. 16. 8. 1984. 3.6 269. 0.
8. 16. 8. 1984. 3.6 243. 0.
9. 16. 8. 1984. 4.7 240. 0.
-1. 1. 1. 1. 1. 1. 1. 1.
```

Station No. 8.   Arnot.   File METD+7 (logical unit 27)

```
9. 15. 8. 1984. 5.1 60. 0.
10. 15. 8. 1984. .4 127. 0.
11. 15. 8. 1984. 1.2 339. 0.
12. 15. 8. 1984. 2.0 267. 0.
13. 15. 8. 1984. 0.4 235. 0.
14. 15. 8. 1984. 0.4 277. 0.
15. 15. 8. 1984. 2.2 261. 0.
16. 15. 8. 1984. 3.3 186. 0.
17. 15. 8. 1984. 3.7 196. 0.
18. 15. 8. 1984. 3.0 215. 0.
19. 15. 8. 1984. 1.6 207. 0.
20. 15. 8. 1984. 1.3 294. 0.
21. 15. 8. 1984. 3.2 331. 0.
22. 15. 8. 1984. 4.2 345. 0.
23. 15. 8. 1984. 4.4 341. 0.
0. 16. 8. 1984. 3.8 336. 0.
1. 16. 8. 1984. 2.2 287. 0.
2. 16. 8. 1984. 4.4 309. 0.
3. 16. 8. 1984. 3.2 306. 0.
4. 16. 8. 1984. 3.0 316. 0.
5. 16. 8. 1984. 2.9 304. 0.
6. 16. 8. 1984. 3.0 307. 0.
7. 16. 8. 1984. 2.7 330. 0.
8. 16. 8. 1984. 1.6 321. 0.
9. 16. 8. 1984. 1.1 193. 0.
-1. 1. 1. 1. 1. 1. 1. 1.
```

Outer layer measurement
Only one option is used (option 3)

Option 3: Format - line 1 :TIME, DAY, MONTH, YEAR
                   line 2 :wind speed ,wind bearing

Fixed heights: starting at 90m and ends at 750m, at 30m intervals

Station No. 1. Elandsfontein. File METD+8 (logical unit 28)

9. 15. 8. 1984.
6.2 69.
6.6 65.
6.7 60.
7.2 52.
6.9 49.
6.4 46.
6.3 42.
5.7 35.
4.9 28.
4.1 21.
3.4 7.
2.6 352.
2.5 334.
2.4 318.
2.4 309.
2.3 305.
2.3 298.
2.3 289.
2.4 279.
2.7 272.
3.0 273.
3.6 263.
3.4 277.
10. 15. 8. 1984.
4.4 32.
4.4 32.
4.6 34.
4.6 35.
4.8 35.
4.8 33.
4.5 29.
4.1 25.
3.5 20.
2.6 12.
2.0 356.
1.8 325.
2.1 303.
2.3 295.
2.7 291.
2.8 288.
3.2 279.
3.5 277.
3.9 266.
4.0 258.
2.9 305.
2.9 305.
3.8 345.

```
11. 15. 8. 1984.
3.9 341.
3.9 341.
3.8 340.
3.7 340.
3.6 342.
3.6 342.
3.7 341.
3.7 340.
3.6 340.
3.5 336.
3.3 330.
2.9 325.
2.8 316.
2.6 304.
2.7 295.
2.9 290.
3.0 283.
3.3 279.
3.7 273.
3.8 272.
4.4 266.
4.9 261.
6.3 252.
12. 15. 8. 1984.
3.7 290.
3.8 293.
3.7 289.
3.6 289.
3.6 287.
3.4 284.
3.4 280.
3.3 280.
3.1 279.
3.1 277.
3.1 274.
3.1 275.
3.2 268.
3.2 266.
3.3 261.
3.5 259.
3.7 259.
4.1 255.
4.5 246.
4.8 242.
5.1 240.
5.4 235.
5.5 230.
```

13. 15. 8. 1984.
5.7 264.
5.8 266.
6.0 265.
6.1 265.
6.2 264.
6.0 264.
5.9 263.
5.9 262.
5.9 264.
5.7 267.
5.5 264.
5.5 266.
5.6 264.
5.5 263.
5.7 264.
5.7 263.
5.9 261.
5.9 256.
5.6 254.
5.5 254.
5.3 253.
5.4 251.
5.0 242.
14. 15. 8. 1984.
4.4 247.
4.5 251.
4.8 253.
4.6 254.
4.5 252.
4.6 253.
4.8 253.
4.8 252.
4.9 251.
5.0 252.
4.9 252.
4.8 250.
4.9 251.
4.7 249.
4.5 250.
4.6 247.
4.7 246.
4.5 246.
4.8 245.
4.4 247.
4.3 238.
4.5 243.
4.0 245.

```
15.  15.  8.  1984.
4.8 246.
5.2 246.
5.4 248.
5.3 247.
5.5 246.
5.8 247.
5.8 246.
5.7 247.
5.6 245.
5.5 247.
5.6 246.
5.3 246.
5.2 245.
5.3 246.
5.2 245.
5.0 246.
5.1 246.
4.9 248.
4.9 252.
4.4 256.
4.4 249.
4.3 254.
4.5 258.
16.  15.  8.  1984.
4.8 219.
4.9 224.
4.9 224.
5.1 221.
5.0 223.
5.0 225.
5.1 223.
5.0 225.
4.9 223.
4.9 224.
4.9 226.
5.0 225.
5.1 225.
5.0 226.
4.9 226.
5.0 223.
5.1 225.
5.1 225.
4.9 225.
5.1 226.
5.0 228.
5.2 230.
5.0 232.
```

17. 15. 8. 1984.
5.9 231.
5.8 235.
6.0 230.
6.1 229.
6.2 229.
6.2 229.
6.2 230.
6.3 228.
6.3 228.
6.2 230.
6.3 231.
6.2 232.
6.0 231.
6.2 233.
6.1 229.
6.5 227.
6.3 225.
6.3 227.
6.4 227.
6.2 233.
6.6 231.
5.7 236.
5.2 238.
18. 15. 8. 1984.
6.5 206.
7.9 201.
5.6 194.
5.1 200.
2.7 286.
7.3 214.
6.3 231.
5.2 228.
7.8 234.
8.8 214.
4.6 215.
7.0 207.
6.2 184.
4.1 207.
6.1 236.
3.4 214.
8.0 218.
6.3 220.
6.6 225.
5.4 227.
5.9 207.
5.9 218.
5.3 205.

19. 15. 8. 1984.
7.2 215.
7.4 215.
7.4 216.
7.8 216.
7.5 215.
7.5 216.
7.4 217.
7.3 218.
7.1 219.
7.1 220.
6.8 222.
6.9 220.
6.6 221.
6.4 227.
6.7 223.
6.5 226.
7.0 226.
6.8 229.
4.5 246.
4.7 229.
4.2 264.
3.0 229.
2.0 171.
20. 15. 8. 1984.
7.4 215.
7.4 215.
7.0 211.
7.0 211.
7.0 211.
5.6 224.
5.6 224.
5.6 224.
5.6 224.
5.6 224.
5.6 224.
5.6 224.
5.6 224.
5.6 224.
5.6 224.
5.6 224.
5.6 224.
5.6 224.
5.6 224.
5.6 224.
6.6 219.

```
21. 15. 8. 1984.
6.3 236.
6.3 236.
6.3 236.
6.3 236.
6.3 236.
6.3 236.
6.3 236.
6.3 236.
6.3 236.
6.0 319.
6.0 319.
6.0 319.
6.0 319.
6.0 319.
6.0 319.
6.0 319.
6.0 319.
6.0 319.
6.0 319.
6.0 319.
6.0 319.
22. 15. 8. 1984.
7.4 234.
8.5 230.
8.5 230.
8.5 230.
8.5 230.
8.5 230.
8.5 230.
7.7 232.
7.2 233.
7.0 229.
7.0 229.
7.0 229.
7.6 222.
7.6 222.
7.6 222.
6.8 315.
6.8 315.
6.8 315.
6.8 315.
11.6 198.
11.6 198.
11.6 198.
5.4 254.
```

```
23. 15.  8. 1984.
7.9 232.
9.6 231.
9.6 231.
9.6 231.
9.6 231.
9.6 231.
9.6 231.
9.6 231.
9.6 231.
9.6 231.
9.6 231.
8.1 231.
8.1 231.
8.1 231.
8.1 231.
8.1 231.
7.1 183.
15.8 266.
6.4 228.
4.2 217.
4.0 246.
6.8 258.
9.6 229.
0.  16.  8. 1984.
8.5 222.
8.8 215.
8.8 215.
8.8 215.
8.8 215.
2.6 254.
2.6 254.
8.6 216.
8.6 216.
8.6 216.
8.6 216.
8.6 216.
8.6 216.
8.6 216.
8.6 216.
8.6 216.
8.6 216.
8.6 216.
8.6 216.
9.1 265.
7.2 257.
7.2 257.
```

```
1. 16. 8. 1984.
5.0 209.
6.4 207.
7.2 207.
7.6 202.
7.6 202.
7.6 202.
7.6 202.
8.6 223.
8.2 222.
8.2 222.
8.2 222.
8.2 222.
8.2 222.
8.2 222.
8.2 222.
8.2 222.
8.2 222.
8.2 222.
8.2 222.
8.2 222.
2. 16. 8. 1984.
4.0 198.
4.0 198.
4.0 198.
4.0 198.
4.0 198.
4.0 198.
4.0 198.
4.0 198.
4.0 198.
4.0 198.
4.0 198.
4.0 198.
4.0 198.
4.0 198.
4.0 198.
4.0 198.
10.5 168.
10.5 168.
10.5 168.
10.5 168.
10.5 168.
10.5 168.
```

```
3.  16.  8.  1984.
2.2 220.
3.1 219.
3.1 219.
3.1 219.
3.1 219.
3.1 219.
3.1 219.
3.1 219.
3.1 219.
3.1 219.
3.1 219.
3.1 219.
3.1 219.
3.1 219.
3.1 219.
3.1 219.
3.1 219.
3.1 219.
3.1 219.
3.1 219.
12.5 209.
16.9 140.
16.9 140.
5.  16.  8.  1984.
3.0 262.
3.8 262.
3.4 241.
3.8 229.
4.3 220.
4.8 214.
5.2 211.
5.4 212.
4.6 206.
4.6 206.
4.6 206.
4.6 206.
4.6 206.
4.6 206.
4.6 206.
4.6 206.
4.6 206.
4.6 206.
4.6 206.
4.6 206.
4.6 206.
```

```
6.  16.  8.  1984.
3.6 250.
3.5 239.
3.9 229.
4.3 225.
5.0 220.
5.0 220.
5.0 220.
5.0 220.
5.0 220.
5.0 220.
5.0 220.
5.0 220.
5.0 220.
5.0 220.
5.0 220.
5.0 220.
5.0 220.
5.0 220.
5.0 220.
7.5 241.
7.5 241.
7.5 241.
7.  16.  8.  1984.
4.6 242.
4.6 242.
4.6 242.
4.6 242.
4.6 242.
4.6 242.
4.6 242.
4.6 242.
4.6 242.
4.6 242.
4.6 242.
4.6 242.
4.6 242.
4.6 242.
4.6 242.
4.6 242.
13. 249.
13. 249.
2.1 180.
2.1 180.
15.1 260.
16.7 275.
```

8. 16. 8. 1984.
4.6 223.
4.4 231.
4.6 224.
5.2 218.
5.6 213.
4.0 228.
4.5 277.
2.5 266.
4.4 266.
3.7 299.
4.3 308.
4.5 300.
1.0 0.
2.7 293.
2.1 255.
3.8 217.
2.9 254.
4.6 224.
5.1 248.
6.2 227.
5.7 249.
3.8 270.
3.1 253.
9. 16. 8. 1984.
4.4 226.
4.7 224.
4.7 221.
4.6 217.
4.8 218.
4.8 216.
5.0 219.
6.1 213.
5.8 218.
6.2 247.
4.8 277.
3.0 61.
4.0 200.
8.3 280.
4.5 209.
5.1 206.
6.8 230.
7.7 223.
4.0 204.
3.0 234.
1.5 260.
3.1 223.
3.7 227.
-1. 1. 1. 1.

Boundary layer height estimate
Only one option is used (option 4, Doppler Acoustic Sounder)

Option 4: Format - line 1: TIME, DAY, MONTH, YEAR
                    line 2: intensity of vertical signal

Fixed heights: starting at 60m and ends at 750m with 30m intervals.

Station No. 1. Elandsfontein. File METD+9 (logical unit 29)

9. 15. 8. 1984.
0.
11.
22.
25.
28.
28.
27.
34.
37.
38.
40.
48.
59.
63.
64
62.
53.
40.
28.
26.
30.
26.
20.
15.
13.

10. 15. 8. 1984.
0.
12.
26.
33.
37.
42.
45.
52.
61.
68.
72.
74.
76.
69.
57.
44.
30.
23.
19.
17.
13.
9.
7.
5.
5.
11. 15. 8. 1984.
0.
12.
29.
38.
44.
48.
48.
51.
54.
56.
57.
56.
55.
55.
56.
52.
46.
39.
34.
31.
31.
33.
35.
26.
16.

12. 15. 8 1984.
0.0
12.
27.
36.
41.
44.
44.
45.
44.
45.
45.
45.
45.
45.
43.
41.
38.
38.
38.
36.
34.
31.
29.
29.
29.
13. 15. 8. 1984.
0.0
13.
29.
38.
41.
44.
44.
44.
45.
46.
45.
44.
44.
42.
41.
38.
34.
32.
29.
28.
26.
25.
24.
22.
21.

```
14.  15.  8.  1984.
0.0
12.
28.
35.
39.
39.
39.
40.
41.
41.
41.
40.
38.
37.
34.
33.
31.
31.
30.
28.
25.
24.
23.
21.
20.
15.  15.  8.  1984.
0.
12.
25.
34.
36.
38.
39.
39.
39.
40.
40.
39.
38.
38.
36.
33.
30.
30.
28.
26.
25.
24.
20.
17.
18.
```

16. 15. 8. 1984.
0.
10.
19.
23.
27.
28.
28.
30.
29.
31.
33.
34.
34.
34.
34.
32.
32.
31.
30.
29.
27.
24.
22.
21.
20.
17. 15. 8. 1984.
0.
9.
16.
21.
23.
23.
25.
23.
23.
23.
23.
22.
22.
23.
23.
23.
21.
22.
20.
19.
18.
17.
15.
15.
14.

18. 15. 8. 1984.
0.
6.
9.
10.
12.
10.
8.
9.
9.
9.
10.
9.
10.
10.
10.
9.
9.
9.
9.
9.
8.
8.
8.
8.
8.
19. 15. 8. 1984.
0.
9.
13.
14.
16.
17.
18.
19.
21.
22.
22.
23.
23.
23.
24.
22.
22.
21.
21.
20.
20.
18.
16.
14.
14.

20. 15. 8. 1984.
0.
9.
9.
9.
10.
11.
12.
12.
14.
19.
11.
9.
10.
9.
9.
7.
7.
8.
6.
6.
5.
4.
5.
6.
4.
21. 15. 8. 1984.
0.
11.
10.
8.
10.
10.
11.
10.
9.
10.
9.
9.
9.
11.
11.
12.
10.
9.
9.
10.
9.
8.
8.
8.
8.

22. 15. 8. 1984.
0.
9.
16.
14.
9.
8.
9.
12.
10.
9.
11.
12.
14.
14.
14.
11.
11.
12.
10.
7.
9.
9.
9.
8.
7.
23. 15. 8. 1984.
0.
13.
15.
9.
9.
9.
7.
8.
10.
10.
10.
10.
9.
9.
8.
8.
5.
6.
6.
6.
8.
9.
11.
10.
10.

0. 16. 8. 1984.
0.
11.
10.
11.
10.
10.
17.
16.
12.
7.
7.
7.
7.
7.
7.
5.
4.
8.
5.
4.
6.
5.
5.
5.
5.
1. 16. 8. 1984.
0.
14.
28.
33.
25.
16.
10.
10.
12.
11.
11.
11.
11.
11.
11.
6.
8.
8.
8.
8.
8.
9.
8.
7.
7.

2. 16. 8. 1984.
0.
11.
15.
11.
11.
11.
11.
8.
28.
58.
12.
7.
5.
4.
5.
5.
5.
5.
6.
3.
6.
8.
8.
9.
7.
3. 16. 8. 1984.
0.
7.
15.
15.
9.
9.
9.
9.
9.
9.
9.
9.
9.
9.
9.
9.
9.
9.
9.
9.
9.
9.
9.
9.

4. 16. 8. 1984.
0.
4.
7.
9.
10.
12.
9.
9.
9.
9.
9.
9.
9.
9.
9.
9.
9.
9.
9.
9.
9.
9.
9.
9.
5.
5. 16. 8. 1984.
0.
4.
10.
15.
16.
20.
24.
26.
21.
20.
24.
10.
10.
10.
10.
10.
10.
5.
5.
5.
5.
4.
6.
5.
5.

6. 16. 8. 1984.
0.
6.
15.
18.
20.
24.
19.
9.
9.
9.
9.
9.
9.
5.
5.
10.
10.
11.
11.
10.
9.
8.
9.
9.
8.
7. 16. 8. 1984.
0.
7.
9.
10.
13.
11.
11.
11.
4.
4.
4.
4.
4.
9.
9.
9.
9.
9.
9.
9.
9.
8.
6.
6.
5.

```
8. 16. 8. 1984.
0.
12.
14.
14.
18.
16.
12.
11.
4.
9.
8.
6.
6.
8.
7.
9.
10.
10.
10.
10.
10.
8.
9.
12.
14.
9. 16. 8. 1984.
0.
11.
18.
22.
23.
27.
30.
30.
24.
11.
9.
8.
6.
5.
5.
7.
9.
8.
8.
8.
7.
5.
5.
8.
6.
-1. 1. 1. 1.
```

a_k = coefficient used in the limiting value method (equation 3.79)

A = total plan area when determining roughness length m^2

A, A_0, A_m = similarity functions used in equations (2.36), (2.37), and (2.38)

A_ℓ = angle correction of the average height above sea level radians

A_0 = obstacle plan area when determining roughness length m^2

$A(k)$ = Fourier coefficients in equation (3.75)

$A(t)$ = random acceleration (equation 3.130)

b_k = coefficient used in the limiting value method (equation 3.79)

B, B_0, B_m = similarity functions used in equations (2.36), (2.37), and (2.38)

B^{-1} = surface transfer coefficient (equation 3.95)

$b(k,t)$ = coefficient used in the modified limiting value method (equation 4.44)

$\tilde{c}$ = Fourier transform of the concentration distribution $g\ m^{-3}$

c_{ij} = transilient coefficient (Section 3.1.2.4)

c_p = specific heat of air at constant pressure $Jg^{-1}K^{-1}$

C = concentration distribution $g\ m^{-3}$

$\overline{C}$ = layer averaged concentration (equation 3.51) $g\ m^{-3}$

C' = deviation from the mean concentration distribution $g\ m^{-3}$

$\langle C \rangle$ = mean concentration distribution $g\ m^{-3}$

C_0 = initial concentration $g\ m^{-3}$

C_{00} = zero'th moment (equation 3.10) $g\ m^{-1}$

C_{10}, C_{01} = first moments (equation 3.10) g

C_{20}, C_{02}, C_{11} = second moments (equation 3.10) $g\ m^{-1}$

C_N = drag coefficient for neutral conditions

C_y, C_z = Sutton parameters (equation 3.34) $m^{n/2}$

d	=	zero-plane displacement distance	m
d_c	=	distance criterion between released puffs	m
d_y	=	day of the year	
D	=	molecular diffusivity	$m^2 s^{-1}$
$d_1(k)$, $d_2(k)$	=	parameters in the modified limiting value method	
$D(x,y)$, $D(i,j)$	=	anomalous divergence at point x,y and i,j, respectively	s^{-1}
$D(z-z')$	=	one-dimensional turbulent diffusivity transfer function (equation 3.59)	$m\ s^{-1}$
dW_t	=	Gaussian white-noise stochastic process	
f	=	Coriolis parameter = $2\Omega\sin\lambda$ where the angular velocity of rotation of the earth, Ω = 7,29 x $10^{-5} s^{-1}$ and λ is the latitude of the observation site	s^{-1}
f_t	=	sampling period used in equation (2.56)	min
f_x, f_y, f_z	=	universal function used in equation (3.124)	
F_b	=	flux buoyancy	$m^4 s^{-3}$
$f(k)$	=	parameter used in the modified limiting value method	
$F(z)$	=	state variable used in Section (3.1.2.4)	
g	=	gravitational acceleration constant	$m^2 s^{-1}$
$\langle G_T \rangle$	=	gust factor used in equation (2.56)	
G	=	soil heat flux	$W\ m^{-2}$
$g(k)$	=	parameter used in the modified limiting value method	
h_*	=	vegetation height	m
h_A	=	hour angle (equation A.1)	hr
h_i	=	inversion height	m
h_m	=	mixing layer height	m
h_p	=	boundary layer depth	m
h_s	=	surface layer depth	m
H	=	sensible heat flux	$W\ m^{-2}$
H^*	=	net radiation	$W\ m^{-2}$
H^0	=	heat flux in the absence of incoming solar radiation	$W\ m^{-2}$
$\Delta h(x)$	=	plume rise at distance x away from the source	m
J	=	rainfall rate	$mm\ h^{-1}$

k	=	von Karmen constant	
k_1	=	rate constant for oxidation of SO_2	s^{-1}
k_2	=	rate constant for oxidation of NO_x to RNO_x and HNO_x	s^{-1}
k_3	=	rate constant for oxidation of NO_x to HNO_x	s^{-1}
k_r	=	chemical reaction rate constant	
k_w	=	washout rate constant	s^{-1}
K_h	=	eddy diffusivity for heat	$m^2 s^{-1}$
K_H	=	horizontal diffusion coefficient	$m^2 s^{-1}$
$\bar{K}_{jj}$	=	diffusion coefficient in the Lagrangian treatment of the advection-diffusion equation	$m^2 s^{-1}$
K_m	=	eddy diffusivity for momentum	$m^2 s^{-1}$
K_v	=	vertical diffusion coefficient	$m^2 s^{-1}$
K_{xx}	=	eddy diffusivity	$m^2 s^{-1}$
$K(\kappa)$	=	diffusion coefficient dependent on the wave number κ used in the spectral diffusivity approach (equation 3.63)	
l	=	mixing length	m
L	=	Monin-Obukhov length	m
N	=	cloud cover fraction	
p	=	exponent used in profile relationships	
q	=	exponent used in profile relationships	
Q	=	sensible heat flux	$W\ m^{-2}$
Q_E	=	equation of time (equation A.3)	hr
$Q(x,t/x_0,t_0)$	=	transitional probability density (equation 3.96)	
$r_{k,ij}$	=	distance away from a sparse measuring point,k, to a grid point, (i,j)	m
r_a	=	aerodynamic resistance	$s\ m^{-1}$
r_c	=	canopy resistance	$s\ m^{-1}$
r_c	=	radiation reduction factor due to the presence of clouds	
r_e	=	earth's radius $=\ 6,37 \times 10^6 m$	
r_s	=	surface resistance	$s\ m^{-1}$
R	=	reaction rate	$gm^{-3}s^{-1}$
R	=	incoming solar radiation	$W\ m^{-2}$

Ri	$=$	Richardson number defined in equation (2.15)	
Ri_B	$=$	bulk Richardson number defined by equation (2.67a)	
$R_E(\xi)$	$=$	Eulerian autocorrelation	
$R_L(\xi)$	$=$	Lagrangian autocorrelation	
$R_{ij}(t,\tilde{t})$	$=$	correlation function at time t with lag $\tilde{t}$, where $i,j = 1,2,3$	
$R(z,z')$	$=$	weighting function (equation 3.67)	
$R(z,z_r)$	$=$	atmospheric resistance	$s\ m^{-1}$
s	$=$	the Shir and Shieh parameter to determine the Monin–Obukhov length (equation 2.57)	
S	$=$	rate of change of concentration due to source addition	$gm^{-3}s^{-1}$
M	$=$	airborne mass	g
M'	$=$	source strength	gs^{-1}
$[S_i]$	$=$	matrix representing the concentration at grid point i in Stull's transilient turbulence theory (Section 3.1.2.4)	
$S(x,t)$	$=$	spatial–temporal distribution of particle sources	
t_E	$=$	Eulerian time scale	s
t_L	$=$	Lagrangian time scale	s
t_{SS}	$=$	time of sunset	hr
t_{SR}	$=$	time of sunrise	hr
Δt	$=$	time step	s
Δt_g	$=$	difference from Greenwich Mean Time (GMT)	hr
Δt_I	$=$	the time interval between updating the concentration distribution output	s
Δt_D	$=$	the time interval between updating the advection–diffusion solution	s
$\Delta t_{release}$	$=$	puff release interval	s
Δt_W	$=$	the time interval between updating the wind field parameters	s
$\bar{T}$	$=$	spatial mean temperature	K
T_g	$=$	ground temperature	K
T_s	$=$	absolute temperature of effluent at stack outlet	K
u'	$=$	deviation in the x–wind velocity	

$\bar{u}$	= wind speed profile	m s^{-1}
u_*	= friction velocity	m s^{-1}
$\bar{u}_c$	= average wind speed for the convective layer	m s^{-1}
$\bar{u}_g$	= wind speed at the boundary layer height	m s^{-1}
$\bar{u}_m$	= layer averaged x-wind velocity component in the outer layer	m s^{-1}
u_{ND}	= correction to the x-wind velocity component in the fixed vorticity method of divergence reduction	m s^{-1}
u_o	= initial estimate of the x-wind velocity component	m s^{-1}
u_{RD}	= correction to the x-wind velocity component due to vorticity	m s^{-1}
u_{RR}	= correction to the x-wind component due to anomalous divergence	m s^{-1}
u_s	= wind speed at the surface layer height	m s^{-1}
$\bar{u}_s$	= solved surface layer averaged velocity in the x-direction (equation 4.28)	m s^{-1}
$\bar{u}_{st}$	= average wind speed for the moderately stable layer	m s^{-1}
$\bar{u}_u$	= average wind speed for the moderately unstable layer	m s^{-1}
$\bar{u}_v$	= average wind speed for the very stable layer	m s^{-1}
U	= mean wind speed used in the Gaussian plume and puff models	m s^{-1}
U_s	= velocity components in the x-direction at the stack height	m s^{-1}
v'	= deviation in the y-wind velocity component	m s^{-1}
v_o	= initial estimate of the y-wind velocity component	m s^{-1}
v_d	= deposition velocity	m s^{-1}
$\bar{v}_m$	= layer averaged y-wind velocity component in the outer layer	m s^{-1}

v_{ND}	=	correction to the y-wind velocity component in the fixed vorticity method of divergence reduction	m s^{-1}
v_{RD}	=	correction to the y-wind velocity component due to vorticity	m s^{-1}
v_{RR}	=	correction to the y-wind velocity component due to anomalous divergence	m s^{-1}
$\bar{v}_s$	=	solved surface layer averaged velocity component in the y-direction	
w'	=	deviation in the vertical wind component	m s^{-1}
$\bar{w}$	=	mean vertical wind component	m s^{-1}
w_b	=	velocity as a result of the buoyancy of a plume	m s^{-1}
w_s	=	sedimentation velocity	m s^{-1}
W	=	vertical velocity resulting from a coordinate transformation of the three-dimensional continuity equation	m s^{-1}
$\bar{W}_s$	=	the solved surface layer averaged vertical velocity	m s^{-1}
$W(r_{j,ij})$	=	interpolation weighting function, where $r_{k,ij}$ is the distance from a sparce point, k, to a grid point, (i,j)	
x_*	=	distance used in Briggs' $^2/3$ plume rise equation (3.132) and (3.133)	m
$\langle X^2 \rangle$	=	mean square of the particle displacement	m^2
Δx	=	finite spatial stepsize in x-direction	m
Δy	=	finite spatial stepsize in y-direction	m
z_0	=	roughness length	m
z_r	=	reference height for evaluating deposition velocity	m
z_t	=	average height above sea level	m
z_T	=	reference height for the temperature profile	m
Δz	=	finite spatial stepsize in z-direction	

Greek Letters

α_p	=	the wind direction at the boundary

		layer height	radians
α_s	=	the wind direction at the surface	
		layer height	radians
β	=	constant used in the stable wind profile	
β_2	=	constant used in the stable temperature	
		profile	
γ	=	constant used in the unstable wind profile	
γ_1, γ_2	=	constants used in the unstable	
		temperature profile	
$\gamma(z,\xi)$	=	transilient rate function defined by	
		equation (3.70), where ξ is the separation	
		distance between two levels being mixed	s^{-1}
Γ	=	adiabatic lapse rate	$K\ m^{-1}$
κ	=	wave number	
θ	=	potential temperature	K
$\bar{\theta}$	=	mean potential temperature	K
θ_*	=	potential temperature scale	K
λ	=	longitude (equation A.1)	radians
$\lambda(t+\Delta t)$	=	random variable used in equation (3.131)	
Λ	=	washout coefficient	s^{-1}
ν	=	kinematic viscosity of air	$gm^{-1}s^{-1}$
μ_x, μ_y	=	x, y coordinates of the puff centroid	m
ξ	=	$\dfrac{z}{L}$ where z height above ground level	
		and L the Monin–Obukhov length	
$\xi(x,y)$	=	vorticity at point x,y	s^{-1}
ρ	=	cross-correlation coefficient	
ρ_m	=	transformed height of the first	
		outer layer in the three-dimensional	
		wind field model	
σ_θ	=	azimuth standard deviation	radians
$\sigma_x, \sigma_y, \sigma_z$	=	variances about the centroid of a	
		distribution	m
$\sigma_u, \sigma_v, \sigma_w$	=	variances of the wind components in	
		the x, y, and z directions	$m\ s^{-1}$
τ	=	time of the day	hours
τ_{ij}	=	time scale	s
τ_{zx}	=	shear stress (Reynold stress) in z–x plane	$N\ m^{-2}$
ϕ	=	potential function defined by $u = \dfrac{\partial\phi}{\partial x}$ or	

$$v = \frac{\partial \phi}{\partial y}$$ where u and v are the wind components
in x and y directions $\qquad$ $m^2 s^{-1}$

ϕ_h $\quad$ = $\quad$ universal function for heat

ϕ_m $\quad$ = $\quad$ universal function for momentum

Ψ $\quad$ = $\quad$ forcing function defined in equation (2.75)
or (2.77) $\qquad$ s^{-1}

Ψ_h $\quad$ = $\quad$ integral function for heat

Ψ_m $\quad$ = $\quad$ integral function for momentum

ω_* $\quad$ = $\quad$ convective velocity scale (equation 3.53) $\qquad$ $m\ s^{-1}$

ω_s $\quad$ = $\quad$ effluent emission velocity at stack outlet $\qquad$ $m\ s^{-1}$

Abbreviations

ABL $\qquad$ — $\quad$ Atmospheric Boundary Layer

ADI $\qquad$ — $\quad$ Alternating Direction Implicit

CPU $\qquad$ — $\quad$ Central Processor Unit

CSIR $\qquad$ — $\quad$ Council for Scientific and Industrial Research

ESCOM $\qquad$ — $\quad$ Electricity Supply Commission

GMT $\qquad$ — $\quad$ Greenwich Mean Time

LV $\qquad$ — $\quad$ Limiting Value

MLV $\qquad$ — $\quad$ Modified Limiting Value

RAM $\qquad$ — $\quad$ Random Access Memory

SOR $\qquad$ — $\quad$ Successive Over-Relaxation

UST $\qquad$ — $\quad$ Universal Standard Time

REFERENCES

A

Abramowitz, M. and Stegun, I.A. 1965. *Handbook of Mathematical Functions*. Dover, New York.

Allen, L.H. 1968. Turbulence and wind speed spectra within a Japanese larch plantation. *J. Appl. Meteorol.*, 7, 73-78.

Altshuller, A.P. 1979. Model predictions of the rates of homogeneous oxidation of sulfur dioxide to sulfate in the troposphere. *Atmospheric Environment*, 13, 1653-1667.

Anderson, G.E. 1971. Mesoscale influences on wind fields. *J. Appl. Meteorol.*, 10, 377-386.

Aris, R. 1956. On the dispersion of a solute in a fluid through a tube. *Proc. R. Soc., Lond.*, A235, 67-77.

Arya, S.P.S. 1977. Suggested revisions to certain boundary layer parameterization schemes used in atmospheric circulation models. *Mon. Weather Rev.*, 105, 215-227.

Arya, S.P.S. 1978. Comparative effects of stability, baroclinicity and the scale-height ratio on drag laws for the atmospheric boundary-layer. *J. Atmos. Sci.*, 35, 40-46.

Arya, S.P.S. 1984. Parametric relations for the atmospheric boundary layer. *Boundary-Layer Meteorol.*, 30, 57-73.

Arya, S.P.S. and Plate, C.D. 1969. Modeling of the stably stratified atmospheric boundary layer. *J. Atmos. Sci.*, 26, 656-665.

Arya, S.P.S. and Sundarajan, A. 1976. An assessment of the proposed similarity theories for the atmospheric boundary. layer. *Boundary-Layer Meteorol.*, **10**, 149-166.

B

Badgley, F.I., Paulson, C.A. and Miyake, M. 1972. *Profiles of wind, temperature and humidity over the Arabian sea.* The University Press of Hawaii, 62pp.

Bagrinowskii, K.A. and Godunov, S.K. 1975. Difference schemes for multidimensional models. *Dokl. Akad. Nauk USSR*, **115**, 431-434.

Barad, M.L. 1958. Project Prairie Grass a field program in diffusion (Vol III). Geophysical Research Papers No. 59, Air Force Cambridge Research Centre - TR-58-235(II).

Barad, M.L. and Fuquay, J.J. 1962. Diffusion in shear flow. *J. Appl. Meteorol.*, **1**, 257-263.

Barker, E.H. and Baxter, T.L. 1975. A note on the computation of atmospheric surface layer fluxes for use in numerical modeling. *J. Appl. Meteorol.*, **14**, 620-622.

Baron, T., Gerhard, E.R. and Johnstone, H.F. 1949. Dissemination of aerosol particles dispersed from stacks. *Ind. Chem. Engng.*, 41, 2403-2408.

Barrie, L.A. 1981. The prediction of rain acidity and SO_2 scavenging in Eastern North America. *Atmospheric Environment*, 15, 31-41.

Batchelor, G.K. 1954. Heat convection and buoyancy effects in fluids. *Quart. J. R. Met. Soc.*, **80**, 339-358

Belt, G.H. 1969. Estimation of sensible heat and momentum fluxes in boundary layer of a pine plantation. *Bull. Amer. Meteor. Soc.*, 50, 491.

Benoit, R. 1977. On the integral of the surface layer profile gradient functions. *J. Appl. Meteorol.*, 16, 859-860.

Berkowicz, R. 1984. Spectral methods for atmospheric diffusion modeling. *Boundary-Layer Meteorol.*, 30, 201-220.

Berkowicz, R. and Prahm, L.P. 1979. Generalization of K-theory for turbulent diffusion. Part I. Spectral turbulent diffusivity concept. *J. Appl. Meteorol.*, 18, 266-272.

Berkowicz, R. and Prahm, L.P. 1980. On the spectral turbulent diffusivity theory for homogeneous turbulence. *J. Fluid. Mech.*, 100, 433-448.

Berkowicz, R. and Prahm, L.P. 1982. Evaluation of the profile method for estimation of surface fluxes of momentum and heat. *Atmospheric Environment*, 16, 2809-2819.

Binkowski, F.S. 1975. On the empirical relationship between the Ricardson number and the Monin-Obukhov stability parameter. *Atmospheric Environment*, 9, 453-454.

Boegman, N. 1985. Major sources of sulphur dioxide emissions in the Eastern Transvaal. Environmental Advisory Services, C/85/13, Pretoria.

Boris, J.P. and Brook, D.L. 1973. Flux-corrected transport - I. HASTA, a fluid transport algorithm that works. *J. Comp. Phy.*, II, 38-69.

Boris, J.P. and Brook, D.L. 1976. Flux-corrected transport - III. Minimal-error FCT algorithms. *J. Comp. Phys.* 20, 397-431.

Briggs, G.A. 1969. *Plume Rise*. United States Atomic Energy Commission Critical Review Series TID-25075.

337

Brost, R.A. and Wyngaard, J.C. 1978. A model study of the stably stratified planetary boundary layer. *J. Atmos. Sci.*, 35, 1427-1440.

Brown, R.A. 1982. On two-layer models and the similarity functions for the PBL. *Boundary-Layer Meteorol.*, 24, 451-463.

Burger, L.W. 1984. Continuous pollutant distribution monitor. M.Sc. thesis, Dept. of Chemical Engineering, University of Natal, Durban.

Burger, L.W. 1986. Listing of the dispersion package WIZARD and the installing program INSTALL. Deposited at the Dept. of Chemical Engineering, University of Natal, Durban, and the Council for Scientific and Industrial Research, Pretoria.

Burger, L.W. and Mulholland, M. 1987. Real-time prediction of point-source distributions using an anemometer-bivane and a microprocessor. Submitted for publication in *Atmospheric Environment*.

Businger, J.A., Wyngaard, J.C., Izumi, Y. and Bradley, E.F. 1971. Flux-profile relationships in the atmospheric surface layer, *J. Atmos. Sci.*, 30, 788-794.

C

Calder, K.L. 1965. On the equation of atmospheric diffusion. *Quart. J. R. Met. Soc.*, 91, 514-517.

Carl, D.M, Tarbell, T.C. and Panofsky, H.A. 1973. Profiles of wind and temperature from towers over homogeneous terrain. *J. Appl. Meteorol.*, 30, 783-794.

Carson, D.J. and Richards, P.J.R. 1978. Modelling surface turbulent fluxes in stable conditions. *Boundary-Layer Meteorol.*, 14, 67–81.

Chamberlain, A.C. 1953. Aspects of travel and deposition of aerosol and vapour clouds. Atomic Energy Research Establishment, HP/R 1261, Harwell, Berkshire, England.

Chapman, M. 1981. FRAM—nonlinear damping algorithms for the continuity equation. *J. Comp. Phys.*, 44, 84–103.

Charnock, H. 1955. Wind stress on the water surface. *Quart. J. R. Met. Soc.*, 81, 639–640.

Chock, D.P. 1985. A comparison of numerical methods for solving the advection equation – II. *Atmospheric Environment*, 19, 571–586.

Chock, D.P. and Dunker, A.M. 1983. A comparison of numerical methods for solving the advection equation. *Atmospheric Environment*, 17, 11–24.

Christensen, O. and Prahm, L.P. 1976. A pseudospectral model for dispersion of atmospheric pollutants. *J. Appl. Meteorol.*, 15, 1284–1294.

Cocks, A.T., Fletcher, I.S. and Kallend, A.S. 1983. Chemical modelling studies of the long range dispersion of power plumes, in *Air Pollution Modelling and its Application II*, ed. C. Wispelaere, 137–157, Plenum, New York.

Corrsin, S. 1953. Proc. First Iowa Symposium on Thermodynamics, Iowa State University.

Counihan, J. 1971. Wind tunnel determination of roughness length as a function of the fetch and the roughness density of three-dimensional roughness elements. *Atmospheric Environment*, 5, 637–642.

Counihan, J. 1975. Adiabatic atmospheric boundary layers: review
and analysis of data from the period 1880-1972. *Atmospheric
Environment*, 9, 871-905.

Cowan, I.R. 1968. Mass, heat and momentum exchange between stands
of plants and their atmospheric environment. *Quart. J. R. Met.
Soc.*, 94, 524-544.

Cressman, G.R. 1959. An operational objective analysis system. *Mon.
Weather Rev.*, 87, 367-374.

Crane, G., Panofsky, H.A. and Zeman, O. 1977. A model for
dispersion from area sources in convective turbulence.
Atmospheric Environment, 11, 893-900.

Csanady, G.T. 1972. Crosswind shear effects on atmospheric
diffusion. *Atmospheric Environment*, 6, 221.

D

Davenport, A.G. 1965. The relationship of wind structure to wind
loading. in "Wind effects on buildings and structures,"
National Physical Laboratory, Symposium 16, Her Majesty's
Stationary Office, London.

Davis, M.L. 1970. Modelling urban atmospheric temperature
profiles. *Atmospheric Environment*, 4, 277-288.

Deacon, E.L. 1949. Vertical diffusion in the lowest layers of the
atmosphere. *Quart. J. R. Met. Soc.*, 75, 89-103.

Deacon, R.R. 1979. Modelling the results of two recent mesoscale
dispersion experiments. *Atmospheric Environment*, 13,
1523-1533.

Deardorff, J.W. 1966. The counter gradient heat flux in the lower atmosphere and in the laboratory. *J. Atmos. Sci.*, 23, 503-506.

Deardorff, J.W. 1970. A three-dimensional numerical investigation of the idealized planetary boundary layer. *Geophys. Fluid. Dyn.*, 1, 377-410.

Deardorff, J.W. 1972. Numerical investigation of neutral and unstable planetary boundary layers. *J. Atmos. Sci.*, 29, 91-115.

Deardorff, J.W. and Willis, G.E. 1975. A parameterization of diffusion into the mixed layer. *J. Appl. Meteorol.*, 14, 1451-1458.

De Bruin, H.A.R. and Holtslag, A.A.M. 1982. A simple parameterization of the surface fluxes of sensible and latent heat during daytime compared with the Penman-Monteith concept. *J. Appl. Meteorol.*, 21, 1610-1621.

De Haan, B.J. 1980. A comparison of finite difference schemes describing the two dimensional advection equation. Proc. 11th Int. Techn. Meeting on Air Pollution Modelling and its Application, NATO-CCMS, Amsterdam.

De Marrais, G.A. 1959. *J. Meteorol.*, 16, 181.

Demuth C. 1978. A contribution to the analytical steady solution of the diffusion equation for line sources. *Atmospheric Environment*, 12, 1255-1258.

Dickerson, M.H. 1978. MASCON - A mass consistant atmospheric flux model for regions with complex terrain. *J. Appl. Meteorol.*, 17, 241-253.

Dilley J.F. and Yen K.T. 1971. Effect of a mesoscale type wind on the pollutant distribution from a line source. *Atmospheric Environment*, 5, 845-851.

Donaldson, C. du P., Sullivan, R.D. and Rosenbaum, H. 1972. A theoretical study of the generation of atmospheric clear-air turbulence. *AIAA J.*, 10, 162-170.

Donea, J., Giuliani, S. and Laval H. 1979. Accurate explicit finite element schemes for convective-conductive heat transfer problems. *Finite Element Methods for Convection Dominated Flows*, ed. J.R. Hughes, AMD-34, 149-166. *Am. Soc. of Mech. Engng.*

Draxler, R.R. 1976. Determination of atmospheric diffusion parameters. *Atmospheric Environment*, 10, 99-105.

Draxler, R.R. 1979. Modelling the results ot two recent mesoscale dispersion experiments. *Atmospheric Environment*, 13, 1523-1533.

Dyer, A.J. 1974. A review of flux-profile relationships. *Boundary-Layer Meteorol.*, 7, 363-372.

Dyer, A.J. and Bradley, E.F. 1982. An alternative analysis of flux-gradient relationships at the 1976 ITCE. *Boundary-Layer Meteorol.*, 22, 3-19.

Dyer, A.J. and Hicks, B.B. 1970. Flux-gradient relationships in the constant flux layer. *Quart. J. R. Met. Soc.*, 96, 715-721.

E

Eimutis, E.C. and Konicek, 1972. Derivations of continuous functions for the lateral and vertical atmospheric dispersion coefficients. *Atmospheric Environment*, 6, 859-863.

Egan, B.A. and Mahoney, J.R. 1972. Applications of a numerical air pollution transport model to dispersion in the atmospheric boundary layer. *J. Appl. Meteorol.*, 11, 1023-1039.

Ekman, V.W. 1905. On the influence of the earth's rotation on ocean currents. *Arkiv. Mat. Astr. Fysik. K. Sv. Vet. Ak.*, **2**, (11), 1-51.

Ellison, T.H. 1957. *J.Fluid Mech.*, **2**, 456.

Endlich, R.M. 1967. An iterative method for altering the kinematic properties of wind fields. *J. Appl. Meteorol.*, **6**, 837- 844.

Endlich, R.M., Ludwig, F.L., Bhumralkar, C.M. and Estoque, M.A. 1982. A diagnostic model for estimating winds at potential sites for wind turbines. *J. Appl. Meteorol.*, 21, 1441-1454.

Endlich, R.M., Nitz, K.C., Brodzinsky, R. and Bhumralkar, C.M. 1984. Along-range air pollution transport model for Eastern North America - I. Sulpfur oxides. *Atmospheric Environment*, **18**, 2345-2360.

Estoque, M.A. 1961. A theoretical investigation of the sea breeze. *Quart. J. R. Met. Soc.*, **87**, 136-146.

Estoque, M.A. 1968. Vertical mixing due to penetration convection. *J. Atmos. Sci.*, **25**, 1046-1051.

F

Falls, A.H. and Seinfeld, J.H. 1978. Continued development of a kinetic mechanism for photochemical smog. *Atmospheric Environment*, **12**, 1398-1406.

Falls, A.H. McRae, G.J. and Seinfeld, J.H. 1979. Sensitivity and uncertainty of reaction mechanisms for photochemical air pollution. *Int. J. Chem. Kinet.*, **11**, 1137-1162.

Fichtl, G.H. and Mc Vehil, G.E. 1970. Longitudinal and lateral
spectra of turbulence in the atmospheric boundary layer at the
Kennedy Space Centre. *J. Appl. Meteorol.*, **9**, 51–63.

Fiedler, B.H. 1984. An integral closure model for the vertical
turbulent flux of a scalar in a mixed layer. *J. Atmos. Sci.*,
41, 674–680.

Forester, K.C. 1977. Higher order monotonic convective difference
schemes. *J. Comp. Phys.*, **23**, 1–22.

Fromm, J.E. 1969. Practical investigation of convective difference
approximations of reduced dispersion. *Phys. Fluids.*, **12**,
Suppl. II, 3–12.

G

Gandin, L.S. 1963. Objective Analysis of Meteorological Fields.
Translated from Russian by the Isreal Program for Scientific
Translations, 1965.

Garland, J.A. 1978. Dry and wet removal of sulphur from the
atmosphere. *Atmospheric Environment*, **12**, 349–362.

Garratt, J.R. 1980. Surface influence upon vertical profiles in the
atmospheric near–surface layer. *Quart. J. R. Met. Soc.*, **106**,
803–819.

Garratt, J.R. 1982. Observations in the nocturnal boundary layer.
Boundary-Layer Meteorol., **22**, 21–48.

Garratt. J.R. 1983. Surface influence upon vertical profiles in the
nocturnal boundary layer. *Boundary-Layer Meteorol.*, **26**, 69–80.

Garratt, J.R. and Brost, R.A. 1981. Radiative cooling effects within and above the nocturnal boundary layer. *J. Atmos. Sci.*, **38**, 2730-2746.

Garratt, J.R., Wyngaard, J.C. and Francey, R.J. 1982. Winds in the atmospheric boundary layer - predictions and observations. *J. Atmos. Sci.*, **39**, 1307-1316.

Gee, J.H. 1965. An approximate treatment of the effect of thermal stability on turbulent diffusion. *Quart. J. R. Met. Soc.*, **91**, 301-305.

Gifford, F.A. 1959. Statistical properties of a fluctuating plume dispersion model. *Atmospheric Diffusion and Air Pollution*, ed. F.N. Frenkiel and P.A. Sheppard, *Advan. Geophys.*, **6**, 117, Academic Press.

Gifford, F.A., 1961. Uses of routine meteorological observations for estimating atmospheric dispersion. *Nuclear Safety*, **2**, 47

Gifford, F.A., 1968. An outline of theories of diffusion in lower layers of the atmosphere. in *Meteorology and Atomic Energy, 1968.* ed. D.H. Slade, U.S. Atomic Energy Commission, Oak Ridge, Tennessee.

Gifford, F.A. 1976. Turbulent diffusion typing schemes: a review. *Nuclear Safety*, **17**, 68-86.

Gifford, F.A. 1982. Horizontal diffusion in the atmosphere: a Lagrangian-dynamical theory. *Atmospheric Environment*, **16**, 505-512.

Gilchrist, B. and Cressman, G.P. 1954. An experiment in objective analysis. *Tellus*, **6**, 309-318.

Gillani, N.V. 1978. Project MISTT: mesoscale plume modeling of the dispersion transformation and ground removal of SO_2, *Atmospheric Environment*, **12**, 569-588.

Glendening, J.W., Businger, J.A. and Farber, R.J. 1984. Improving plume rise prediction accuracy for stable atmospheres with complex vertical structure. *JAPCA*, 1128-1133.

Golder, D. 1972. Relations among stability parameters in the surface layer. *Boundary-Layer Meteorol.*, 3, 47-57.

Goodin, W.R. and McRae, G.J. 1980. A procedure for wind field construction from measured data which utilizes local surface roughness, Proc. Second Conf. on Coastal Meteorology, AMS Los Angeles, Calif., 233-239.

Goodin, W.R., McRae, G.J. and Seinfeld, J.H. 1979. A comparison of interpolation methods for sparce data: application to wind and concentration fields. *J. Appl. Meteorol.*, 18, 761-771.

Goodin, W.R., McRae, G.I. and Seinfeld, J.H. 1980. An objective analysis technique for constructing three-dimensional urban-scale wind fields. *J. Appl. Meteorol.*, 19, 98-108.

Goroch, A.K. 1976. Comparison of radiosonde and acoustic echo sounder measurements of atmospheric thermal strata. *J. Appl. Meteorol.*, 15, 520-521.

Gurvich, A.S. 1965. Vertical temperature and wind velocity profiles in the atmospheric surface layer. *Izv. Acad. Sci. USSR, Atmos. Ocean Phys.*, 1, 31-36.

H

Hall, F.F.(jr), Edinger, J.G and Neff, W.D. 1975. Convective plumes in the planetary boundary layer investigated with an acoustic echo sounder. *J. Appl. Meteorol.*, 14, 513-523.

Haltiner, G.J. and Williams, R.T. 1980. *Numerical Prediction and Dynamic Meteorology*. John Wiley and Sons, New York.

Hameed, S. 1974. A modified multi-cell method for simulation of atmospheric transport. *Atmospheric Environment*, 8, 1003-1008.

Hanna, S.R. 1979. A statistical diffusion model for use with variable wind fields, in Fourth Symposium on Turbulent Diffusion and Air Pollution, American Meteorological Society, 15-18.

Hanna, S.R., Briggs, G.A., Deardorff, J., Egan, B.A., Gifford, F.A. and Pasquill, F. 1977. AMS workshop on stability classification schemes and sigma curves - Summary of recommendations. *Bull. Amer. Meteor. Soc.*, 58, 1305-1309.

Hay, J.S. and Pasquill, F. 1959. Diffusion from a continuous source in relation to the spectrum and scale of turbulence. *Atmospheric Diffusion and Air Pollution*, ed. F.N. Frenkiel and P.A. Sheppard, *Advances in Geophysics*, 6, 345, Academic Press.

Heines, T.S. and Peters, L.K. 1973. The effect of a horizontal impervious layer cuased by a temperature inversion aloft on the dispersion of pollutants in the atmosphere. *Atmospheric Environment*, 7, 39-48.

Heines, T.S. and Peters, L.K. 1974. The effect of ground level absorption on the dispersion of pollutants in the atmosphere. *Atmospheric Environment*, 8, 1143-1153.

Henry, R.C. and Hidy, G.M. 1981. (Discussion) Multivariate analysis of particulate sulfate and other air quality variables - I. Annual data from Los Angeles and New York. *Atmospheric Environment*, 15, 424-426.

Henry, R.C. and Hidy, G.M. 1982. Multivariate analysis of particulate sulfate and other air quality variables by principle components - II. Salt Lake City, Utah and St. Louis, Missouri. *Atmospheric Environment*, 16, 929-943.

Hess, G.D., Hicks, B.B. and Yamada, T. 1981. The impact of the Wangara experiment. *Boundary-Layer Meteorol.*, 20, 135-174.

347

Hicks, B.B. 1976. Wind profile relationships from the Wangara experiment, *Quart. J. R. Met. Soc.*, 102, 535-551.

Hicks, B.B., Hyson, P. and Moore, C.J. 1975. A study of eddy fluxes over a forest. *J. Appl. Meteorol.*, 14, 58-66.

Hino, M. 1968. Computer experiment on smoke diffusion over complicated topography. *Atmospheric Environment*, 2, 541-558.

Hogstrom, U. 1964. An experimental study on atmospheric diffusion. *Tellus*, 16, 205-251.

Hunt, J.C.R. and Richards, K.J. 1984. Stratified airflow over one or two hills. *Boundary-Layer Meteorol.*, 30, 223-259.

I

Irwin, J.S. 1983. Estimating plume dispersion - a comparison of several sigma schemes. *J. Climate Appl. Meteorol.*, 22, 92-114.

Irwin, J.S. and Binkowski, F.S. 1981. (Technical Note) Estimation of the Monin-Obukhov scaling length using on-site instrumentation. *Atmospheric Environment*, 15, 1091-1094.

Ito, S. 1970. A mechanism of turbulent diffusion in the atmospheric surface layer. *Papers in Meteorology and Geophysics*, 21, 141.

J

Jensen, M. and Franck, N. 1963. *Model-scale tests in turbulent wind*, Part 1. Danish Technical Press, Copenhagen, Denmark.

Jones, P.M., De Larrinaga, M.A.B. and Wilson, C.B. 1971. *Atmospheric Environment*, 5, 89.

Joynt, R.C. and Blackman, D.R. 1976. A numerical model of pollutant transport, *Atmospheric Environment*, 10, 433-442.

K

Kaimal, J.C., Wyngaard, J.C., Haugen, D.A., Cote, O.R., Izumi, Y., Caughey, S.. and Readings, C.J. 1976. Turbulent structure in the convective boundary layer. *J. Atmos. Sci.*, 33, 2152-2169.

Kazanski, A.B. and Monin, A.S. 1956. *Izv. Akad. Nauk. USSR.*, Geophys. Series, 1, 79pp.

Kazanski, A.B. and Monin, A.S. 1960. A turbulent regime above the ground atmospheric layer. *Izv. Akad. Nauk. USSR.*, Geophys. Series, 1, 110-112.

Klug, W. 1967. Determination of turbulent fluxes of heat and momentum from the wind profile, *Quart. J. R. Met. Soc.*, 93, 101-104.

Knox, J.B. 1974. Numerical modeling of the transport diffusion and deposition of pollutants for regions and extended scales. *JAPCA*, 24, 660-664.

Kondo, O. and Yamazawa, 1986. Aerodynamic roughness over an inhomogeneous ground surface, *Boundary-Layer Meteorol.*, 35, 331-348.

Kullenberg, G. 1971. Vertical diffusion in shallow waters. *Tellus*, 23, 129-135.

Kung, E. 1963. Climotology of aerodynamic roughness parameter and energy dissipation in the planetary boundary layer of the Northen Hemisphere. Studies of the effects of variations in boundary conditions on the atmospheric boundary layer, Annual Rept. 1963, Dept. of Meteorology, University of Wisconsin, Madison, 37-96.

L

Lamb, R.G. 1973. Note on application of K-theory to turbulent diffusion problems involving chemical reaction. *Atmospheric Environment*, **7**, 235.

Lamb, R.G. 1978. A numerical simulation of dispersion from an elevated point source in the convective boundary layer. *Atmospheric Environment*, **12**, 1297-1304.

Lamb, R.G. 1979. The effects of release heights on material dispersion in the convective planetary boundary layer, preprint volume, Fourth Symposium on Turbulance, Diffusion, and Air Pollution, Reno, Navada, 15-18 Jan., 27-33.

Lamb, R.G., Chen, W.H. and Seinfeld, J.H. 1975. Numerico-empirical analysis of atmospheric diffusion theories. *J. Atmos. Sci.*, **32**, 1794-1807.

Lange, R. 1978. ADPIC - a three-dimensional particle in cell model for the dispersal of atmospheric pollutants and its comparison to regional tracer studies. *J. Appl. Meteorol.*, **17**, 320-329.

Lapidus L. and Pinder, G.F. 1982. *Numerical Solution of partial Differentail Equations in Science and Engineering*. Wiley, New York.

Lax, P.D. and Wendorff, B. 1960. Systems of conservation laws. *Comm. Pure Appl. Math.*, **13**, 217-237.

350

Leahey, D.M. 1975. An application of a simple advective pollution model to the city of Edmonton. *Atmospheric Environment*, 9, 817-823.

Lebedeff, S.A. and Hameed, S. 1975. Study of atmospheric transport over area sources by an integral method. *Atmospheric Environment*, 9, 333-338.

Lebedeff, S.A. and Hameed, S. 1976. Laws of effluent dispersion in the steady-state atmospheric surface layer in stable and unstable conditions. *J. Appl. Meteorol.*, 15, 326-336.

Lee, H.N. and Kau, W.S. 1984. Simulation of three-dimensional wind flow over complex terrain in the atmospheric boundary layer. *Boundary-Layer Meteorol.*, 29, 381-396.

Leonard, R.E. and Federer, C.A. 1973. Estimation and measured roughness parameters for a pine forest. *J. Appl. Meteorol.*, 12, 302-307.

Lettau, H. 1969. Note on aerodynamic roughness - parameter estimation of the basis of roughness-element description. *J. Appl. Meteorol.*, 8, 828-832.

Lettau, H.H. 1970. Physical and meteorological basis for mathematical models of urban diffusion processes. *Proceedings of Symposium on Multiple Source Urban Diffusion Models*. USEPA Publication AP-86.

Lettau, H.H. 1979. Wind and temperature profile prediction for diabatic surface layers including strong inversion cases. *Boundary-Layer Meteorol.*, 17, 443-464.

Levine, S.Z. and Scwartz, S.E. 1982. In-cloud and below-cloud of scavenging of nitric acid vapor. *Atmospheric Environment*, 16, 1725-1734.

Lewellen, W.S. and Teske, M. 1973. Prediction of the Monin-Obukhov similarity functions from an invariant model of turbulence. *J. Atmos. Sci.*, **30**, 1340-1345.

Lewellen, W.S. and Teske, M. 1976. Second-order closure modeling of diffusion in the atmospheric boundary layer. *Boundary-Layer Meteorol.*, 10, 69-90

Ley, A. 1982. A random walk simulation of two-dimensional diffusion in the neutral surface layer. *Atmospheric Environment*, 16, 2799-2808.

Ley, A. and Thomson, D.J. 1983. A random walk model of dispersion in the diabatic surface layer, *Quart. J. R. Met. Soc.*, 109, 847-880.

Lin, C.C. and Reid, W.H. 1963. Turbulent flow, theoretical aspects. In *Handbuch der Physik*, ed. S. Fuggle, VIII/2, Springer, Berlin.

Ling, C. 1976. On the calculation of surface shear stress using the profile method. *J. Geophys. Res.*, 81, 2581-2582.

Liu, C.Y. and Goodin, W.R. 1976. An iterative algorithm for objective wind field analysis. *Mon. Weather Rev.*, 104, 784-792.

Liu M.K. and Seinfeld J.H. 1975. On the validity of grid and trajectory models of urban air pollution. *Atmospheric Environment*, 9, 555-574.

Lo, A.K. 1977. An analytical-empirical method for determining the roughness length and zero plane displacement. *Boundary-Layer Meteorol.*, 12, 141-151.

Lo, A.K. 1978. A method for determining flux parameters in the absence of a temperature profile. *Boundary-Layer Meteorol.*, 15, 195-204.

Lo, A.K. 1979. On the determination of boundary-layer parameters using velocity profile as the sole information. *Boundary-Layer Meteorol.*, 17, 465-484.

Lo, A.K. and McBean, G.A. 1978. On the relative errors in methods of flux calculations. *J. Appl. Meteorol.*, 17, 1704-1711.

Long, P.E. and Pepper, D.W. 1976. A comparison of six numerical schemes for calculating the advection of atmospheric pollution. Third Symposium on Atmospheric Turbulance, Diffusion and Air Quality, 19-20 Oct. 1976, Raleigh, NC, U.S.A.

Ludwig, F.L. 1981. A model for simulating the behaviour of pollutants emitted at ground level under time-varying meteorological conditions. *Atmospheric Environment*, 15, 989-999.

Ludwig, F.L., Gasiorek, L.S. and Ruff, R.E. 1977. Simplification of a Gaussian puff model for real-time minicomputer use. *Atmospheric Environment*, 11, 431-436.

Lumley, J.L. and Panofsky, H.A. 1964. *The Structure of Atmospheric Turbulence*, Interscience, London, 239pp.

Lumley, J.L. 1978. Computational modeling of turbulent flows. in *Advances in Applied Mechanics*, ed. C.-S. Yih, 18, 123-176. Academic Press, New York.

Lumley, J.L. and Mansfield, P. 1984. Second order modeling of turbulent transport in the surface mixed layer. *Boundary-Layer Meteorol.*, 30, 109-142.

Lupini, R. and Tirabassi, T. 1983. Solution of the advection-diffusion equation by the moments method. *Atmospheric Environment*, 17, 965-971.

Mac Cracken, M.C. and Sauter, G.D. (Eds.) 1975. *Development of an air pollution model for the San Francisco Bay area*. Vol. 2, Appendices Lawrence Livermore Laboratory, UCRL-51920, 229-230. [NTIS UCRL-51920].

Mahrer, Y. and Pielke, R.A. 1975. A numerical study of the air flow over mountains using the two-dimensional version of the University of Virginia Mesoscale model. *J. Atmos. Sci.*, **32**, 2144-2155.

Manins, R.T. and Sawford, B.L. 1979. A model of Katabatic winds. *J. Atmos. Sci.*, **36**, 619-630.

Marchuk, G.I. 1975. *Methods of Numerical Mathematics*. Springer, New York.

Maul, P.R. 1978. The effect of the turning of the wind vector with height on the ground level trajectory of a diffusing cloud. *Atmospheric Environment*, **12**, 1045-1050.

Maul, P.R. 1980. Atmospheric transport of sulphur compound pollutants. Central Electricity Generating Bureau MID/SSD/80/0026/R, Nottingham, England.

McMahon, T.A., Denison, P.J. and Fleming, R. 1976. A long-distance air pollution transportation model incorporating washout and dry deposition components. *Atmospheric Environment*, **10**, 751-761.

McRae, G.J., Goodin, W.R. and Seinfeld, J.H. 1982. Development of a second-generation mathematical model for urban air pollution - I. Model formulation. *Atmospheric Environment*, **16**, 679-696.

McVehil, G.E. 1964. Wind and temperature profiles near the ground in stable stratification. *Quart. J. R. Met. Soc.*, **90**, 136-146.

Mellor, G.L. 1973. Analytical prediction of the properties of
    stratified planetary surface layers *J. Atmos. Sci.*, 30,
    1061-1069.

Mellor, G.L. and Yamada, T. 1974. A hierarchy of turbulence closure
    models for planetary boundary layers. *J. Atmos. Sci.*, 31,
    1791-1806.

Misra, P.K. 1980. Dispersion from tall stacks into a shore line
    environment. *Atmospheric Environment*, 14, 397-400.

Molenkamp C.R. 1968. Accuracy of finite-difference methods applied
    to the advection equation. *J. Appl. Meteorol.*, 7, 160-167.

Molion, L.C.B. and Moore, C.J. 1983. Estimating the zero-plane
    displacement for tall vegetation using a mass conservation
    method. *Boundary-Layer Meteorol.*, 26, 115-125.

Moller, D. 1980. Kinetic model of atmospheric SO_2 oxidation based
    on published data. *Atmospheric Environment*, 14, 1067-1079.

Monin, A.S. 1965. On the symmetry properties of turbulence in the
    surface layer of air. *Atmos. Ocean. Phys.*, 1, 45-54.

Monin, A.S. and Obukhov, A.M. 1954. Basic regularity in turbulent
    mixing in the surface layer of the atmosphere. *Frud. Geofig.
    Inst. Akad. Nauk*, SSSR, 24, 151, 163.

Monin, A.S. and Yaglom, A.M. 1965. *Statistical Fluid Mechanics*.
    1971 English translation. MIT Press, Cambridge, Mass. 769pp

Monin, A.S. and Yaglom, A.M. 1967. *Statistical Fluid Mechanics*.
    1971 English translation. MIT Press, Cambridge, Mass.

Monin, A.S. and Yaglom, A.M. 1971. *Statistical Fluid Mechanics*,
    Vol. 1., MIT Press, Cambridge, Mass.

Monro, D.M. 1983. *Fortran 77*, Edward Arnold, London.

Moore, G.E., Liu, M.K. and Shi, L.H. 1985. Estimates of integral time scales from a 100m meteorological tower at a plains site. *Boundary-Layer Meteorol.*, 31, 349-368.

Morton, B.R., Taylor, G.I. and Turner, J.S. 1956. Turbulent gravitational convection from maintained and instantaneous sources. *Proc. R. Soc.*, **A234**, 1-23.

Munro, D.S. and Davies, J.A. 1978. On fitting the log-linear model to wind speed and temperature profiles over a melting glacier. *Boundary-Layer Meteorol.*, 15, 423-437.

Mulholland, M. 1977. Formulation and application of a dynamic model for atmospheric point sources. Ph.D. thesis, Dept. of Chemical Engineering, University of Natal.

Mulholland, M. 1980. Simulation of tracer experiments using a numerical model for point sources in a sheared atmosphere. *Atmospheric Environment*, 14, 1347-1360.

Myrup, L.O. and Ranzieri, A.J. 1976. A consistant scheme for estimating diffusivities to be used in air quality models. California Department of Transportation Report CA-DOT-TL-7169-3-76-32, 69pp.

N

Neiburger, M. 1974. Private conversation with Liu and Goodin (1974)

Neumann, J. 1978. Some observations on the simple exponential function as a Lagrangian velocity correlation function in turbulent diffusion. *Atmospheric Environment*, 12, 1965-1968.

Neumann, J. and Maher, Y. 1971. A theoretical study of the land and sea breeze circulations. *J. Atmos. Sci.*, 28, 532-542.

Nieuwstadt, F.T.M. 1978. The computation of the friction velocity u_* and the temperature scale T_* from temperature and wind profiles by least square methods. *Boundary-Layer Meteorol.*, 14, 235-246.

Nieuwstadt, F.T.M. 1980. An analytical solution of the time-dependent, one-dimensional diffusion equation in the atmospheric boundary layer. *Atmospheric Environment*, 14, 1361-1364.

Nieuwstadt, F.T.M. 1983. On the solution of the stationary, baroclinic Ekman-layer equations with a finite boundary height. *Boundary-Layer Meteorol.*, 26, 377-390.

Nieuwstadt, F. and De Bruin, H.A.R. 1981. Comment on 'On the determination of boundary-layer parameters using velocity profile as the sole information'. *Boundary-Layer Meteorol.*, 20, 125-126.

O

O'Brien, J.J. 1970. A note on the vertical structure of the eddy exchange coefficient in the planetary boundary layer. *J. Atmos. Sci.*, 27, 1213-1215.

Obukhov, A.M. 1959. Description of turbulence in terms of Lgrangian variables. *Advan. Geophys.*, 6, 113-116.

Okubu, A. 1967. The effect of shear in an oscillatory current on horizontal diffusion from an instantaneous source. *Int. J. Oceonol. Limnol.*, 1, 194-204.

Orlenko, L.R. 1970. in *Building Climatology*, Tech. Note No. 109. World Meteorol. Organ., Geneva, Switzerland.

Orszag, S.A. 1971. Numerical simulation of incompressible flows within simple boundaries I. Galerkin (spectral) representations. *Stud. Appl. Math.*, **50**, 293–326.

Overcamp, T.J. 1976. A Gaussian diffusion–deposition model for elevated point sources. *J. Appl. Meteorol.*, **15**, 1167–1171.

P

Pandolfo, J.P. 1966. Wind and temperature profiles for constant-flux boundary layers in lapse conditions with a variable eddy conductivity to eddy viscisity ratio. *J. Atmos. Sci.*, **23**, 495–502.

Panofsky, H.A. 1961. *Quart. J. R. Met. Soc.*, **87**, 109.

Panofsky, H.A. 1962. Determination of stress from wind and temperature measurements. *Quart. J. R. Met. Soc.*, **88**, 85–94.

Panofsky, H.A., Blackadar, A.K. and McVehil, G.E. 1960. The diabatic wind profile. *Quart. J. R. Met. Soc.*, **86**, 390–398.

Parry, H.D., Sanders, M.J. and Jensen, H.P. 1975. Operational Applications of a pure acoustic sounding system. *J. Appl. Meteorol.*, **14**, 67–77.

Pasquill, F. 1961. The estimation of the dispersion of windborne material, *Met. Mag.*, **90**, 33

Pasquill, F. 1962. *Atmospheric Diffusion*. 1st ed., Van Nostrand, London.

Paquill F. 1969. The influence of the turning of wind with height on crosswind diffusion. *Phil. Trans. R. Soc.*, **A** 265, 173–181.

Pasquill, F. 1971. Atmospheric dispersion of pollution. *Quart. J. R. Met. Soc.*, 97, 369-395.

Pasquill, F. 1974. *Atmospheric Diffusion*. 2nd ed., John Wiley and Sons, London.

Pasquill, F. and Smith, 1971. The physical and meteorological basis for the estimation of the dispersion, in "Proceedings of the Second International Clean Air Congress," eds. H.M. Englund and W.T. Beery, Academic Press, New York.

Paulson, C.A. 1970. The mathematical representation of wind speed and temperature profiles in the unstable atmospheric surface layer. *J. Appl. Meteorol.*, 9, 857-861.

Peaceman, D.W. and Rachford, H.H.,Jr. 1955. The numerical solution of parabolic and elliptical differential equations. *J. Soc. Ind. Appl. Math.*, 3, 28-41.

Peters, L.K. and Klinzing, G.E. 1971. The effect of variable diffusion coefficients and velocity on the dispersion of pollutants. *Atmospheric Environment*, 5, 497-504.

Pielke, R.A. and Mahrer, Y. 1975. Technique to represent the heated-planetary boundary layer in mesoscale models with course vertical resolution. *J. Atmos. Sci.*, 32, 2288-2308.

Pielke, R.A., Panofsky, H.A. and Segal, M. 1983. A suggested refinement for O'Brian's Convective boundary layer eddy exchange coefficient formulation. *Boundary-Layer Meteorol.*, 26, 191-195.

Plate, E.J. 1971. The aerodynamics of shelter belts. *Agric. Met.*, 8, 203-222.

Prahm, L.P. and Christensen, O. 1977. Long-range transport of pollutants simulated by the 2-D pseudospectral dispersion model. *J. Appl. Meteorol.*, 16, 896-910.

Prandtl, L. 1925. Bericht uber Untersuchungen zur ausgebildeten Turbulenz. *Z. Anew. Math. Mech.*, 5(No. 2), 136-139.

Prater, B.E. and Colls, J.J. 1981. Correlations between acoustic sounder dispersion estimates, meteorological parameters and pollution concentrations. *Atmospheric Environment*, 15, 793-798.

Priestley, C.H.B. 1959. Turbulent transfer in the lower atmosphere. Univ. of Chicago Press.

Pruitt, W.O., Morgan. D.L. and Lourence, F.J. 1973. Momemtum and mass transfers in the surface boundary layer. *Quart. J. R. Met. Soc.*, 99, 370-386.

Q

Quesada A.F. 1971. Some solutions of the diffusion equation for an expanding gas cloud in a constant shear flow. Physical Science Research Papers No. 446, Air Force Cambridge Research Laboratories 71-0111.

R

Raffinerieerlaß 1975. Verwaltungsvorshrift zur Genehmigungsverfahren nach § 4.15 BIMSchG Fur Mineralolraffinerien und petrochemische Anlagen, Technische Richtlinie zur Luftreinhaltung. Ministerialblatt 28, 966.

Ragland, K.W. 1973. Multiple box model for dispersion of air pollutants from area sources. *Atmospheric Environment*, 7, 1017-1032.

Ragland, K.W., and Dennis, R.L. 1975. Point source atmospheric
    diffusion model with variable wind and diffusivity profiles.
    Atmospheric Environment, **9**, 175-189.

Ranca, E. and Sardei, F. 1975. Numerical treatment of time
    dependent advection and diffusion of air pollutants.
    Atmospheric Environment, **9**, 69-80.

Randerson, D. 1970. A numerical experiment in simulating the
    transport of sulphur dioxide through the atmosphere.
    Atmospheric Environment, **4**, 615-632.

Rao, K.S., Wyngaard, J.C. and Cote, O.R. 1974. Local advection of
    momentum, heat and moisture in micrometeorology.
    Boundary-Layer Meteorol., **7**, 331-348.

Rao, K.S. and Snodgrass, H.F. 1981. A nonstationary noctural
    drainage flow model. *Boundary-Layer Meteorol.*, **20**, 309-320.

Raupach, M.R. 1979. Anomalies in flux-gradient relationships over
    forest. *Boundary-Layer Meteorol.*, **16**, 467-486.

Reible, D.D., Shair, F.H. and Ares, R. 1983. A two-layer model of
    the atmosphere indicating the effects of mixing between the
    surface layer and the air loft. *Atmospheric Environment*, **17**,
    25-33.

Reid, J.D. 1979. Markov chain simulations of vertical dispersion in
    the neutral surface layer for surface and elevated releases.
    Boundary-Layer Meteorol., **16**, 3-22.

Reiquam, H. 1970. An atmospheric transport and accumulation model
    for airsheds. *Atmospheric Environment*, **4**, 233-247.

Richtmyer, R.D. 1963. A survey of difference methods for non-steady
    fluid dynamics. National Center for Atmospheric Research, Tech
    Notes, No. 63-62, 25pp.

Richtmyer, R.D. and Morton K.W. 1967. *Difference Methods for Initial-Value Problems*. Interscience, New York.

Rittmann, B.E. 1982. Application of two-thirds law to plume rise from industrial-sized sources. *Atmospheric Environment*, 16, 2575-2579.

Roache, P.J. 1972. *Computational Fluid Dynamics*. Interscience, New York.

Roberts O.F.T. 1923. The theoretical scattering of smoke in a turbulent atmosphere, *Proc. R. Soc., Lond.*, A104, 640-657.

Roberts, K.V. and Wiess, N.O. 1966. Convective difference schemes. *Math. Comp.*, 20, 272-299.

Robinson, S.M. 1962. Computing wind profile parameters. *J. Atmos. Sci.*, 19, 189-190.

Roffman, A., Rao, R.K. and Grimble, R. 1975. Application of a three dimensional diffusion model for predicting air pollution under thermal inversion breakup fumigation conditions. 68th Annual Meeting of the Air Pollution Control Association., June 15-20, 1975, Boston, Massachsetts.

Rossby, C.G. and Montgomery, R. 1935. The layers of frictional influence in wind and ocean currents. MIT paper 3, 3-101.

Rounds, W., (Jr.) 1955. Solution of the two-dimensional diffusion equation. *Trans. Amer. Geophys. Union.*, 36, 395-405.

Rubin, E.L. and Burstein, S.Z. 1967. Difference methods for the inviscid and viscous equations of compressible gas. *J. Comp. Phys.*, 2, 178-196.

Saffman P.G. 1962. The effect of wind shear on horizontal spread from an instantaneous ground source. *Quart. J. R. Met. Soc.*, **88**,382–393.

Sasaki, Y. 1970. Some basic formulations in numerical variational analysis. *Mon. Weather Rev.*, **98**, 875–883.

Sawford, B.L. 1984. The basis for, and some limitations of, the Langevin equation in atmospheric relative dispersion modelling. *Atmospheric Environment*, **18**, 2405–2411.

Sceicz, G. *et al*. 1969. Aerodynamic and surface factors in evaporation. *Water Resource Research*. **5**, 380–394.

Scholtz, M.T. and Brouckaert, C. 1978. Modeling of stable air flow over a complex region. *J. Appl. Meteorol*., **17**, 1249–1257

Schultz, P. 1979. Estimation of surface stress from wind. *Boundary-Layer Meteorol*., **17**, 265–267.

Schotz, S. and Panofsky, H.A. 1980. Wind characteristics at the Boulder Atmospheric Observatory. *Boundary-Layer Meteorol*., **19**, 155–164

Scire, J.S., Lurman, F.W., Base, A. and Hanna, S.R. 1984. Development of the MESOPUFF II dispersion model. Report No. EPA–600/3–84–057, Environmental Sciences Research Laboratory, Research Triangle Park, NC.

Scott, B.C. 1978. Parameterization of sulfate removal by precipitation *J. Appl. Meteorol*., **17**, 1375–1389.

Scott, B.C. 1981. Sulfate washout ratios in winter storms. *J. Appl. Meteorol*., **20**, 619–625.

Sedefian, L. and Benett, E.   1980.   A comparison of turbulent
        classification schemes. *Atmospheric Environment*, 14, 741-750.

Sehmel, G.A.   1980.   Particle and gas dry deposition - a review.
        Atmospheric Environment, 14, 983-1011.

Seinfeld, J.H.   1975.   *Air Pollution*, McGraw-Hill Co., New York.

Sellers, W.D.   1962.   *J. Atmos. Sci.*, 19, 180.

Sellers, W.   1965.   *Physical Climatology*. University of Chicago
        Press, 272pp.

Sethuraman. S. and Brown, R.M.   1976.   Validity of the log-linear
        profile relationship over rough terrain during stable
        conditions. *Boundary-Layer Meteorol.*, 10, 489-301.

Shepherd, J.G.   1974. Measurements of the direct deposition of
        sulphur dioxide onto grass and water by the profile method.
        Atmospheric Environment, 8, 69-74.

Sherman, C.E. .1978.   A mass-consistant model for wind fields over
        complex terrain. *J. Appl. Meteorol.*, 17, 312-319.

Shieh, C.M.   1978.   A puff pollutant dispersion model with wind shear
        and dynamic plume rise. *Atmospheric Environment*, 12,
        1933-1938.

Shieh, C.M., Wesely, M.L. and Hicks, B.B.   1979.   Estimated dry
        deposition velocities of sulfur over the Eastern United States
        and surrounding regions. *Atmospheric Environment*, 13,
        1361-1368.

Shiozawa, K., Okamoto, S. and Ootaki, A.   1975.   A diffusion model
        for air quality simulation. Paper #75-04.4 in 68'th Annual
        Meeting of the Air Pollution Control Association, Boston,
        Mass.

Shir, C.C. 1973. A preliminary numerical study of atmospheric turbulent flows in the idealized planetary boundary layer. *J. Atmos. Sci.*, **30**, 1327-1339.

Shir, C.C. and Shieh, L.J. 1974. A generalized urban air pollution model and its application to the study of SO_2 distributions in the St.Louis metropolitan area. *J. Appl. Meteorol.*, **13**, 185-204.

Singer, I., Frizzola, J.A. and Smith, M.E. 1966. *JACPA*, 594.

Skibin, D. and Businger, J.A. 1985. The vertical extent of the log-linear wind profile under stable stratification. *Atmospheric Environment*, 19, 27-30.

Sklarew, R.C., Fabrik, A.J. and Prager, J.E. 1971. A particle-in-cell method for numerical solution of the atmsopheric diffusion equation, and application to air pollution problems. Report No. 3SR-844, Systems, Science and Software, La Jolla, CA.

Slade, D.H. (ed). 1968. *Meteorology and Atomic Energy.* U.S. Atomic Energy Comm., Oak Ridge, Tennessee.

Slawson, P.R. and Csanady, G.T. 1967. The effect of atmospheric conditions on plume rise. *J. Fluid. Mech.*, **47**, 33-49.

Slinn, W.G.N. 1976. Formulation and a solution of the diffusion-deposition-resuspension problem. *Atmospheric Environment*, 10, 763-768.

Smith F.B. 1957. *J. Appl. Mech.*, **3**, 49

Smith, F.B. 1968. Conditioned particle motion in a homogeneous turbulent field. *Atmospheric Environment*, 2, 491-508.

Smith, M.E., Carlson, J.H., Martin, J.R. and Lawrence, J.L. 1983. Atmospheric modeling for emergencies. *Plant/Operations Progr.*, 2, 61-66.

Smith, F.B. and Thomson, D. 1984. Solutions of the integral equation of diffusion and the random walk model for continuous plumes and instantaneous puffs in the atmospheric boundary layer. *Boundary-Layer Meteorol.*, 30, 143-157.

Smith, T.B., Marsh, S.L., White, W.H., Jerskey, T.N., Lamb, R.G., Durbin, P.A. and Killus, J.P. 1976. Analysis of the data from the three-dimensional gradient study, Final report submitted to the California Air Resources Board under contracts ARB-4-051 and ARB-4-250 by Meteorology Research, Inc., Pasadena, California, and System Applications, Inc., San Rafeal, California, 124.

Spiegel, E.A. 1963. A generalization of the mixing length theory of turbulent convection. *Astrophys. J.*, **138**, 216-225.

Stanhill, G. 1969. A simple instrument for the field measurement of turbulent diffusion flux. *J. Appl. Meteorol.*, **8**, 509-513.

Stearns, C.R. 1970. Determining surface roughness and displacement height. *Boundary-Layer Meteorol.*, 1, 102-111.

Stephens, J.J. 1967. On convergence of the Endlich iteration method. *J. Appl. Meteorol.*, 6, 845-847.

Stephens, J.J. and Stitt, J.M. 1970. Optimum influence radii for interpolation with the method of successive corrections. *Mon. Weather Rev.*, **98**, 680-687.

Stoker, J.J. 1957. *Water Waves*. Wiley-Interscience, New York.

Strom, G.H. 1976. Transport and diffusion of stack effluents. in *Air Pollution*, Vol.I, ed. A.C. Stern, 401-501, Academic Press, New York.

Stull R.B.   1984.   Transilient turbulence theory. Part I: The concept
of eddy-mixing across finite distances.   *J. Atmos. Sci.*, 41,
3351–3367.

Sutton, O.G.   1953.   *Micrometerology*. McGraw–Hill Book Co., London.

Swinbank, W.C.   1964.   The experimental wind profile. *Quart. J. R.
Met. Soc.*, 97, 416–428.

Swinbank, W.C.   1968.   A comparison between predictions of
dimensional analysis for constant flux layer and observations
in unstable conditions. *Quart. J. R. Met. Soc.*, 94, 460–467.

T

Tadmor, B.D. and Gur, Y.   1969.   Analytical expressions for the
vertical and lateral dispersion coefficients in the
atmospheric diffusion. *Atmospheric Environment*, 3, 688–689.

Tajchman, S.J.   1981.   Comments on measuring turbulent exchange
within and above forest canopy. *Bull. Am. Meteorol. Soc.*, 62,
1550–1559.

Takeuchi, K.   1961.   *Met. Soc. Japan*, Ser. II, 39, 346.

Taylor, G.I. 1921.   Diffusion by continuous movements, *Proc. Lond.
Math. Soc.*, Ser. 2, 20, 196.

Taylor, G.I.   1953.   Dispersion of soluble matter in solvent flowing
slowly through a tube. *Proc. R. Soc., Lond.*, A219, 446–468.

Taylor G.I.   1954.   The dispersion of matter in turbulent flow
through a pipe. *Proc. R. Soc., Lond.*, A223, 446–468.

Taylor, R.J. 1960 Similarity theory in the relation between fluxes and gradients in the lower atmosphere. *Quart. J. R. Met. Soc.*, **86**, 67-78.

Tennekes, H. and Lumley, J.L. 1972. *A Course in Turbulence*. M.I.T. Press, Cambridge, Mass.

Thom, A.S. 1971. Momentum absorption by vegetation. *Quart. J. R. Met. Soc.*, **970**, 414-428.

Thomson, R. 1971. Numeric calculation of turbulent diffusion. *Quart. J. R. Met. Soc.*, **97**, 93-98.

Touma, J.S. 1977. Dependance of the wind profile power law on stability for various locations. *J. Air Pollu. Control Ass.*, **27**, 863-866.

Turner, D.B. 1964. A diffusion model for an urban area, *J. Appl. Meteorol.*, **3**, 83.

Tyldesley, J.B. and Wallington, C.E. 1965. The effect of wind shear and vertical diffusion on horizontal dispersion. *Quart. J. R. Met. Soc.*, **91**, 158-174.

V

Van Egmond, N.D. and Kesseboom, H. 1983. Mesoscale air pollution dispersion models - I. Eulerian grid model. *Atmospheric Environment*, **17**, 257-265.

Van Dop, H., De Haan, B.J. and Engeldal, C. 1982. The KNMI mesoscale air pollution model. KNMI Scientific report W.R., 82-86, De Bilt.

Van Dop, H., Steenkist, R. and Nieustadt, E.T.M. 1979. Revised estimates for continuous shoreline fumigation. *J. Appl. Meteorol.*, 18, 133-137.

Van Egmond, N.D. and Kesseboom, H. 1983. Mesoscale air pollution dispersion models-II. Lagrangian puff model and comparison with Eulerian grid model. *Atmospheric Environment*, 17, 267-274.

Venkatram, A. 1980. Estimation of turbulence velocity scales in the stable and the unstable boundary layer for dispersion applications. In Eleventh NATO-CCSM International Technical Meeting on Air Pollution Modeling and its Application, 54-56.

Venkatram, A. 1980a. Dispersion from an elevated source in a convective boundary layer. *Atmospheric Environment*, 14, 1-10.

Venkatrem, A. and Vet, R. 1981. Modeling of dispersion from tall stacks. *Atmospheric Environment*, 15, 1531-1538.

Venter, G.P.N., Haliday, E.C. and Prinsloo, L.A. 1973. The determination of the Sutton diffusion parameters for the Highveld of South Africa. *Atmospheric Environment*, 7, 593-602.

Villadsen, J.V. and Stewart, W.E. 1967. Solution of boundary-value problems by orthogonal collocation. *Chem. Engng. Sci.*, 21, 1483-1501.

Viswanadham, Y. 1982. Eximination of the empirical flux-profile models in the atmospheric surface boundary layer, *Boundary-Layer Meteorol.*, 22, 61-77.

Von Gogh, R.G. 1983. Preliminary measurements and assessment of the impact of emissions from burning colliery discard dumps. CSIR report ATMOS/83/16, Pretoria.

Walters T.S. 1969. The importance of diffusion along the mean wind direction for a ground-level crosswind line source. *Atmospheric Environment*, **3**, 461-466.

Webb, E.K. 1970. Profile relationships: the log-linear range, and extension to strong stability. *Quart. J. R. Met. Soc.*, **96**, 67-90.

Webb, E.K. 1982. Profile relationships in the superadiabatic surface layer. *Quart. J. R. Met. Soc.*, **108**, 661-688.

Weber, A.H. 1976. Atmospheric Dispersion Parameters in Gaussian Plume Modeling, Part 1, Review of Current Systems and Possible Future Developments. EPA-600/4-76-030a, Washington, D.C.

Weber, A.H., Irwin, J.S., Kahler, J.P. and Peterson, W.B. 1975. Atmospheric turbulence in the lowest 300metres. US. Environmental Protection Agency Report 600/4-75-004, 152pp.

Weil, J.C. 1977. Evaluation of the Gaussian plume model at Maryland power plants. Report No. PPSP-MP-16, Martin Marietta Corporation, Baltimore, Maryland.

Wendell, L.L. 1972. Mesoscale wind fields and transport estimates determined from a network of wind towers. *Mon. Weather Rev.*, **100**, 565-578.

Wesely, M.L. and Hicks, B.B. 1977. Some factors that affect the deposition rates of sulfur dioxide and similar gases on vegetation. *JAPCA*, **27**, 1110-1116.

Wetzel, P.J. 1982. Toward parameterization of the stable boundary layer. *J. Appl. Meteorol.*, 21, 7-13.

Wieringa, J. 1976. An objective exposure correction method for average wind speeds measured at a sheltered location. *Quart. J. R. Met. Soc.*, 102, 241-253.

Wieringa, J. 1980. Representation of wind observations at airports. *Bull. Amer. Met. Soc.*, 61, 962-971.

Wilson, J.D., Thurtell, G.W. and Kidd, G.E. 1981. Numerical simulation of particle trajectories in inhomogeneous turbulance, III: Comparison of predictions with experimental data for the atmospheric surface layer. *Boundary-Layer Meteorol.*, 21, 443-463.

Willis, G.E. and Deardorff, J.W. 1976. A laboratory model of diffusion into the convective boundary layer. *Quart. J. R. Met. Soc.*, 102, 427-445.

Wyckoff, R.J., Beran, D.W. and Hall, F.F.(Jr) 1973. A comparison of the low-level radiosonde and the acoustic echo sounder for monitoring atmospheric stability. *J. Appl. Meteorol.*, 12, 1196-1204.

Wyngaard, J.C. 1982. Boundary layer modeling. Chapter 3 of the collection of papers by F.T.M. Nieustadt and Van Dop: *Atmospheric Turbulence and Air Pollution Modelling, A Course held in the Hague, 21-25 September 1981*. Reidel, 69 -106.

Wyngaard, J.C., Arya, S.P.S. and Cote, O.R. 1974. Some aspects of the structure of convective planetary boundary layers. *J. Atmos. Sci.*, 31, 747-754.

Wyngaard, J.C. and Brost, R.A. 1984. Top-down and bottom-up diffusion in the convective boundary layer, *J. Atmos. Sci.*, 41, 102-112.

Wyngaard, J.C., Cote, O.R. and Rao, K.S. 1974. Modeling the atmospheric layer. *Advan. Geophys.*, 18A, 193-212, Academic Press, New York.

Yaglom, A.M. 1977. Comments on wind and temperature flux-profile relationships. *Boundary-Layer Meteorol.*, 11, 89-102.

Yaglom, A.M. 1977a. Semi-empirical equations of turbulent diffusion in boundary layers. *Fl. Dyn. Trans.*, Polish Acad. Sci., 7, 99-144.

Yamada, T. 1976. On the similarity functions A, B and C of the planetary boundary layer. *J. Atmos. Sci.*, 33, 781-793.

Yamada, T. 1979. PBL similarity profiles determined from a level - 2. turbulence closure model. *Boundary-Layer Meteorol.*, 17, 333-351.

Yamada, T. 1981. A numeric simulation of nocturnal drainage. *J. Met. Soc. Japan*, 59, 108-122.

Yamamoto, G. 1959. *J. Met. Soc. Japan*, 37, 60.

Yamamoto, G. 1975. Generalization of the KEYPS formula in diabatic conditions and related discussion on the critical Richardson number, *J. Met. Soc. Japan*, 53, 189-194.

Yanenko, N.N. 1971. *The Method of Fractional Steps*. Springer, Berlin.

Yardanov, D. 1968. On some asymptotic formulae describing diffusion in the surface layer of the atmosphere. *Atmospheric Environment*, 2, 167-180.

Yardanov, D..1975. A simple baroclinic model of the planetary boundary layer. *Atmos. Ocean Phys.*, 11, 387-389.

Yelagina, L.G., Koprov, B.M. and Timanovsky, D.F. 1978. Certain characteristics of the atmospheric surface layer above snow. *Izv. Acad. Sci. USSR, Atmos. Ocean Phys.*, 14, 652-655.

Yocke, M.A., Liu, M.K. and McElroy, J.L. 1978.. The development of a three-dimensional wind model for complex terrain. Proc. Joint Conf. Applications of Air Pollution Meteorology, Salt Lake City, *Amer. Meteor. Soc.*, 209-214.

Yu, T. 1977. A comparative study on the parameterization of vertical turbulent exchange processes. *Mon. Weather Rev.*, 105, 57-66.

Yu, T. 1978. Determining height of the nocturnal boundary layer. *J. Atmos. Sci.*, 17, 28-33.

Z

Zalesak, S.T. 1979. Fully multidimensional flux-corrected transport algorithms for fluids. *J. Comp. Phys.*, 31, 335-362.

Zanetti, P. 1981. An improved puff algorithm for plume dispersion simulation. *J. Appl. Meteorol.*, 20, 1203-1211.

Zeman, O. 1979. Parameterization of the dynamics of stable boundary layers and nocturnal jets. *J. Atmos. Sci.*, 36, 792-804.

Zeman, O. and Lumley, J.L. 1976. Modeling buoyancy driven mixed layers. *J. Atmos. Sci.*, 33, 1974-1988.

Zilitinkevich, S.S. and Chalikov, D.V. 1968. Determining the universal wind-velocity and temperature profiles in the atmospheric boundary layer. *Izv. Acad. Sci. USSR, Atmos. Ocean. Phys.*, 4, 165-170.

Zilitinkevich, S.S. 1972. On the determination of the height of the Ekman boundary layer. *Boundary-Layer Meteorol.*, 3, 141-145.

Zilitinkevich, S.S. and Chalikov, D.V. 1969. On the computations of
the vertical turbulent fluxes in the surface layer of the
atmosphere from data of porfile observations. *Izv. Acad. Sci.
USSR, Atmos. Ocean. Phys.*, **4**, 915-929.

Zlatev, Z., Berkowicz, R. and Prahm, L.P. 1983. Three-dimensional
advection-diffusion modelling for regional scale. *Atmospheric
Environment*, **17**, 491-499.